Bangor University

DOCTOR OF PHILOSOPHY

Detection of Volatile Organic Compounds Using Fuel Cell Sensors

Wheldon-Williams, Robyn

Award date:
2002

Awarding institution:
Bangor University

Link to publication

Detection of Volatile Organic Compounds Using Fuel Cell Sensors

by

Robyn Wheldon-Williams

(B.Sc Hons)

A thesis submitted for the degree of

<u>Doctor of Philosophy</u>

Adran Cemeg

Department of Chemistry

Submitted July, 2002

Acknowledgements

i

UNIVERSITY OF WALES, BANGOR

<u>ABSTRACT</u>

DEPARTMENT OF CHEMISTRY

<u>Doctor of Philosophy</u>

Detection of volatile organic compounds using fuel cell sensors

By **Robyn Wheldon-Williams** BSc (Hons)

In this study the development of an improved electrochemical fuel cell sensor for the detection of low-levels of formaldehyde vapour is described. Current fuel cell sensors used in the commercial Formaldemeter™ instrument lack sensitivity, respond to methanol, and show an interference response to humidity. For the detection and accurate determination of low-level concentrations of formaldehyde an improvement in these characteristics is essential. Two routes were investigated to achieve these requirements.

Firstly the oxygen reduction reaction at the cathode was replaced with that of a conducting polymer, polyaniline (PANI). Before construction of the fuel cells the stability and open circuit behaviour of various PANI films were investigated in order to assay their suitability as a cathode material in a fuel cell application. Based on these results various fuel cells containing PANI as the cathode were prepared and incorporated into the Formaldemeter™. The cells were then evaluated using a calibrated vapour stream. Fuel cells containing a Pt-black anode and a PANI/SO_4^{2-} coated Pt-black cathode in H_2SO_4 electrolyte displayed a significant improvement in sensitivity, selectivity and a reduced humidity response. In addition a fast response time, excellent reproducibility and a long shelf life was demonstrated. It is proposed that a PANI film coated on Pt-black behaves as a more stable electron sink for the cathodic reaction instead of the oxygen reduction reaction which is dependent on the diffusion of oxygen. The fast fuel cell response time is explained by the fast switching of PANI (< 10μs).

In the second part of the work, the effect of changing fuel cell catalyst was investigated. Initially, the electrocatalytic activity of various noble metals and alloys electrodeposited on glassy carbon were investigated. Based on these results several fuel cell electrodes were prepared and characterised by SEM and EDAX. Fuel cells were then constructed and their performance evaluated. Cells made up of 50:50 % atomic weight ratio of platinum and palladium showed that while the fuel cell was active towards low levels of formaldehyde, its response to equivalent levels of methanol was very small.

Table of Contents

Chapter III – The Use of Polyaniline as a Cathode in Fuel Cell Sensors

Chapter IV – The Catalytic Activity of Fuel Cell Electrodes - Electrocatalysis

Chapter V – General Conclusions and Recommendations

Chapter I - Introduction

1.0 General introduction

For thousands of years the nose has frequently been relied upon as the only gas detector available, often with dismal or fatal consequences. As a result animals were often used to make life safer; these "biomonitors" would help in situations that could be hazardous to humans. In the early days, miners discovered that small birds such as canaries were much more susceptible to noxious fumes than they were, so it became common to carry canaries into mines as a safeguard against "bad air"; however, inflammable gases were rarely detected and explosions were still common. Many lives were lost in industry and unpleasant and incurable illnesses were contracted as a result of exposure to toxic gases and vapours. Sadly, at that time people were unaware of the link between the working environment and certain illnesses. To this day more is constantly being learnt of the toxic effects of commonly encountered gases which were once considered safe or which have become a new problem as a result of developing industry and technology.

Over the last thirty years in the United States bodies such as the National Institute for Occupational Safety and Health (NIOSH) and the Occupational Safety and Health Administration (OSHA) have been set up to protect people in their working environment. The United Kingdom adopted a similar system under the Health and Safety at Work Act 1974. As a result strict regulations have been introduced with hefty penalties if they are broken. The permissible exposure limit (PEL) for toxic gases and vapours is now common in today's society, however as more is learnt on the environmental and health effects of toxic gases regulations are constantly being revised.

The constantly increasing demands of society has created the need for the detection and measurement of various gases and vapours and has aroused new areas of research into the field of sensors. Over the last twenty years many analytical techniques have been conceived as a direct result of this demand and development is still proceeding at a rapid pace. Today, gas detection has become a lucrative multi-million pound industry and is set to expand sharply into the foreseeable future as more markets are discovered and exploited.

1.1 Air pollution

The problem of air pollution is not new but has gone hand-in-hand with man's technical and industrial development. Although scientists have only become concerned with the problem within the last century, Parliament saw fit to prohibit the burning of coal in London as early as 1273 [1]. The steep rise in the use of fossil fuels during the industrial revolution over the last century, coupled with the simultaneous development of the internal combustion engine resulted in the dramatic increase of air pollution and gave rise to atmospheric conditions which were both unpleasant and dangerous to live in from a health point of view.

In recent years, further industrialization and increased use of motor vehicles have resulted in rising emissions of harmful gaseous pollutants. Fortunately, society is becoming increasingly aware of the potential health effects and dangers of air pollution, and as a response the levels of harmful gases and vapours which are emitted into the environment are strictly controlled through 'Air Quality Standards', which define the maximum allowable concentrations of the major atmospheric pollutants [2]; these include SO_2, O_3, NO_x, CO and a wide range of volatile organic compounds (VOCs). In spite of these standards, air pollution is still a major environmental health problem affecting developed and developing countries around the world. The World Health Organisation (WHO) recently estimated that 3 million people die each year as a result of air pollution and in addition many more suffer serious health effects such as respiratory diseases, asthma, cardiovascular diseases and cancer of the lung [3]. In addition to the common environmental pollutants it is now realised that there are many other gases and vapours which have a toxic effect on man when present at very low concentrations in industrial working environments.

1.1.1 Industrial air pollution

The Common Law of England has, for centuries, required that no master or employer shall put his servant at risk; however, until recently no truly scientific attempts at controlling the workers' environment were made. The exposure of workers in the industrial environment is now controlled through the application of occupational exposure limits and in the UK this is enacted through the Control of Substances Hazardous to Health (COSHH) regulations.

In most countries control measures are implemented through permissible exposure limits (PEL) for gases and vapours, however, as some substances are extremely toxic in the short-term and others require frequent exposure over a long-term period before any adverse symptoms can be noticed, the permissible exposure limit includes a long-term time weighted average limit (TWA) and a short term exposure limit (STEL). Both exposure limits are expressed as airborne concentrations averaged over a specified period of time. The TWA limit is usually 8 hours while the STEL is 15 minutes in the UK and differs from country to country. Based on this system in the UK, the Health and Safety at Work Act, 1974, gives the factory inspectorate the power to close any factory if the level of a gas or vapour is considered too high. As a result there has been increased demand for instruments to detect and measure the concentration of various gases and vapours.

In addition to environmental and industrial air pollution recent years has seen the rise of air pollution in the indoor environment, this is of particular concern since there are different population groups, such as children and old people who are more at risk from pollutants [3]. The regulations, which were initially implemented for industry, have been extended to cover all working environments; however, there are still no satisfactory regulations in the non-occupational environment.

1.1.2 Indoor air pollution

In developed countries people typically spend most of their time indoors, which makes indoor spaces important microenvironments when addressing risks from air pollution. The indoor environment is generally considered to be a safe haven from all air pollutants but due to the amount of time spent indoors and the higher pollution levels that can be encountered as a result of poor ventilation, most of a person's daily exposure to many air pollutants comes through inhalation of indoor air.

The air quality inside buildings is affected by many factors. In an effort to conserve energy, modern building design has favoured tighter structures with lower rates of ventilation, however, lower ventilation rates and the presence of products and materials that emit a large variety of compounds contribute to most of the pollution problems. Indoor air quality problems affect all types of buildings including homes, schools, offices, health care facilities and other public and commercial buildings. Pollution and degradation of indoor air cause illness, increased mortality, loss of productivity and have major economic and social implications. The medical and

social cost associated with these illnesses, and the related reduction in human productivity result in staggering economic losses [3].

Indoor concentrations of air pollutants are influenced by outdoor levels, indoor sources, the rate of exchange between indoor and outdoor air, and the characteristics and furnishings of buildings. The sources of indoor air pollution and the principal pollutants, grouped by outdoor and indoor origin are summarized in table 1. This is not a complete listing of all sources of indoor air pollutants, as there is continuous air exchange between indoors and outdoors, and most pollutants in the outdoor air are also found indoors [3].

As the health effects of exposure to indoor air pollution, both short-term and long-term are slowly being learnt, it is speculated that similar exposure limits to those in the working environment will be implemented in the home environment, a measure that is already in place in the United States [4]. If such regulations are introduced into the home environment there will be increased demand for reliable and cheap instruments to monitor air quality.

1.2 Volatile Organic Compounds

In addition to the familiar air pollutants it is now realised that there are many other gases and vapours that may exert toxic effects when present in low concentrations. Much of the knowledge gained in this field has only come about as a result of new methods sensitive enough to detect and measure those chemical species which were once unknown to be present in the atmospheric environment.

Volatile organic compounds or VOCs are an important class of air pollutants and are commonly found in the atmosphere at ground level in all urban and industrial centres. VOCs are classified as organic compounds which are present in the atmosphere as gases, but which under normal conditions of temperature and pressure are liquids or solids [5]. VOCs are the subject of increasing concern as they are one type of pollutant commonly found in the air of non-industrial buildings. Recent work has shown that construction materials and furnishings are major sources of VOCs in indoor air [6,7]. Various studies of indoor air quality have identified more than 250 organic compounds at a level exceeding 1 ppb with many hundreds of additional compounds existing at lower levels [8].

Principal Pollutant	Sources, predominantly outdoor
SO_2, SPM/RSP	Fuel combustion, smelters
O_3	Photochemical reactions
Pollens	Trees, grass, weeds, plants
Pb, Mn	Automobiles
Pb, Cd	Industrial Emissions
VOCs, PAH	Petrochemical Solvents, Vaporisation of unburned fuels
Principal Pollutant	**Sources, both indoor and outdoor**
NO_x, CO	Fuel burning
CO_2	Fuel burning, metabolic activity
SPM, RSP	Environmental tobacco smoke, resuspension, condensation of vapours and combustion products
Water vapour	Biological activity, combustion, evaporation
VOCs	Volatilisation, fuel burning, paint, metabolic action, pesticides, insecticides, fungicides
Principal Pollutant	**Sources, predominantly indoor**
Radon	Soil, burning construction materials, water
HCHO	Insulation, furnishing, environmental tobacco smoke
Asbestos	Fire-retardant, insulation
NH_3	Cleaning products, metabolic activity
PAH, Arsenic, Nicotine, Acrolein	Environmental tobacco smoke
VOCs	Adhesives, solvents, cooking, cosmetics
Mercury	Fungicides, paints, spills or breakage of mercury containing products
Aerosols	Consumer products, house dust

Table 1 Principal pollutants and sources of indoor air pollution, grouped by origin [3]. SPM = Suspended Particulate Matter, RSP = Respirable Particulate Matter, PAH = Polycyclic Aromatic Hydrocarbons, VOCs = Volatile Organic Compounds.

Health effects of VOCs are similar to those of Sick Building Syndrome. Some organic compounds can affect the human senses through their odour, some others exert a narcotic effect, and certain species are toxic [2]. The term 'air toxics' is given to those organic compounds that are present in the ambient atmosphere and have the potential to induce cancer in the human population. The most important VOCs that belong to the air toxics category are; benzene, 1,3-butadiene, which are potential leukaemia inducing agents and formaldehyde (methanal), which is a potential nasal carcinogen. Due to the severe health effects of these chemicals to the human population there has been increasing demand for efficient analytical techniques to determine the concentration of the gases in the atmosphere. One of the air toxics, formaldehyde is of great concern to society as so many of the population are exposed to its health effects on an occupational and on a non-occupational level. The next section will review formaldehyde in detail; in addition, current methods for its detection will be discussed.

1.3 Formaldehyde

Formaldehyde, one of the best known VOCs in the atmosphere has received considerable attention in recent years due to its harmful effects on health. Concerns were raised in the 1970s when reports of health effects in buildings, including residential and mobile homes, were associated with building materials manufactured with formaldehyde, particularly pressed wood products such as particleboard and urea-formaldehyde foam insulation (UFFI) [9]. Further concerns were raised in 1979 when Kerns and co-workers discovered that formaldehyde induced cancer in the nasal cavity of both sexes of rats when administered by inhalation [10,11]. Questions were soon asked about workers routinely exposed to the substance. These initial findings caused the next twenty years to become a frenzy of activity by toxicologists, epidemiologists and industry workers all striving to answer the question 'Is formaldehyde a human carcinogen?'.

The causative association of long-term formaldehyde exposure with cancer in humans is controversial and still unproven. Occupational studies have noted statistically significant associations between exposure to formaldehyde and increased incidence of lung and nasopharyngeal cancer, however the evidence is still considered to be limited [12]. As a result of the research by Kerns and subsequent studies on humans

by various groups, formaldehyde is listed in the Ninth Annual Report on Carcinogens and is classified as a suspected human carcinogen [13].

Formaldehyde was first prepared by Butlerov in 1859 by hydrolysing methylene acetate [14]. The gas was characterised by its pungent, suffocating odour and its irritant effect on the mucous membrane of the eyes, nose and throat. Today formaldehyde is one of the most common chemicals in use. Annual world production of formaldehyde is around 12 million tonnes and in the United States it is consistently ranked among the top 50 highest volume chemicals produced each year [13]. Formaldehyde occurs naturally in the environment and is produced by mammalian cells in the course of normal metabolism. It has been in widespread use for over a century as a disinfectant and preservative agent due to its denaturing action on proteins, and more recently in a number of industrial products.

As a chemical building block, it can be traced to consumer goods through a wide spectrum of manufacturing processes; this arises largely from its high chemical reactivity and relatively low cost which are the main reason for its rôle in the synthesis of organic compounds. It is commonly used as formalin, a mixture containing 30-50% formaldehyde and 10-20% methanol in water, as formaldehyde on its own tends to polymerise in solution.

Formaldehyde is primarily used in the manufacture of urea-formaldehyde resins (25% produced), phenol- formaldehyde resins (20%), plastics (15%) and intermediates (22%) [13]. Urea-formaldehyde resins and phenol-formaldehyde resins are primarily used as adhesives in the manufacture of pressed wood products, and for molding, paper treating and coating, textile treating, surface coating and foams for insulation.

1.3.1 Health effects of formaldehyde

The primary routes of potential human exposure to formaldehyde (gas) are inhalation, dermal contact and ingestion. Exposure to formaldehyde vapours at levels as low as 1 ppm irritates the eyes, nose and throat. Low-level exposure can cause teariness, and burning of the eyes, sneezing and coughing. It can also cause allergic reactions of the skin (dermatitis) and the lungs (asthma). The severity of irritation increases as concentrations increase; table 2 summarises the general effects at different concentrations of formaldehyde [2].

Approximate Formaldehyde Air Concentrations, ppm	Reported Health Effects
0.05 - 1.0	Odour threshold
0.01 - 2.0	Eye irritation
1.0 - 3.0	Irritation of the eyes/nose/throat/upper respiratory system
4.0 - 5.0	Inability to tolerate prolonged exposures
10.0 - 20.0	Severe respiratory symptoms, difficulty in breathing
>50.0	Serious injury to the respiratory tract
>100.0	Death

Table 2 Health Effects of formaldehyde exposure in parts per million parts air [2].

It can be seen that at 100 ppm it is immediately dangerous to life and health, high levels cause throat spasms and a build up of fluid in the lungs, leading to death. Direct contact can cause severe eye and skin burns, leading to permanent damage. These may appear hours after exposure, even if no pain is felt. Even though the health effects of short-term exposure to the substance are well documented, the health effects of long-term low-level exposure are still under investigation.

A number of studies point to formaldehyde as a potential factor predisposing certain groups, particularly children, to respiratory tract infections. It has not been definitely established that formaldehyde gas causes respiratory tract allergy, but occupational studies indicate that 1-2 % of the population exposed to high concentrations may develop asthma [15,16]. A study in Arizona, USA reported that children exposed to 60-120 ppb formaldehyde at home, and particularly if also exposed to tobacco smoke, had an increased likelihood of suffering from asthma or chronic bronchitis [17].

In recent decades the prevalence of allergic diseases has increased substantially in many Western countries [18] and at the same time, materials emitting formaldehyde have become increasingly popular in homes [19]. Thus, it is possible that at least some part of the increase in allergic disease could have been brought about by an increase in indoor formaldehyde exposure.

1.3.2 Formaldehyde exposure and sources

It is estimated that several million people are exposed to formaldehyde in industrialised countries alone, with people working directly with the substance most likely to be at risk; these include anatomists, embalmers, pathologists, other medical workers and industrial workers. In the industrial environment the highest continuous exposures (frequently greater than 0.8 ppm) have been measured in particleboard mills, during the varnishing of furniture and wooden floors, in foundries, during the finishing of textiles and in fur processing. Exposure to more than 0.8 ppm also occurs in some facilities where resins, plastics and special papers are produced. The average formaldehyde level measured in plywood mills and in embalming establishments is about 0.8 ppm. Lower levels are encountered, for example, during the manufacture of garments, man-made mineral fibres, abrasives and rubber [13].

Formaldehyde levels in buildings depend mainly on what is releasing the formaldehyde (the source), the temperature, the humidity, and air exchange rate (the amount of outdoor air entering or leaving the indoor area). An increase in the temperature or humidity will increase the amount of formaldehyde emitted. There are many sources from which formaldehyde is released; significant contamination of indoor air is most likely from products manufactured using urea-formaldehyde resins. These include; particleboard (flooring, panelling, cabinetry, furniture), medium density fibreboard (MDF), hardwood plywood panelling and urea-formaldehyde foam insulation (UFFI). Due to the common use of formaldehyde-emitting materials in buildings, indoor concentrations generally exceed those outdoors [4].

Two subpopulations that are particularly at high risk of potential exposure are residents of mobile homes containing plywood (with an average exposure of 0.4 ppm formaldehyde) and people living in conventional homes insulated with urea-formaldehyde foam (with a potential average exposure of 0.12 ppm). The formaldehyde release can be due to volatile unreacted formaldehyde trapped in the resin and from the hydrolytic decomposition of the resin polymer itself.

During the 1970s, many homeowners installed UFFI to save energy, however, many of these homes had high levels of formaldehyde soon afterwards. As a result, the sale of UFFI largely stopped. A recent UK study of the exposure to formaldehyde from the use of UFFI in residential houses revealed that houses built in the 1980s had formaldehyde levels three times as high as houses built before the 1920s. Another

study in Australia found that schools panelled with particleboard had twice the average formaldehyde level than schools panelled without [16].

The general population is exposed to formaldehyde mainly by inhalation, smokers receiving about 0.3 ppm / day by this route. Studies have shown that where smoking rates are high and ventilation minimal there is a clear contribution to formaldehyde concentration of the order of a few ppb. Automobile exhaust is a major source of formaldehyde in air. Typical concentrations of formaldehyde range from sub-ppb levels in remote and rural areas to higher levels (up to 10–20 ppb) in urban atmospheres [20,21]. In general the formaldehyde concentration in the atmosphere is in the low ppb region, this is because it has a short half-life in air due to degradation by photochemical processes.

1.3.3 Control of Indoor Formaldehyde Pollution

In the industrial environment pollution of the indoor air is controlled through regulations and occupational exposure standards that define maximum exposure limits. In the early seventies, exposure limits for formaldehyde at workroom environment were fixed in most European countries in the region of 5 ppm, however during the following years as the health effects of exposure were being learned the limits were tightened with exposure limits ranging from 0.5 - 2 ppm. Regulations and exposure limits to formaldehyde and various other gases vary from country to country [22]. Table 3 summarises the exposure limits of some countries to formaldehyde.

| Country | Year | Living Space | | Workplace | | | |
| | | | | TWA [1] | | STEL [2] | |
		PPM	mg m^{-3}	PPM	mg m^{-3}	PPM	mg m^{-3}
United Kingdom	1993	No Regulation		2	2.5	2	2.5
France	1999	No Regulation		0.5	0.6	1	1.5
Germany	1999	0.1	0.15	0.5	0.6	1	1.5
Sweden	1999	0.2	0.30	0.5	0.6	1	1.5
Australia	1993	0.1	0.15	1	1.5	2	2.5
United States	OSHA[3] 1993	0.4	0.5	0.75	0.9	2	2.5
	NIOSH[4] 1993	-	-	0.016	0.02	0.1	0.15

Table 3 Exposure limits for formaldehyde in various countries [22]. [1] Time Weighted Average; [2] Short Term Exposure Level; [3] Occupational Safety and Health Administrative ; [4] National Institute of Safety and Health

Presently the permissible exposure limit (PEL) for formaldehyde in all workplaces in the United Kingdom (including general industry, construction, and maritime) is 2 ppm measured as an 8-hour time weighted average (TWA). The standard also includes a 2 ppm short-term exposure limit (STEL) (*i.e.* maximum exposure allowed during a 15-minute period). However there is no limit for living space exposure in the United Kingdom. The World Health Organisation (WHO) recommends that in order to avoid complaints of sensitive people about indoor air in non-industrial buildings the formaldehyde concentration should be below 0.050 ppm as a 30 minute average and this is recommended as an air quality guideline value [2]. In addition to exposure limits and guidelines, there are also building regulations and product standards relating to the quality and installation procedure for the use of UFFI for cavity walls and the free formaldehyde content of particleboard and fibreboard. These standards limit the amount of formaldehyde emitted from the product into the occupied space of a building [23].

In order to determine the concentration of formaldehyde in the indoor air and to adhere to legal limits and regulations, gas sensors for formaldehyde are required by industries worldwide. In addition new markets are emerging with some countries implementing regulations in non-industrial buildings such as the home environment. In light of recent health findings, indoor exposure limits and guidelines for formaldehyde are set to be revised again [15]. As a result the demand for a reliable analytical method to detect formaldehyde has never been greater. As exposure limits are decreasing constantly over time in response to health effects, older analytical techniques are slowly becoming obsolete. In addition, the technologies of most modern gas sensors have to be improved in order to achieve the necessary low limits of detection.

1.4 Analytical methods for formaldehyde detection

One of the earliest methods for collecting and analysis of formaldehyde in air was published in 1943 [24]. Over the years numerous sampling and analytical methods have been developed for formaldehyde. These include passive samplers that can be used to provide information on mean concentrations for periods of typically 1-3 days and a variety of active or pumped samplers that provide concentration data for periods of 30 minutes to few hours. Although passive sampling devices are highly selective and accurate they are time consuming, require laboratory back-up services and do not

11

give an instant on-the-spot reading. Most active samplers suffer from the same disadvantages, however they are generally quicker and cheaper.

Grab air sampling is the most popular method for the detection of formaldehyde. Grab sampling of formaldehyde is generally rapid and may be carried out efficiently by relatively unskilled personnel. In addition grab sampling monitors are portable and relatively cheap, however they are not as accurate and selective as passive sampling techniques. This is because grab sampling depends on small samples of air in an atmosphere that might not be homogeneous.

A number of analytical techniques are currently marketed for the detection of formaldehyde. The following review of those methods currently used or under development for the detection of formaldehyde will show the limitations of many of these and ultimately illustrate that fuel cell sensors, the target technology of this work based on electrochemical oxidation / reduction processes, are an alternative proposition.

1.4.1 Chemical derivatisation methods

Chemical derivatisation methods have long been used for formaldehyde detection [25]. As the technique is simple and relatively low cost it is recommended as standard procedure for formaldehyde analysis. The latest most accurate and universally accepted method of formaldehyde analysis is a chemical derivatisation procedure recommended by the Occupational Safety and Health Administration (OSHA) [26]. A diffusion type air monitoring system is recommended; air samples are collected by drawing known volumes of air through sampling tubes containing XAD-2 adsorbent which have been coated with the derivatizing agent, 2-(hydroxymethyl) piperidine. When it reacts with formaldehyde it forms a stable oxazolidine complex. The samples are desorbed with toluene and then analysed by gas chromatography using a nitrogen selective detector. The quantitative limit for this method is 16 parts per billion (ppb).

The US Environmental Protection Agency recommends a similar procedure using sampling tubes containing silica gel treated with 2, 4-dinitrophenylhydrazine (DNPH). The derivatized analyte is then extracted from the cartridge and analysed by HPLC or GC. As mentioned earlier these methods require laboratory 'back-up' services, are time consuming and do not give an instant 'on-the-spot reading'.

1.4.2 Colorimetric detector tubes

Colorimetric analytical methods are based on the measurement of the colour change undergone by a chemical reagent on reacting with the gas of interest. The detector tube is the most widely used colorimetric method of detection, especially in the industrial environment. Detector tubes have been available since the late 1940s [27] and various types have been developed which are claimed, by their manufacturers, to be specific for one or more of a whole range of commonly encountered air-borne chemical species.

The detector tube is essentially a glass tube packed with crystalline carrier with a colorimetric reagent solution adsorbed onto its surface. To detect the gas components, a known volume of air is passed through the tube by pulling a specified number of air strokes with a manual pump. As the gas components are passed through the tube adsorption occurs onto the carrier and a reaction takes place between gas components and the colorimetric reagents. The length of the colour change and the scale on the tube directly determine the concentration of the particular gas component in the air sample. Selectivity is achieved by virtue of the reagent used and varies from total to partial.

A wide range of detector tubes for various gases and vapours are produced by Dräger [28]. Early versions of the breathalyser were based on the alcohol detector tubes produced by Dräger. Alcohol oxidation by an acidified solution of potassium dichromate would produce a quantitative yellow Cr(VI) to green Cr(III) colour change. Detector tubes for formaldehyde are very popular and are based on the following reaction

$$HCHO + C_6H_4(CH_3)_2 + H_2SO_4 \rightarrow \text{quinoid reaction products}$$
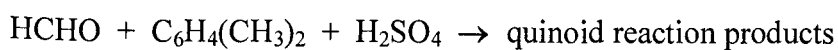
The detector tube contains xylene and sulfuric acid. As formaldehyde comes into contact with these reagents a reaction occurs forming quinoid reaction products which are indicated by a white to pink colour change, the "length" of the colour change corresponds to the concentration of formaldehyde.

Although colorimetric detector tubes are simple to use, they tend to be non-specific, and consume costly analytical materials continuously.

1.4.3 Colorimetric paper tape method

Another type of colorimetric technique is the paper tape method where the colorimetric reagent is impregnated onto a test paper against which the gas under analysis is blown. The colour change of the paper is then compared spectrophotmetrically and taken as a measure of the gas concentration.

The paper tape method was previously the standard technique recommended in the 1980s for the detection of formaldehyde [29] and a number of instruments are still produced. An example of which is the 3M-brand Formaldehyde Monitor [30]. The formaldehyde vapour passes through a diffusion barrier and is adsorbed on bisulfite-impregnated paper contained within the monitor. The formaldehyde collected by the monitor is laboratory analysed by desorbing the formaldehyde-bisulfite adduct from the treated paper with formaldehyde-free deionised water. Chromotropic acid and sulfuric acid are added to an aliquot of the sample to form a purple mono-cationic chromogen. The absorbance of this coloured solution is read in a spectrophotometer at 580 nm and is proportional to the amount of formaldehyde collected.

1.4.4 Semiconductor gas sensors

Semiconductor gas detectors have been available since the 1960s. They are now commonly used for the measurement of a wide variety of organic gases and vapours. Seiyama *et al.* in 1962 [31] demonstrated that thin films of ZnO, heated to ~300°C in air, exhibited conductivity which was very sensitive to the presence of traces of reactive gases in the air. Taguchi, also in 1962, [32] demonstrated similar properties for sintered SnO_2, with the advantage of greater stability. Taguchi subsequently established Figure Engineering Inc. [33], which still remains a major manufacturer of gas sensor devices. Since then, there have been many thousands of papers on the properties and uses of semiconducting oxides (mainly SnO_2) as gas sensors,

Semiconducting gas sensors consist of a heated semiconducting oxide bead or film. The conductance of the semiconductor bead is a function of the temperature and the partial pressure of oxygen. The principle is that oxygen adsorbed from the air acts as an electron acceptor state, lying within the band gap of the oxide but located at the surface of the material. When a gas is adsorbed on to the surface it reacts with some of the oxygen causing a change in the fractional surface coverage of the acceptor state, hence resulting in a change in conductivity. The conductivity is therefore dependent on the rate constant of the surface reactions.

Although semiconductor sensors are cheap and are used for the detection of a wide variety of organic gases they have high energy consumption, lack selectivity and stability and are non-linear in response. In addition, water vapour has a large interference effect on the conductivity over the range 200 – 400 °C. Arrays of these devices are currently being used, in conjunction with pattern recognition techniques, to enhance their specificity. Devices that operate at room temperature are also being developed.

1.4.5 Fuel cell sensors

A fuel cell is an electrochemical system that can convert the chemical energy of a fuel directly into electrical energy. The basic operating principle of fuel cells was discovered by Sir William Grove in 1839 [34,35]. He showed that by supplying hydrogen and oxygen to two separate platinum electrodes, which were submersed in sulfuric acid electrolyte and connected electrically by a voltmeter, an open circuit of 1 V could be set up. Since this early discovery considerable research has been carried out in developing fuel cells for power production [36-40] with some already commercialised [41-43]. Fuel cells have also attracted considerable interest in their use as analytical sensors, particularly for gases and vapours. The first reported use of fuel cells for gas analysis was published in 1965 by NASA [44]; descriptions were given of a low temperature hydrogen-oxygen fuel cell which could be used as an oxygen sensor. Many fuel cell detectors soon followed for a range of atmospheric pollutants [45-49].

A basic fuel cell consists of two catalytically active electrodes; an anode at which one fuel is electrochemically oxidised and a cathode, at which the other fuel is electrochemically reduced. The two electrodes are connected through an external circuit *via* an electrolyte solution. In the cell electrons are lost from the oxidised fuel at the anode and flow through the electrical circuit to the cathode. It is this flow of electrons which is made to do useful work or which is used in electroanalysis.

The general principle of operation of an analytical fuel cell is represented in figure 1 The sample under analysis is supplied to the anode in such a way that the resulting electrical output is proportional to the concentration of the particular species in the gas under analysis. The only requirement is that the chemical is either oxidisable or reducible, the former applying to most situations, as oxygen can be supplied to the cathode where its reduction occurs. Since the quantity of oxidisable species in the fuel

cell is low, the oxygen requirement is correspondingly small, so that diffusion from the air is sufficient. By suitable choice of the electrode materials and electrolyte it is possible to design a fuel cell that can selectively analyse many gases and vapours of analytical importance.
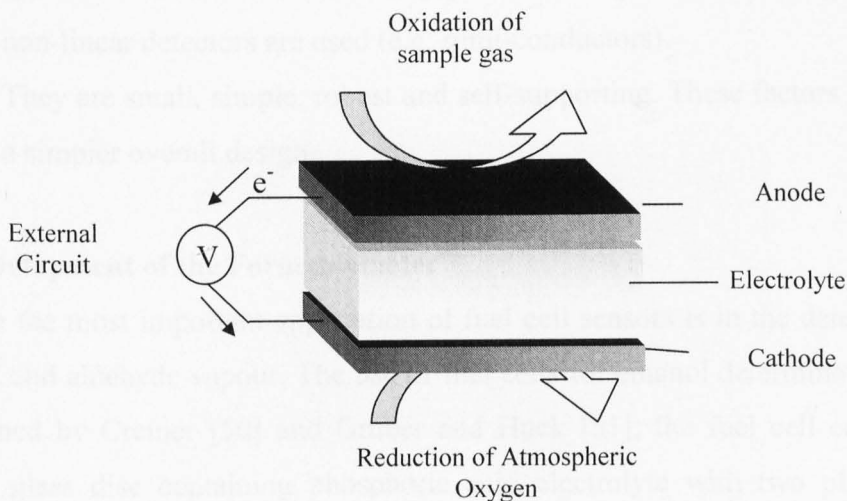
Figure 1 The fuel cell as an analytical sensor

The electrical output from the fuel cell can be measured either as current, or more usually as voltage. A measurable signal is achieved by connecting the two electrode terminals *via* a resistor – termed the "load resistance", and measuring the potential change across the resistor in response to the vapour introduced. The rate at which this happens is highly dependent on the load resistor. By increasing the load resistance the cell-produced current will be converted to a higher voltage.

1.4.5.1 Advantages of fuel cell sensors

Although the precision of the fuel cell may not always be as high as that of some of the more established detectors, such as those using infrared radiation, it is usually more than adequate for the particular application. When comparing fuel cells sensors with other detection methods in the same market, they offer ample advantages.

1. They are highly selective in response. The need for separating column or sample pre-treatment stages is eliminated with the effect of reducing the complexity and the cost of the final instrument.

2. They are highly sensitive to low concentrations of sample vapour so that small sample volumes are required.

3. Their response to the presence of the sample under analysis is immediate and linear. This means that the display can be calibrated directly and linearly in concentration units and not simply as a fixed point, as in the practice when non-linear detectors are used (e.g. semi-conductors).

4. They are small, simple, robust and self-supporting. These factors again lead to a simpler overall design.

1.5 Development of the Formaldemeter™

To date the most important application of fuel cell sensors is in the determination of alcohol and aldehyde vapour. The use of fuel cells for ethanol determination was first mentioned by Cremer [50] and Gruber and Huck [51]; the fuel cell consisted of a porous glass disc containing phosphoric acid electrolyte with two platinum-black electrodes on either face. The detector showed sensitivity to primary and secondary alcohols and aldehydes. These types of sensors were considered to be ideal as detectors for simple pocket size instruments for blood alcohol determination by breath analysis. Later work by Williams [52] on the Gruber and Huck fuel cell led to a modified version utilising sintered PVC as the support matrix, the design later being incorporated into the Alcometer® [53] range of breath screening devices sold by Lion Laboratories plc. Jones and Wright subsequently patented the device in 1976[54]. These devices are used by police forces worldwide for evidential breath testing.

A similar device for the detection of formaldehyde in the air was developed by Lion Laboratories plc in 1981; the device was termed the Formaldemeter™ [55]. As formaldehyde is a primary aldehyde no major modifications were required to the existing fuel cell, however one major problem of the detector was the high specificity to methanol. Further work by Nurton [56] resulted in a modified fuel cell for the determination of formaldehyde in the air; he found that fuel cells made up of 50/50% atomic weight ratio of platinum and palladium were active towards low-levels of formaldehyde with minimal response towards methanol.

1.5.1 The Formaldemeter™

The Formaldemeter™ instrument is now sold by PPM Technology Ltd. Many modifications have been done to the instrument, however, the fuel cell detector is essentially the same and is still produced by Lion Laboratories plc and is based on the sensor studied by Williams and Nurton [55,56]. The Formaldemeter™ and its components are shown in figure 2.
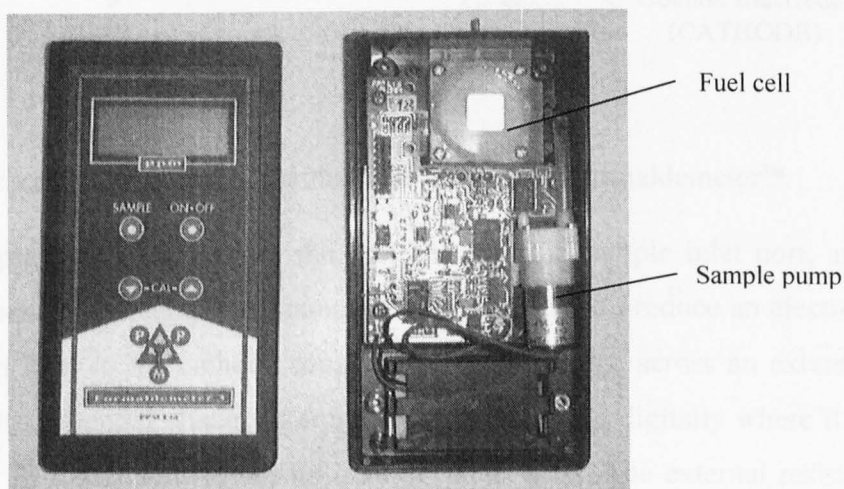
Figure 2 Photograph of the PPM Formaldemeter™; left; display cover; right; bottom case containing fuel cell sensor

The fuel cell detector, (shown simplified in figure 3) is constructed from a thin disc of porous PVC, (32mm diameter, 1mm thick) which acts as an electrode separator, onto either side of which, gold is coated by means of vacuum evaporation to make them electrically conducting. An electrodeposition process is then undertaken where a layer of highly active 50/50% atomic weight ratio of palladium and platinum black is deposited.

The two catalytic electrodes are brought into contact by immersing the disc in an acid electrolyte, usually phosphoric acid, and after an "ageing process", mounted in a plastic case fitted with electrical contacts to each electrode. The plastic case provides a small volume above each electrode, together with a sample inlet and outlet ports above the anode. The method of sampling typically used with this type of device involves drawing in a volume of approximately 10 cm^3 from the atmosphere, through the fuel cell by means of a small pump.

18
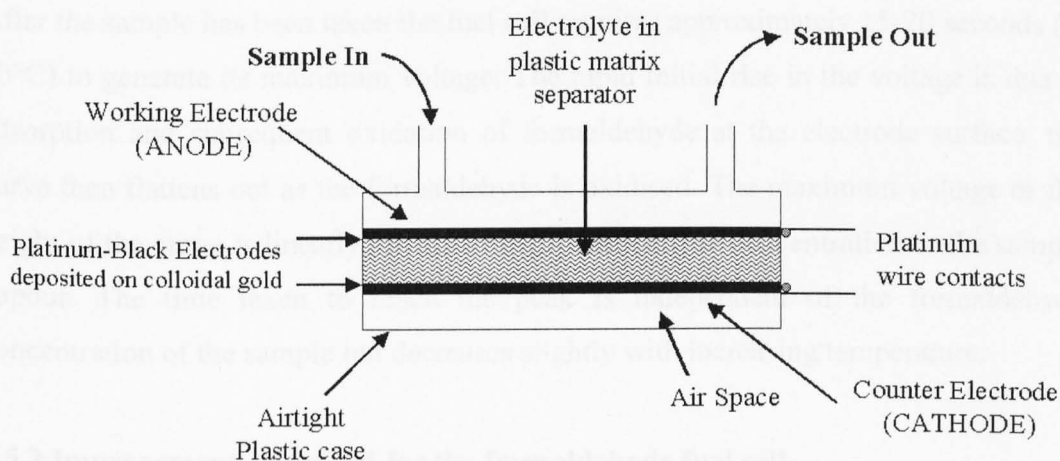
Figure 3 Schematic diagram of the fuel cell used in the Formaldemeter™

When an air sample is introduced into the fuel cell, *via* the sample inlet port, any formaldehyde present in the sample is spontaneously oxidised to produce an electron flow. The electron flow to the cathode causes a potential change across an external load resistance. This potential change is amplified and displayed digitally where it is calibrated directly in formaldehyde vapour concentration units. The external resistor in the Formaldemeter™ instrument is $1k\Omega$. This is the optimum value for the existing fuel cell. Typically the output current from the cell rises from zero to a peak, and then ultimately decays back to zero. A profile for a fuel cell response to formaldehyde is shown in figure 4.
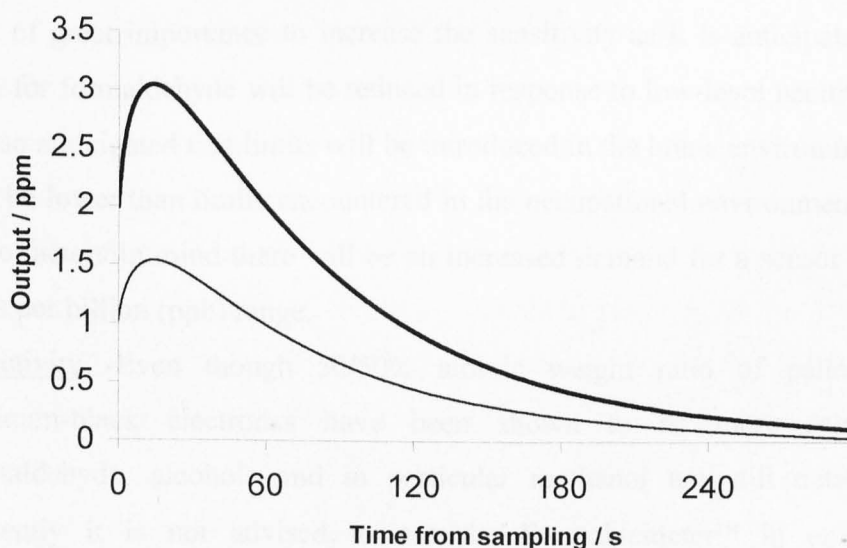
Figure 4 Typical output of Formaldemeter™ for two different concentrations of formaldehyde

After the sample has been taken the fuel cell requires approximately 15-20 seconds (at 20°C) to generate its maximum voltage. The rapid initial rise in the voltage is due to adsorption and subsequent oxidation of formaldehyde at the electrode surface, the curve then flattens out as the formaldehyde is oxidised. The maximum voltage or the height of the curve is linearly related to the formaldehyde concentration in the sample vapour. The time taken to reach the peak is independent of the formaldehyde concentration of the sample but decreases slightly with increasing temperature.

1.5.2 Improvements required for the formaldehyde fuel cell

Although fuel cell sensors offer many advantages over other analytical methods for formaldehyde detection, significant improvements are required to the existing fuel cell in the Formaldemeter™. Since the formaldehyde fuel cell was first developed by Lion Laboratories plc in 1981 no modifications have been done to the sensor itself [55]. This is of particular concern since competition in the formaldehyde detector market has increased considerably in the last few years. Over the years it has become apparent that the fuel cell sensor in the Formaldemeter™ needs to be improved in the following areas:

(i) Sensitivity - Currently, the threshold limit of detection of the formaldehyde fuel cell is 0.05 ppm [57]. Results below this level are treated with caution, since other gases or electronic noise could induce such 'formaldehyde' readings. It is also estimated that the precision of the detector is 10 % at a 2.0 ppm level [57]. It is of great importance to increase the sensitivity as it is anticipated that the PEL for formaldehyde will be reduced in response to low-level health effects. It is also anticipated that limits will be introduced in the home environment, which will be lower than limits encountered in the occupational environment. With all these factors in mind there will be an increased demand for a sensor in the low parts per billion (ppb) range.

(ii) Selectivity -Even though 50/50% atomic weight ratio of palladium and platinum-black electrodes have been shown to be more selective for formaldehyde, alcohols and in particular methanol are still detected [56]. Presently it is not advised to use the Formaldemeter™ in environments containing high levels of methanol. It is therefore essential to have a fuel cell with a reduced response to methanol.

(iii) <u>Humidity effects</u> – In the last few years it has become apparent that the response of the formaldehyde fuel cell is affected by fluctuations in humidity. This is of particular concern since it becomes difficult to detect low levels of formaldehyde in areas of high humidity. A signal swamping effect is created when the response to humidity is greater than that of formaldehyde. There are many environments where humidity can have an effect on the fuel cell; therefore it is of great importance that any modified fuel cell should have reduced response to humidity.

Any modification to the formaldehyde fuel cell must meet the above requirements as these are pertinent in the field of gas and vapour analysis. In addition the simplicity and low cost of the instrumentation must be maintained, since these are the main advantages of the Formaldemeter™ over other analytical methods of formaldehyde detection.

1.5.3 Methods to improve the fuel cell sensor

Modifying one or more of the following characteristics may improve the sensitivity and selectivity of the fuel cell to formaldehyde and could also reduce the response to humidity:

(i) A different electron sink may be used at the cathode instead of the oxygen reduction reaction which is dependent on the diffusion of air. This may be performed by the use of a different reactant other than oxygen at the cathode or by the use of a different redox couple such as conducting polymer coated on the cathode.

(ii) The anode may be chosen so as to adsorb and/or oxidise only formaldehyde. This may be done in the form of a single metal or alloy of two metals or more.

(iii) The modification of the concentration, pH and nature of the electrolyte.

(iv) The potential across the two electrodes may be adjusted to that of the oxidation (or reduction) potential of the species of interest. This may be done by selection of an appropriate reference electrode or by the use of an external supply.

(v) A selectively permeable membrane may be placed across the anode hence restricting the range of compounds adsorbed. In this method the cell reaction becomes diffusion controlled and hence diffusion dependent.

In this work, two pathways are studied; firstly, the effect of replacing the cathodic reaction with that of a conducting polymer is investigated; and secondly a host of various noble metals and alloys are investigated for the selective oxidation of formaldehyde.

1.6 The cathode - Oxygen reduction reaction

The oxygen electrode occupies a unique position in electrochemical energy conversions in that it forms the cathode in almost all fuel cells. It owes its popularity to the combination of near infinite capacity while not needing storage of any reactant. Consequently the oxygen electrode reaction has been the subject of extensive investigations [58-63].

It has proved particularly difficult to identify catalysts for the reduction of oxygen as a result of the strong O-O bond. The selection of cathodes for oxygen reduction has also posed a materials problem, particularly in acidic environments, where few materials are stable to anodic dissolution at potentials close to the equilibrium potential for oxygen reduction where a good catalyst would operate. Moreover, even with the more noble metals which do not dissolve, the study of oxygen reduction is hampered by oxidation and/or reduction of their surface within the potential range of interest, which may lead to a change in mechanism when the electrode surface changes from metal oxide to metal or vice versa [64].

Although many mechanisms exist for the reduction of oxygen in acidic solutions [63], it is generally accepted that the reduction may proceed either directly or indirectly depending on the choice of electrode material [64].

A - Direct Reduction

$$O_2 + 4H^+ (aq) + 4e^- \rightarrow 2H_2O \qquad 1.23 \ V \ (RHE)$$

B - Indirect Reduction

Step (i)	$O_2 + 2H^+ (aq) + 2e^- \rightarrow H_2O_2$	0.68 V (RHE)
Step (ii)	$H_2O_2 + 2H^+ (aq) + 2e^- \rightarrow 2H_2O$	1.77 V (RHE)
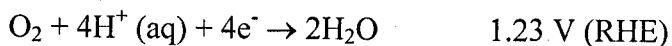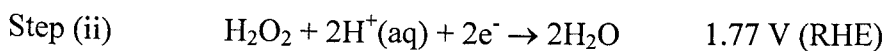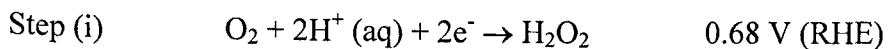
Route A leads to water as the only identifiable product, while in route B the reduction to water clearly occurs in two steps with hydrogen peroxide as an intermediate. Route

A implies the cleavage of the O-O bond by dissociative adsorption at an early stage in the reduction, whereas in route B the first step is the reduction of oxygen to superoxide. Route A offers the best chance of effective electrocatalysis and is also necessary to ensure the full free energy output from the $4e^-$ reduction and an approach to the equilibrium potential of 1.23 V. Nevertheless, the reduction of oxygen is a slow reaction, large overpotentials are observed as a consequence of low exchange current density, which leads to a very poor reproducibility of the rest potential of the electrode. This restriction can be overcome, but only by the development of extremely active electrocatalysts. At the present time dispersed Pt remains the best catalyst cathode for oxygen reduction, however much work is still required to achieve a fully efficient catalyst for oxygen reduction.

Clearly the mechanism of oxygen reduction is very complex and in some cases, depending on the electrode material, is very inefficient. The situation is further complicated when using the oxygen reduction reaction as a cathodic reaction in a fuel cell sensor since there are environmental conditions affecting the concentration of oxygen in air. With all these factors in mind it can be seen that there are many limitations to the oxygen reduction reaction as the cathodic reaction in the fuel cell.

1.7 Conducting polymer cathode

Replacing the oxygen reaction in a fuel cell sensor with another reactant is impractical since a storage device would have to be incorporated into the sensor instrument. Another way to overcome this problem is to coat a conducting polymer on the cathode. In this way the conducting polymer would act as the electron sink.

In principle if the conducting polymer on the cathode is in its oxidised state a supply of electrons from the oxidation of formaldehyde at the anode would cause the polymer to switch to its reduced state, making the fuel cell response dependent on the rate of electron transfer rather than the diffusion of oxygen. A set up of this type of fuel cell is shown in figure 5.

Anode Reaction   **Cathode Reaction**

$HCHO + H_2O$ Oxidised polymer

$CO_2 + 4H^+ + 4e^-$ Reduced polymer

Platinum on PVC   Conducting polymer
                                                 on platinum
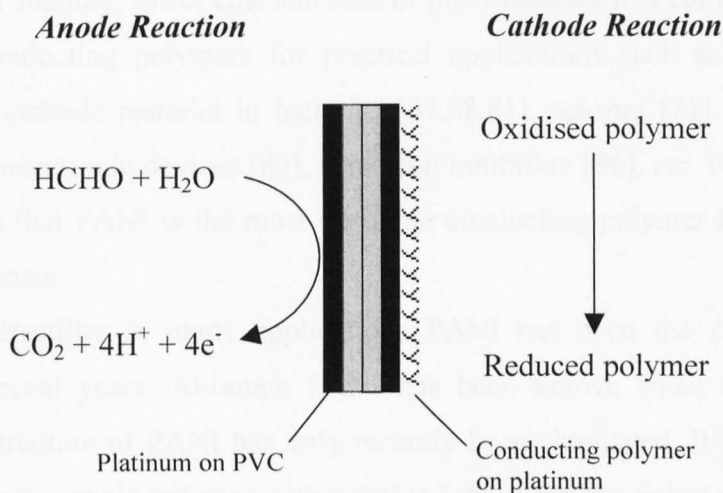
Figure 5 A conducting polymer modified fuel cell

Electronically conducting polymers were first reported in 1977 by Heeger and MacDiarmid who discovered that doping polyacetylene with iodine resulted in metallic properties in the polymer with the conductivity increasing by nearly ten fold [65,66]. The ability of polyacetylene to be doped (in electrochemical terminology the equivalent of oxidation and reduction) made it a good material for use in rechargeable batteries [67,68]. In the ensuing period, other conducting polymers were discovered with polypyrrole (PPy), polythiophene (PTh) and polyaniline (PANI) being the most studied.

A conducting polymer has the structural characteristic of an extended π-conjugated system (alternating single and double bonds along the polymer chain) at least in their doped forms. It is this feature that allows current to flow through the polymer and make them conducting. Over the years many applications have been proposed for conducting polymers [69-71]. However, a comprehensive review of the literature reveals that the utilisation of a conducting polymer as the cathode in a fuel cell sensor has not been previously reported.

An ideal conducting polymer for use as a cathode in fuel cell sensors is polyaniline (PANI). Of all the conducting polymers PANI is commonly referred to as the most stable [72,73]; it is stable in air and in strongly aggressive acidic environments [74-78]. In solution it can be switched between the insulating and conducting states up to

10^6 times if the potential is kept within a certain range [79]. Due to its higher environmental stability, lower cost and ease of processability it is commonly preferred over other conducting polymers for practical applications such as electrochromic devices [80], cathode material in batteries [67,68,81], sensors [71], electrocatalysis [82-84], microelectronic devices [85], corrosion inhibition [86], *etc*. For these reasons it can be seen that PANI is the most desirable conducting polymer for utilisation in the fuel cell sensor.

Due to its versatility in many applications PANI has been the subject of much research in recent years. Although PANI has been known since the last century [87,88], the structure of PANI has only recently been elucidated. It has been shown that PANI is not a single polymer with a defined structure, but rather a complex series of the different repeat units depending on the oxidation and doping level. MacDiarmid *et al.* have described the polymer by the general formula shown below [89,90].

| Reduced unit | | Oxidised unit |
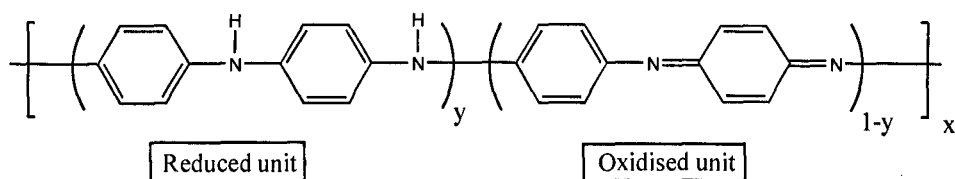
The oxidation state of the polymer can then be defined by the value of (1-*y*). The non-conducting form of this polymer can, in principle, exist in a continuum of oxidation states ranging from completely reduced leucoemeraldine (*y* = 1) to completely oxidised pernigraniline (*y* = 0). PANI is particularly interesting in that its conductivity depends not only on its oxidation state, but also the extent of protonation, the highest conductivity being the 50 % protonated Emeraldine salt (*y* = 0.5).

The structure of PANI has been studied by many workers using a variety of techniques [91-96]; these and other studies have led to the current model of PANI as shown in figure 6. It consists of five forms of the polymer, each represented by an octamer.
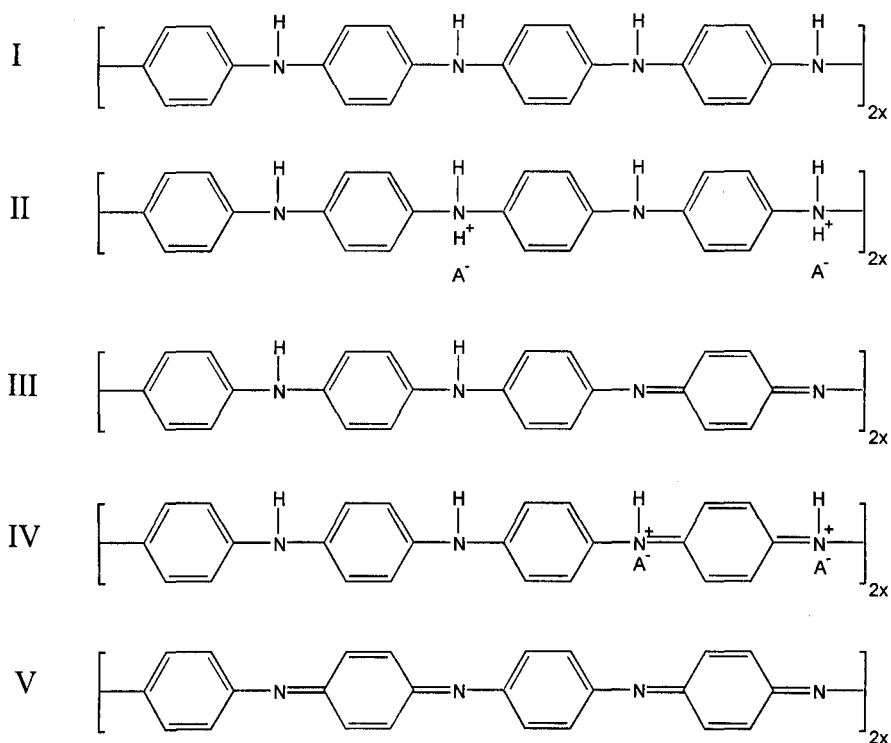
Figure 6 Proposed structure of the five forms of polyaniline [97],
(I) leucoemeraldine base, (II) leucoemeraldine salt, (III) emeraldine base,
(IV) emeraldine salt, (V) pernigraniline

Electronically conducting polymers coated on electrodes can undergo a transition between the insulating and the conducting states depending on the applied potential. In the case of polyaniline the switching process of oxidising the reduced insulating form to the conducting emeraldine salt or *vice versa* has been shown to be extremely rapid (less than 10 μs) and is controlled by the RC time constant of the cell [98]. As the switching time is rapid in PANI it would be fair to assume that it would be a more reliable and efficient cathode for the fuel cell sensor in comparison to the oxygen reduction reaction, which is dependent on the slow diffusion of oxygen. In the fuel cell the electrons produced from the oxidation of formaldehyde would cause the PANI to switch from the oxidised conducting state to reduced insulating state. Once PANI is reduced after the electrochemical reaction, the polymer should be oxidised back to its original state to make successive formaldehyde vapour determinations possible. Based on fundamental corrosion [74,78,99] and electrocatalysis [82,83] studies it is anticipated that the spontaneous reaction of reduced PANI with atmospheric oxygen will restore the polymer to its original emeraldine salt oxidation state. To the best of

the author's knowledge, this is the first reported application of the use of a PANI film as a cathode in a fuel cell.

1.8 Aims of the present work

The aim of this work is to improve the performance and reliability of fuel cells used in the detection of formaldehyde. Increasing sensitivity, selectivity and minimising the response to humidity are essential improvements required for the existing fuel cell sensor. Two routes are investigated to achieve these requirements:

Firstly the oxygen reduction reaction at the cathode is replaced with that of a conducting polymer, polyaniline (PANI). It is anticipated that a PANI film coated on platinum-black would act as a more stable electron sink for the cathode instead of the oxygen reduction reaction. In principle, this would have the effect of increasing reliability and reducing humidity effects. The response time would also be controlled by the rate of electron transfer rather than diffusion of oxygen. The fuel cell response is explained by fundamental investigations on the redox behaviour of PANI in acidic media by means of open circuit potential (OCP) and cyclic voltammetry (CV) experiments. These experiments are also used to investigate the feasibility and long-term stability of PANI in a fuel cell environment. PANI films are characterised by cyclic voltammetry (CV) and scanning electron microscopy (SEM).

In the second part of the work, the effect of changing the composition of the catalyst is investigated. Several noble metals and alloys are investigated for their selectivity and sensitivity towards the oxidation of low-levels of formaldehyde. Solution based electrochemical (CV) studies are initially performed on metal deposits on a glassy carbon electrode. The most electrocatalytic electrodes are then electrodeposited on gold coated PVC for utilisation in the fuel cell sensor. SEM and CV investigations are used to characterise the electrodes.

1.9 References

1   P. Brimblecombe *"The Big Smoke"* Routledge, London, UK. (1987)

2   WHO – *"Air Guidelines for Europe"*, WHO-Regional Publications, ES No. 23, (1987)

3   WHO *"Guidelines for Air Quality"*, Geneva (2000)

4   Occupational Safety and Health Regulations (OSHA), http//www.osha-slc.gov

5 R. E. Hester, R. M. Harrison, *"Volatile Organic Compounds in the Atmosphere"*, Issues in Environmental Science and Technology, The Royal Society of Chemistry (1995)

6 H. Gustafsson, *"Document D10"*, Swedish Council for Building Research, Stockholm, (1992)

7 V. Brown, S. Coward, D. Crump, M. Gavin, C. Hunter, J. Llywellyn, G. Raw, *"The ALSPAC Indoor Air Environment Study"*, Building Research Establishment Report, BRE, Watford, (1995)

8 J. Namiesnik, T. Gorecki, B. Mozdron-Zabiegala, J. Lukasiak, *"Building and Environment"*, 27 (1992), 339

9 B. Meyer, *"Indoor Air Quality"*, Addison-Wesley, Massachusetts, (1983)

10 W. D. Kerns, *Cancer Research*, 43 (1983) 4382

11 W. D. Kerns, *Formaldehyde Toxicit.*, (1983) 111

12 J. K. McLaughlin, *Int. Arch. Occup. Environ. Health* 66 (1994) 295

13 *"Formaldehyde"*, Ninth Report on Carcinogens, (2000)

14 H. M. Leicester, *J. Chem. Ed.,* 17 (1940) 203

15 M. H. Garrett, M. A. Hooper, B. M. Hooper, P. R. Rayment, M. J. Abramson, *Allergy*, 54 (1999) 330

16 F. Wantke, C. M Demmer, P. Tappler, M. Götz, R. Jarisch, Clin. *Exp. Allergy*, 26 (1996) 276

17 M. Kryzanowski, J. Quackenboss, M. Mebowitz, *Environ. Res.,* 52 (1990) 117

18 D. P. Strachan, *Clin. Exp. Allergy*, 25 (1995) 791

19 S. C. Stenton, D.J. Hendrick, *Immunol Allergy Clin. North Am.*, 14 (1994) 635

20 P. Carlier, H. Hannachi, G. Mouvier, *Atmos. Environ.*, 20 (1986) 2079

21 Y-.N. Lee, X. Zhou, K. Hallock, *J. Gophys. Res.*, 1999 (1995) 25933

22 *Sigma-Aldrich Material Safety Data Sheet*, (2000)

23 D. Crump, *Proceedings of the Investigation of Air Pollution Standing Conference*, paper 15/3, London, (1993)

24 F. H. Coleman, H. Yagoca, *Ind. Lug. Chem.* 15 (1943) 377

25 A. Vairavamurthy, J. Roberts, L. Newman, *Atmos. Environ.*, 26 (1992) 1965

26 OSHA Regulations (Standards – 29 CFR), *"Sampling strategy and analytical methods for formaldehyde – 1910.1048 App B"*, http//www.osha-slc.gov

27 N. L. Allport, J. W. Keyser, *"Colorimetric Analysis"*, Chapman and Hall, London, (1957)

28 Dräger Safety Technology, http://www.draeger.com

29 NIOSH Analytical Methods, P. and Cam 125

30 3M Brand Formaldehyde Monitors 3750/3751, 3M Company, St Paul, MN

31 T. Seyama, A. Kato, K. Fulshi, M. Nagatani, *Anal. Chem.*, 34 (1962) 1502

32 N. Taguchi, *US Patents* 3,676,820 (1972) and 3,732,519 (1973)

33 A. Chiba, *"Chemical Sensor Technology, Vol. 4."* Ed. Yamauchi S (Tokyo: Kodansha) (1992) 1

34 W. R. Grove, *Phil Mag.*, 14 (1839) 127

35 W. R. Grove, *Phil Mag.* 21 (1842) 417

36 L. Mond and C. Langer, *Proc. Roy. Soc.*, 46 (1889) 269

37 W. Ostwald. *Z. Elektrochem.*, 1 (1894) 122

38 F. T. Bacon, *Ind. Chem. Eng.* 52 (1960) 301

39 A. C. Ching, A. P. Gillis, F.M. Plauche, *Proc. 7th Intersociety Energy Conversion Engineering Conference*, (1965) 368

40 S. Wasmus, A Kuver, *J. Electroanal. Chem.*, 461 (1999) 14

41 *Chem. Br.*, Sept. (1995) 655

42 *Chem. Br.*, June. (2000) 24

43 *New Scientist*, Nov (2000) 36

44 NASA. *Technical Brief*, 65-10060, (1965)

45 M. Shaw, *US Patent* 3,622,487 (1971)

46 M. Shaw, *US Patent* 3,622,488 (1971)

47 S. I. Bykov, *Zavod.Lab.*, 35 (1969) 920

48 F. A. Prohol, *German Patent* 1,905,056 (1972)

49 F. A. Prohol, *Technica*, 25 (1976) 10,

50 E. Cremer, *J. Chromatog.*, 3 (1967) 329

51 E. Cremer, H. L. Gruber, H. Huck, *Chromatographia*, 2 (1969) 197

52 P.M. Williams, *MSc Thesis*, University of Wales, Cardiff, (1974)

53 Alcometer® Breath Alcohol Instruments, Lion Laboratories plc, Barry, South Glamorgan, Wales, UK

54 T. P. Jones, B. M. Wright, *US Patent* 3,940,251 (1976)

55 P. M. Williams, I. R. Whiteside, T. P. Jones. *Int. Environ. Safety*, (1981) 15

56 R. L. Nurton, *MSc. Thesis*, University of Wales, Cardiff, (1985)

57 Formaldemeter™ 3 Technical Specifications, PPM Technology Ltd, Parc Menai, Bangor, Gwynedd, Wales, UK

58 T. Toda, H. Igarashi, H. Uchida, M. Watanabe, *J. Electrochem. Soc.* 146 (1999) 3750

59 D. Chu, *Electrochim. Acta.*, 43 (1998) 3711

60 S. Mukerjee, S. Srinivasan, *J. Electroanal. Chem.* 357 (1993) 201

61 S. Mukerjee, S. Srinivasan, A. J. Appleby, *Elecrochim. Acta.* 38 (1993) 1661

62 K. L. Hsueh, E. R. Gonzalez, S. Srinivasan, D. T. Chin, *J. Electrochem Soc.* 131 (1984) 823

63 J. O'M Bockris, S. Srinivasan, "*Fuel Cells: their electrochemistry*", McGraw-Hill (1969) 437

64 Southampton Electrochemistry Group, "*Instrumental Methods in Electrochemistry*" Ellis Horwood (1990)

65 H. Shirakawa, E. J. Louis, A. G. MacDiarmid, C. K. Chiang, A. J. Heeger, *J. Chem. Commun.*, 1977 (1978) 578

66 C. K. Chiang, Y. W. Park, A. J. Heeger, H. Shirakawa, E. J. Louis and A. G. MacDiarmid, *J. Chem Phys.* 69 (1978) 5098

67 P. J. Nigrey, A. G. MacDiarmid, A. J. Heeger, *J. Chem. Soc., Chem, Commun.*, (1979) 598

68 D. MacInnes Jr, M. A. Druy, P. J. Nigrey, D. P. Nairns, A. G. MacDiarmid, A. J. Heeger, *J. Chem. Soc., Chem, Commun.*, (1981) 317

69 M.G. Kanatzidis, *Chem. Eng. News*, 3 (1990) 36

70 D. Kumar, R. C. Sharma, *Eur. Polym. J.*, 34 (1998) 1053

71 A. G. MacDiarmid., *Synth. Met.*, 84 (1997) 27

72 J. R. Ellis in T. A. Skotheim (ed.) "*Handbook of Conducting Polymers*", Vol. 1, Marcel Dekker, New York, (1986)

73 S. Pitchumani, V. Krishnan, *Bull. Electrochem.*, 3 (1987) 117

74 D. W. DeBerry, *J. Electrochem. Soc.* 132 (1985) 1022

75 W. K. Lu, R. L. Eisenbaumer, B. Wessling, *Synth. Met.* 71 (1995) 2163

76 P. Rao, J. Anand, S. Palaniappan, D. N. Sathyanarayana, *Eur. Polym. J.*, 36 (2000) 915

77 M. A. Malik, M. T. Galkowski, H. Bala, B. Grzybowska, P. J. Kulesza, *Electrochim. Acta*, 44 (1999) 2157

78 A. P. Monkman, P. N. Adams, P. J. Laughlin, E. R. Holland, *Synth. Met* 69 (1995) 183

79 T. Kobayashi, H. Yonemana, H. Tamura, *J. Electroanal. Chem.* 161 (1984) 419

80 V. W. Jones, *PhD Thesis*, University of Wales, Bangor, (1995)

81 N. L. D. Somasiri, A. G. MacDiarmid, *J. Appl. Electrochem.* 18 (1988) 92

82 G. Mengoli, M. M. Musiani, G. Zotti, S. Valcher, *J. Electroanal. Chem.*, 202 (1986) 217

83 L. Doubova, G. Mengoli, M. M. Musiani, S. Valcher, *Electrochim. Acta.*, 34 (1989) 337

84 C. Q. Cui, J. Y. Lee, *J. Electroanal. Chem.*, 367 (1994) 205

85 E. W. Paul, A. J. Ricco, M. S. Wrighton, *J. Phys. Chem.*, 89 (1985) 1441

86 M. C. Bernard, S. Joiret, A. H-L. Goff, P. V. Phong, *J. Electrochem. Soc.* 148 (2001) B12

87 H. Letheby. *J. Chem.Soc.*, 15 (1862) 161

88 E. M. Genies, A. Boyle, M. Lapkowski, C. Tsintavis, *Synth. Met.*, 36 (1990) 139

89 G. E. Asturias, A. G. MacDiarmid, R. P McCall and A. J Epstein, *Synth. Met.*, 29 (1989) E157

90 W. S. Huang, A. G. MacDiarmid, *Polymer*, 34 (1993) 1833

91 J. Nakajima, M. Harada, R. Osawa, T. Kawagoe, Y. Furakawa, I. Harada, *Macromolecules*, 22 (1989) 2644

92 C. E. Brown, P. Kovacic, K. J. Welch, R. B. Cody, R. E. Hein, J. A. Kinsinger, *J. Polymer Sci. Part A: Polymer Chemistry*, 26 (1988) 131

93 C. E. Brown, P. Kovacic, K. J. Welch, R. B. Cody, R. E. Hein, J. A. Kinsinger, *J. Polymer Sci. Part A: Polymer Chemistry*, 26 (1988) 131

94 T. Ohsaka, Y. Ohnuki, N. Oyama, G. Katagiri, Kamisako, *J. Electroanal. Chem.*, 161 (1984) 399

95 S. Ni, J. Wang, F. Wang, *Synth. Met.*, 24 (1988) 231

96 H. Choi, E. J. Mele. *Physical Review Letters*, 59 (1987) 2188

97 M. Kalaji, L. Nyholm, L. M. Peter, *J. Electroanal. Chem.* 313 (1991) 271

98 M. Kalaji, L. M. Peter, L. M. Abrantes, J. C. Mesquita, *J. Electroanal. Chem.* 274 (1989) 289

99 R. Gasparac, C. R. Martin, *J. Electrochem. Soc.*, 148 (2001) B138

Chapter II - Experimental

2.0 Introduction

In this chapter the following techniques and preparation methods are described.

1. Cyclic Voltammetry
2. Preparation of Fuel Cells
3. Formaldemeter™ sampling device
4. Aldehyde and Alcohol Vapour sampling / Vapour Generator
5. Characterisation of fuel cells - SEM / EDAX

Cyclic voltammetry is a standard technique used in electrochemistry, therefore only a brief description will be given. The preparation of various fuel cells is described in detail along with the sampling method and generation of vapour with the custom-built vapour generator. The characterisation of the fuel cell electrodes with scanning electron microscopy (SEM) and energy dispersive analysis by X-rays (EDAX) is also described. Fundamental electrochemical experiments and conditions are described in more detail in the relevant chapters/sections.

2.1 Solutions and materials

All the reagents used in this work were of 'Analar' grade purity and were obtained from Sigma-Aldrich unless otherwise stated. In all experiments the electrolyte solutions were prepared with ultra pure water produced by an ELGASTAT UHQII water purifier.

2.2 Cyclic voltammetry [1-4]

Cyclic voltammetry has become a popular tool for studying electrochemical reactions; over the years it has been applied to an ever-increasing range of systems [1-4]. It is of particular interest since many experiments can be carried out within a few minutes. Because of its versatility it is often the first technique that is employed to study a system for the first time. Voltammetry permits the mechanistic and kinetic study of systems in which electron transfers are coupled to chemical reactions [4], this is possible by mathematical descriptions of cyclic voltammetry which have been

developed sufficiently to enable kinetic parameters to be determined for a wide variety of mechanisms.

In this technique a potential time waveform is applied between a working electrode (the surface where the electrochemical reaction takes place) and a counter electrode (a conductive but chemically inert material). The potential (E) recorded relative to a stable potential produced by a reference electrode, is swept from E_1 to E_2 at a constant sweep rate, v. The current of the electrode is measured as a function of the potential (E) applied. At potential E_2 the reaction may be stopped, allowed to proceed back to E_1 or allowed to continue between E_1 and E_2 depending upon the type of study required.
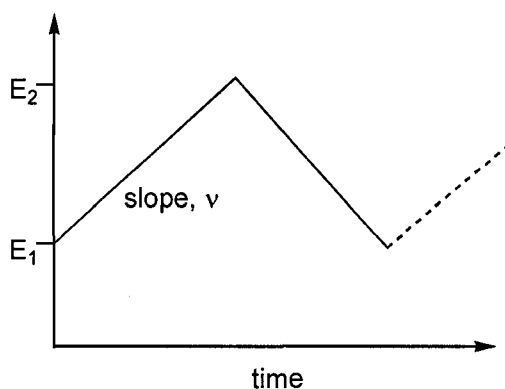
Figure 1 Potential-time profile for a cyclic voltammogram for a single sweep

Voltammetry yields a lot of information about the electrochemical reactions taking place at the electrode surface, due to the interaction with chemical species in solution. The overall shape of the curve gives details of the electrode processes, as well as the potential at which a reaction occurs and whether the process is reversible or not. At the same time, from the sweep rate dependence of the peak amplitudes the role of adsorption, diffusion, and coupled homogeneous chemical reactions may be identified. The difference between the first and subsequent cyclic voltammograms frequently provides useful mechanistic information. Using this technique an 'electrochemical spectrum' can be rapidly obtained [1,2]

In this work cyclic voltammetry experiments were performed using a home built potentiostat equipped with positive feedback iR compensation, and a waveform

generator (HI-TEK Generator, PPR1). The cyclic voltammograms were recorded using an X-Y recorder (Lloyd Instruments or Philips PM 8272).

2.2.1 Electrochemical cell

Cyclic voltammetry experiments and basic electrochemical investigations on Pt-black and Au coated PVC electrodes were performed in a specially constructed three-electrode glass cell as shown in figure 2. The electrochemical cell is divided into three special compartments for each electrode, the reference electrode (RE) - saturated calomel electrode (SCE), working electrode (WE), and counter electrode (CE) – platinum mesh.
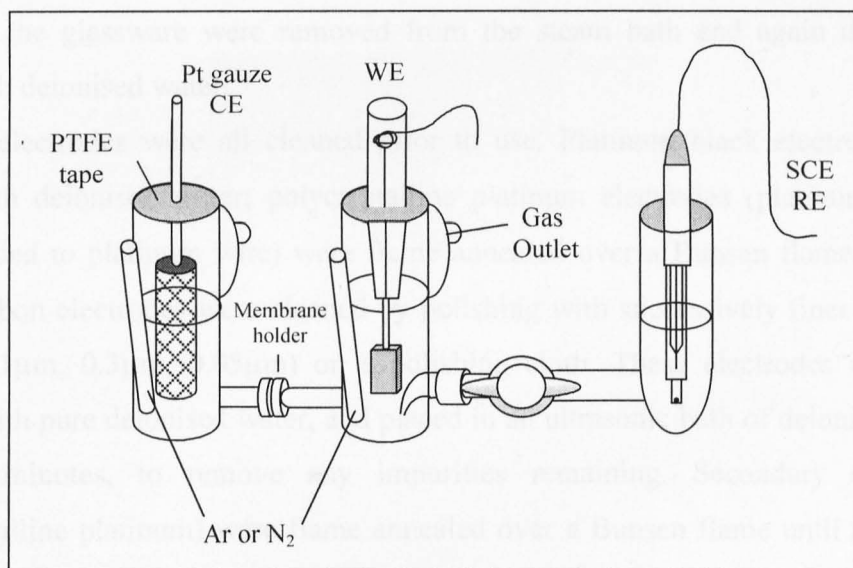
Figure 2 Electrochemical three-electrode cell

The cell is different to standard three-electrode cells in that a membrane can be utilised in between the working and counter electrode compartments; this is useful for separating the electrolyte in both compartments. The compartments may be isolated using ion exchange membranes such as Nafion®. Both compartments have individual gas inlets for gas bubbling (degas or for introducing other gases or vapours) and gas outlets fitted with gas bubblers. When the bubbler is filled with supporting electrolyte, it acts as a one-way valve and allows the gas escape from the cell and prevents gases re-entering the cell. The reference electrode (SCE) is brought close to the working electrode *via* a narrow Luggin capillary that minimises errors in the potential that may

34

arise from solution resistance [1-2]. All compartments can be sealed by covering the ports with thick PTFE tape. Experiments utilising normal polycrystalline platinum or glassy carbon electrodes were performed in a standard three-electrode cell. This is described in more detail in section 4.1.3.

2.2.2 Preparation for electrochemical experiments

It was essential before any experiment that all glassware and electrodes were thoroughly cleaned. All glassware was left overnight in concentrated nitric/sulphuric acid mixture (1:1) to ensure there were no impurities present. This was followed by washing in deionised water and steaming for 20 minutes. The steam bath allows steam to freely circulate around the glassware thus removing any acid traces. After steaming, the glassware were removed from the steam bath and again thoroughly rinsed with deionised water.

Working electrodes were all cleaned prior to use. Platinum black electrodes were rinsed with deionised water; polycrystalline platinum electrodes (platinum coupon sheet welded to platinum wire) were flame annealed over a Bunsen flame; flat disc glassy carbon electrodes were cleaned by polishing with successively finer grades of alumina (1µm, 0.3µm, 0.05µm) on a polishing cloth. These electrodes were then washed with pure deionised water, and placed in an ultrasonic bath of deionised water for five minutes, to remove any impurities remaining. Secondary electrodes (polycrystalline platinum) were flame annealed over a Bunsen flame until a uniform red glow was attained thereby preventing the risk of contamination.

In all experiments it was essential that the electrolyte solution was completely degassed; this was achieved by degassing the solution with nitrogen from the in-house nitrogen line or with argon from a gas cylinder. Before any experiment solutions were degassed for 30 minutes.

More details on the conditions used for cyclic voltammetry and basic electrochemical experiments will appear in the relevant results and discussion sections.

2.3 Preparation of fuel cells

In this work fuel cells smaller than the ones used in the commercial Formaldemeter™ were used. This meant that smaller electrodes could be utilised which simplified the electrode preparation process and made the overall fuel cell detector more cost effective. The disc electrodes currently used in the Formaldemeter™ have a geometric

surface area of 8.04 cm^2; the smaller electrodes used in this work have a geometric surface area of 0.98 cm^2. In addition to the preparation and cost benefits smaller electrodes reduce resistance (iR) effects.

Two types of fuel cells were used in this work; the basic components of each fuel cell are shown in figures 3a and 3b. The main difference between the two is that type I has two separate platinum-coated PVC sheets positioned back-to-back while type II has the catalyst coated on either side of one PVC sheet. Both types have electrode dimensions of 14 x 7 x 1 mm. The preparation of each fuel cell is described in the proceeding sections.
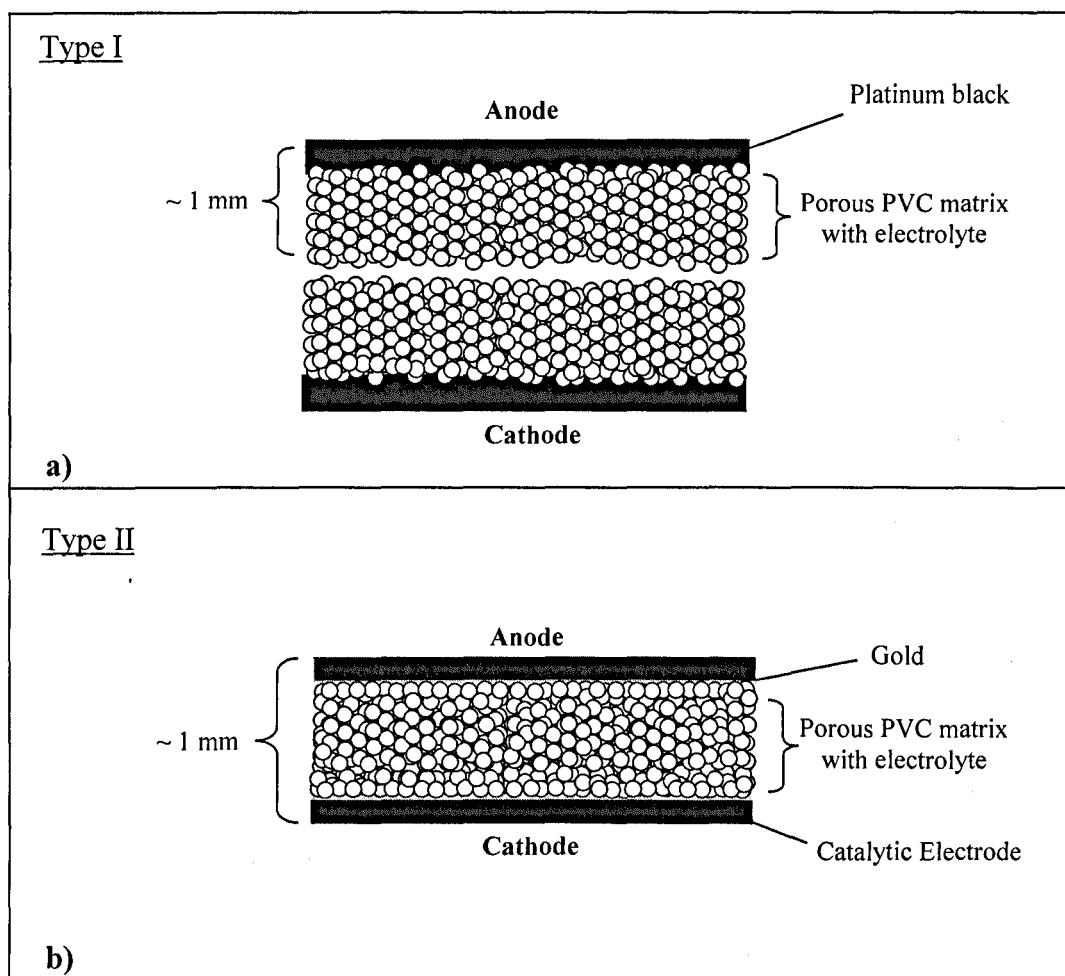
Figures 3 Schematic diagram showing transverse sections of the electrode in **(a)** type I and **(b)** type II fuel cells

To study the effect of a polyaniline (PANI) cathode on the response of the fuel cell, type I fuel cells (figure 3a) were used since it was possible to coat PANI on one electrode surface. This would have been hard to achieve with type II, since it would

be difficult to prevent the anode from being coated with the polymer. The effect of different electrocatalysts on the response of the fuel cell was investigated by preparing type II fuel cells (figure 3b). These were more advantageous since both electrodes could be prepared at the same time giving electrodes of the same quality.

2.3.1 Preparation of Type I fuel cells

The platinum-black fuel cell electrodes, supplied by PPM Technology Ltd [5] and produced by Lion Laboratories plc [6], were of the type used in a wide range of ethanol-monitoring devices. Essentially the electrodes consisted of a thin disc of porous polyvinyl chloride (PVC) sheeting (0.1 cm thick and 3.2 cm in diameter) which behaved as an electrode separator with platinum black coated on one side. Deposition was achieved from a slurry of platinum black in distilled water. The electrodes were then dried and pressed at a pressure of 4 tons for 3 minutes. This method of deposition was developed by Lion Laboratories and is based on the method described by Woodward [7]. The platinum black discs supplied were cut into 14 x 7 mm rectangles to fit the fuel cell casing. Fuel cell electrodes were then immersed in 6 mol dm^{-3} H$_2$SO$_4$ electrolyte for 30 minutes, after which excess electrolyte was wiped off with a dry tissue. A standard fuel cell was prepared by bringing the two platinum black electrodes into contact by placing them back-to-back in the fuel cell casing (described in section 2.3.4).

2.3.2 Preparation of PANI-modified fuel cells

As mentioned the type I fuel cell assembly was used for the PANI-modified fuel cells. Modification was achieved by depositing PANI on the cathode (Pt black or Au-PVC). Full details on the synthesis conditions are described in chapter 3. After synthesis, PANI films were tested for their redox behaviour in a monomer free solution. PANI electrodes were then taken out of solution in the emeraldine salt oxidation state (+ 500 mV) ready to be utilised as the cathode in the fuel cells. All polymerisations and polymer investigations were performed in a standard three-electrode cell. A high surface area platinum gauze electrode was utilised as the counter electrode and a saturated calomel electrode (SCE) was used as a reference electrode.

Before use in the fuel cell, PANI-coated electrodes were immersed in the intended fuel cell electrolyte for 30 minutes; the same procedure was used for the platinum black working electrode. Fuel cells were prepared by placing the PANI-coated

cathode and platinum black anode back-to-back in a fuel cell casing (section 2.3.4). The component structure of the fuel cell is shown in figure 4.
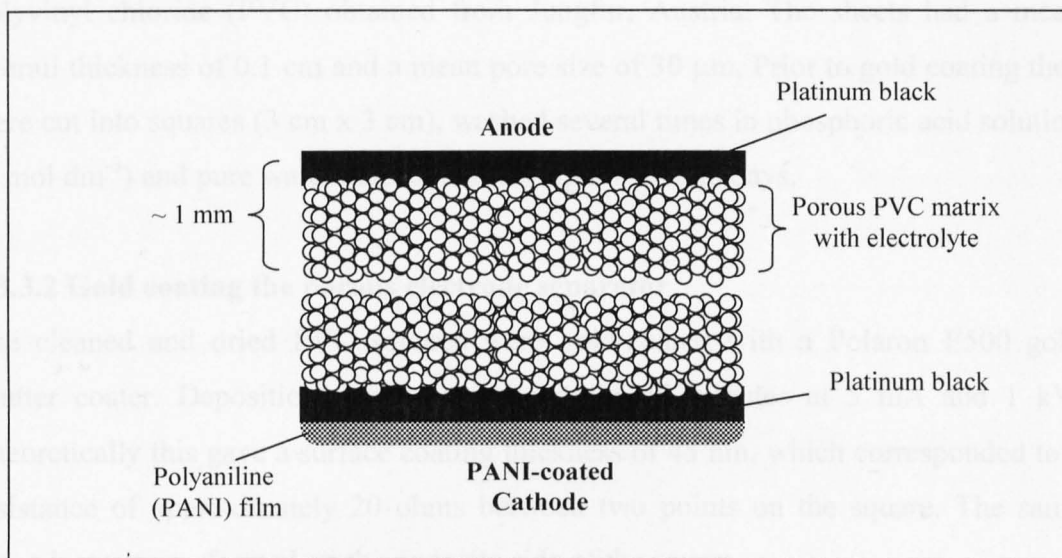
Figure 4 Transverse section through a PANI based fuel cell

All PANI based fuel cells were based on variants of the type I assembly; further details of other PANI fuel cells are discussed in section 3.3.2.

2.3.3 Preparation of Type II fuel cells

As described previously type II fuel cells were utilised in the second part of the work. Fuel cells were prepared in a similar manner to that described by Williams [8,9], Harrison [10] and Nurton [11]. Essentially, the fuel cell consisted of a thin rectangle of porous material (the electrode separator) onto either side of which was electrodeposited the metal or alloy so as to form two electrically isolated catalytic electrodes. Electrodeposition of the metal / alloy was made possible by pre-coating the separator faces with a thin film of gold, by means of gold sputtering. The two catalytic electrodes were brought into contact by impregnation of the porous PVC with a suitable electrolyte, usually ortho-phosphoric acid (76 %), to give a complete fuel cell. After electrolyte impregnation the fuel cells were subjected to a number of pre-treatment procedures which had previously been shown to enhance and prolong the activity of the fuel cells [8-11]. The experimental procedure for the preparation of the electrode is described next.

2.3.3.1 Preparation of the porous electrode separator

The electrode separator was prepared from sheets (15 cm x 15 cm) of porous polyvinyl chloride (PVC) obtained from Jungfur, Austria. The sheets had a mean overall thickness of 0.1 cm and a mean pore size of 30 µm. Prior to gold coating they were cut into squares (3 cm x 3 cm), washed several times in phosphoric acid solution (1 mol dm^{-3}) and pure water before final drying for several days.

2.3.3.2 Gold coating the porous electrode separator

The cleaned and dried PVC squares were gold-coated with a Polaron E500 gold sputter coater. Depositions were carried out for 45 minutes at 5 mA and 1 kV. Theoretically this gave a surface coating thickness of 45 nm, which corresponded to a resistance of approximately 20 ohms between two points on the square. The same procedure was performed on the opposite side of the square.

2.3.3.3 Electrodeposition of the metal electrodes

Before electrodeposition, the gold-coated PVC squares were cut into smaller rectangles of 18 mm x 7 mm. Although the fuel cell casing dimension was 14 mm x 7 mm the extra area was used as a contact point for electrodeposition, in this way the incompletely coated contact point could be cut off afterwards. The gold-coated PVC rectangles were subsequently clipped to a special platinized-titanium holder. The vessel used for the plating was a 25 ml glass beaker which had been thoroughly cleaned. Electroplating solutions were made up to 20 ml. The composition and operating conditions of the electroplating baths used in the preparation of the different metal electrodes are described in more detail in section 4.3.1. During electrodeposition the gold-coated PVC and holder formed the cathode, whilst the anode consisted of a 4 cm x 10 cm platinum anode, this was bent around both sides of the anode to enable uniform current distribution.

2.3.3.4 Electrolyte impregnation

After electrodeposition, fuel cell electrodes, still in their wire holders, were thoroughly rinsed with pure water and immersed in a solution of phosphoric acid (76 %) in a 100 ml glass beaker. This was placed in a vacuum desiccator which was connected to a vacuum pump in order to remove the air within the porous matrix. The

cells were left under vacuum for 30 minutes after which time they were removed and excess liquid allowed to drain off for several minutes.

2.3.3.5 Fuel cell compression

After electrolyte impregnation the fuel cells were mounted between two clean stainless steel plates (7 mm thick). These were then compressed at a pressure of 3 tons for 10 minutes by means of a hydraulic press of the type used in the preparation of KBr discs for use in infrared spectroscopy. Because of the radial expansion of the electrodes during pressing they were subsequently retrimmed to size (14 mm x 7 mm) to fit inside the fuel cell casing. Afterwards the electrodes were returned to the wire holders ready for activation.

2.3.3.6 Electrode activation

The fuel cells were activated by repetitive cycling the potential of the electrodes in phosphoric acid solution (76 %) by means of cyclic voltammetry between limits of – 200 and 1000 mV (vs. SCE), which correspond to hydrogen and oxygen evolution respectively. Cycling continued for 1 hour at a sweep rate of 50 mV s^{-1} before the process was stopped at the negative limit. On completion of the activation process the cells were removed from the acid and placed in a sealed plastic bag in a dark cupboard to protect from light, dust, or other possible contaminants.

2.3.4 Fuel cell cases

Throughout this work specially constructed fuel cell holders supplied by PPM Technology Ltd [7] were used to accommodate the fuel cell electrodes. The holders, which were made of ABS plastic, included sample inlet/outlet ports and were fitted with platinum wire contacts. The fuel cell holders had dimensions of 27 x 13 x 7 mm, and the inlet/outlet ports had internal diameters of 2 mm. The complete assembly, with electrodes in place is shown schematically in figure 5.
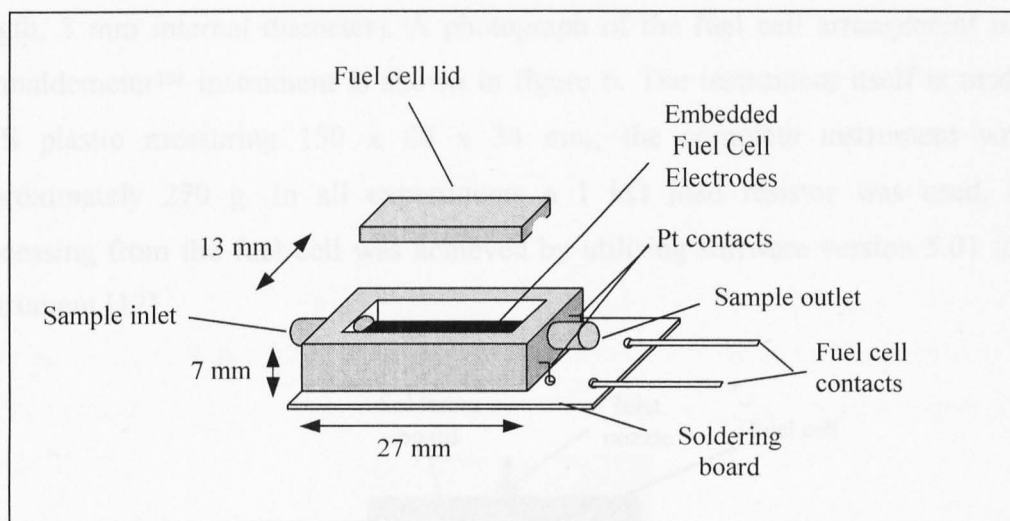
Figure 5 A diagram of the fuel cell casing assembly; inset, the dimensions of the
fuel cell holder

The electrode contacts were prepared from lengths (2 cm) of platinum wire (0.35 mm
diameter) and were fitted to the casing through small holes leaving approximately 1
cm exposed to the electrode surface. Epoxy resin was used to seal the points of exit of
the platinum wires from the plastic case. The fuel cell casing was then attached to a
special soldering board with adhesive tape and the fuel cell contact points were
soldered in position. Flexible wire cabling were soldered to respective contact points
on the board which were then used as fuel cell contacts to the printed circuit board
(PCB) of the Formaldemeter™ instrument.

Having mounted the fuel cell electrodes in the plastic case the lid was pushed firmly
into place and the joint sealed with epoxy resin. As some of the fuel cells needed to be
opened to adjust the electrodes it was necessary to use several layers of insulating tape
instead of epoxy resin. It was essential that the detector was completely airtight to
ensure that the fuel cell electrodes were not exposed to air from leakages in the seal.
The fuel cells were then prepared for sampling by fitting a metal nozzle to the fuel
cell inlet. Again it was essential that the connection was completely airtight.

2.4 Incorporation of fuel cells into Formaldemeter™

All fuel cells prepared were incorporated into the Formaldemeter™ sampling
instrument. Fuel cell contacts were soldered to the relevant pads on the PCB and the
fuel cell outlet was connected to the sampling pump *via* silicone tubing (3.5 cm

41

length, 3 mm internal diameter). A photograph of the fuel cell arrangement in the Formaldemeter™ instrument is shown in figure 6. The instrument itself is made of ABS plastic measuring 150 x 80 x 34 mm; the complete instrument weighs approximately 270 g. In all experiments a 1 kΩ load resistor was used. Data processing from the fuel cell was achieved by utilising software version 5.01 in the instrument [12].
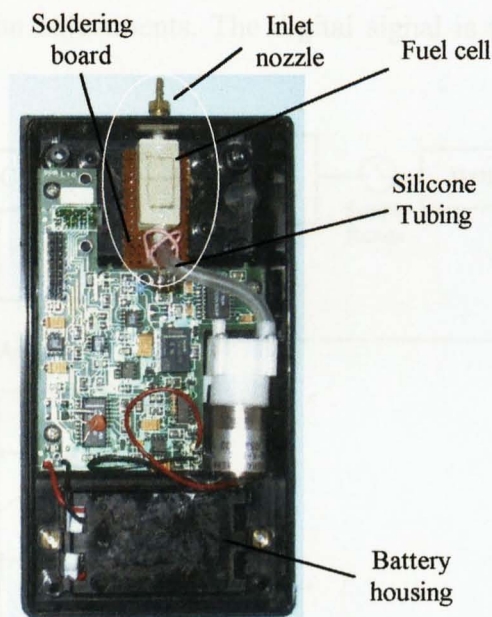
Figure 6 Photograph of the fuel cell incorporated into the Formaldemeter™ casing

2.4.1 Sampling system

Williams has shown that the fuel cell response to a gas or vapour depends on the total amount of the reactant introduced into it [8,9]. It is essential, therefore, that the volume of the gaseous sample be reproducible if comparative and quantitative measurements are to be made. Having fixed the volume of the sample then the fuel cell response may be taken as proportional, within limits, to the concentration of the reactant gas species present in the gas or vapour sample. In the Formaldemeter™ this is achieved by utilising a sampling pump which draws in a fixed volume of gas (10 cm^3), this may be varied by changing the pump run time.

2.4.2 Electronic circuitry of the Formaldemeter™

The basic electronic system is shown in figure 7. The electrical response of the fuel cell to formaldehyde vapour oxidation is analogue in nature, so that after amplification the voltage is converted to a digital signal and finally shown on a liquid crystal display meter calibrated directly in vapour concentration units. The meter, which extends from 0.05 to 50 ppm, is calibrated by incorporating a potentiometer in the gain section of the amplifier circuitry; the user may reset this potentiometer during subsequent, routine calibration adjustments. The digital signal is then processed *via* the software.
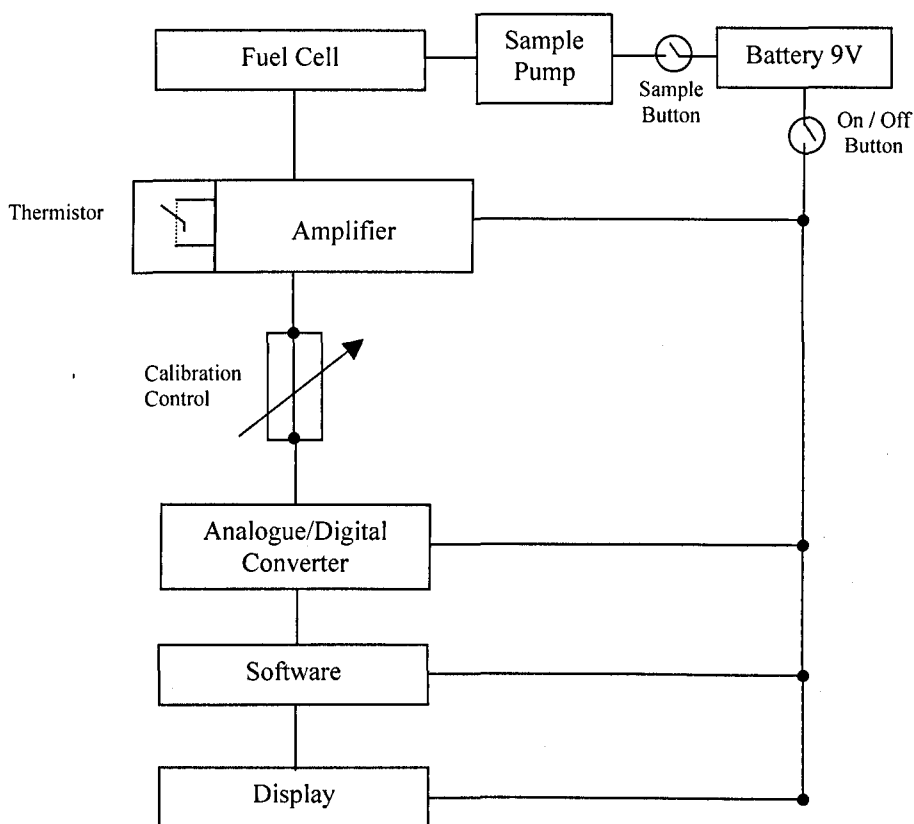
Figure 7 Block diagram of the electronic circuitry used in the Formaldemeter™

Most fuel cell detectors have a positive temperature coefficient. This is countered by incorporating a thermistor of the same, but negative coefficient in the gain control section of the amplifier, so enabling the instrument to be used under field conditions. The electronic circuits use proven, solid-state integrated devices and are both hardwearing and reliable. A PP3 sized alkaline battery is used which has sufficient power for up to 300 field tests.

2.4.3 Fuel cell response measurements

The response of the fuel cells to formaldehyde can be monitored directly on the Formaldemeter™ display or by connecting the Formaldemeter™ to a computer. In this work the second method was preferred since the whole process, from the beginning of sampling until recovery of the fuel cell could be monitored and plotted. This information was possible by utilising a specially designed computer programme in Microsoft QuickBasic language [5].

The Formaldemeter™ was connected to the serial port of the computer *via* data cable from the instrument. Fuel cell output data was directly supplied from the analogue/digital converter in the instrument, as a result readings in parts per million (ppm) were not possible since the signal bypasses the Formaldemeter™ software. The output using the computer is quoted in Test Mode (TM) units; although they are not calibrated to parts per million (ppm) units the TM values are sufficient in qualitatively investigating and comparing fuel cells. In all experiments, the fuel cell output was monitored over 500 seconds with the computer taking 10 readings every second. In all PANI experiments a pump run time of 0.2 seconds was used.

2.4.4 Calibration standard

Fuel cells are neither absolute detectors, nor is their sensitivity constant with time [13]; therefore, they require calibration when first produced, followed by periodic checks and adjustments. Calibration allows accurate readings in parts per million (ppm) to be obtained consistently from the fuel cell. For this purpose a calibration standard is often utilised.

The calibration standard is essentially a glass tube containing silica gel onto which is adsorbed 0.03 % w/v formaldehyde. Glass wool is positioned on either end of the tube to keep the silica gel in place. The vapour concentration of formaldehyde inside the tube is approximately 2 ppm; however, this changes with temperature. A correlation between temperature and the concentration in ppm of formaldehyde in the calibration standard is known from previous studies and is printed on the side of the glass tube. This data are used to calibrate the fuel cell sensor to a known concentration of formaldehyde at a particular temperature. A component structure of the calibration standard is shown in figure 8.
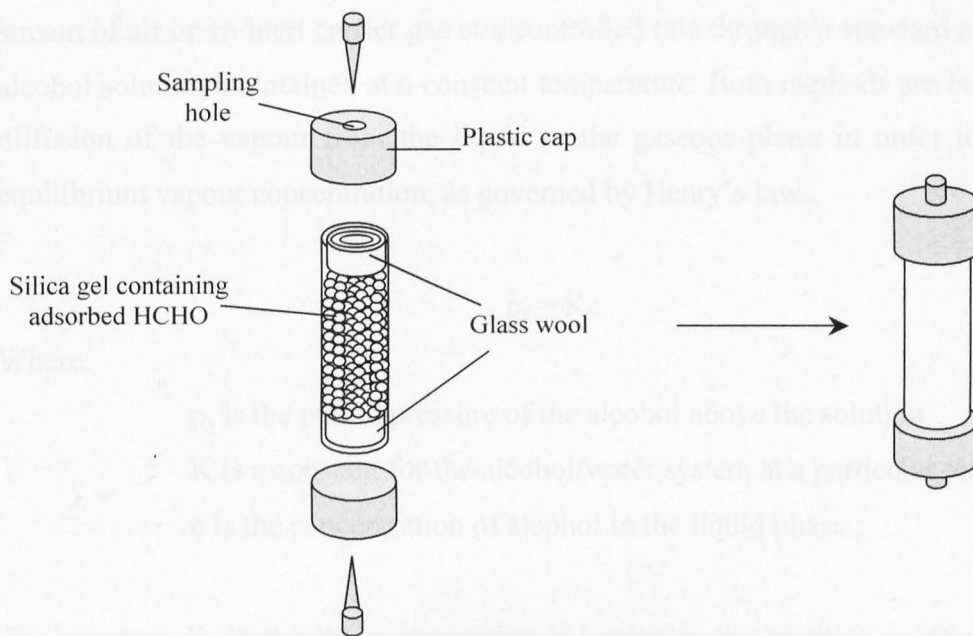
Figure 8 Component structure of the calibration standard

The calibration standard may be used by removing the stoppers from the plastic caps on each end of the tube. The nozzle of the Formaldemeter™ is then pressed tightly against a rubber seal around the outlet. As the Formaldemeter™ withdraws a sample an airflow causes the formaldehyde to be released from the silica gel and into the fuel cell sensor.

In this work all fuel cells were initially checked for their response to formaldehyde with the calibration standard. The standard was also used to check the long-term sensitivity and reproducibility of the fuel cells. More detailed investigations on the response of the fuel cells to formaldehyde and other vapours were performed using a vapour generator. As well as being able to control the vapour concentration, the temperature and humidity of the vapour could also be controlled using this equipment. The vapour generator is discussed in more detail in section 2.5.3.

2.5 Aldehyde and alcohol vapour standards

Aldehyde and alcohol vapours of known concentration may be produced by static or dynamic methods, as described by Hill and Newall [14]. In the static method a small volume of standard aqueous aldehyde or alcohol solution is sealed in a glass vessel, the sample then diffuses from the liquid to the vapour phase until equilibrium is established. Dynamic methods of generating vapour standards are used whenever a

continuous stream of such a vapour is required. This method consists of passing a stream of air or an inert carrier gas at a controlled rate through a standard aldehyde or alcohol solution maintained at a constant temperature. Both methods are based on the diffusion of the vapour from the liquid to the gaseous phase in order to attain an equilibrium vapour concentration, as governed by Henry's law.

$$p_s = Kc$$

Where:

p_s is the partial pressure of the alcohol above the solution

K is a constant for the alcohol/water system at a particular temperature

c is the concentration of alcohol in the liquid phase

The constant, K, in the above expression is known as the partition coefficient and is defined as:

$$K_{air/water} (K_{a/w}) = \frac{\text{Concentration of alcohol in the vapour}}{\text{Concentration of alcohol in solution}}$$

The value of $K_{a/w}$ for alcohols between air and water has been studied by many workers [8,9] so that the molar concentration of an alcohol in the head-space above a standard solution may be readily calculated.

Alcohol	$K_{a/w}$ x 10^3
Methanol	0.196
Ethanol	0.215

Aqueous methanol vapour standards were made up using the formula:

$$ppm = \frac{\mu g \times V_n}{V \times M_{wt}}$$

Where

V_n = molar gas volume at 25 °C (24.45 dm^3)

μg = micrograms methanol in vapour phase

V = volume of methanol/air mixture

M_{wt} = molecular weight of methanol

46

e.g. weight of methanol contained in 1 dm^3 of 10 ppm methanol vapour

$$10 = \frac{\mu g \times 24.45}{1 \times 32} = 13.09 \ \mu g$$

From Henry's law and $K_{a/w}$ for methanol

$$\text{Concentration of methanol in solution} = \frac{13.09}{0.196 \times 10^{-3}} = 0.0668 \ g \ dm^{-3}$$

Therefore a solution of methanol containing 0.0668 g dm^{-3} generates a 10 ppm methanol/air mixture.

2.5.1 Preparation of standard solutions of methanol

Standard solutions of methanol were prepared by the volumetric addition of the pure methanol to pure water. The addition of methanol was carried out as rapidly as possible to reduce evaporation losses and did not, in any case, exceed 30 seconds. The solutions were made up to 1 dm^3 with pure water and mixed thoroughly.

2.5.2 Preparation of standard solutions of formaldehyde

The preparation of formaldehyde standards were carried out in exactly the same way as methanol; 0.03 % w/v aqueous solutions of paraformaldehyde were prepared. Previous studies have shown that a 0.03 % w/v solution of paraformaldehyde corresponds to 2 ppm vapour concentration of formaldehyde [12]. Further dilutions of this solution were necessary to prepare lower vapour concentrations.

2.5.3 The Vapour Generator

Throughout this work a continuous method of producing vapour was utilised. This method was preferred over static sampling since the temperature and relative humidity of the sample vapour could be controlled. A diagram and photograph of the custom-made vapour generator which was used to generate the vapour standards are shown in figures 9a and 9b.
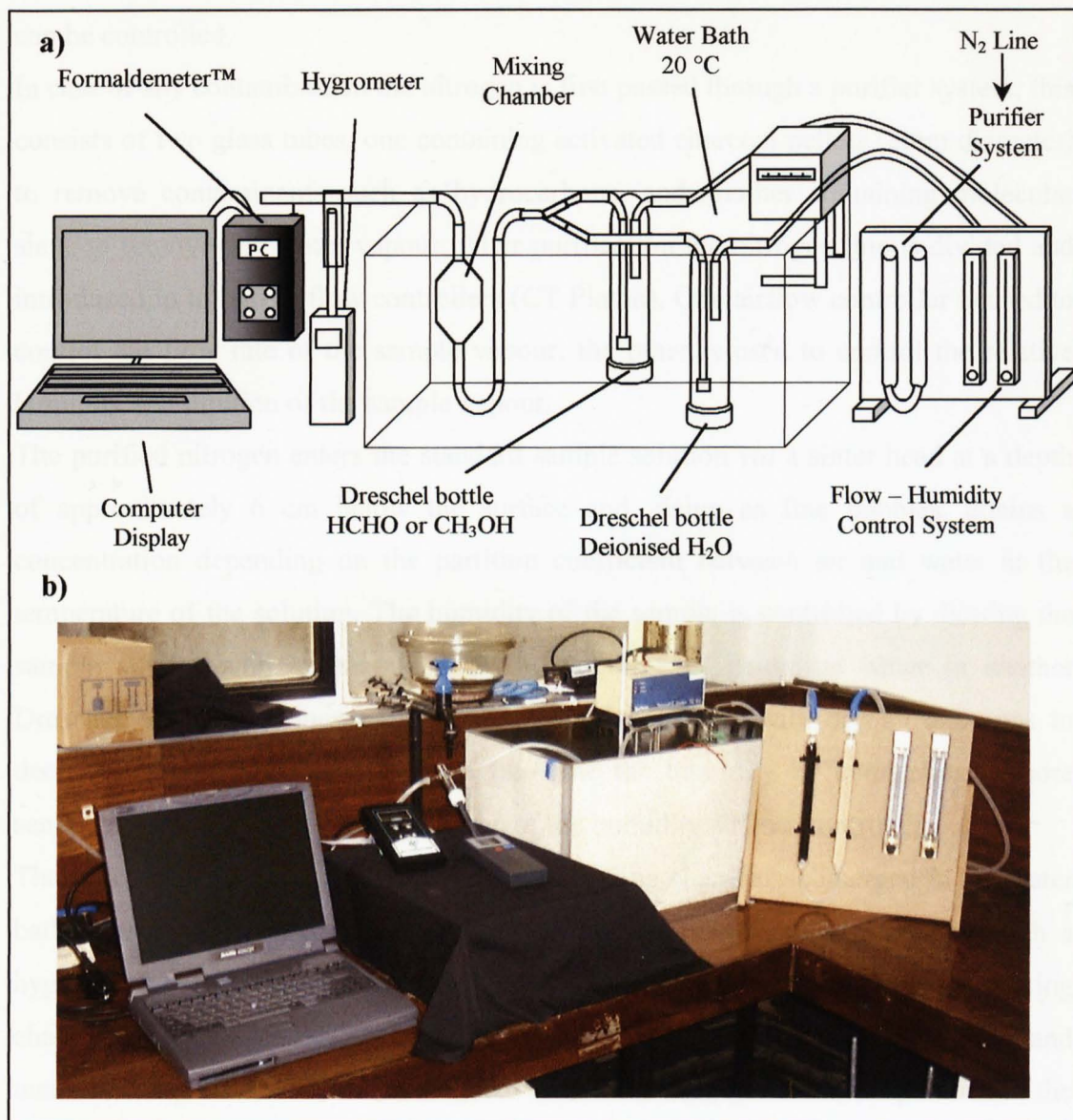
Figures 9 (a) Schematic diagram of the vapour generator used at the Department of Chemistry **(b)** photograph of the vapour generator apparatus

Testing of the PANI-modified fuel cells was carried out at PPM Technology Ltd. where purified air was the carrier gas, while testing of the different electrocatalysts was carried out at the Department of Chemistry where nitrogen was the carrier gas. Essentially, the vapour is produced by passing a controlled stream of purified inert carrier gas (N_2) or air through standard solutions of formaldehyde and methanol contained in 500 ml Dreschel bottles (SGL). Mixing the sample vapour with dry or wet air controls the humidity and by immersing the Dreschel bottles and mixing

chamber in a constant temperature water bath the temperature of the sample vapour can be controlled.

In case of any contamination the nitrogen is first passed through a purifier system; this consists of two glass tubes, one containing activated charcoal pellets (2mm diameter) to remove contaminants such as hydrocarbons, and another containing molecular sieve to remove any water vapour. After purification the nitrogen line is divided and introduced in to two airflow controllers (CT Platon). One airflow controller is used to control the flow rate of the sample vapour; the other is used to control the relative humidity and dilution of the sample vapour.

The purified nitrogen enters the standard sample solution *via* a sinter head at a depth of approximately 6 cm below the surface and, rising as fine bubbles, attains a concentration depending on the partition coefficient between air and water at the temperature of the solution. The humidity of the sample is controlled by diluting the sample vapour with humid air from the bubbling of deionised water in another Dreschel bottle, thus increasing humidity, or by diluting with dry nitrogen gas to decrease humidity. It is possible to fine-tune the humidity by connecting a more sensitive needle valve to the output tube of the humidity airflow controller.

The dilution is achieved by virtue of a glass mixing chamber submerged in the water bath. The humidity and temperature of the vapour is constantly monitored with a hygrometer (Rotronic), which is attached to a special glass port just after the mixing chamber. A stable reading on the hygrometer indicates steady state conditions and means the vapour is ready to be sampled. A small needle hole in the output tube of the hygrometer port is used as the sampling port for the Formaldemeter™ instrument, and provides space for the fuel cell nozzle. The response of the fuel cell in the Formaldemeter™ is monitored on a computer supported with Microsoft QuickBasic (QBasic) software (section 2.4.3). The vapour stream eventually leads to the fume hood where it is released. Main parts of the vapour generator are summarised in the flow chart diagram in figure 10.

Because of the large air/liquid volume ratio within the Dreschel bottles, the liquid standards required replacement only infrequently, however to reduce discrepancies the solutions were changed according to age and use.
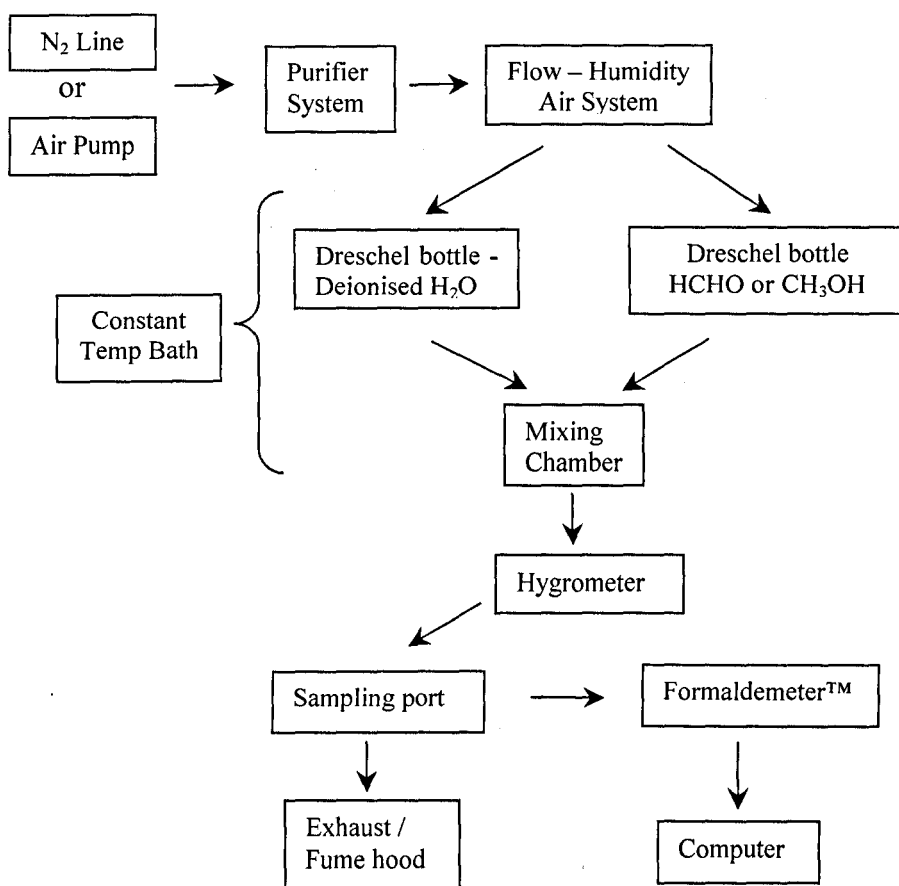
Figure 10 A flow chart diagram of the vapour generator

In all experiments Dreschel bottles were filled with 300 ml standard solutions and fitted with Dreschel heads (porosity 4). The Dreschel bottles and mixing chamber were submerged as deeply as possible in the water bath at 20 °C ± 0.1 °C. The flow rate in all experiments was adjusted to deliver 600 ml/min of sample vapour. Sampling of the vapour stream commenced once the desired humidity of the vapour sample attained a steady state reading on the hygrometer.

2.6 Characterization of the fuel cell electrodes

In this work a Hitachi S-520 Scanning Electron Microscope was used to examine the surface of the fuel cell electrodes. Prior to examination in the microscope the samples were dried under vacuum and the surface cleaned from any contaminants by blowing the surface with nitrogen. The samples were then mounted onto Cambridge stereo scan stubs (1.25 cm diameter) using double-sided conductive graphite tape. As all the sample electrodes were coated on PVC it was necessary to daub the corner of each mounted sample electrodes with silver paint to ensure electrical continuity from the

surface of the electrode to the stub. In some experiments it was necessary to sputter coat the samples with a gold conduction film (10 nm), this was necessary to prevent a build up of excess charge on the sample surface which would result in impaired resolution of the electron image. To prevent damage to the PVC separator, the samples were coated at milder conditions than standard; samples were coated for 10 minutes at 5 mA and 1 kV. The prepared samples were finally stored in a clean dry vacuum desiccator before SEM examination. The optical images obtained from SEM investigations were recorded on 35 mm Ilford FP4 black and white negative material using a Nikon 35 mm camera

The Hitachi S-520 SEM used for microscopic examination was linked to an analytical limited QX2000I EDS system. This achieved an energy dispersive analysis by x-rays of the sample. The instrument worked by extracting the characteristic secondary x-rays generated as the electron beam (high energy x-rays) interacted with the specimen. The x-ray fluorescence detector (an L24 windowless detector) then sorted the x-ray photons according to their energies. These were recorded as x-ray energy spectra and printed on a Mitsubishi thermal printer.

When irradiated using high energy x-rays, elements emit x-ray photons of characteristic energies; as a result peaks in the spectrum can be directly related to elements present within the samples. Lighter elements generally produce lower energy secondary x-rays. A reasonable concentration of elements in the region of the sample to be analysed allows qualitative analysis of individual elements to be recorded with an accuracy of ± 1 %. The x-ray detector used restricted identification to elements heavier than sodium. Therefore a complete major elemental composition of a feature as small as a few micrometers across could be determined within a matter of seconds. The theoretical and experimental details of SEM and EDAX are discussed in detail elsewhere [15,16].

2.7 References

1   Southampton Electrochemistry Group, *"Instrumental Methods in Electrochemistry,"* Ellis Horwood (1990)

2   C. H. Hamann, A. Hamnett, W. Vielstich, *"Electrochemistry,"* Wiley VCH Weinheim, (1998)

3   G. A. Mabbott, *J. Chem. Ed.*, 60 (1983) 697

4   J. A. Alden, R. G. Compton, *Anal. Chem.*, (2000) 199A

5 PPM Technology Ltd, Parc Menai, Bangor, Gwynedd, Wales, UK

6 Alcometer Breath Alcohol Instruments, Lion Laboratories plc, Barry, South Glamorgan, Wales, UK

7 S. F. Woodward, *Ph.D. Thesis*, University of Wales, Cardiff, (1985)

8 P.M. Williams, *MSc Thesis*, University of Wales, Cardiff, (1974)

9 P.M. Williams, *Ph.D Thesis*, University of Wales, Cardiff, (1978)

10 I. D. Harrison, *Ph.D Thesis*, University of Wales, Cardiff, (1982)

11 R. L. Nurton, *MSc. Thesis*, University of Wales, Cardiff, (1985)

12 PPM Technology Ltd, Parc Menai, Bangor, Gwynedd, Wales, UK, *Private Communication* (2001)

13 P. M. Williams, I. R. Whiteside, T. P. Jones. *Int. Environ. Safety*, (1981) 15

14 D. W. Hill, H. A. Newall, *J. Sci. Instrument*, 42 (1965) 783

15 J.W.S. Hearle, J.T. Sparrow, P.M. Cross, *"The Use of the Scanning Electron Microscope,"* Pergamon Press, Oxford (1972)

16 J.I. Goldstein, D.E. Newburry, P. Echlin, D.C. Joy, C. Fiori, E. Lifshin, *"Scanning Electron Microscopy and X-Ray Microanalysis,"* Plenum Press, New York (1981)

Chapter III
The use of Polyaniline as a Cathode in Fuel Cell Sensors

3.0 Introduction

The use of conducting polymers as materials in many devices depends on their conversion from one state to another. In the case of PANI the switching time has been shown to be particularly rapid [1], which makes it a desirable material as a cathode in a fuel cell sensor. The behaviour of PANI as a cathode in a fuel cell sensor will essentially depend on the redox state of the polymer at open circuit. The redox state of the polymer can be influenced by either injecting electric charge or by adding a reagent that interferes with the redox equilibrium [2]. The principle of the PANI cathode is based on these two factors.

In theory if PANI is in its oxidised state, electrons produced at the anode from the oxidation of formaldehyde will cause PANI to switch to its reduced state, thus behaving as an electron reservoir. It is also anticipated that on completion of formaldehyde oxidation the reaction of reduced PANI with atmospheric oxygen will switch the polymer back to its original oxidised state, thus an electrochemical – chemical reversible switching process is proposed for PANI. A diagram of the proposed processes occurring in the fuel cell is shown in figure 1.
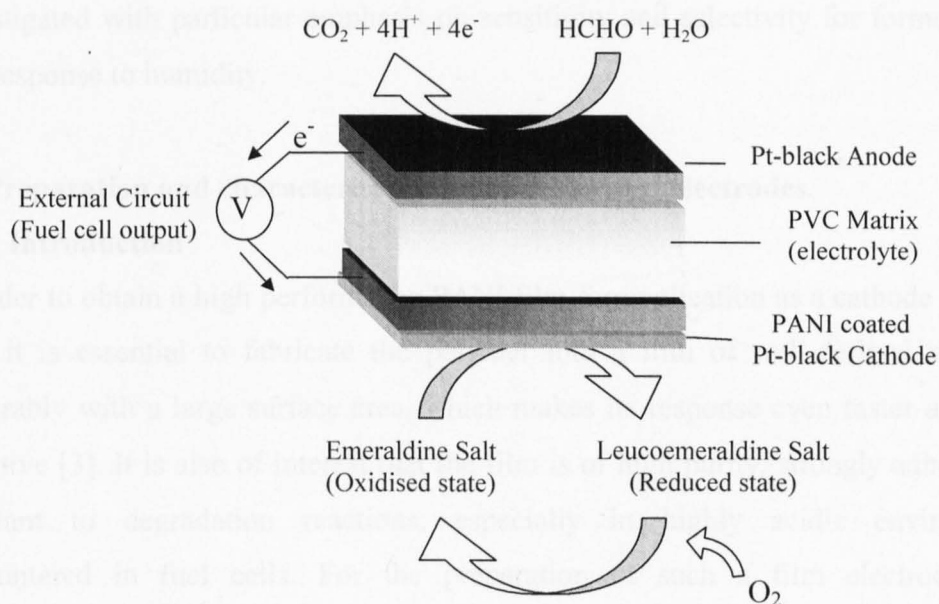
Figure 1 Proposed processes occurring in a PANI-modified fuel cell

In principle the PANI cathode seems ideal, however, in practice the polymer must fulfil a number of conditions before utilisation in a fuel cell environment. If a PANI based cathode is used in a commercial fuel cell sensor, a durable good quality film is essential. The redox properties of the film at open circuit must also be preserved over a long period of time. Clearly the loss of film stability would be a major problem for the maintenance of the fuel cell. In addition, a good understanding of the factors that affect the redox switching of PANI at open circuit is important. It is with these prerequisites in mind that the open circuit behaviour and feasibility of PANI-coated electrodes are investigated. The work is divided into three sections

3.1 Electrochemical deposition and characterisation of PANI-coated platinum black and gold-coated PVC electrodes

3.2 Stability and open circuit behaviour of PANI-coated electrodes in various acidic media

3.3 Performance of PANI-modified fuel cells

In the first section the electrochemical synthesis and redox behaviour of PANI on platinum black and gold-coated PVC are described. In the second part of the work the stability and open circuit behaviour of PANI coated electrodes in various acidic media are investigated by means of cyclic voltammetry and open circuit measurements. In the third and final part of the work the performance of the PANI-modified fuel cells is investigated with particular emphasis on sensitivity and selectivity for formaldehyde and response to humidity.

3.1 Preparation and characterisation of PANI-coated electrodes

3.1.1 Introduction

In order to obtain a high performance PANI film for application as a cathode in a fuel cell, it is essential to fabricate the polymer into a film of well-defined structure, preferably with a large surface area, which makes its response even faster and more effective [3]. It is also of interest that the film is of high purity, strongly adhered and resistant to degradation reactions, especially in highly acidic environments encountered in fuel cells. For the preparation of such a film electrochemical polymerisation by potential cycling is the preferred method [4-6].

Over the last few years polyaniline (PANI) films have been studied on many different substrates, including Pt [7,8], Au [9,10], Pd [11], C [12,13], Al [14], Zn [15], Cu [16], stainless steel [17], TiO_2 [18], SnO_2 [19] and RuO_2 [20]; however, there are no reports in the literature of PANI synthesised on platinum black, which is quite surprising considering the number of applications utilising the material. Previous studies have indicated that the choice of substrate is a key factor in determining the growth rate, structure and electrochemical behaviour of PANI films [21]. A number of researchers reported that PANI films polymerised under different conditions possess not only a different primary structure but also different gross morphology [1,22-24], which as a result exhibit different properties and responses [25].

In this study the electrochemical growth and characterisation of PANI-coated platinum black is described. In addition a PANI film deposited directly on gold-coated porous PVC is investigated. If the behaviour of such a film in a fuel cell is similar to PANI-coated Pt-black, then the need for a Pt-black substrate at the cathode could be eliminated, thus reducing the unit cost of the fuel cell sensor.

3.1.2 Experimental

Three different types of PANI films were prepared and investigated. For the first type, PANI was grown on Pt-black in a solution containing aniline (0.1 mol dm^{-3}) in sulfuric acid (1 mol dm^{-3}) (Pt-black/PANI/SO_4^{2-}). The redox properties of this type were investigated in 1 mol dm^{-3} H_2SO_4. The second type was grown in a solution containing aniline (0.1 mol dm^{-3}) in hydrochloric acid (1 mol dm^{-3}) (Pt-black/PANI/Cl^-) with the redox properties investigated in 1 mol dm^{-3} HCl. Both films were grown for 50 cycles from −200 mV to +750 mV *vs.* SCE with the first 3 cycles taken to 1 V to facilitate nucleation and growth of the polymer. The third type comprised a PANI film deposited on gold-coated porous PVC. The film was grown in aniline (0.1 mol dm^{-3}) in sulfuric acid (1 mol dm^{-3}) (Au-PVC/PANI/SO_4^{2-}) for 25 cycles under the same potential limits as the others. In all experiments a potential scan rate of 50 mV/s was used. The redox properties of all the films were investigated between the potential limits −200 mV and +600 mV. The charges contained in the PANI voltammograms were calculated by integrating the area between these limits. Morphological properties of the PANI films were investigated by SEM. Throughout the work platinum black electrodes used were supplied by PPM Technology Ltd (section 2.3.1) and were cut into dimensions of 10 x 6 mm prior to PANI deposition.

However due to the lack of available literature on the substrate it was necessary to characterise the surface of the supplied platinum black electrodes before the deposition of PANI.

3.1.3 Characterisation of Pt-black

Platinum black is different to standard polycrystalline platinum in that it has a much higher surface area and as a result a better catalytic activity; the main reason why it is used for electrocatalysis, e.g. fuel oxidation and oxygen reduction in low-temperature fuel cells [26-31]. A typical cyclic voltammogram of a pristine platinum black electrode is shown in figure 2.
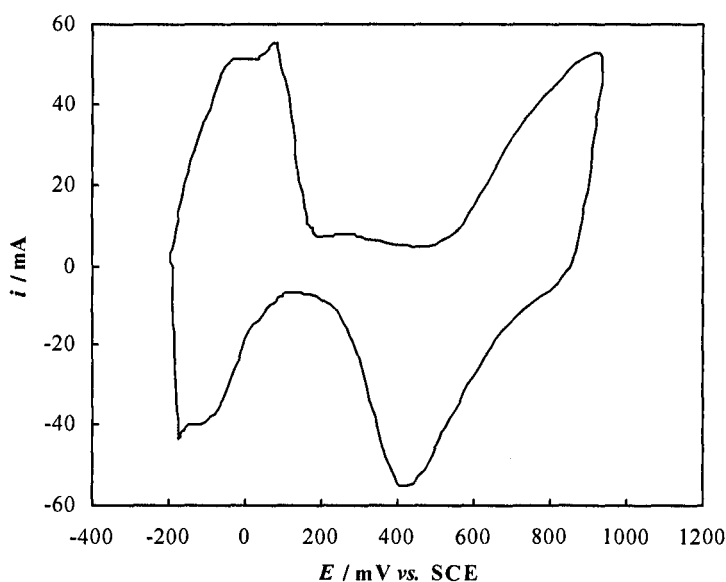
Figure 2 Cyclic voltammogram of a pristine Pt-black electrode in 1 mol dm^{-3} H$_2$SO$_4$.

The response is typical of platinum and is similar to that of polycrystalline platinum in acid [31]. However, the main difference between this voltammogram and that of polycrystalline Pt is the large amplitude of the faradaic and capacitive currents observed with Pt-black, which is indicative of a high surface area electrode, in particular the hydrogen adsorption/desorption region. This is expected as the electrode is composed of compressed platinum powder. The cyclic voltammogram of platinum is well documented and more details of the processes can be found in the literature [30,31] or in chapter 4 where electrocatalysis on noble metal electrodes is discussed.

An SEM image of pristine Pt-black electrode is shown in figure 3, and as can be seen the electrode is fractured in some places.
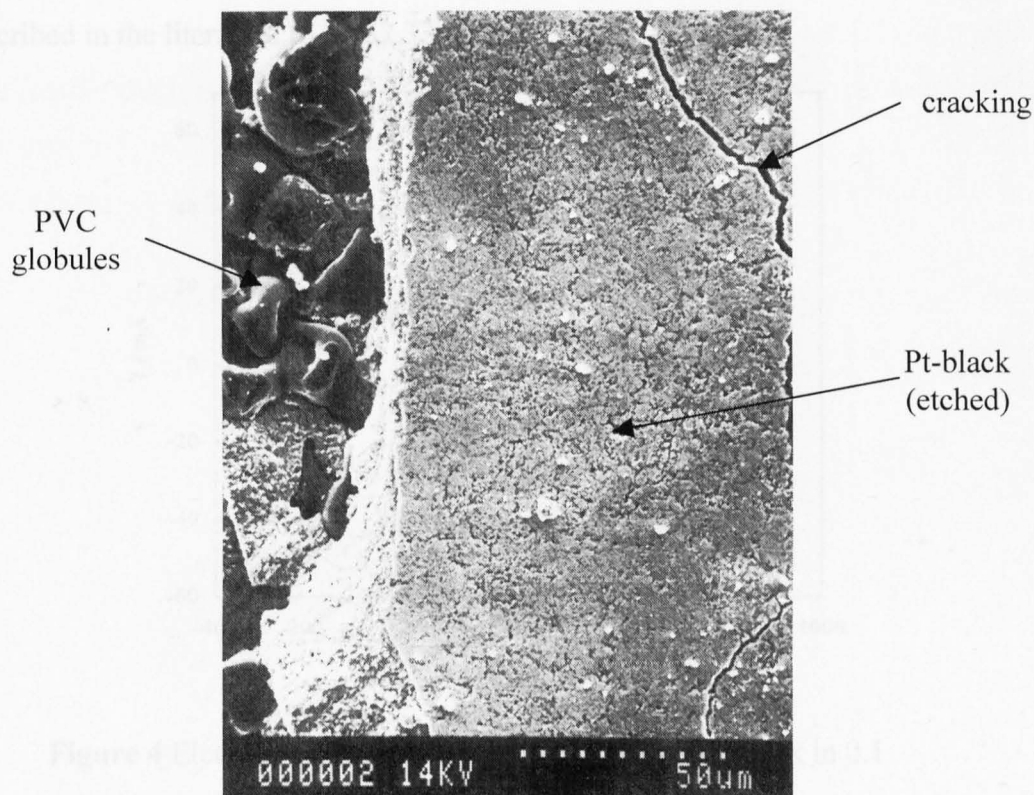
Figure 3 SEMs of platinum black electrode (× 600)

Further examination of the electrode shows the thickness of the film to be approximately 5 μm. The cracks and fractures in the surface of the electrode have been reported to be as a result of the preparation procedure, which consists of compression and an activation procedure as described in section 2.3.1. [27]. Closer investigation by SEM reveals the width of the cracks to be in the order of 1-3 μm. The extent of cracking of the platinum black surface, however, does not result in the loss of conductivity. It is therefore assumed that the fracturing of the platinum black substrate should not affect the deposition of PANI. The effect of compression and activation on the surface characteristics of fuel cell electrode is discussed further in chapter 4.

3.1.4 Deposition of PANI films

Figure 4 show typical cyclic voltammograms recorded during the growth of Pt-black/PANI/SO_4^{2-}. The voltammograms shows peaks and features that are well described in the literature [6,21,32,33].
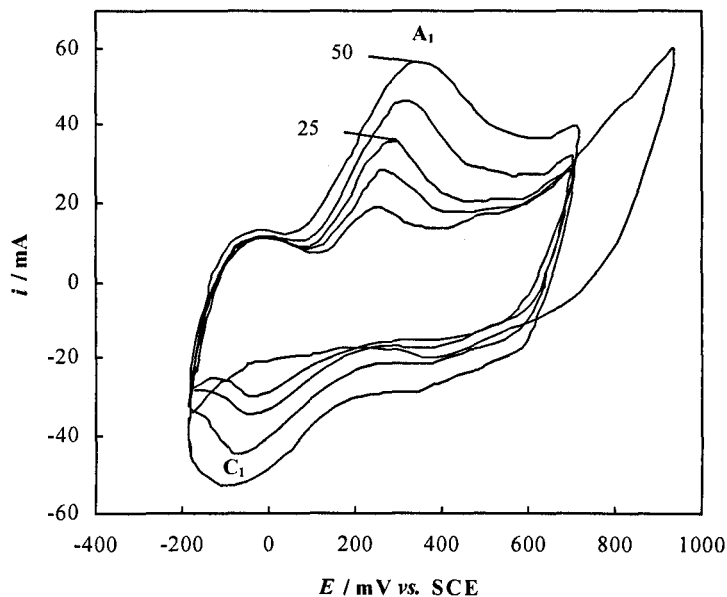
Figure 4 Electrochemical growth of PANI-coated Pt-black in 0.1 mol dm^{-3} aniline/ 1 mol dm^{-3} H_2SO_4

A_1 and C_1 peaks are associated with the oxidation/reduction of the leucoemeraldine salt / emeraldine salt states of PANI. As the film begins to form A_1 and C_1 peaks occur at 260 mV and –50 mV respectively, however with increasing film thickness the peaks shift to 370 mV and –80 mV by the last sweep. Increasing film thickness has the effect of increasing the resistance in the film, thus causing the potential shift in the peaks [22,35]. Compared to a PANI film coated on polycrystalline platinum [21,34] for the same number of cycles the growth rate is much quicker on platinum black. The peak separation and large peak current are indicative of this. This enhanced behaviour is most probably due to the extremely high catalytic surface area of the electrode in comparison to polycrystalline platinum [31]. This is denoted by the large capacitive region in the voltammogram between –20 mA and 10 mA which is consistent with the voltammogram of bare Pt-black shown in figure 2. Another interesting feature in the voltammogram is the anodic peak at 0 V which corresponds to the hydrogen desorption region of platinum [36]. Normally when a PANI film is coated on a Pt electrode this feature is not observed due to passivation by the film.

Although the region is much suppressed in comparison to pristine platinum black as shown in figure 2 the response is most likely due to the porous nature of the film in addition to the high surface area of the Pt-black electrode.

The same features and response described were also observed for Pt-black/PANI/Cl$^-$, as a result the growth voltammogram is not shown here. The redox properties of the film however, are described in the section 3.1.5.

Figure 5 shows a typical growth cyclic voltammogram of Au-PVC/PANI/SO$_4{}^{2-}$.
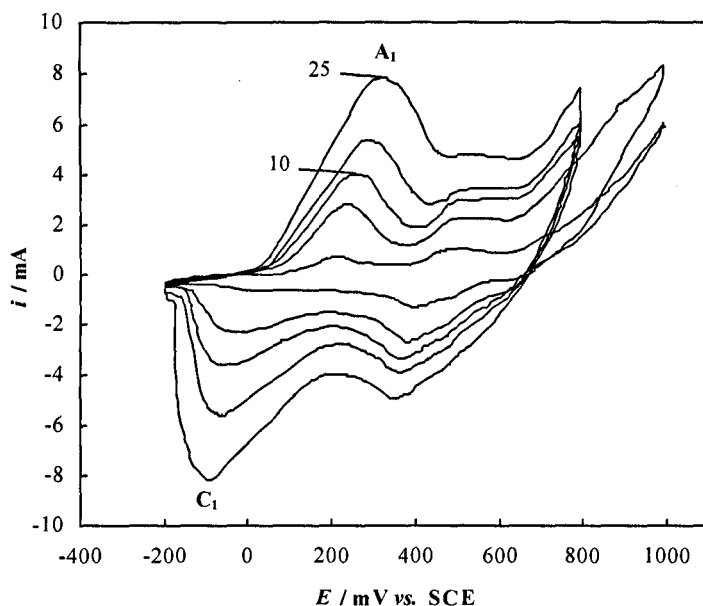
Figure 5 Electrochemical growth of PANI on Au coated PVC in 0.1 mol dm^{-3} aniline/ 1 mol dm^{-3} H$_2$SO$_4$

The voltammogram is typical of a film grown on gold [6] and is quite similar to the PANI grown on Pt-black. This behaviour is consistent with previous studies which show that the choice between gold and platinum substrates does not affect the rate or voltammogram characteristics of PANI [21]. In common with PANI grown on Pt-black the leucoemeraldine salt/ emeraldine salt peaks A$_1$ and C$_1$ again shift with additional growth cycles indicating the formation of a relatively thick PANI film.

The main difference between the voltammograms is the smaller current scale observed with Au and the disappearance of the capacitive and hydrogen regions observed in the voltammogram on Pt-black. These differences are partially due to the much smaller surface area of the gold electrode, which contains a very thin layer of approximately 45 nm, coated on PVC, in comparison to Pt-black electrodes which have a Pt thickness of 5 μm after compression onto the PVC substrate.

As the contribution from the surface area is small on the growth voltammogram on gold, other peaks are more clearly seen. In the first few potential cycles, a pronounced redox couple occurs at 500-600 mV, which is due to the redox peaks of degradation products, containing aromatic quinoid groups that have been identified as benzoquinone/hydroquinone, quinoneimines, or oligomers of aniline [37,38]. In subsequent cycles this peak does not increase further in size and the main PANI redox peaks, centred at 250 mV begin to dominate the voltammetric response.

The mechanism of aniline polymerisation is well documented [39,40] and the first step in the oxidation of aniline has been shown to be the formation of a radical cation followed by radical coupling to form dimer molecules [41]. Oligomerisation reactions follow in the earlier stages of polymer growth and once short chain oligomers are formed, they grow to polymers *via* what is known as the autocatalytic growth mechanism where the polymerisation reaction is catalysed by the film itself. [23,33].

3.1.5 Redox behaviour of PANI films

Figure 6 shows a typical cyclic voltammogram of Pt-black/PANI/SO_4^{2-}. Shown in grey is the normal redox behaviour of the PANI film and it can be seen that the appearance of the voltammogram is distorted, most probably due to the iR drop within the thick polymer layer [35]. It is well known that iR errors can substantially distort cyclic voltammograms by altering peak positions and the shape of the voltammogram [30,42]. This problem is mostly encountered in poor conducting electrolytes or with resistive electrode films or deposits. A normal procedure in such cases is to apply positive feedback iR compensation, a facility that is standard on most modern potentiostats to correct for any iR errors. Shown in black is the iR compensated response of the same PANI film; clearly the shape of the voltammogram and peak positions are much better defined. In almost all experiments on Pt-black/PANI iR compensation was utilised. All voltammograms of PANI coated Pt-black from this point forward will only contain the iR compensated response.
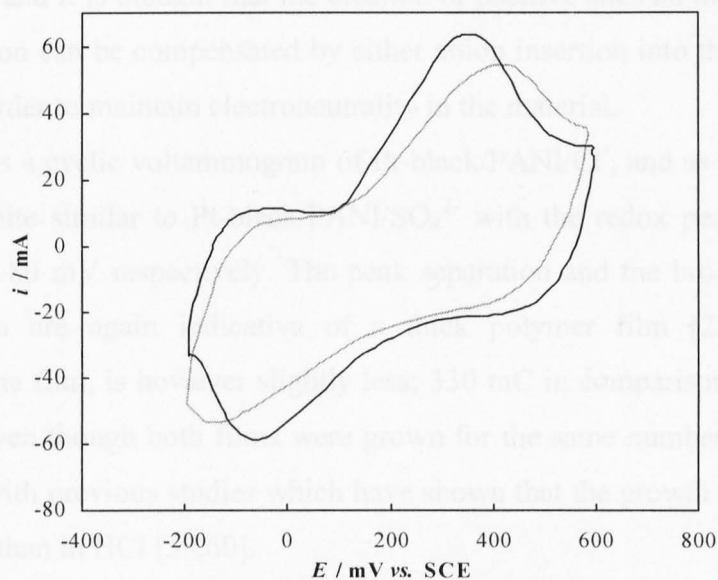
Figure 6 Cyclic voltammogram of Pt-black/PANI/SO$_4$$^{2-}$ in 1 mol dm^{-3} H$_2$SO$_4$.
Grey – uncompensated response; black - iR compensated

In comparison to a typical voltammogram of PANI coated on polycrystalline Pt the redox peaks occurring at 370 mV and 60 mV respectively, are very broad with a greater anodic / cathodic peak separation, which again as already established, demonstrate the thick nature of the PANI film [22]. The redox couple corresponds to the switching reaction of the first oxidation / reduction process of PANI and accounts for the dramatic change in conductivity of the polymer [6,7]. The anodic peak corresponds to the oxidation of the reduced PANI from the leucoemeraldine salt state to the conductive emeraldine state. The opposite transition occurs on the reverse sweep. The redox process is also accompanied by the well known electrochromic property of PANI [33-45], in this case changing colour from light green to dark green on the anodic sweep and the reverse on the opposite sweep. Diaz [46], Kobayashi [47], McManus [48], Watanabe [49] and Genies *et al.* [50] have observed a wide range of colours from pale yellow to blue for both thin and thick polymer films on various types of electrodes.

The second oxidation/reduction process becomes visible if the potential limit is taken sufficiently positive, however as this involves the concurrent oxidation of the emeraldine form and deprotonation of the polymer it leads to the eventual degradation of the polymer [51]. This was avoided in all experiments with PANI in order to preserve its redox properties. There have been many studies on the redox processes in

PANI [51-58] and it is thought that the creation of positive sites on the polymer chain during oxidation can be compensated by either anion insertion into the film or cation expulsion in order to maintain electroneutrality in the material.

Figure 7 shows a cyclic voltammogram of Pt-black/PANI/Cl⁻, and as can be seen, the response is quite similar to Pt-black/PANI/SO_4^{2-} with the redox peaks occurring at 380 mV and −80 mV respectively. The peak separation and the broad nature of the voltammogram are again indicative of a thick polymer film [22]. The charge contained in the film, is however slightly less; 330 mC in comparison to 410 mC for PANI/SO_4^{2-} even though both films were grown for the same number of cycles. This is consistent with previous studies which have shown that the growth rate in H_2SO_4 is slightly faster than in HCl [59,60].
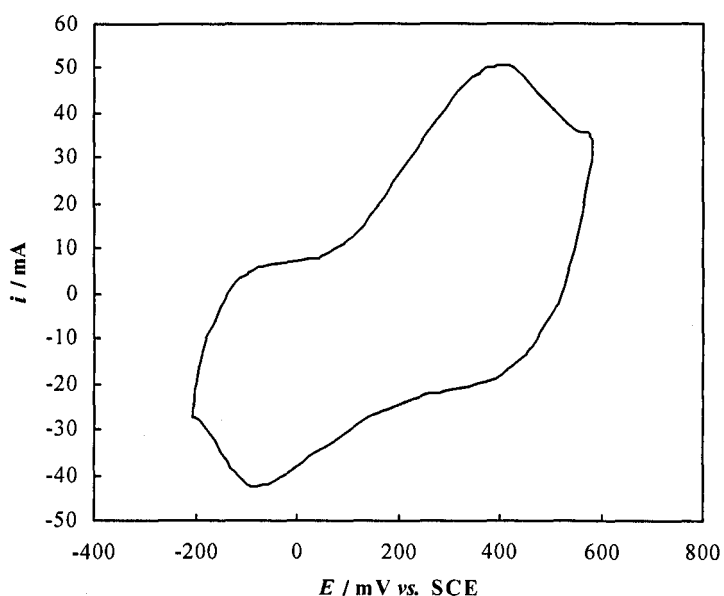
Figure 7 Cyclic voltammogram of Pt-black/PANI/Cl⁻ in 1 mol dm⁻³ HCl

Figure 8 shows a cyclic voltammogram of Au-PVC/PANI/SO_4^{2-}. Initial voltammograms for the film displayed a resistive effect, therefore voltammograms were performed with iR compensation, however, the resistive effect was much reduced in comparison to PANI films coated on Pt-black.
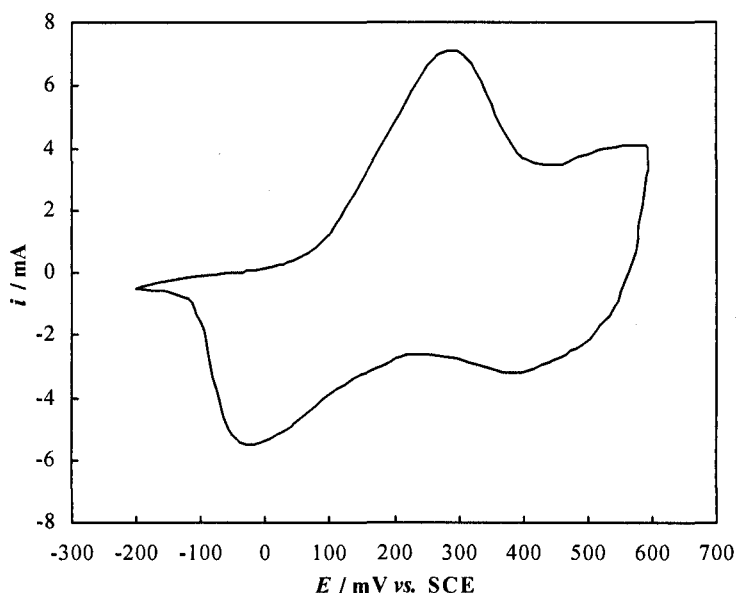
Figure 8 Cyclic voltammogram of Au-PVC/PANI/SO_4^{2-} in 1 mol dm^{-3} H_2SO_4

As can be seen, the voltammogram is quite different to PANI-coated Pt-black; the peak currents are much smaller and the capacitive behaviour associated with the high surface area of Pt-black is not shown, especially in the region –200 mV < 0 mV.

The scale of the voltammogram and charge associated in the film, 45 mC, indicates that the amount of PANI coated is smaller than the typical deposits on Pt-black. Nevertheless the film is reasonably thick as indicated by the relatively large anodic/cathodic peak separation occurring at 300 mV and –80 mV respectively. The colour change associated with the switching process was similar to PANI on Pt-black changing colour from very light green to dark green.

3.1.6 Morphological properties of PANI films

Morphological studies of PANI are not as widespread as might be expected [61,62]. In addition the origin of the morphological differences among the films studied is still a controversial subject [5]. Recent work has shown that film thickness, electrolyte pH, electrosynthesis technique and the nature of the anions used during the growth, affect the morphology of PANI [23,24]. Zotti *et al.* have studied the effects of anions on the morphology and have grouped them into two types, class 1 (BF_4^-, ClO_4^- and CF_3COO^-) and class 2 (SO_4^{2-}, NO_3^- and Cl^-) [24]. Class 1 anions promote a fibrous compact structure, while class 2 anions result in a granular open structure. When the

experimental parameters are controlled to give deposits with obvious fibrous structures, the deposits show fibres of different diameters which decrease in order: $HSO_4^- > NO_3^- > Cl^- > ClO_4^-$ [59].

SEM images of PANI/SO_4^{2-} coated Pt-black are shown in figure 9(a-d) and as can be seen from figure 9a, the film is homogeneous with excellent surface coverage. It is also visible in figure 9b that the surface cracking of Pt-black does not affect the morphology of PANI; the film can be seen covering the fractures. From these images it is apparent that the film is very porous and has a substantial surface area, which is consistent with the voltammetric behaviour of the film. SEM measurements reveal the thickness of the film to be approximately 50 µm. In addition it can be seen in figure 9c and d that the film has a fibrous morphology, further increasing the surface area of the film. The fibrils have an average diameter of about 0.3 µm with a distance of about 2 µm between branch points. As described previously a high surface area polymer is suitable for practical applications promoting a faster and more efficient response for the polymer. In addition it has been reported that a polymer with a highly fibrilar morphology exhibits a greater reactivity for oxygen [63] which makes it especially suitable for the reverse reaction in the fuel cell, when a conversion back to the oxidised state of the polymer is required.
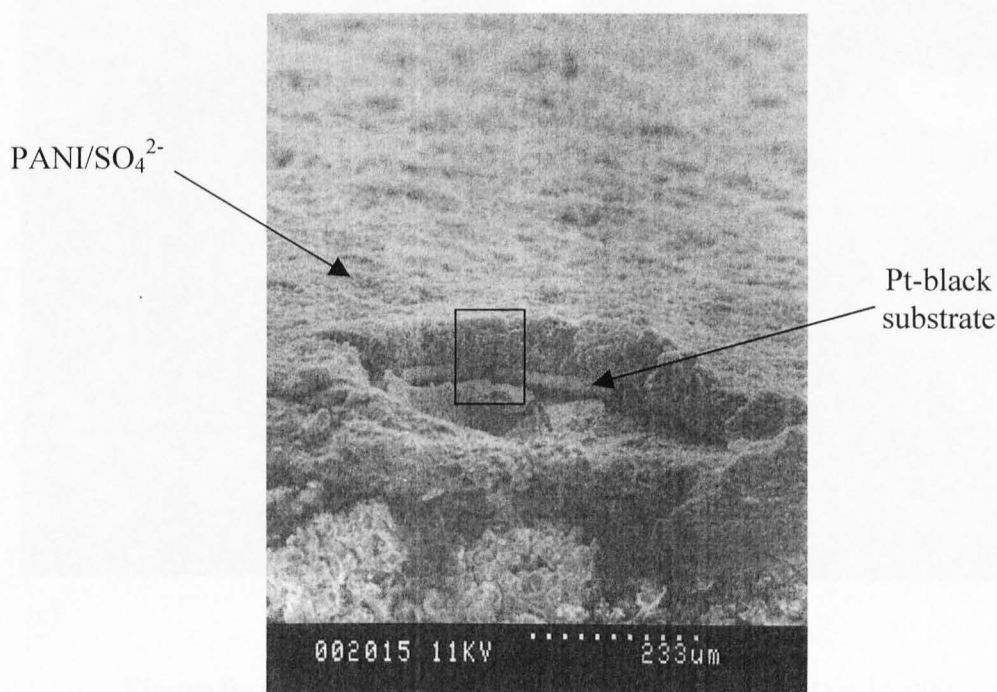
Figure 9a SEM of Pt-black/PANI/SO_4^{2-}, thickness ~ 50µm (× 140 magnification)

64

PANI/SO$_4^{2-}$

Crack in Pt-black

Pt-black substrate

002017 11KV   43um
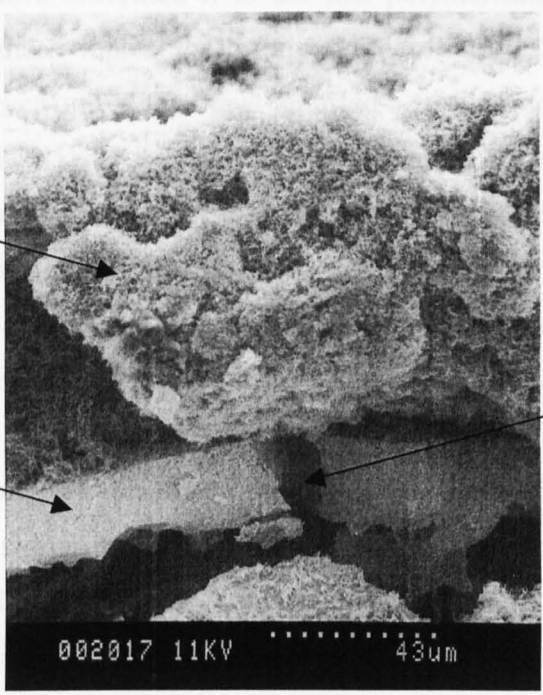
Figure 9b Magnification of region enclosed in square in figure 9a (× 700)

(c)

002008 10KV   10.0um

(d)

002009 10KV   2.00um
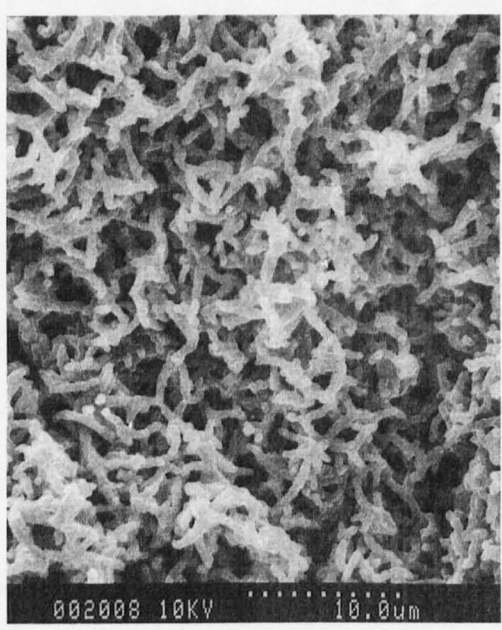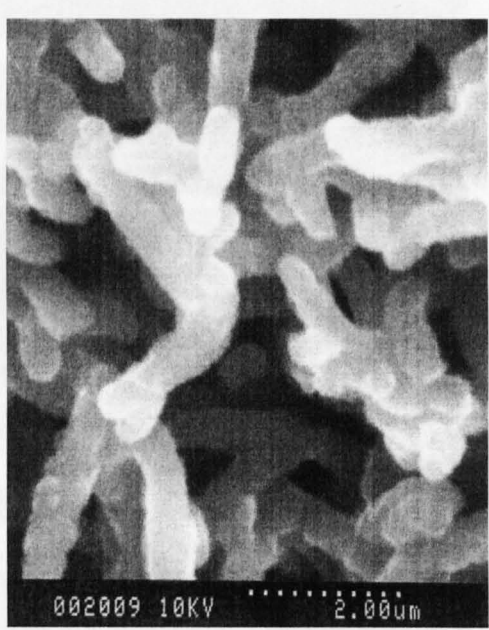
Figure 9c Close-up of PANI/SO$_4^{2-}$ strands × 3,000 **(d)** × 15,000

Other authors have reported a porous structure for PANI films grown in H_2SO_4 medium [5,64] and have attributed it to the fast polymerisation rate in this acidic medium. Several authors report the morphology of PANI/SO_4^{2-} to be granular [4,22,24,65,66], however only a few have reported a fibrilar morphology as observed in our experiments [24,65]. Our results closely resemble those of Zotti *et al.* who report a fibrilar morphology of PANI/SO_4^{2-} under controlled parameters [24].

The effect of changing the positive potential limit on the morphology of PANI has only come to light recently. Zhang *et al.* reported a distinct difference in the morphology when the upper anodic limit was reduced from 1 V to 0.8 V [65]. A granular morphology was observed for the film cycled to 1 V, while a fibrilar morphology was found for the lower limit. A fibrilar morphology has also been observed for slower sweep rate [5]. It is therefore fair to assume that the fibrous morphology observed in our investigations is most probably due to the controlled anodic potential limit of 0.75 V during growth.

Figure 10a and b shows SEM images of the Pt-black/PANI/Cl⁻ and as can be seen the morphology is quite different to Pt-black/PANI/SO_4^{2-}.

000025 14KV X2.19K 14.3um   000027 14KV X6.00K 5.0um
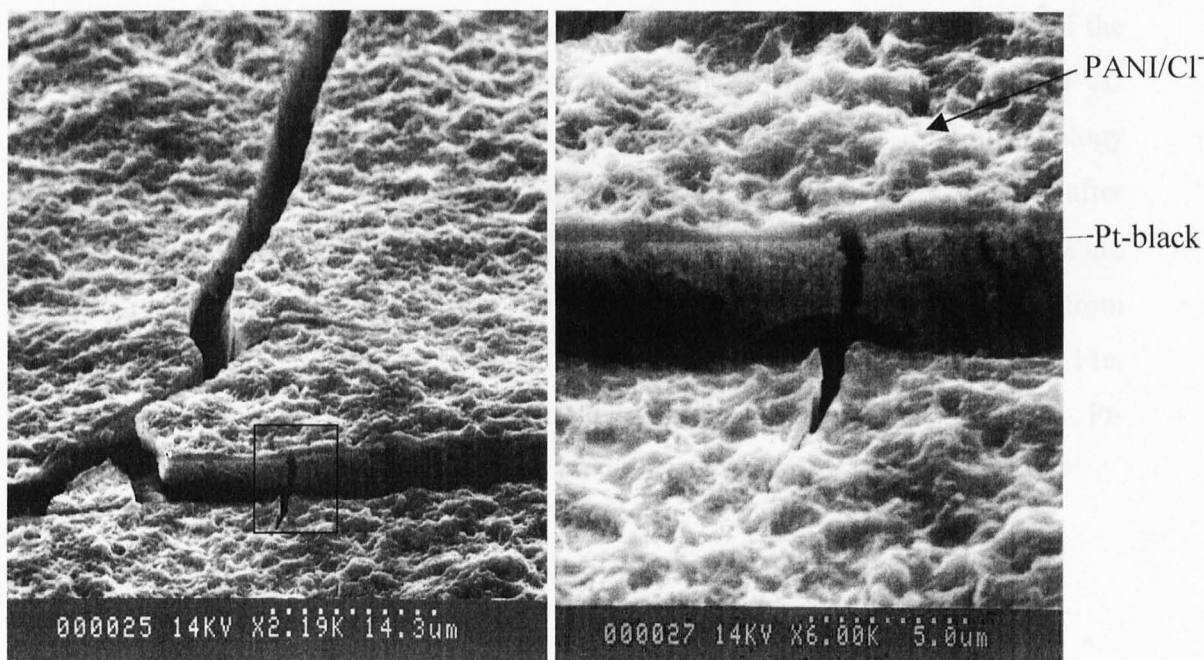
PANI/Cl⁻

Pt-black

Figure 10 (a) SEM image of PANI/Cl⁻ coated Pt-black (× 2100) **(b)** Magnification of region enclosed in square (× 6,000)

Although the polymer was grown for exactly the same number of cycles and demonstrated similar growth voltammogram and redox behaviour in acid, it can be seen that the PANI film is very dense and compact. Although not clear in the SEM presented, the film on closer inspection showed a poorly defined fibrous morphology. This is in agreement with work carried out by Okamoto *et al.* [3] and other workers [61,67] who reported a smaller structural size and a more dense texture in the HCl system, although a more clearly defined fibrous morphology was also demonstrated. The densely compact morphology observed for Pt-black/PANI/Cl$^-$ is however, in contrast to work by Zotti *et al.* who proposed that class 2 anions (SO$_4^{2-}$, NO$_3^-$ and Cl$^-$) promoted an open structure [24].

From the SEM images shown for PANI/SO$_4^{2-}$ and PANI/Cl$^-$ it is clear that the morphology depends greatly upon the anion present in the supporting electrolyte during electropolymerisation. This is in agreement with work carried out by many other workers [3,5,59,61,64,65]. Tang *et al.* recently reported that anions promoted PANI growth in the order, H$_2$SO$_4$ > HCl > HClO$_4$ [59]. Cordóva *et al.* explained that this behaviour indicates that nucleation and growth of PANI depends on the nature of the anion, thus determining polymer morphology [64].

Figure 11(a-c) shows SEM images of PANI/SO$_4^{2-}$ coated Au-PVC. The nature of the substrate is shown in figure 11a and it can be seen that it contains a network of PVC nodules linked at different points and intersected by random pores. The morphology and nature of the PVC substrate is described further in chapter 4. The difference after PANI deposition is clearly seen in figure 11b where the gold-coated PVC nodules are almost completely covered with the polymer and in some places adjoining from separate nodules. The nature of the polymer is fibrilar, as can be seen in figure 11c, however it is much more compact and dense in comparison to the Pt-black/PANI/SO$_4^{2-}$.

Network of PVC globules
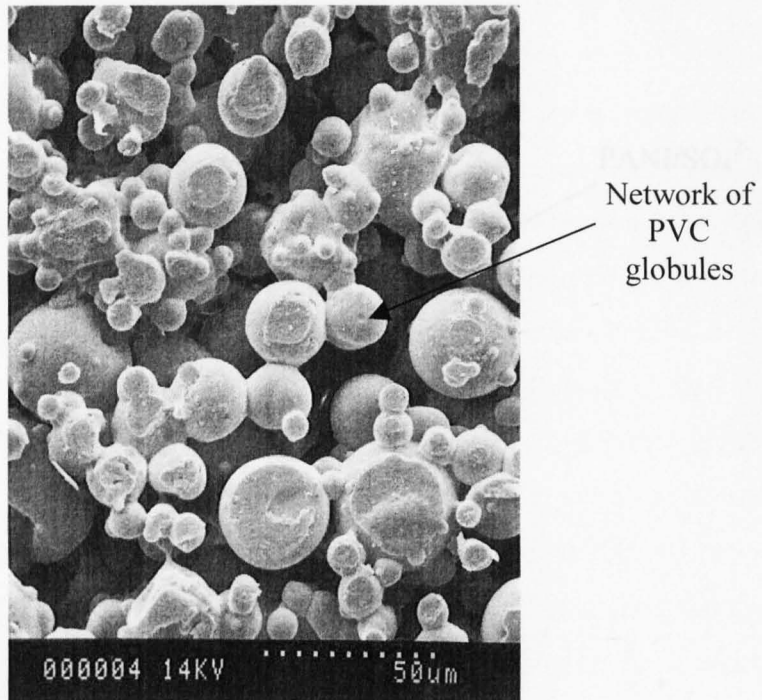
Figure 11a SEM of Au-coated PVC before modification by PANI (× 600)

PANI/SO$_4^{2-}$

PVC globule

Adjoining PANI/SO$_4^{2-}$ from separate PVC globules
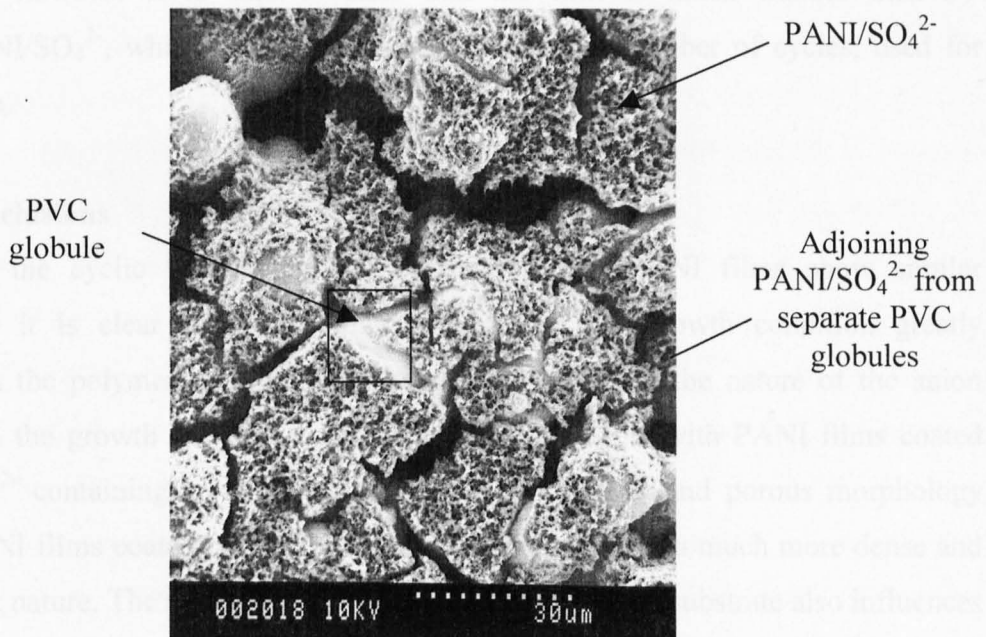
Figure 11b Au-coated PVC after modification by PANI (× 1,000)

68

Figure 11c Magnification of region enclosed in square in 9b (× 10,000)

Film thickness is difficult to estimate due to the extremely uneven nature of the electrode, however it is safe to state that the film is much thinner than Pt-black/PANI/SO_4^{2-}, which is consistent with the smaller number of cycles, used for deposition.

3.1.7 Conclusions

Although the cyclic voltammograms of the different PANI films show similar behaviour it is clear from the SEM images that the growth condition greatly influences the polymer morphology. The results show that the nature of the anion present in the growth medium is of particular importance, with PANI films coated from SO_4^{2-} containing solutions showing a highly fibrilar and porous morphology while PANI films coated from Cl^- containing solutions show a much more dense and a compact nature. The results also show that the nature of the substrate also influences the morphology, although to a lesser extent than the anion.

3.2 Stability and open circuit behaviour of PANI in various acidic media

3.2.1 Introduction

All the films prepared in the last section exhibited good redox properties and favourable morphology with good adherence and high surface area which are essential for practical applications [3]. For use in practical devices, it is vital that the polymer keeps these properties; thus, one of the most important factors in the utilisation of PANI is the stability of the polymer. In particular, retention of the excellent kinetic characteristics (<10 μs switching time between conducting and non-conducting states [1]) is critical for the efficient operation of the polymer in the fuel cell.

PANI is commonly referred to as the most stable material within the class of conducting polymers [68-70]. However a comprehensive look at the related articles reveals that only a few investigations have been devoted to its stability. Considering the many practical applications of PANI films, this is rather surprising. Most of these applications require repeated injection and removal of charge from the polymer by doping and undoping processes. The doping process, which is accomplished by the oxidation of PANI, produces positively charged polymeric species which are susceptible to nucleophilic attack by electrolytes and/or solvents, resulting in the gradual degradation of the film [71]. The loss of film and/or electrical contact to segments of the film would pose a problem for PANI films used in applications such as batteries, supercapacitors and electrochromic devices [44,45,72-76], let alone in the proposed fuel cell sensor. Previous studies on PANI stability have been mainly concerned with its electrochemical and thermal stability under extreme conditions (*i.e.* at high temperatures [77] or at high potentials [38]); however, stability investigations in conditions that could be encountered in practical devices is also required in order to assess the full feasibility of the polymer.

In this section the stability and open circuit behaviour of various PANI films are reported. Initially PANI films coated on polycrystalline platinum were investigated and used as a model to describe the stability of such films under various conditions. Similar studies were carried out on films coated on various substrates that can be used in fuel cells. Different conditions were explored in a bid to discover the most desirable conditions for the operation of PANI in a fuel cell environment. In particular, the effect of different growth conditions, substrate and aqueous electrolyte (HCl, H_2SO_4, H_3PO_4) were investigated.

3.2.2 Experimental

The stability and open circuit behaviour of PANI were investigated by cyclic voltammetry (CV) and open circuit potential (OCP) measurements. In addition to the films described in section 3.1.1, PANI films coated on polycrystalline platinum (1 cm^2) were also investigated. These films were grown from aniline solutions (0.1 mol dm^{-3}) in sulfuric acid (1 mol dm^{-3}) for 20 cycles under the same potential limits as described previously in section 3.1.2. Details are specified where different growth conditions were employed. Experiments on PANI films coated on Pt-black and Au-PVC were performed in a specially constructed three-electrode cell as described in section 2.2.1. Experiments on PANI-coated polycrystalline platinum were performed in a standard three-electrode cell; this is described in more detail in section 4.1.3.

Prior to OCP measurements the polymer was cycled once between –200 and 600 mV and taken to the desired applied potential on the forward sweep. After holding the applied potential for 10 minutes the change in OCP as a function of time was measured with a digital voltmeter. The behaviour of the polymer was investigated in acidic solutions of similar pH [H$_2$SO$_4$ (1 mol dm^{-3}) HCl (1 mol dm^{-3}) and H$_3$PO$_4$ (7 mol dm^{-3})]. Investigations were performed in either nitrogen saturated, argon saturated, oxygen saturated or air equilibrated solutions; all gases were bubbled for 45 minutes prior to the experiment. The effect of adding a reducing agent such as Na$_2$SO$_3$ (0.25 mol dm^{-3}) to the electrolyte (1 mol dm^{-3} H$_2$SO$_4$) on the open circuit behaviour of PANI was also investigated.

Where stated a revised degassing technique was employed, in these experiments the nitrogen flow was supplied to the cell *via* a 500 cm^3 Dreschel bottle containing Na$_2$SO$_3$ (0.5 mol dm^{-3}) in deionised water. The sulfite anion is an effective oxygen scavenger [78-83] which should ensure that only N$_2$ enters the cell. During the experiment N$_2$ was continuously supplied over the electrolyte (quiescent wave technique), again to ensure that no O$_2$ could enter the cell.

3.2.3 PANI-coated polycrystalline platinum
3.2.3.1 Effect of different acids on the OCP of PANI

The open circuit behaviour of PANI in nitrogen saturated HCl (1 mol dm^{-3}) and H$_2$SO$_4$ (1 mol dm^{-3}) from initial applied potentials of –200 mV and + 700 mV are shown in figure 12.
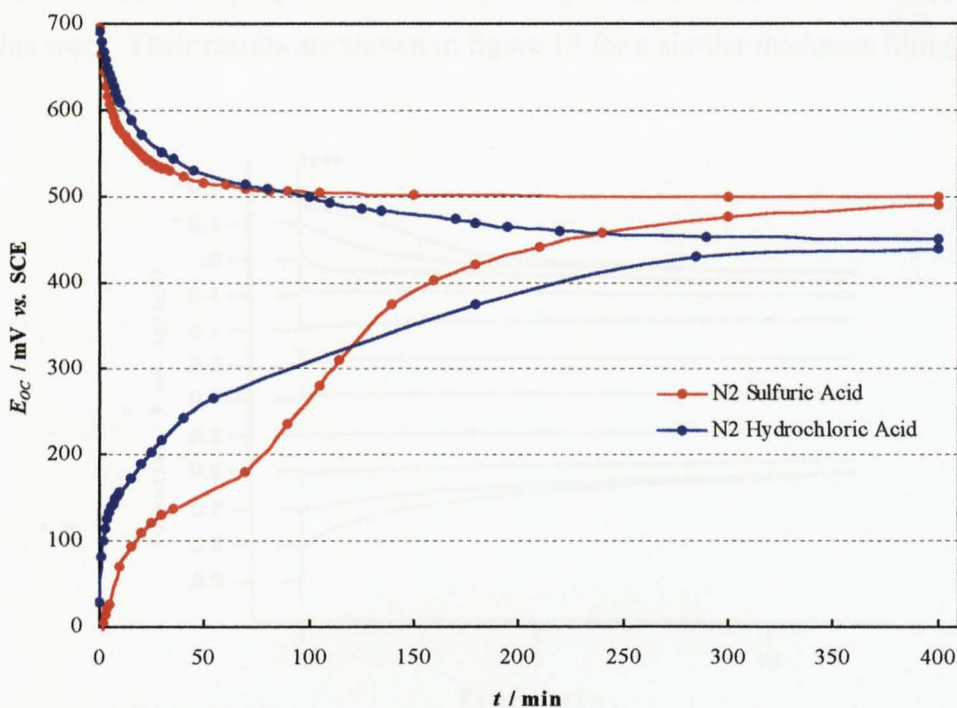
Figure 12 Open circuit behaviour of PANI-coated polycrystalline Pt, polarised in N_2 saturated 1 mol dm^{-3} H_2SO_4 (red) and 1 mol dm^{-3} HCl (blue) for 10 minutes. Both films were coated from 0.1 mol dm^{-3} aniline + 1 mol dm^{-3} H_2SO_4. Film thickness ~ 0.5 μm

The OCP values decay from the values corresponding to the reduced leucoemeraldine salt (-200 mV) and the oxidised pernigraniline (+ 700 mV), and converge towards a value that corresponds to the emeraldine salt (400-500 mV). Although the overall trend is the same for all the curves, the rate of decay varies between PANI/Cl⁻ and PANI/SO$_4$²⁻. This is particularly evident when examining the OCP decay from the potential of the reduced state. The gradient, dE/dt, of the PANI/SO$_4$²⁻ exhibited two maxima. Furthermore, a difference was observed in the final equilibrium values reached after nearly 7 h. The OCP of PANI/SO$_4$²⁻ was stable at 500 mV whereas PANI/Cl⁻ attained 450 mV. The difference is most likely due to the different chemical potentials of these two different salts. Remarkably the value of PANI/Cl⁻ is very similar to 435 mV (*vs.* SCE) quoted by Huang *et al.* [84].

One of the most intriguing aspects about the OCP measurements is establishing what causes the change in potential if the solution is degassed. Reports of the open circuit behaviour of PANI in the literature are scarce and one of the main reports published is

by Stilwell and Park [85] whose results are very much in contrast to the ones reported in this work. Their results are shown in figure 13 for a similar thickness film (0.5 μm).
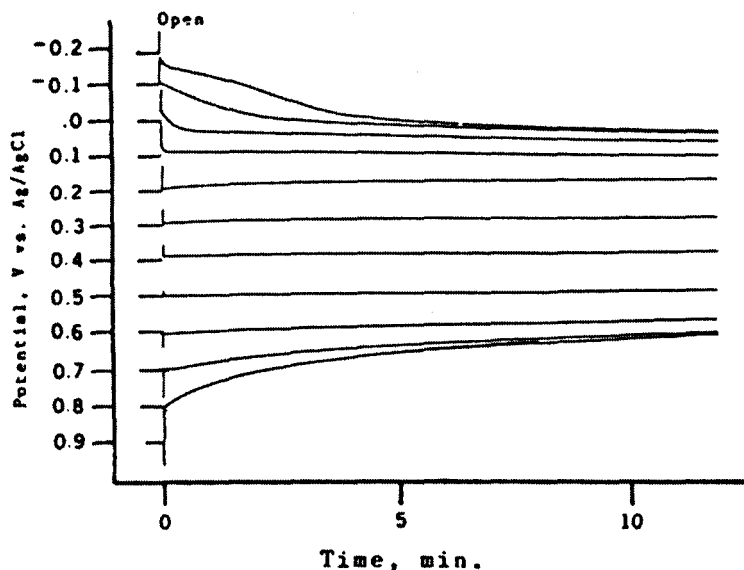
Figure 13 OCP behaviour for PANI from a number of initially stepped potentials. Data taken for film in the reduced to the oxidised form by stepping the closed circuit potential 0.1 V [85].

Stilwell and Park suggested that the initial fast decay in the open circuit potentials for the extreme positive (0.7 V) and negative potentials (-0.2 V) can be attributed to the overpotential decay, however this is only suggested for the first 30 seconds. Although overpotential decay can be attributed to the initial rapid change in potential it is clear from the results presented here that the change in OCP is a continuous process until an equilibrium potential is reached. Stilwell and Park reported slow oxidation of PANI upon opening the circuit, at potentials negative of 0 V and attributed the change to trace amounts of oxidising agents in solution, however their OCP values stabilised at 0 V *vs.* Ag/AgCl. They also observed a slow reduction in potentials positive of 0.7 V (*vs.* Ag/AgCl) and attributed the change to the formation of degradation products which result in changes in the film composition and thus in a different equilibrium potential, however, yet again their OCP stabilised quickly (within 0.1 V). In addition their results indicated that PANI states defined by the potential range of 0-0.6 V are stable. The striking aspect about Stilwell and Park's experiments is that the OCP was only measured for 10 minutes and for the extreme potentials stability was maintained

after just 2 minutes. The data presented in this work were obtained over a much longer period of time. Furthermore, the starting potential was applied for a longer period of time to ensure that all parts of the polymer were in the oxidation state that corresponds to the applied potential.

In view of these contrasting results and to gain better understanding of what causes the electrochemical switching of PANI at open circuit, the OCP of PANI was investigated further using oxidising and reducing agents.

3.2.3.2 Effect of oxygen on the OCP of PANI (Leucoemeraldine salt)

The effect of oxygen on the open circuit profiles of PANI is shown in figure 14 and, as can be seen, the change in potential is rapid, especially in H_2SO_4. In nitrogen purged H_2SO_4, the polymer takes approximately 6 hours to reach the equilibrium potential, while in oxygen saturated H_2SO_4 the polymer only takes 20 minutes. Similarly in nitrogen saturated HCl the polymer takes 5 hours to reach equilibrium, while under oxygen the polymer takes 2 hours. It is possible that the slower rate in oxygen saturated HCl in comparison to H_2SO_4 is due to the shielding of the active sites of the polymer by Cl⁻ which according to Tang et al. [59] and Choi et al. [86] forms a stronger ion-pair with the polymer, thus making it more difficult for oxygen to react. The results indicate that the reaction of reduced PANI (leucoemeraldine state) with oxygen is quite fast, especially in H_2SO_4 which is extremely promising for the fuel cell sensor application where oxidation of the polymer to the emeraldine salt state is required for efficient multiple sampling.

It has been previously demonstrated that PANI is effective in catalysing oxygen reduction and a number of applications are dependent on the principle [63,87-96]. It has been proven that PANI is a reliable cathode for oxygen reduction in acidic media for a working model of a H_2-O_2 fuel cell [63]. Shim et al. reported the use of PANI as a potentiometric sensor for dissolved oxygen in aqueous media [91]. They showed that PANI could be oxidised by oxygen and restored to its reduced state by treatment with an inert atmosphere. The results indicated that both the dissolution of gaseous oxygen and the diffusion of the dissolved oxygen into the PANI determined the response time, which showed a linear dependence on the film thickness. Kanakare et al. proposed a theory based on the formation of charge-transfer complexes between oxygen molecule and the reduced form of the conducting polymer [90]. The principle of oxygen reduction at PANI has also been applied to corrosion studies [91-96]; open

circuit measurements by a number of investigators [92,94-96] indicate that the reaction of the reduced leucoemeraldine form of PANI with oxygen keeps the film in its oxidised state, thus protecting the metal from corrosion processes.
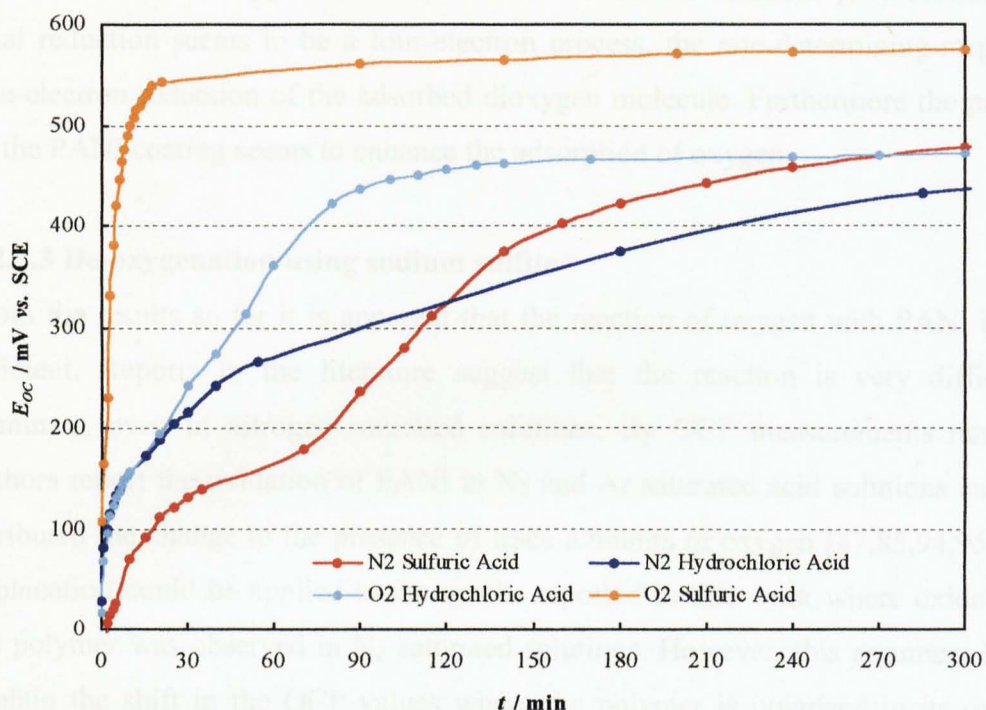
Figure 14 Effect of oxygen saturation on the open circuit behaviour of the same PANI films as in figure 12

The mechanism of interaction of oxygen with conductive polymers is still somewhat obscure, and reports in the literature are controversial. Shim *et al.* suggested charge transfer from leucoemeraldine (base) to oxygen whereupon superoxide is formed by the following reaction [91]

Superoxide ion is unstable in aqueous solutions and disproportionates to hydroxide and peroxide ions.

PANI has been studied in strongly acidic solutions, and a two-electron reduction of oxygen limited to the H_2O_2 stage has been suggested based on the stoichiometry of leucoemeraldine oxidation (studied by potentiometry) and the apparent low reactivity of H_2O_2 with the polymer [63,87]. In a more recent paper Cui and Lee studied the effect of PANI on oxygen reduction in buffered neutral solutions [89]. Although the total reduction seems to be a four-electron process, the rate-determining step is the one-electron reduction of the adsorbed dioxygen molecule. Furthermore the presence of the PANI coating seems to enhance the adsorption of oxygen.

3.2.3.3 De-oxygenation using sodium sulfite

From the results so far it is apparent that the reaction of oxygen with PANI is quite efficient. Reports in the literature suggest that the reaction is very difficult to eliminate, even in nitrogen saturated solutions. By OCP measurements numerous authors report the oxidation of PANI in N_2 and Ar saturated acid solutions and have attributed the change to the presence of trace amounts of oxygen [47,85,94,95]. This explanation could be applied to the results reported in this work where oxidation of the polymer was observed in N_2 saturated solutions. However, this argument fails to explain the shift in the OCP values where the polymer is polarised in its oxidised pernigraniline form.

With these results and those reported in the literature in mind a revised method of degassing was utilised which could eliminate oxygen from entering the cell. This consisted of passing the N_2 flow to the cell *via* a solution containing sodium sulfite (0.5 mol dm^{-3}), which was used as an oxygen scavenger, for 15 hours. Over this time the polymer was also held at the applied potential of -200 mV to make sure that the polymer was completely reduced. Full details of the revised procedure are described in the experimental section.

The effect of using the revised method of degassing on the OCP is shown in figure 15 and, as can be seen, the profiles follow the same trend as PANI in N_2 saturated H_2SO_4. This is an extremely important result as it proves that PANI is oxidised in the absence of O_2, thus disproving the mechanism proposed be Stilwell and Park [85] and various other workers who have attributed the change to adventitious traces of O_2 in the system [47,94,95].
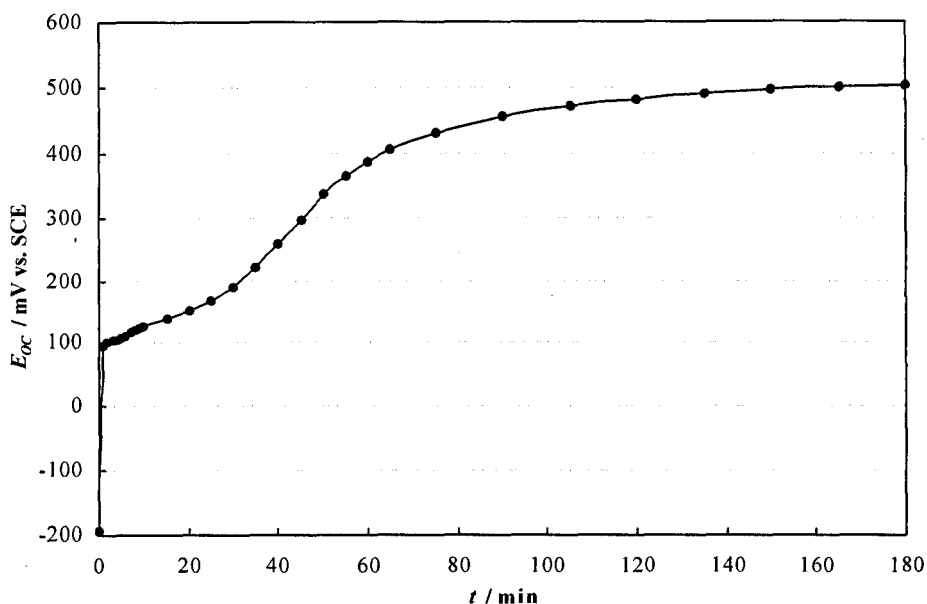
Figure 15 OCP of PANI in H_2SO_4 saturated with N_2 bubbled *via* a solution of sodium sulfite (0.5 mol dm^{-3} Na_2SO_3) to remove O_2. Film thickness ~ 0.6 μm

3.2.3.4 OCP of PANI/SO_4^{2-} in air equilibrated H_2SO_4

Similar experiments to those described by Stilwell and Park [85] were performed on PANI films in air equilibrated H_2SO_4 and in N_2 saturated solution of H_2SO_4 + Na_2SO_3 by measuring the OCP from different applied potentials. The OCP behaviour of PANI in air equilibrated H_2SO_4 (1 mol dm^{-3}) is shown in figure 16.

It can be seen that irrespective of the applied potential the OCP profile tends towards the reproducible equilibrium value of 480 mV ± 30 mV over the period of 160 minutes. It is interesting to note that the OCP profiles from –200 mV and 700 mV are very similar to the ones obtained in N_2 saturated solutions (figure 12); however, the decay is much faster, which can be attributed to the presence of oxygen in solution.

From initial applied potentials negative of the equilibrium potential (480 mV), it can be seen that there are two types of transients. At potentials negative of 200 mV the profiles involve two steps while positive of this potential the profiles change in a one step exponential manner. From an initial applied potential of –200 mV the two changing points occur at approximately 110 mV where the rate of change rapidly decreases and the second at approximately 200 mV, where the rate of change increases. These changing points are particularly interesting when compared with the cyclic voltammogram of the polymer shown in figure 17.
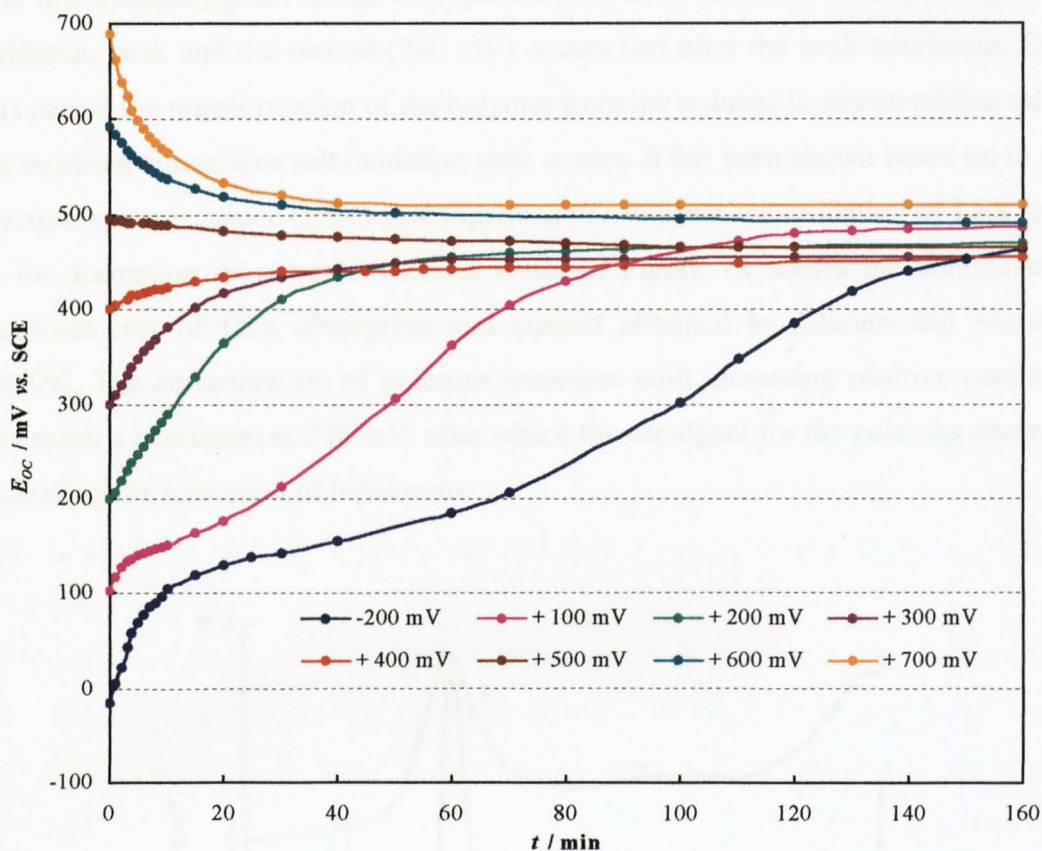
Figure 16 Open circuit behaviour of PANI in air equilibrated 1 mol dm^{-3} H$_2$SO$_4$ solution. PANI was polarised for 10 min at various potentials before opening circuit. Film thickness ~ 1.6 µm
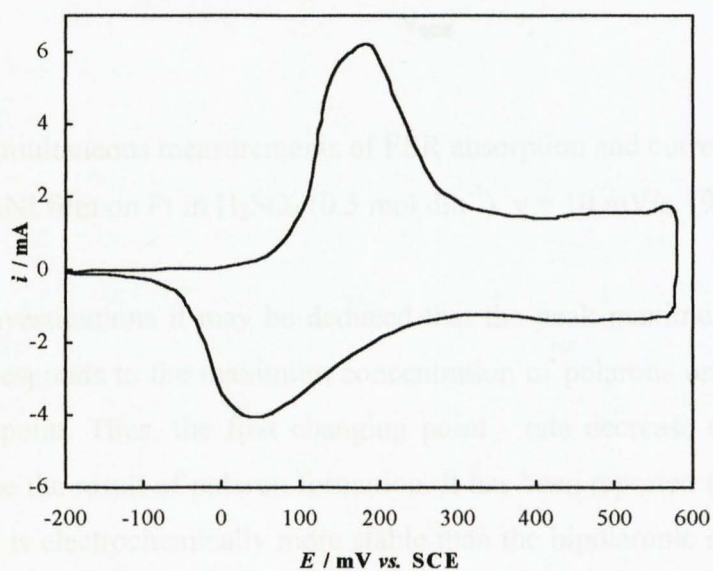
Figure 17 Cyclic voltammogram of the PANI film in H$_2$SO$_4$ (1 mol dm^{-3}) solution

The first changing point on the OCP profile (110 mV) occurs at the beginning of the oxidation peak and the second (200 mV) occurs just after the peak maximum. Over this period the transformation of the polymer from the reduced leucoemeraldine salt to the oxidised emeraldine salt oxidation state occurs. It has been shown based on *in situ* electron spin resonance (ESR) investigations [97-99] that the oxidation of LES leads to the formation of polarons (radical cations). Figure 18 shows the simultaneous measurements of ESR absorption and current obtained by Glarum and Marshall [98,99]. The concentration of polarons increases with increasing positive potentials and reach a maximum at 200 mV, after which the esr signal for the polarons decrease, indicating the formation of bipolarons.
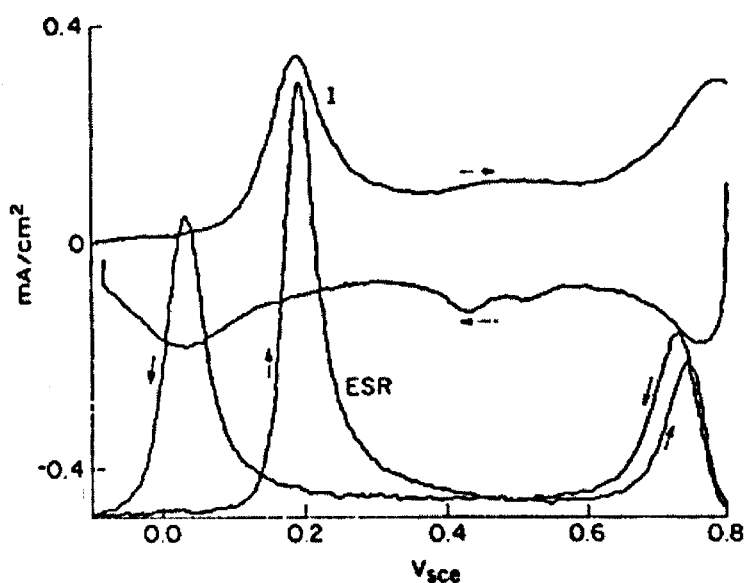
Figure 18 Simultaneous measurements of ESR absorption and current for a 100 nm PANI film on Pt in H_2SO_4 (0.5 mol dm^{-3}), v = 10 mV/s. [98-99]

From these investigations it may be deduced that the peak maximum at 185 mV in figure 17 corresponds to the maximum concentration of polarons on the PANI chain at any given point. Thus, the first changing point - rate decrease seen in the OCP profile must be the result of polaron formation. It has been reported that the polaronic state of PANI is electrochemically more stable than the bipolaronic state [100] which could account for the rate change and stabilisation of the OCP at 110 mV. Similar behaviour is observed from an initial applied potential of 100 mV, with maximum

gradients occurring at approximately 120 mV and again at around 200 mV. It is also interesting to note that the switching time at open circuit from initial applied potentials of –200 mV and 100 mV are also the slowest, reaching equilibrium after approximately 160 and 120 minutes respectively, in comparison to 40 minutes for all the other OCP profiles. The longer time scale suggests that the formation of polarons is the rate-determining step in the switching of the polymer at open circuit conditions.

As PANI is polarised at more positive potentials (200 mV, 300 mV, 400 mV) the profiles increase in an exponential manner and converge at approximately 460 mV after 50 minutes, the initial rate decrease is not observed. At these potentials the transformation of the polymer to the emeraldine salt state has occurred and the concentration of polarons decreases which could account for the one step exponential increase.

At an applied potential of 600 mV the same decay as 700 mV is observed, with the potential reaching equilibrium within 50 minutes. This is quite interesting as Stilwell and Park suggested that the degradation processes occurring at 700 mV brings about the shift in OCP [85], literature reports suggest that this is only relevant at potentials above 600 mV [47], thus it can be surmised that degradation processes occurring at 600 mV are minimal. To support this assumption, a slight negative shift is also observed after holding the potential at 500 mV. Thus, the possibility of degradation products causing a shift in the OCP can be discounted.

The result obtained in N_2 saturated H_2SO_4 electrolyte using the modified degassing technique *via* Na_2SO_3 solution (figure 15) suggests that the same profiles in air equilibrated H_2SO_4 would also be observed in N_2 saturated solutions with the only difference being the longer time scale of the experiment. Therefore the results reported by Stilwell and Park which have already been shown in figure 13 must be treated with scepticism. The question of what causes the change in OCP, however, still remains unanswered. The only fair assumption at this moment is that PANI must react with some species in solution or on the chain itself (disproportionation or comproportionation) for the switching process to occur. This is demonstrated better by the mathematical treatment of the transients in section 3.2.3.6.

3.2.3.5 OCP of PANI/SO_4^{2-} in N_2 saturated H_2SO_4 + Na_2SO_3

Figure 19 shows the OCP behaviour of PANI in N_2 saturated H_2SO_4 (1 mol dm^{-3}) + Na_2SO_3 (0.25 mol dm^{-3}) using the modified degassing technique (section 3.2.2).
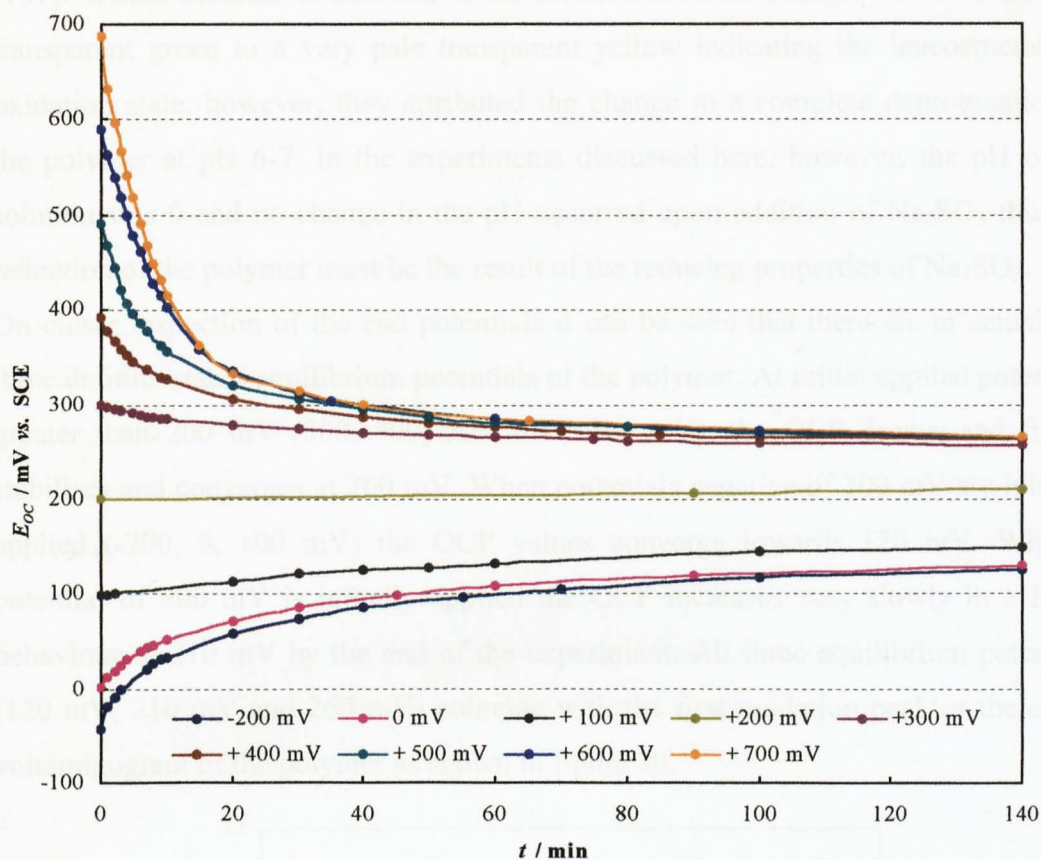
Figure 19 Open circuit behaviour of PANI in N_2 saturated 1 mol dm^{-3} H_2SO_4 + 0.25 mol dm^{-3} Na_2SO_3 solution. (Film thickness = 1.8μm)

The behaviour is quite different to PANI in air equilibrated H_2SO_4 and in N_2 saturated solutions. In general the profiles tend towards a modified equilibrium potential, which can be taken as 200 mV ± 60 mV, a shift of -280 mV in comparison to a solution without Na_2SO_3. Sodium sulfite is a moderately strong reducing agent, for this reason it is an excellent oxygen scavenger, but also could result in the reduction of the polymer.

The magnitude of the shift in the equilibrium potential is very similar to that of the standard electrode potential of the following redox reaction:

$$2H_2O + S_2O_6^{2-} \rightleftharpoons 2SO_4^{2-} + 4H^+ + 2e^- \qquad 0.22 \text{ V}$$
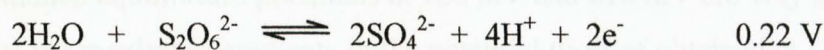
Huang and MacDiarmid have shown that a chemically prepared PANI film in the emeraldine salt state can be reduced by sodium dithionite ($Na_2S_2O_4$) solution (pH ~ 6)

[101]. Within seconds of addition of the solution the film changed colour from dark transparent green to a very pale transparent yellow indicating the leucoemeraldine oxidation state, however, they attributed the change to a complete deprotonation of the polymer at pH 6-7. In the experiments discussed here, however, the pH of the solution was 0 and no change in the pH occurred upon addition of Na_2SO_3 thus the reduction of the polymer must be the result of the reducing properties of Na_2SO_3.

On closer inspection of the end potentials it can be seen that there are in actual fact three definite stable equilibrium potentials of the polymer. At initial applied potentials greater than 200 mV (300, 400, 500, 600, 700 mV), the OCP decays and finally stabilises and converges at 260 mV. When potentials negative of 200 mV are initially applied (-200, 0, 100 mV) the OCP values converge towards 120 mV. When a potential of 200 mV is initially applied the OCP increases very slowly in a linear behaviour to 210 mV by the end of the experiment. All three equilibrium potentials (120 mV, 210 mV and 260 mV) coincide with the first oxidation peak of the cyclic voltammogram of the polymer as shown in figure 20.
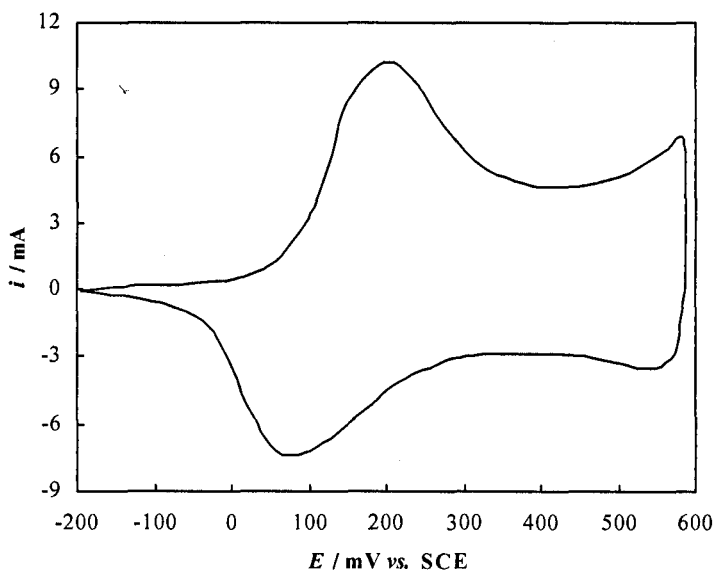
Figure 20 Cyclic voltammogram of the PANI film in H_2SO_4 (1 mol dm^{-3}) + Na_2SO_3 (0.25 mol dm^{-3}) electrolyte using modified degassing technique

The two attained equilibrium potentials at 120 mV and 210 mV are very similar to the positions of the maximum gradients in the potential profiles obtained at –200 mV and 100 mV in air equilibrated H_2SO_4 (figure 16). It can be seen that when the potential was initially polarised at –200 mV, the first 30 minutes of the profile are very similar

to the one observed in the profile of sulfite, until the first changing point in H_2SO_4 (120 mV). After this point, the profile is stable in Na_2SO_3 containing solution, whereas in a solution containing only H_2SO_4 the potential starts to increase. Clearly the formation of polarons is favoured in this system as the presence of sodium sulfite prevents the polymer from oxidising further.

The equilibrium potential of 210 mV is very stable and occurs near the peak maximum on the cyclic voltammogram (200 mV) which corresponds to PANI containing the maximum amount of polarons. The equilibrium potential of 260 mV occurs just after the peak maximum where the polymer contains less polarons. If all the transients are extrapolated it is estimated that the equilibrium potentials of 210 mV and 260 mV will converge after another 8 hours (10 hours in total), however, from the slope of the transients it is very doubtful if the lowest equilibrium potential of 180 mV will converge with the upper two equilibrium potentials. To validate this, the experiment would obviously have to be repeated for a longer time scale, which would be around 5 days, instead of the measured 140 minutes.

The observation of three different equilibrium potentials of PANI is in agreement with work carried out by Albery *et al.* [102] who proposed based on cyclic voltammogram and ESR studies that polymers like PANI can exist in two forms, α and β, in a "scheme of squares" approach. The α form is the stable conformation when the film is reduced but is metastable once the coat becomes oxidised. A different β form is the stable conformation when the polymer is oxidised. The authors propose that the transformation between the two forms is governed by first-order kinetics.

It is possible that the reduced form α corresponds to the equilibrium potential of 120 mV, and the oxidised form β corresponds to the equilibrium potential of 260 mV. The equilibrium potential of 210 mV could correspond to the metastable state proposed.

Many other models have been proposed for the redox switching kinetics of PANI. In 1984 Feldberg proposed a two state model for conducting polymers [103]. In his model he proposed that the change from one state to another took place according to the catastrophe theory. More recent models include the Hillman and Bruckenstein "scheme of cubes" [104] and the "scheme of hypercubes" [105], however the approach made by Albery *et al.* best suits the results described here. Clearly more work is needed to elucidate the different forms of the polymer and to understand the mechanism by which the polymer switch in degassed H_2SO_4 and in Na_2SO_3

containing H_2SO_4. *in situ* ESR and *in situ* IR experiments would be required in future experiments.

3.2.3.6 Origin of the potential transients at open circuit

In this section, an attempt is made to try and explain the shape of the potential transients. As previously mentioned, the reaction can be either due to the reaction of the polymer with a species in solution (such as oxygen), or due to a comproportionation or disproportionation reaction.

The system considered here is a surface redox couple in which one of the components can react with a species in solution. It is considered that the reaction is not diffusionally controlled.

(I)   Initial Conditions

The initial potential is E_i. For this potential, the surface concentrations of the oxidised (Ox) and reduced (R) components are Γ_{ox}^i and Γ_{red}^i respectively. The total concentration (surface) Γ_{total} (Γ_T)

$$\Gamma_{total} = \Gamma_{ox} + \Gamma_{red} \quad (e.g. \ \Gamma_{ES} + \Gamma_{LES}) \tag{1}$$

The electrode potential is assumed to follow the Nernst equation

$$E = E^\theta - \frac{RT}{nF} \ln \frac{\Gamma_{red}}{\Gamma_{ox}} \tag{2}$$

$$\therefore \quad E_i = E^\theta + \frac{RT}{nF} \ln \left(\frac{\Gamma_T - \Gamma_{red}^{(i)}}{\Gamma_{red}^{(i)}} \right) \tag{3}$$

(II)   Rate equation

The reaction considered is ;

$$R + X \xrightarrow{\ k\ } Ox \tag{4}$$

$$i.e. \ LES + X \xrightarrow{\ k\ } ES$$
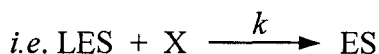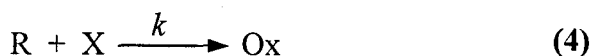
The reaction is totally irreversible and therefore;

$$\frac{-d\Gamma_R}{dt} = k\,\Gamma_R\,[X]^\infty \qquad (5)$$

This assumes no diffusional component

(5) can be directly integrated to give

$$\Gamma_R = \Gamma_R^{(i)}\,e^{-k[X]^\infty t} = \Gamma_R^{(i)}\,e^{-k't} \qquad (6)$$

where $k' = k[X]^\infty$

$[X]^\infty$ = bulk concentration

(III)   Time dependence of the potential at open circuit

(1), (2) and (6)

$$E = E^\theta + \frac{RT}{nF}\,\ln\left(\frac{\Gamma_T}{\Gamma_R} - 1\right) \;=\; E^\theta + \frac{RT}{nF}\,\ln\left(\frac{\Gamma_T}{\Gamma_R^{(i)}}e^{k't} - 1\right) \qquad (7)$$

At long times when $\dfrac{\Gamma_T}{\Gamma_R^{(i)}}e^{k't} \gg 1$,

$$E = E^\theta + \frac{RT}{nF}\,\ln\left(\frac{\Gamma_T}{\Gamma_R^{(i)}}\right) + \frac{RT}{nF}k[X]t \qquad (8)$$

At short times when $\dfrac{\Gamma_T}{\Gamma_R^{(i)}}e^{k't} \ll 1$,   ($e^x \approx 1 + x$)

$$E = E^\theta + \frac{RT}{nF}\,\ln\left[\left(\frac{\Gamma_T}{\Gamma_R^{(i)}} - 1\right) + k't\right] \qquad (9)$$

If the standing potential is <u>very</u> negative with respect to E^θ, $\Gamma_R^{(i)} \approx \Gamma_T$ and (9) becomes

$$E = E^{\theta} + \frac{RT}{nF} \ln\left(k[X]t\right) \qquad \textbf{(10)}$$

The solution of the potential with time (from 8 and 10) will follow (figure 21).
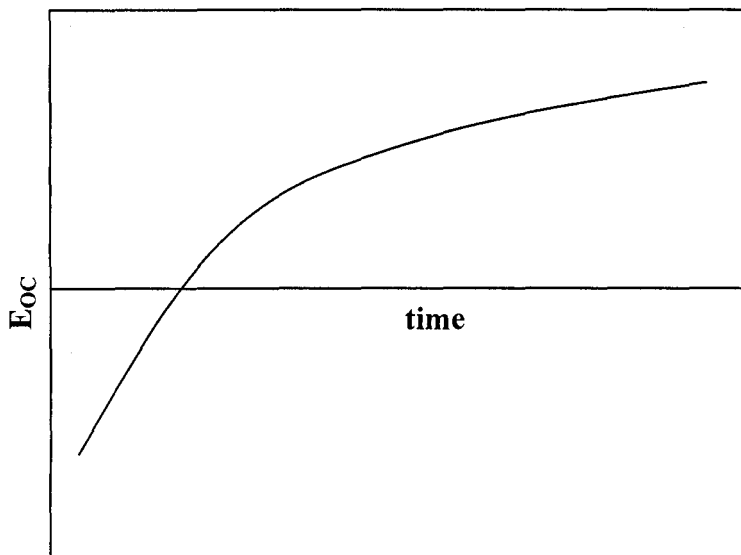
Figure 21 Solution of the potential with time (equations 8 & 10)

Note that the potential will tend to $+\infty$ as $t \to \infty$ since it was assumed that the chemical reaction (4) is irreversible. A final steady state potential will be predicted if the reverse of equation 4 is taken into account. However, it must be emphasised here that even though the nature of the polymer is known at the initial and final potentials, it is unclear as to the nature or indeed identity of the other reactants.

Armed with the knowledge about the behaviour of the OCP of PANI films, the chemical stability of such films is reported in the next section.

3.2.4 Long term stability of PANI and the overoxidation effect

For any application of PANI, its long term stability is of particular importance. The OCP measurements performed thus far suggest that PANI films are quite stable in the short term, *i.e.* the polymer reaches an equilibrium potential. The long term stability of the various films were investigated by cyclic voltammetry in air equilibrated solutions; in addition, the effect of applying a potential of 700 mV (overoxidation) was investigated.

Cyclic voltammograms of PANI/SO_4^{2-} coated polycrystalline platinum in H_2SO_4 (1 mol dm^{-3}) recorded over 72 hours are shown in figure 22.
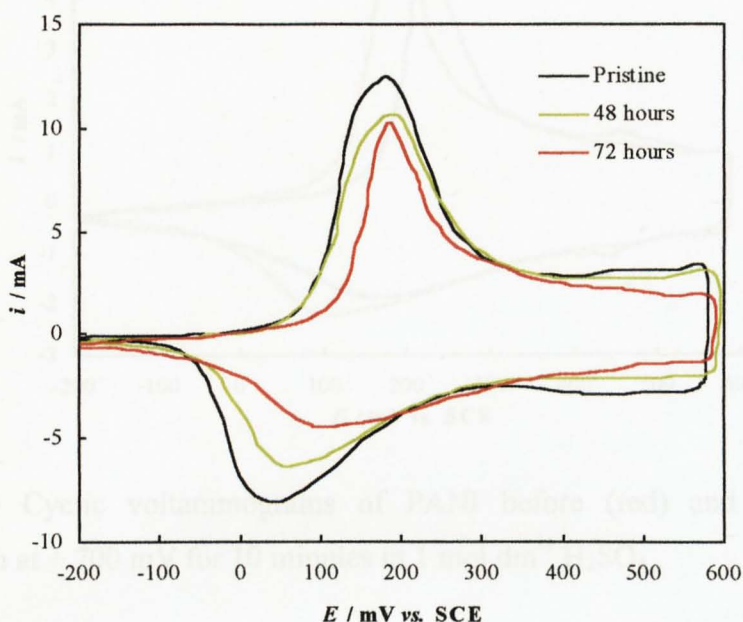
Figure 22 Cyclic voltammograms of PANI/SO_4^{2-} in 1 mol dm^{-3} H_2SO_4.
Film thickness ~ 1.6 μm

As can be seen, over 3 days the intensity of the peak corresponding to the switching reaction is reduced and a 40 % decrease in coulombic capacity occurs, which clearly corresponds to the degradation of the polymer. LaCroix and Diaz [67] and Pasquali *et al.* [106] have observed the instability of PANI on polycrystalline Pt in H_2SO_4 (1 mol dm^{-3}) solution. At room temperature LaCroix and Diaz [67] reported a positive shift in the open circuit potential to 0.65 V within an hour but reported no loss of coulombic capacity; this is particularly interesting as the OCP of the polymers in this study showed good stability. In a study on the storage characteristics of electrochemically prepared PANI in 1 mol dm^{-3} H_2SO_4 + 0.5 mol dm^{-3} Na_2SO_4 Pasquali *et al.* reported that degradation proceeded at room temperature only after several hours which seems to be in agreement with this work [106]. In addition the authors also observed a decrease in coulombic capacity over time.

As can be seen in figure 23, the extent of degradation increases when the polymer is subjected to a constant potential of 700 mV for 10 minutes
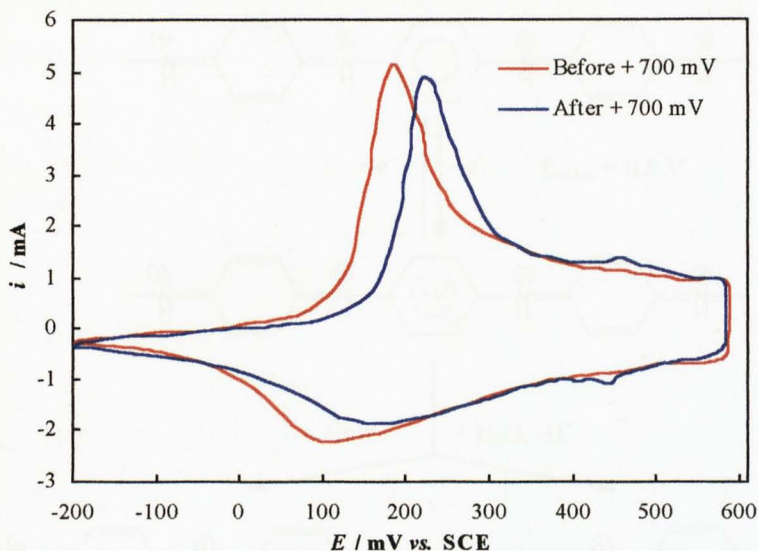
Figure 23 Cyclic voltammograms of PANI before (red) and after (blue) polarisation at + 700 mV for 10 minutes in 1 mol dm^{-3} H$_2$SO$_4$

As can be seen, an irreversible change in the voltammogram occurs which points to the degradation effect of PANI. Features of degradation are given by the reduced coulombic capacity (further 10 % loss), shifted PANI oxidation – reduction peaks and the appearance of a redox couple at 450 mV which can be attributed to the benzoquinone / hydroquinone (BQ/HQ) redox couple. BQ and HQ are degradation products of PANI [37,38]. It is well known that, particularly in acidic solutions, PANI films are susceptible to dissolution processes at potentials greater than 650 mV *versus* SCE [47]. The principal product is thought to be soluble benzoquinone (BQ) [32,47,85,107] which has been detected in solution by ring-disc studies [85,107], spectrophotometry [47,65,85] and by comparison of the new cyclic voltammetric peak which appears at *ca*. 500 mV *versus* SCE, with the redox peaks of the BQ/HQ couple when it is added intentionally into solution. Other insoluble degradation products have been suggested to remain on the electrode surface, including PANI strands containing quinoneimine end groups [32,85] and ortho-coupled polymers [65].

On the basis of these data and results of electrooxidation of aniline in acidic solutions, obtained by Hand and Nelson [108,109], Yonemana and co-workers suggested the following scheme for PANI oxidative degradation [47]:

88
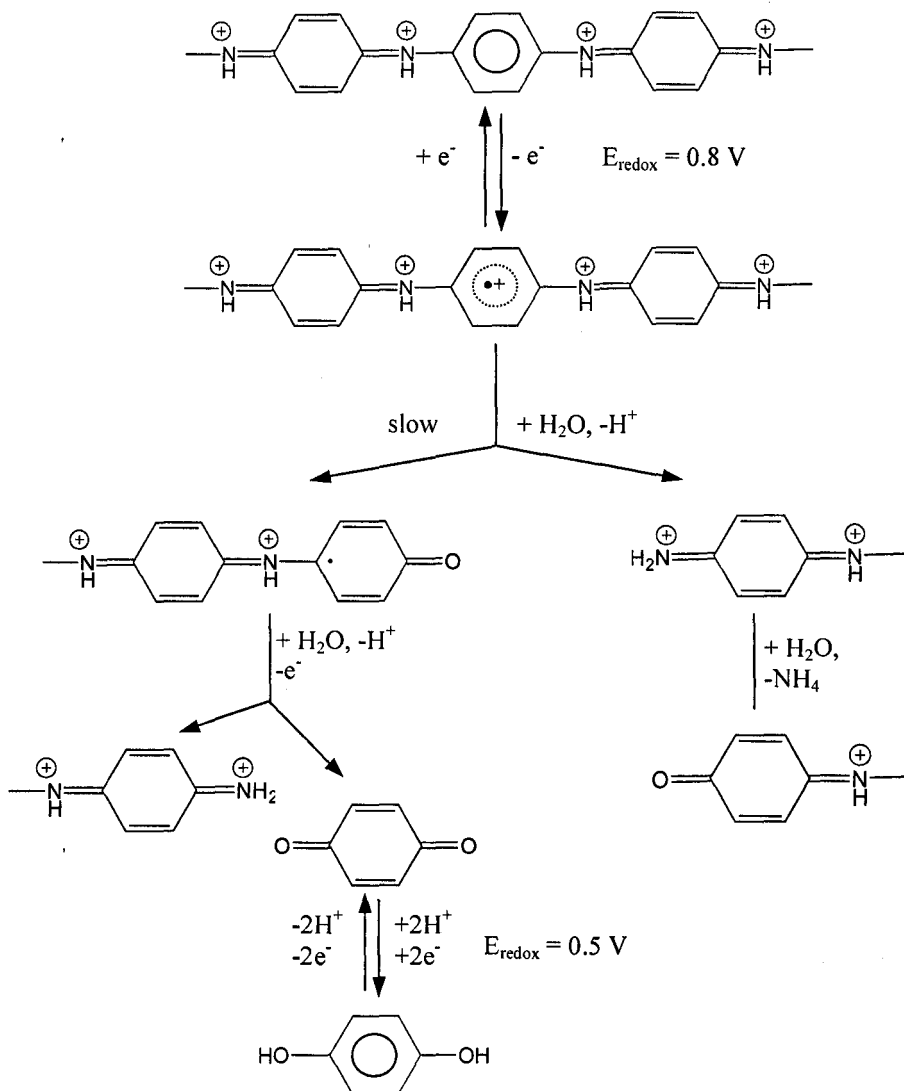
Figure 24 Proposed reaction scheme for oxidative degradation of PANI [47]

In addition to the appearance of the BQ/HQ redox couple and in agreement with the results reported here Dinh *et al.* [38] have also reported a shift in the PANI redox peaks. Whereas the data reported here show that the anodic peak shifts positive by 40 mV after holding the potential at 700 mV for 10 minutes, Dinh *et al.* reported a peak shift of *ca.* 100 mV after holding for 30 minutes at a similar potential for a similar film thickness. A relationship between the extent of degradation and the holding time was confirmed by ellipsometric measurements together with an increase in film porosity and film thinning. The irreversible change in the voltammogram was suggested to be the consequence of the development of a new polymer phase, perhaps having a PANI skeleton interspersed by quinoneimine groups or a cross-linked

polymer consisting of PANI and benzoquinone. This seems to be in agreement with the early work carried out by Kitani [98] and Bruners et al. [110] who believed that irreversible conversion of PANI could be connected with crosslinking between linear polymer chains, leading in the end to its insolubility and decrease in electrical activity.

According to Batich et al. [111] PANI degradation is seen more distinctly, not under conditions of cyclic voltammetry, but in the potentiostatic mode, under which PANI degradation at 500 mV in 1 mol dm^{-3} H$_2$SO$_4$ was registered. In a recent report Mažeikienè et al. [100] indicated that the degradation of PANI in H$_2$SO$_4$ (0.5 mol dm^{-3}) proceeds at a remarkable rate over a wide potential range, even as low as 300 mV, although the rate of electrochemical degradation in the low potential region appeared to be one or two orders of magnitude less. Okamoto and Kotaka [112] noted that the degradation proceeds faster at higher anodic potentials (800 mV), although no degradation was reported for lower potentials. Mažeikienè et al. suggested that the fast degradation observed at higher electrode potentials could be attributed to the higher rate of degradation of the bipolaronic form, which is predominant in this potential region [100]. At lower electrode potentials, a polaronic form of PANI dominates resulting in slower degradation, probably due to the higher electrochemical stability of the polymer

The observation of film instability at higher anodic potentials is consistent with those of other groups that have observed a decay in the electrochemical response for PANI [32,38,85,100,107-112] however only few reports are in agreement with the observations of film instability at open circuit [106]. Reports on the open circuit stability of PANI in acidic media are scarce and of the reports published there remain key disagreements. According to Stilwell and Park, PANI hydrolysis in a sulfuric solution is only significant in the high oxidation state and ceases at open circuit [85]. Clearly the observations reported here and those of Pasquali et al. [106] contradict those of Stilwell and Park [85]. According to Stilwell and Park's scheme for PANI degradation [85], oxidation is a necessary prerequisite and this can only take place if the circuit is closed. They propose that at open circuit, an equilibrium is set up between the potential of PANI and that of benzoquinone (~ 500 mV vs. SCE), which stops degradation. Pasquali et al. dismiss this and they propose that PANI oxidation in nonhermetically sealed vessel can be triggered and nourished by dissolved oxygen. So an equilibrium can hardly be reached, also oxygen in solution could reoxidise

hydroquinone formed by the reduction of benzoquinone, the latter could, in turn, act as an oxidising agent towards PANI.

Interesting behaviour of the long term stability and overoxidation effect were obtained for PANI films in HCl electrolyte. The cyclic voltammograms of PANI/SO_4^{2-} coated polycrystalline platinum in HCl (1 mol dm^{-3}) recorded over 39 days are shown in figure 25.
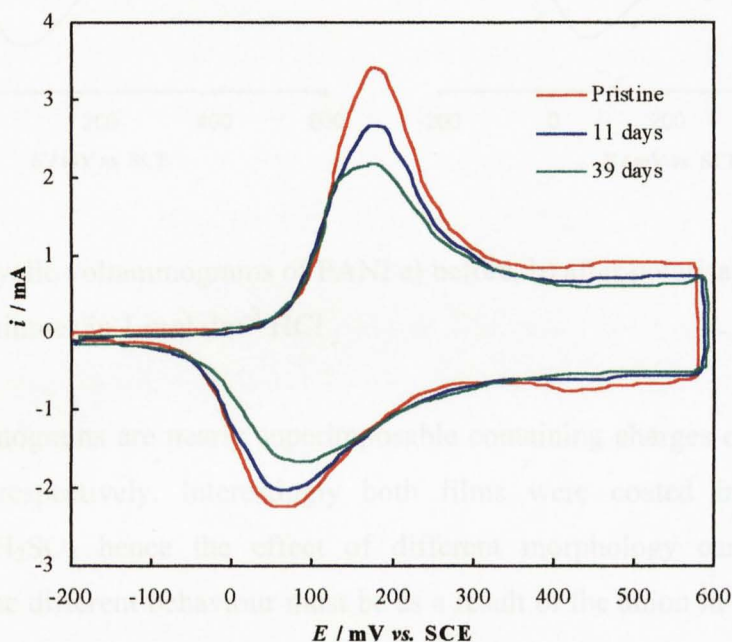
Figure 25 Cyclic voltammograms of PANI/SO_4^{2-} in 1 mol dm^{-3} HCl over time
Film thickness ~ 0.4 μm

As can be seen, the PANI film is much more stable in HCl electrolyte. Over a period of 39 days a 20 % loss in coulombic capacity is observed compared to a 40 % loss in 4 days in H_2SO_4 electrolyte. The effect of applying 700 mV on the electrochemistry of a PANI/SO_4^{2-} coated film in 1 mol dm^{-3} HCl is shown in figure 26, and as can be seen, the polymer retains its electroactivity completely which is in contrast to the previous film in H_2SO_4.

91
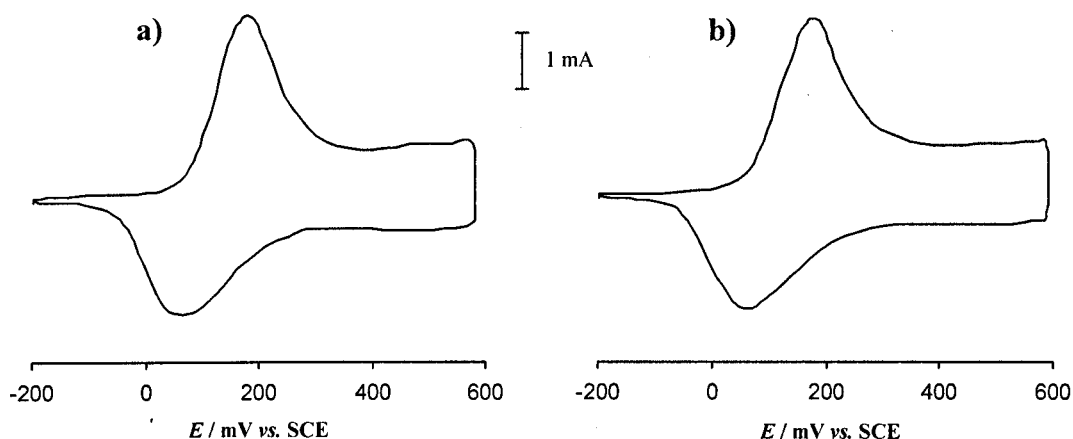
Figure 26 Cyclic voltammograms of PANI a) before, b) after polarisation at + 700 mV for 10 minutes in 1 mol dm^{-3} HCl

The voltammograms are nearly superimposable containing charges of 13.55 mC and 13.45 mC respectively. Interestingly both films were coated in an electrolyte containing H_2SO_4 hence the effect of different morphology can be ruled out. Therefore, the different behaviour must be as a result of the anion in solution. Clearly the presence of the sulfate anion promotes the degradation at open circuit and at increased applied potentials (700 mV). Considerable irreversible changes have been reported for PANI in HCl (1 mol dm^{-3}), albeit at an applied potential of 800 mV [53,110]. Tang *et al.* attributed the behaviour to the "anion effects" [59]. They reported that PANI degradation is dependent on the anion present in solution for the oxidation, but independent of the anion present in the growth solution of the polymer film. The anion in solution accelerated the degradation of PANI in the order H_2SO_4 > HCl > HClO$_4$. It is worthwhile noting that the anion promotes the growth of PANI and the overoxidation of PANI in the same order. A similar effect was observed by Lippe and Holze [113]. In perchloric acid the shape of the voltammogram was barely changed compared with the voltammograms recorded earlier at an anodic potential limit of 300 mV. In the presence of H_2SO_4, however, the PANI film was completely overoxidised at the high potentials. They deduced that the anion effect in the overoxidation of PANI originates primarily from the specific interaction between the anions and the charge carriers, the bipolarons, which results in a different stability of the PANI-acid complexes.

Some researchers have tried to explain the strong promoting effect of sulfate anions on electrochemical degradation of PANI. Stilwell and Park proposed that sulfate anions may catalyse the hydrolysis reaction of PANI whereas chloride anions do not [114]. They suggested the formation of intermediate species involving SO_4^{2-} and HSO_4^- to account for catalytic effects of sulfate ions. Park suggested that the greater stability of PANI in HCl in comparison to H_2SO_4 could be due to the fact that Cl^- is the weakest base [40]. Alternatively, Lippe and Holze [113] have proposed a shielding model: perchlorate ions shield the bipolarons from nucleophilic attack by either OH^- ions or H_2O molecules much better than sulfate ions do, because sulfate ions cannot shield the two positive charges of each bipolaron as efficiently as in the case of two perchlorate ions, which is illustrated in figure 27. However, no suitable explanation was suggested for their results with chloride and nitrate ions. Nonetheless, the shielding model remains an interesting approach to understanding the different anion-specific effects.
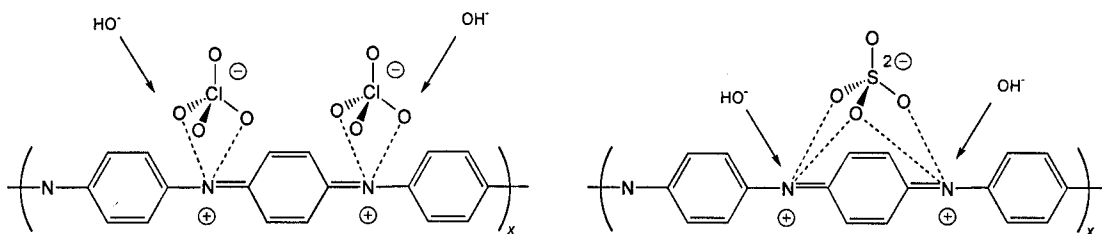
Figure 27 Illustration of the shielding effect that different anions can have on the nucleophilic attack of OH^- ions at bipolaron sites on a PANI chain

It is possible that the greater degree of hydration of the chloride ion, which makes it a larger anion in comparison to the HSO_4^- ion, could result in the Cl^- behaving in a similar way to the ClO_4^- complex limiting the approach of hydroxyl ions to the reactive sites. The observed "anion effects" may also be explained by considering the Hofmeister series of anions, which represents their lyophilicity [86],

$$ClO_4^- > SCN^- > I^- > NO_3^- > Br^- > Cl^- \gg HCO_3^- \sim OAc- \sim SO_4^{2-} \sim HPO_4^{2-}$$
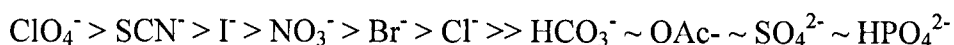
That is, perchlorate ions are the most lyophilic while sulfate ions are the most hydrophilic, thus attracting nucleophilic constituents like OH^- and H_2O. For this

reason, it has been reported that perchlorate anions are expected to form the most stable ion pairs with anilinium ions [86], likewise it may also be surmised that such affinity persists even in PANI [65]. Therefore the Hofmeister series can be correlated to the stability of the polymer which is in agreement with the observed instability in H_2SO_4 compared to HCl. Choi *et al.* also linked the Hofmeister series of anions with the different morphologies observed in various acids, the origin of the differences attributed to the strength of ion-pairs [86]. Like the explanations available in the literature further investigations need to be performed to confirm the origin of the greater stability in the PANI-Cl$^-$ complex.

A dramatic improvement in the long term stability of PANI in H_2SO_4 was observed when the solution contained Na_2SO_3 (0.25 mol dm^{-3}). The cyclic voltammograms over 3 days are shown in figure 28.
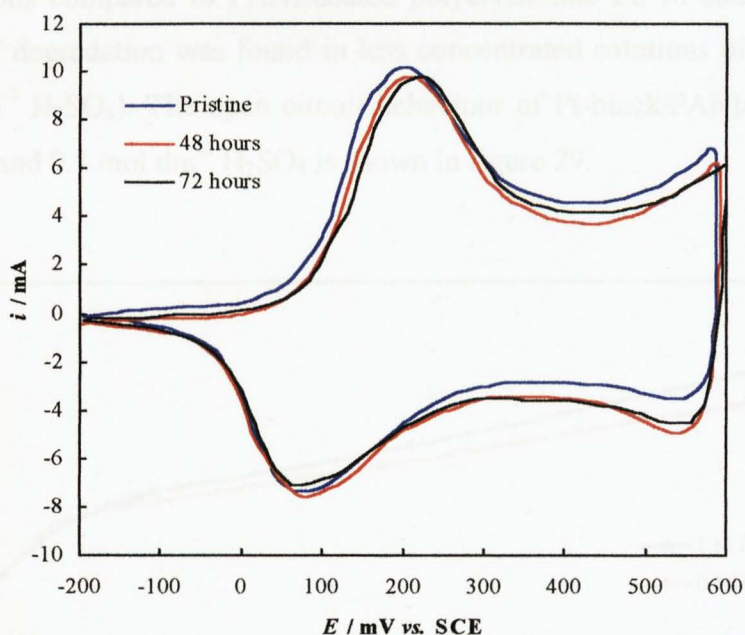
Figure 28 Cyclic voltammograms of PANI/SO$_4^{2-}$ over time in 1 mol dm^{-3} H_2SO_4 + 0.25 mol dm^{-3} Na_2SO_3. Film thickness ~ 1.8 μm

Over a period of 72 hours only a 1.4 % decrease in the coulombic charge is observed. As the decrease is so small it is debatable whether in fact the change is due to degradation processes. It is possible that the increased stability is due to the adjusted equilibrium potential of the polymer in a solution containing Na_2SO_3. As shown previously the equilibrium potential for PANI in a solution containing Na_2SO_3 is shifted negatively to approximately 200 mV in comparison to PANI in a solution

containing just the acid, which is approximately 500 mV. The adjusted equilibrium favours the polaronic form of the polymer which has been previously shown to be more stable than the bipolaronic form.

Even though the results discussed so far have revealed interesting information about the stability of PANI films, it must be remembered that in fuel cell-based sensors, the electrode material is Pt-black, which exhibits different reactivity when compared with Pt. The behaviour and stability of PANI films coated on Pt-black are discussed in the following section.

3.2.5 Long term stability and open circuit behaviour of PANI-coated Pt-black
3.2.5.1 Pt-black/PANI/SO$_4^{2-}$

The degradation of PANI/SO$_4^{2-}$ coated Pt-black is much more rapid in H$_2$SO$_4$ (1 mol dm^{-3}) solutions compared to PANI-coated polycrystalline Pt. In addition, a similar rapid rate of degradation was found in less concentrated solutions of the electrolyte (0.1 mol dm^{-3} H$_2$SO$_4$). The open circuit behaviour of Pt-black/PANI/SO$_4^{2-}$ in 1 mol dm^{-3} H$_2$SO$_4$ and 0.1 mol dm^{-3} H$_2$SO$_4$ is shown in figure 29.
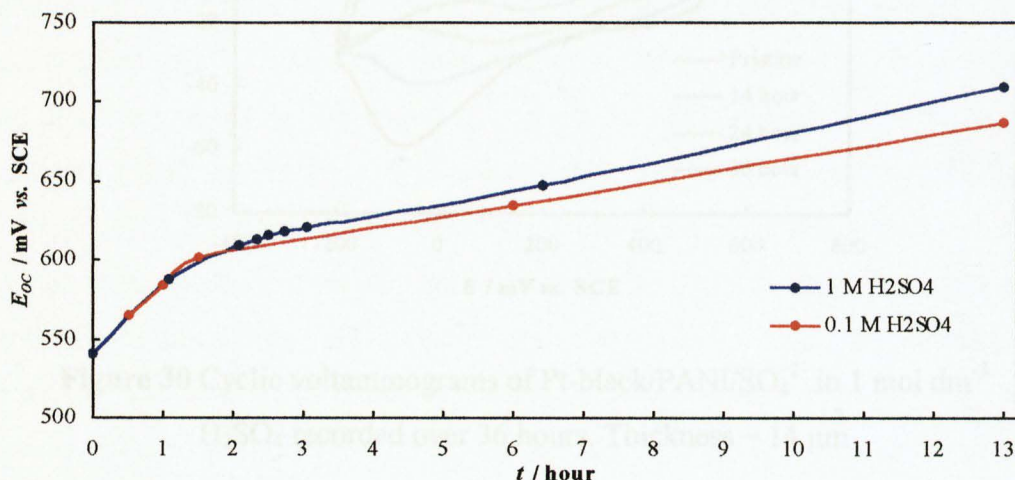
Figure 29 Open circuit behaviour of Pt-black PANI/SO$_4^{2-}$ in 1 mol dm^{-3} H$_2$SO$_4$ ~ 14 μm thick and 0.1 mol dm^{-3} H$_2$SO$_4$ ~10 μm thick, over 13 hours. Initial applied potential = −200 mV

Freshly prepared films on Pt-black exhibit a redox behaviour which is typical of that of a pristine film in that the initial potential at open circuit is 540 mV. However, as

can be seen, a rapid increase in the open circuit potential occurs over a relatively short period of time, reaching 710 mV after 13 hours in 1 mol dm^{-3} H$_2$SO$_4$ and 690 mV for a similar film in 0.1 mol dm^{-3} H$_2$SO$_4$. As described previously, potentials above 600 mV *vs.* SCE are clearly outside the redox threshold for stable PANI [47]. At these increased potentials, hydrolysis reactions take place leading to the formation of degradation products, which have the effect of further catalysing the degradation of the PANI film. Such high OCP values were not observed in studies on PANI-coated polycrystalline Pt films.

The extent of degradation is shown more clearly in the cyclic voltammograms in figure 30. Over a period of 36 hours there is a 60 % decrease in the coulombic capacity of the film with little or no change in colour during the switching reaction.
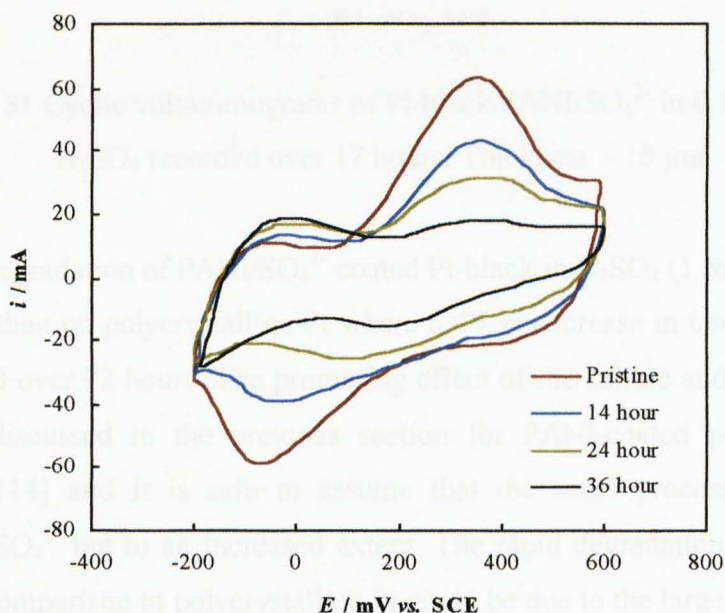
Figure 30 Cyclic voltammograms of Pt-black/PANI/SO$_4^{2-}$ in 1 mol dm^{-3} H$_2$SO$_4$ recorded over 36 hours. Thickness ~ 14 μm

The same effect was also observed in 0.1 mol dm^{-3} H$_2$SO$_4$, as shown in figure 31, where over a period of 17 hours a 46 % decrease in the coulombic capacity of the film was observed.
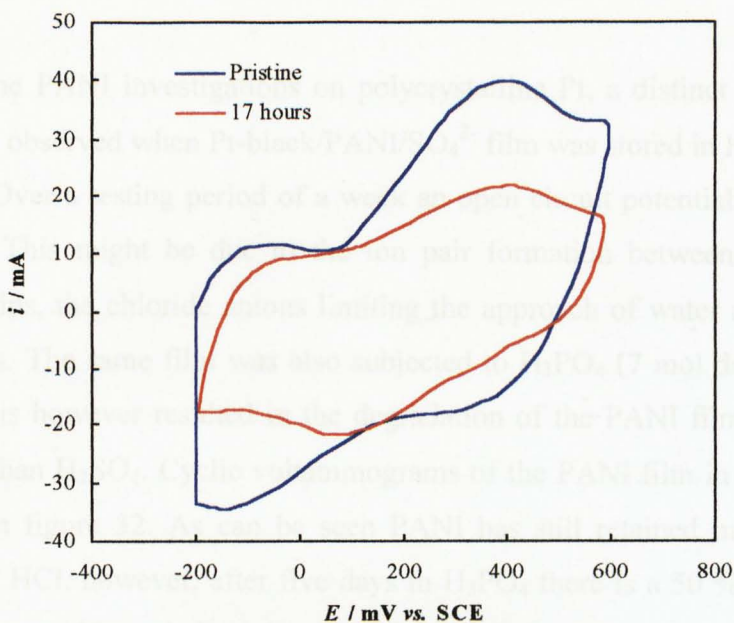
Figure 31 Cyclic voltammograms of Pt-black/PANI/SO_4^{2-} in 0.1 mol dm^{-3}
H_2SO_4 recorded over 17 hours. Thickness ~ 10 µm

The rate of degradation of PANI/SO_4^{2-} coated Pt-black in H_2SO_4 (1 & 0.1 mol dm^{-3}) is much faster than on polycrystalline Pt where a 40 % decrease in coulombic capacity was observed over 72 hours. The promoting effect of the sulfate and bisulfate anions have been discussed in the previous section for PANI-coated polycrystalline Pt electrodes [114] and it is safe to assume that the same process occurs for Pt-black/PANI/SO_4^{2-} but to an increased extent. The rapid degradation of PANI-coated Pt-black in comparison to polycrystalline Pt could be due to the large surface area and highly porous morphology of the film as shown in figure 9, section 3.1.6. Zhang *et al.* report that polymer degradation is promoted in this open structure [65], which imposes little restriction to the polymer interior by any solution constituents, as compared to a PANI film grown in perchloric acid or hydrochloric acid, which render a more compact structure that is more resistant to polymer degradation.

MacDiarmid *et al.* have reported that the electrochemistry of PANI is highly reversible when the pH of H_2SO_4 is carefully controlled [115], especially if the pH is greater than zero, more preferably, between about 2 and 10 and still more preferably between about 2 and 6. Retention of coulombic efficiency, capacity and stability was observed. In the results shown here severe degradation is still observed when the pH is changed from 0 to 1, The extensive degradation at pH 1 suggests that changing the

pH to the limits suggested by MacDiarmid *et al.* will not stop the degradation of the polymer.

Similar to the PANI investigations on polycrystalline Pt, a distinct improvement in stability was observed when Pt-black/PANI/SO_4^{2-} film was stored in HCl (1 mol dm^{-3}) electrolyte. Over a testing period of a week an open circuit potential of 540 mV was maintained. This might be due to the ion pair formation between the anions and polymer chains, the chloride anions limiting the approach of water molecules to the reactive sites. The same film was also subjected to H_3PO_4 (7 mol dm^{-3}) solution for few days; this however resulted in the degradation of the PANI film, but at a much slower rate than H_2SO_4. Cyclic voltammograms of the PANI film in HCl and H_3PO_4 are shown in figure 32. As can be seen PANI has still retained most of its redox properties in HCl, however, after five days in H_3PO_4 there is a 50 % decrease in the switching charge. Nevertheless the rate of degradation in H_3PO_4 is slower than in H_2SO_4 which exhibited a loss of 60 % in switching charge after only 36 hours.
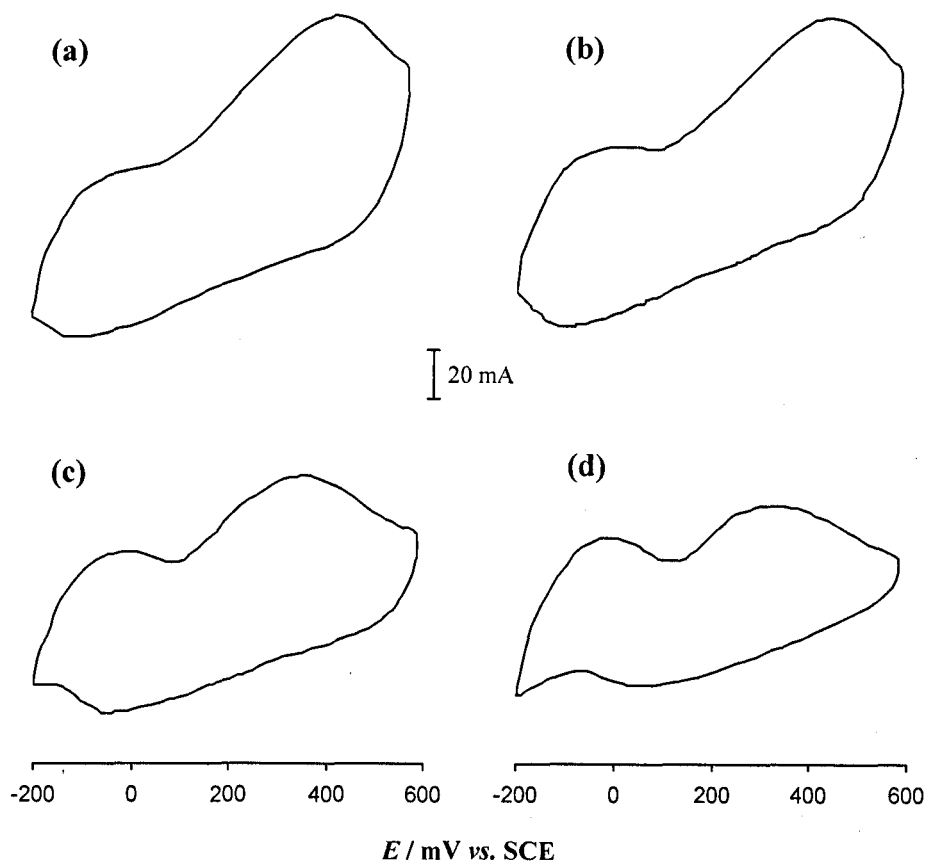
Figure 32 Cyclic voltammograms of Pt-black/PANI/SO_4^{2-} recorded over time in different acids (a) pristine condition 1 mol dm^{-3} HCl (b) 7 days 1 mol dm^{-3} HCl, (c) 7 days 1 mol dm^{-3} HCl + 4 days 7 mol dm^{-3} H_3PO_4 (d) 7 days 1 mol dm^{-3} HCl + 15 days 7 mol dm^{-3} H_3PO_4. Thickness ~ 14 µm

The results discussed so far show that the rate of degradation of Pt-black/PANI/SO$_4$$^{2-}$ in acidic solutions can be related to the anions and occurs in this order;

$$Cl^- < HPO_4^{2-} < SO_4^{2-}$$

which is similar to the Hofmeister series of anions [86] discussed in section 3.2.4 The chloride anion is the most lyophilic in the series used here and thus has a greater ion pair stability.

Figure 33 shows the open circuit behaviour of the same PANI/SO$_4$$^{2-}$ film in various acids over a period of 12 hours.
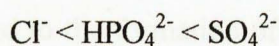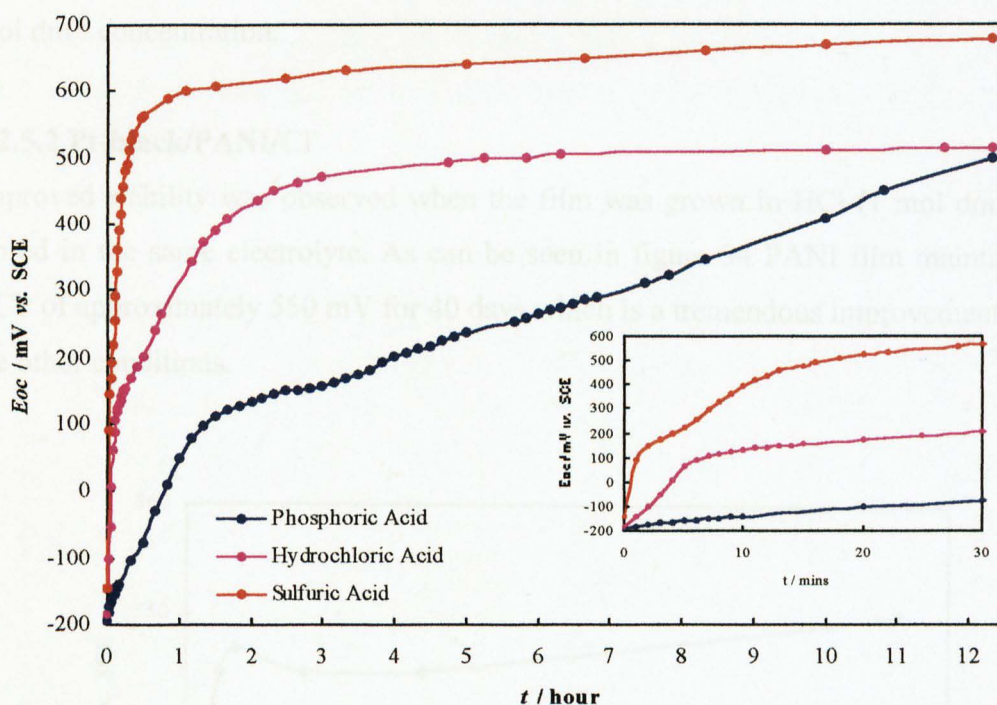
Figure 33 Open circuit behaviour of Pt-black/PANI/SO$_4$$^{2-}$ in H$_2$SO$_4$ (1 mol dm^{-3}), HCl (1 mol dm^{-3}) and H$_3$PO$_4$ (7 mol dm^{-3}); inset - first 30 minutes of profiles.

The time taken to reach a stable equilibrium potential increases in the order H$_2$SO$_4$, HCl, H$_3$PO$_4$. The OCP slopes of PANI/SO$_4$$^{2-}$ in H$_2$SO$_4$ and H$_3$PO$_4$ between 2 and 12 hours suggests that degradation reactions still occur as the potential shifts slowly towards positive values. The OCP in HCl on the other hand is much more stable, possibly owing to the stabilising effect of the ion pairs as proposed by Zhang *et al.*

[65] and Choi *et al.* [86]. A main changing point at approximately 100 mV is seen on all the profiles; it is clearly seen in H_3PO_4 but is also clear in the other acids when looking at the inset which shows the first 30 minutes of the profiles. This is consistent with the OCP investigations on PANI-coated polycrystalline Pt where it was proposed that the rate change was related to the formation of polarons on the PANI chain. On PANI-coated polycrystalline Pt the changing point correlated to the start of the PANI oxidation peak, however on Pt-black the same correlation is not observed as the peak occurs at 400 mV. From an experimental point of view this is not surprising as the polymer was extremely thick (14 μm), consequently introducing *i*R effects to the electrochemical response.

The OCP profile in H_3PO_4 is particularly interesting as the rate of change is extremely slow, this could be the effect of excess anions in the electrolyte as the acid was in 7 mol dm^{-3} concentration.

3.2.5.2 Pt-black/PANI/Cl⁻

Improved stability was observed when the film was grown in HCl (1 mol dm^{-3}) and stored in the same electrolyte. As can be seen in figure 34 PANI film maintains an OCP of approximately 550 mV for 40 days which is a tremendous improvement on all the other conditions.
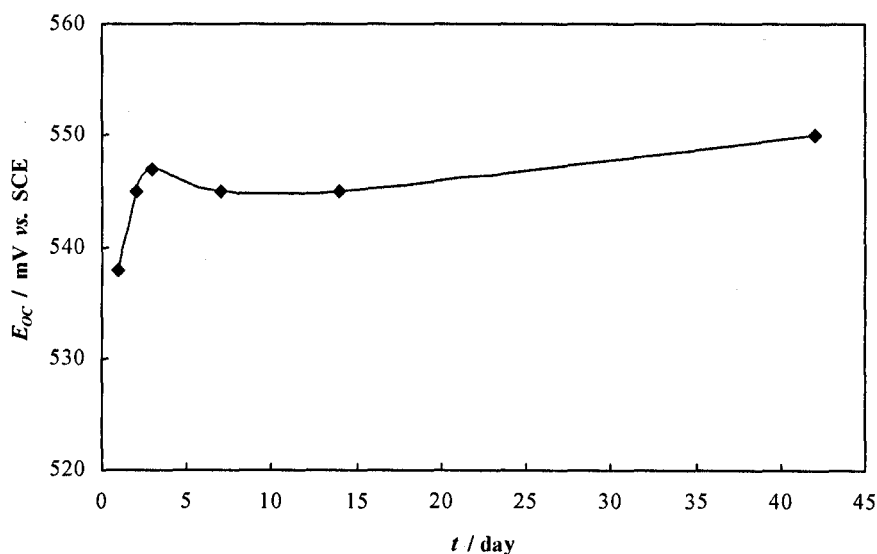
Figure 34 Open circuit behaviour of Pt-black/PANI/Cl⁻ in air equilibrated 1 mol dm^{-3} HCl; Experiment performed over 42 days. Thickness ~ 12 μm

The stable behaviour can be attributed to the compact morphology of the PANI/Cl⁻ film in comparison to the extremely porous morphology of the PANI/SO_4^{2-} polymer. The morphologies of both are described in more detail in section 3.1.6, and a distinct difference is noted. A compact polymer structure has been shown to be more resistant to polymer degradation as it restricts nucleophilic constituents to the polymer interior [65]. Even though the film displays a stable open circuit equilibrium potential, the cyclic voltammograms performed over this period show signs of marked degradation and are shown in figure 35a. A reduction in charge from 372 mC to 136 mC is observed, which corresponds to a 63 % decrease in the coulombic capacity of the polymer. However, the redox behaviour of the polymer remains intact, as can be seen in figure 35b. Also the polymer displayed the characteristic change in colour associated with the switching of PANI. This is notably different to the Pt-black/PANI/SO_4^{2-} film stored in H_2SO_4 which demonstrated a fast degradation accompanied by a severe loss of redox properties as shown by the voltammograms over time (figure 30) and in addition the loss of its electrochromic property.
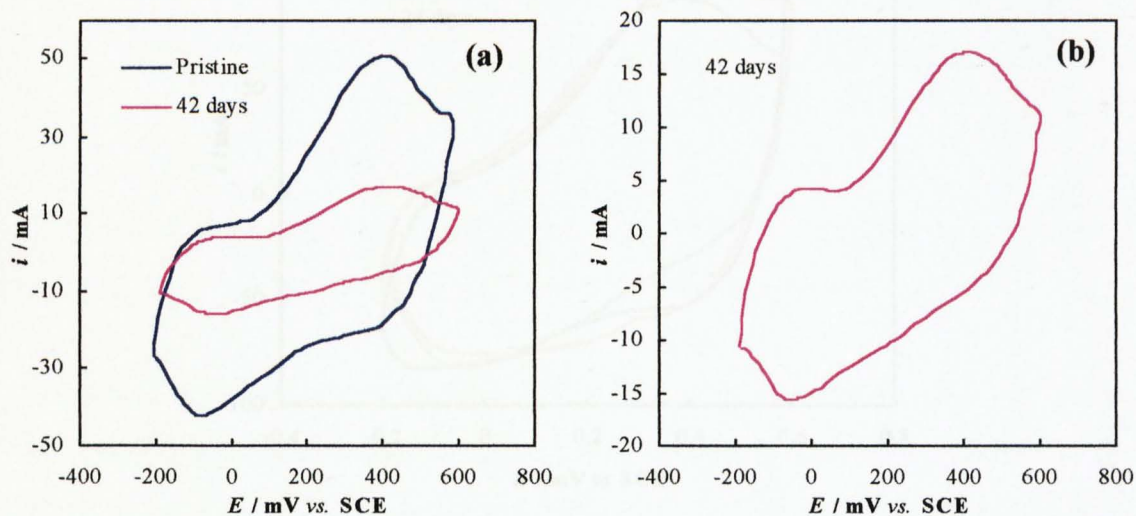
Figure 35 Cyclic voltammograms of Pt-black/PANI/Cl⁻ performed (a) before and after storage in HCl for 42 days (b) expanded view of the PANI voltammogram after 42 days. Thickness in pristine condition ~ 12 μm

101

The observed degradation suggests that nucleophilic constituents attack the active sites of the polymer exterior, be it over a long period of time compared to PANI in H_2SO_4 or H_3PO_4; however, the stable OCP and retention of the redox properties suggest that the polymer still contains active sites which are protected from nucleophilic attack, these are most probably located in the polymer interior.

3.2.5.3 Pt-black/PANI/SO$_4^{2-}$ in Na$_2$SO$_3$

In agreement with the previous work on polycrystalline Pt in H_2SO_4 (1 mol dm^{-3}) + Na$_2$SO$_3$ (0.25 mol dm^{-3}) increased stability was also observed for Pt-black/PANI/SO$_4^{2-}$ in the same electrolyte. Figure 36 shows the cyclic voltammograms recorded over time, and as can be seen, the difference to a solution just containing the acid is astounding; over a period of 24 days a decrease of only 10 % in the coulombic capacity is observed compared to a solution containing just the acid which lost 46 % of the coulombic capacity in 17 hours.
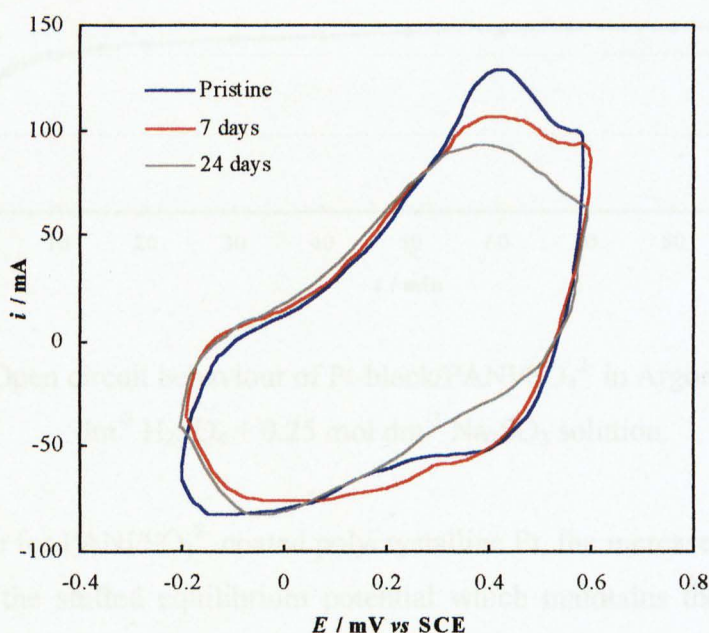
Figure 36 Cyclic voltammograms of Pt-black/PANI/SO$_4^{2-}$ over time in N$_2$ saturated 1 mol dm^{-3} H$_2$SO$_4$ + 0.25 mol dm^{-3} Na$_2$SO$_3$ Thickness ~ 26 µm

In view of the improved stability, the open circuit behaviour at different applied potentials was investigated. Figure 37 shows the effect of applying an initial potential on the OCP behaviour. As can be seen, the OCP profiles are very similar to the ones obtained for PANI-coated polycrystalline Pt under the same conditions. In this case

the equilibrium potential is approximately 100 mV. It is clear from the OCP profiles that the equilibrium potentials observed do not correlate well with the cyclic voltammograms of the polymer, however this effect is most probably a result of iR drop in the thick film on Pt-black.
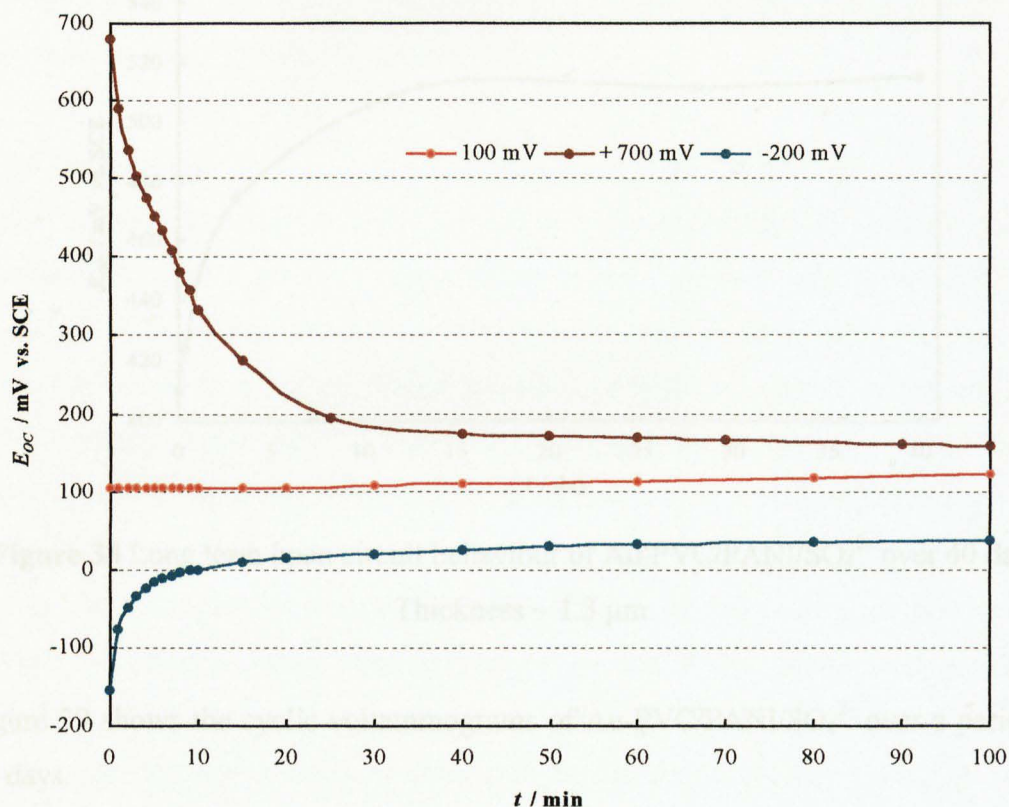
Figure 37 Open circuit behaviour of Pt-black/PANI/SO$_4^{2-}$ in Argon purged 1 mol dm^{-3} H$_2$SO$_4$ + 0.25 mol dm^{-3} Na$_2$SO$_3$ solution.

As in the case for PANI/SO$_4^{2-}$ coated polycrystalline Pt, the increased stability can be attributed to the shifted equilibrium potential which maintains the polymer in the more stable polaronic form, rather than the unstable bipolaronic form which is more liable to nucleophilic attack.

3.2.5.4 PANI-coated Au-PVC

Increased stability of the polymer was also observed when the substrate was changed, figure 38 shows the OCP behaviour of Au-PVC/PANI/SO$_4^{2-}$ in air equilibrated H$_2$SO$_4$ (1 mol dm^{-3}) over 40 days. When the film is in pristine condition an equilibrium potential of 410 mV is observed, over the next 13 days the potential slowly increases

to 510 mV and is maintained for the duration of the experiment (27 days). The rate of change during this period suggests that the film would be stable for many more months or even longer. The initial increase in OCP is likely to be the reaction of the polymer with oxygen in solution.
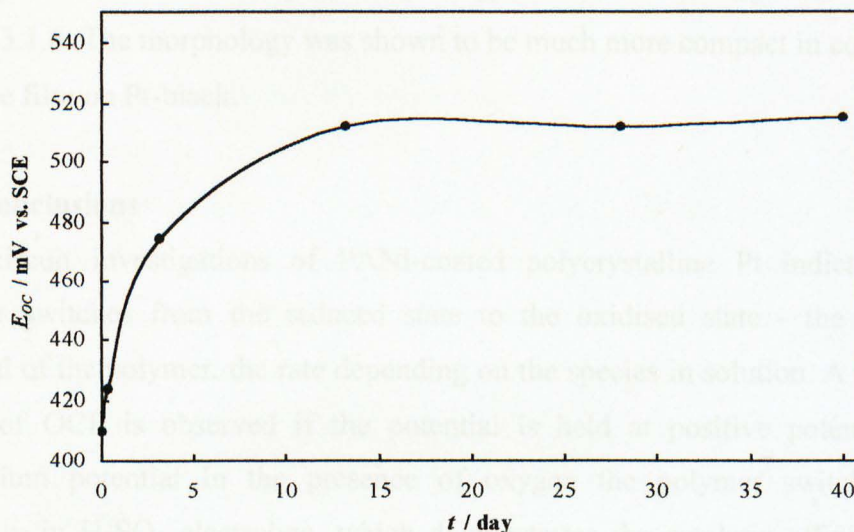
Figure 38 Long term open circuit behaviour of Au-PVC/PANI/SO_4^{2-} over 40 days. Thickness ~ 1.3 μm

Figure 39 shows the cyclic voltammograms of Au-PVC/PANI/SO_4^{2-} over a period of 30 days.
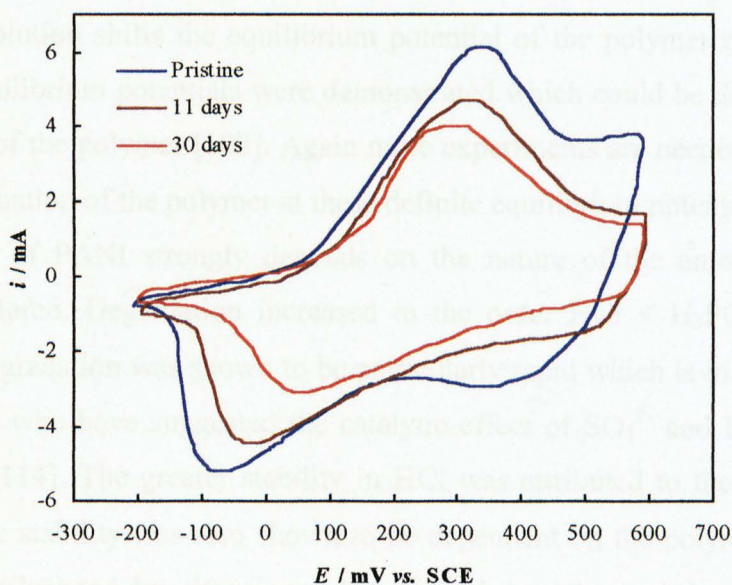
Figure 39 Cyclic voltammograms of Au-PVC/PANI/SO_4^{2-} over time in air equilibrated 1 mol dm^{-3} H_2SO_4. Thickness ~ 1.3 μm

104

Although the OCP study shows the equilibrium potential to be stable over this time, the voltammograms show a decrease in coulombic capacity of 40 % after 30 days, this is in agreement with the work on Pt-black/PANI/SO_4^{2-} except that the OCP is much more stable for Au-PVC/PANI/SO_4^{2-}. The improved stability of the polymer is most probably a result of the compact morphology, which has already been described in section 3.1.6. The morphology was shown to be much more compact in comparison to the same film on Pt-black.

3.2.6 Conclusions

Open circuit investigations of PANI-coated polycrystalline Pt indicate that the polymer switches from the reduced state to the oxidised state - the equilibrium potential of the polymer, the rate depending on the species in solution. A decay in the values of OCP is observed if the potential is held at positive potentials to the equilibrium potential In the presence of oxygen the polymer switches rapidly, especially in H_2SO_4 electrolyte, which demonstrates the catalytic affinity of PANI towards oxygen. However, in a completely de-oxygenated solution the same process occurs but at a much slower rate. It is thought that the reaction of the polymer with species in solution other than oxygen or on the PANI chain itself causes the switching. Mathematical treatment of the OCP transients supported this assumption. More experiments are needed in addition to the utilisation of other techniques such as *in situ* ESR to determine the exact nature of the reacting species. The presence of Na_2SO_3 in solution shifts the equilibrium potential of the polymer negatively; three definable equilibrium potentials were demonstrated which could be due to different α and β forms of the polymer [102]. Again more experiments are needed to confirm the exact conformation of the polymer at these definite equilibrium potentials.

The stability of PANI strongly depends on the nature of the anion in which the polymer is stored. Degradation increased in the order HCl < H_3PO_4 < H_2SO_4. In H_2SO_4 the degradation was shown to be particularly rapid which is in agreement with other authors who have suggested the catalytic effect of SO_4^{2-} and HSO_4^- on PANI degradation [114]. The greater stability in HCl was attributed to the stability of the ion-pairs. The stability was also shown to be dependent on the polymer morphology which was influenced by changing substrate and growth conditions. The compact morphology of Pt-black/PANI/Cl^- was much more stable than the open porous morphology of Pt-black/PANI/SO_4^{2-} which is more prone to nucleophilic attack. The

same reason was attributed to the greater stability of Au-PVC/PANI/Cl⁻. Improved stability was observed when Na_2SO_3 was added into H_2SO_4 electrolyte. It is thought that Na_2SO_3 has a reducing effect on the polymer, thus keeping it in the polaronic form which is less liable to nucleophilic attack by solution constituents.

3.3 Performance of PANI-modified fuel cells

3.3.1 Introduction

Although varying stabilities were observed in H_2SO_4, HCl and H_3PO_4, a combination of fuel cells utilising PANI-coated Pt-black and Au-PVC cathodes in different acid electrolytes were tested. Full details of the preparation conditions are described in the next section. It is worth recalling the issues which require improvement in the current Formaldemeter™ fuel cell the PANI-modified fuel cells were tested for their;

- Sensitivity towards formaldehyde
- Selectivity – response to methanol
- Humidity response
- Fuel cell shelf life

In addition to these points ideal criteria include fast response and clearing times to enable a greater number of measurements in a given time.

3.3.2 Experimental

Six different fuel cells utilising a PANI cathode were investigated. The preparation conditions of the PANI films (substrate and polymer growth conditions) and the electrolyte utilised in the fuel cell are summarised in table 1. PANI films were grown in an identical manner to the ones described in section 3.1.2, in addition to Au – PVC/PANI/Cl⁻ which was grown under the same conditions as Au – PVC/PANI/SO_4^{2-} with 1 mol dm⁻³ HCl. All the fuel cells contained a Pt-black anode. Type I assembly was used for the PANI-modified fuel cells as described in section 2.3.2. This means that the fuel cells were composed of two separate electrodes as opposed to type II fuel cells which were composed of two electrodes on either side of one PVC separator.

Cathode Substrate/PANI/Anion	Growth electrolyte / 1 mol dm^{-3}	Fuel cell electrolyte / 1 mol dm^{-3}
Pt–black/PANI/SO$_4^{2-}$	H$_2$SO$_4$	H$_2$SO$_4$
Pt–black/PANI/Cl$^-$	HCl	HCl
Pt-black/PANI/PO$_4^{3-}$	H$_2$SO$_4$	H$_3$PO$_4$
Au–PVC/PANI/SO$_4^{2-}$	H$_2$SO$_4$	H$_2$SO$_4$
Au–PVC/PANI/Cl$^-$	HCl	HCl
Au-PVC/PANI/PO$_4^{2-}$	H$_2$SO$_4$	H$_3$PO$_4$

Table 1 Preparation and fuel cell conditions of PANI cathodes used in the fuel cells

Preliminary investigations of the performance of the fuel cells were carried out. Simple measurements of response times were taken using gas streams of known concentrations as described in section 2.5. Detailed investigations were then performed on sensors showing good response; these tests were performed using the vapour generator combined with the computer-controlled equipment as described in section 2.5.3. The response of the PANI-modified fuel cell was compared to a standard fuel cell containing a Pt-black anode and cathode in an electrolyte of 1 mol dm^{-3} H$_2$SO$_4$. It is important to note that the electrodes used in the Formaldemeter™ are composed of Pt-Pd in an electrolyte of 7 mol dm^{-3} H$_3$PO$_4$. The response of a fuel cell of this type is described in chapter 4 where the effect of different electrocatalysts is investigated.

3.3.3 Preliminary investigations of PANI-modified fuel cells

Initial investigations of the fuel cells yielded mixed results. Fuel cells containing HCl and H$_3$PO$_4$ electrolyte exhibited a very poor response regardless of the substrate onto which PANI was deposited. The response of Au-PVC/PANI/SO$_4^{2-}$ modified fuel cell in H$_2$SO$_4$ was also poor; however, in complete contrast the Pt-black/PANI/SO$_4^{2-}$ modified fuel cell showed excellent response to formaldehyde. The results are summarised in table 2 which also shows the direct outputs of the fuel cells measured 5 days after assembly.

Cathode utilised in fuel cell	Direct Fuel Cell Output / mV 5 days after assembly	General response to HCHO / MeOH
Pt–black/PANI/SO$_4^{2-}$	+ 140	Excellent
Pt–black/PANI/Cl$^-$	-79	Very poor
Pt-black/PANI/PO$_4^{3-}$	-ve	Very poor
Au–PVC/PANI/SO$_4^{2-}$	-271	Poor
Au–PVC/PANI/Cl$^-$	-67	Very poor
Au-PVC/PANI/PO$_4^{3-}$	-ve	Very poor

Table 2 Direct output and general response to the vapour standards of modified fuel cells

As can be seen, the direct fuel cell output corresponds to the general response of the fuel cell. Values for the polymers containing the PO$_4^{3-}$ anion are not stated due to wild fluctuations in the values obtained; however, the outputs obtained indicated a negative value. In general, fuel cells with a very poor response measured a negative value, while the only fuel cell that worked measured a positive value. At the moment, it is not certain why this occurs, however it is anticipated that the poor response is related to anion adsorption at the electrode. Previous studies have shown that the nature and the concentration of the electrolyte solution has a profound effect on the activity of Pt and Pt-black fuel cells [27, 116-119].

It is well known from work on Pt single crystals, that anions can dramatically affect the kinetics of electrocatalytic reactions, e.g. the oxidation of small organic molecules [120] or oxygen reduction [121,122]. This is readily understood when it is recalled that adsorption from solution involves the replacement of previously adsorbed species by the active gas or its adsorption products. The gas molecules therefore compete with species in solution (O$_2$, H$_2$O and anions) for the adsorption sites and it is to be expected that the species with the greatest strength of adsorption will be preferentially adsorbed on the electrode surface.

The effect of anions on the oxidation of methanol has been investigated by using different electrolytes and measuring current potential curves [123]. It was shown that methanol oxidation was severely inhibited in HCl. The results were attributed to competition between the adsorption of methanol and the adsorption of anions. The

trend in peak currents was explained in terms of the "adsorption strength" of anions which were ordered as $ClO_4^- < HSO_4^- < H_2PO_4^- < Cl^-$ [124]. Many authors are in agreement about the adsorption strength of chloride anions and have discounted it as a potential electrolyte in a fuel cell application [27, 123-126].

Ross [119] examined the electroreduction of oxygen on Pt in 1 M acid solutions ($HClO_4$, H_2SO_4, and H_3PO_4) and 85 % H_3PO_4 and found that the activity in 1M H_3PO_4 was approximately half that observed in 1 M H_2SO_4 and $HClO_4$. This was attributed to a greater degree of surface coverage by the $H_2PO_4^-$ anions in the potential range 0.8 – 1.0 V, in agreement with the work of Bagotsky et al. [127]. Llopis [118] has shown that the formation of adsorbed oxygen layer is hindered by the presence of halide ions which are specifically adsorbed on Pt in preference to oxygen. This effect increased in the order;

$$I^- > Br^- > Cl^-$$
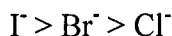
corresponding to the increasing strength of anion adsorption on the electrode surface In agreement with this work more recent work by Schmidt et al. [126] have also shown that the activity of the oxygen reduction reaction (ORR) decreases in the order $ClO_4^- > HSO_4^- > Cl^-$, consistent with the increasing adsorption strength of the anions.

The results for the fuel cell activity are very much in agreement with the work published in the literature with only the Pt-black/PANI/SO_4^{2-} showing good activity compared to fuel cells containing the Cl^- anion or the PO_4^{3-} ($H_2PO_4^-$) anion. Complete drying of the fuel cell in HCl electrolyte was also observed after a period of a week. This was also observed by Williams [26] and Harrison [27] for fuel cells containing Pt-black, although an explanation was not proposed.

The poor activity of the fuel cell containing Au-PVC/PANI/SO_4^{2-} cathode in comparison to a similar film on Pt-black is particularly interesting and can be attributed to the nature of the substrate. Of all the fuel cells, that containing the Au-PVC/PANI/SO_4^{2-} modified cathode had the largest negative direct output value (-271 mV). This is most probably due to the potential difference between the Au-PVC and Pt-black electrode which results in a new equilibrium potential for the fuel cell sensor. The shifted equilibrium potential is certain to have an effect on the electrooxidation of formaldehyde and methanol, and it is possible that it is outside the potential window for the oxidation to actually occur, thus requiring greater overpotentials to oxidise the species successfully.

As a result of these initial investigations only the fuel cell containing the Pt-black/PANI/SO$_4^{2-}$ cathode was further investigated.

3.3.4 Detailed study of Pt-black/PANI/SO$_4^{2-}$ modified fuel cell

3.3.4.1 Direct fuel cell output

The direct output of the PANI-modified fuel cell is shown in figure 40 The output voltage is displayed in Test Mode (TM) units; arbitrary units used by the Formaldemeter™ software before calibration (section 2.4.3). As can be seen there is an initial steep rise over the first 100 seconds until the output reaches a constant level.
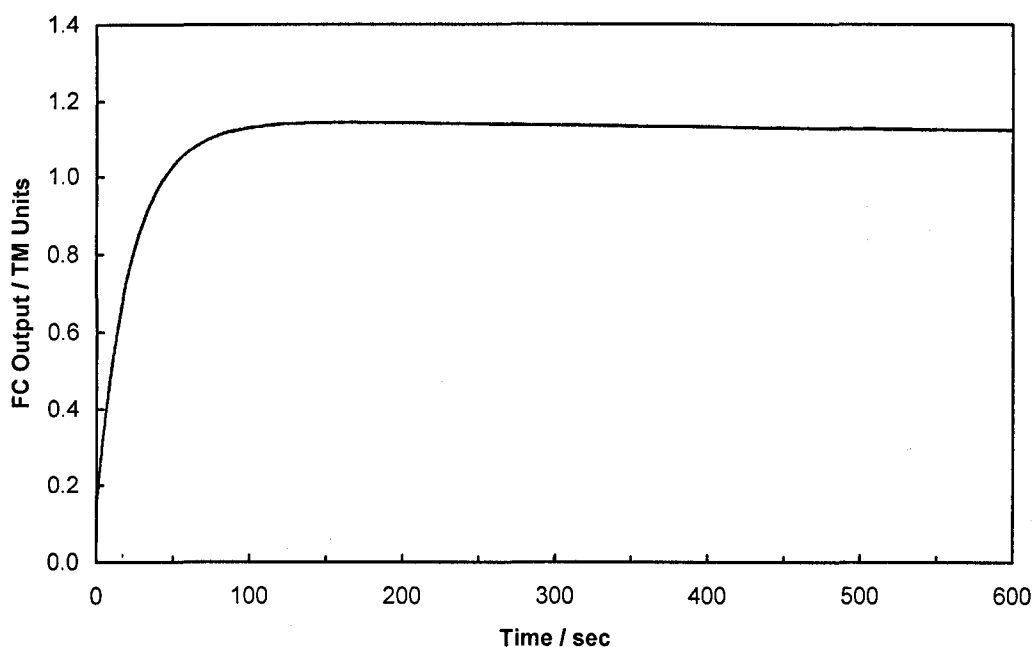
Figure 40 Direct output of PANI fuel cell. No air sample.

This behaviour is different to fuel cells containing identical Pt-black anode and cathode, which normally show a constant output value of 0.056 in TM Units. The difference in behaviour can be directly attributed to the activity of PANI and represents the new equilibrium potential of the fuel cell.

In the Formaldemeter™ when the fuel cell is not in use the electrodes are in direct contact (short-circuited). This is also true before and after sampling and has the effect of discharging the electrodes; for a normal fuel cell this is an extremely efficient process which facilitates in dissipation of the charge that is left over from sampling and ensures that the next reading is taken from a stable baseline. Over time this

process occurs naturally, however short-circuiting the electrodes facilitates making the process faster and the recovery quicker.

In the PANI-modified fuel cell it is anticipated that the initial rise in the output due to the new equilibrium potential could interfere with low level sampling of formaldehyde, therefore to eliminate the effect, the relay in control of the fuel cell short-circuiting was removed. As a result samples were taken not from a zero baseline but from the new equilibrium potential, which was compensated for in the software. From the open circuit behaviour of PANI in oxygen saturated electrolytes it was anticipated that the reaction of reduced PANI with oxygen would be quite fast, thus recovering the fuel cell for multiple samplings, hence short-circuiting the fuel cell was thought to be an unnecessary procedure.

3.3.4.2 Response to formaldehyde

A typical response of the standard Formaldemeter™ fuel cell to 1 and 2 ppm formaldehyde is shown in figure 41. The increase in current corresponds to the rapid dissociative adsorption of formaldehyde on the electrode surface at the anode which slowly decreases in rate as the adsorption approaches equilibrium. A decrease in current then occurs as the slow electrochemical oxidation of the adsorbed species occurs.
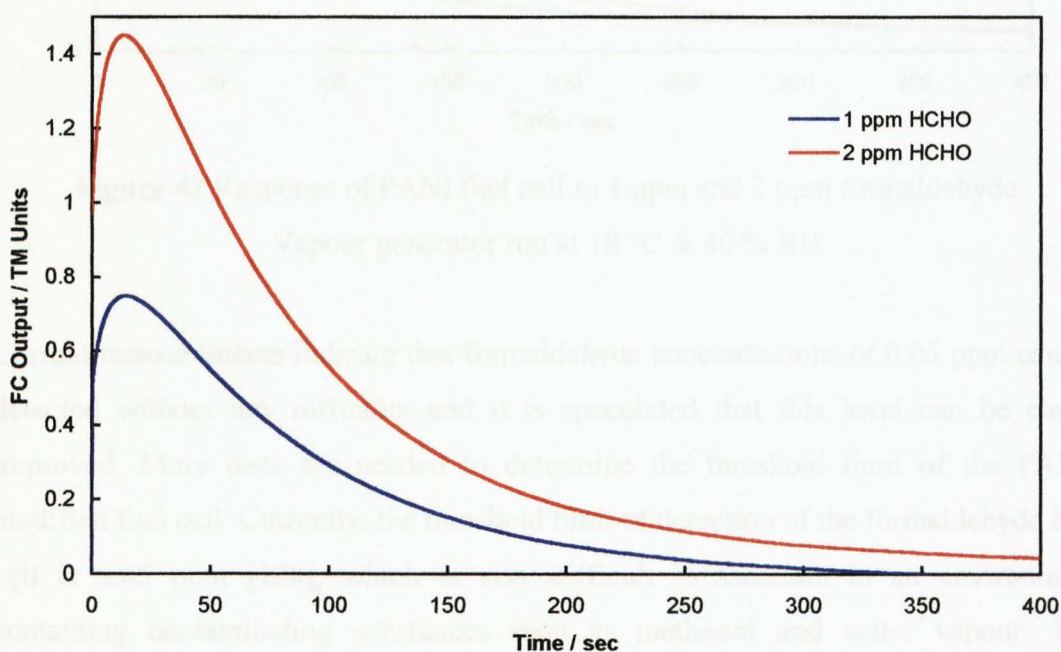
Figure 41 Response of standard fuel cell to 1 ppm and 2 ppm formaldehyde. Vapour generator run at 18 °C & 40 % RH.

111

As can be seen, the peak height is linearly related to the concentration of formaldehyde in the air sample and occurs at 13 seconds, which is consistent for both outputs.

In comparison to the response of the standard fuel cell, it can be seen that the output is approximately doubled in the PANI-modified fuel cell (figure 42); the response is also quicker and sharper, peaking at 10 seconds, 3 seconds sooner than the standard fuel cell, suggesting that the response is much more efficient per ppm of formaldehyde.
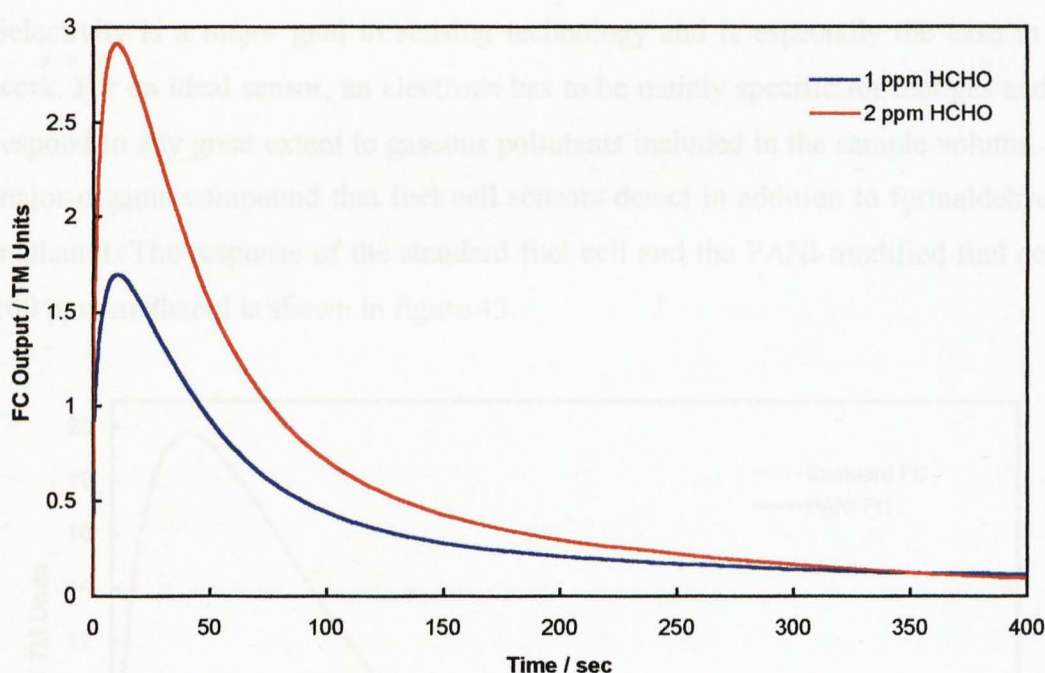
Figure 42 Response of PANI fuel cell to 1 ppm and 2 ppm formaldehyde

Vapour generator run at 18 °C & 40 % RH

Current measurements indicate that formaldehyde concentrations of 0.05 ppm can be detected without any difficulty and it is speculated that this level can be easily improved. More tests are needed to determine the threshold limit of the PANI-modified fuel cell. Currently, the threshold limit of detection of the formaldehyde fuel cell is 0.05 ppm [128], which is very difficult to ascertain in an environment containing contaminating substances such as methanol and water vapour. The improved sensitivity and faster response of the fuel cell to formaldehyde could be as a result of the fast electrochemical switching of the PANI cathode (<10 μs [1]) from the

oxidised form to the reduced form which is thought to be a more efficient process than the oxygen reduction reaction. The fuel cell also displayed good reproducibility enabling measurements to be performed within short recovery time for the fuel cell. This suggests that the reaction of oxygen with the reduced form of the polymer is also efficient, which could be as a result of the large surface area of the polymer.

It is also possible that the new equilibrium potential of the fuel cell, which causes the anode to have a different resting potential, may favour the oxidation of formaldehyde which could result in the improved signal.

3.3.4.3 Response to methanol

Selectivity is a major goal in sensing technology and is especially the case in this work. For an ideal sensor, an electrode has to be mainly specific for that gas and not respond to any great extent to gaseous pollutants included in the sample volume. The major organic compound that fuel cell sensors detect in addition to formaldehyde is methanol. The response of the standard fuel cell and the PANI-modified fuel cell to 100 ppm methanol is shown in figure 43.
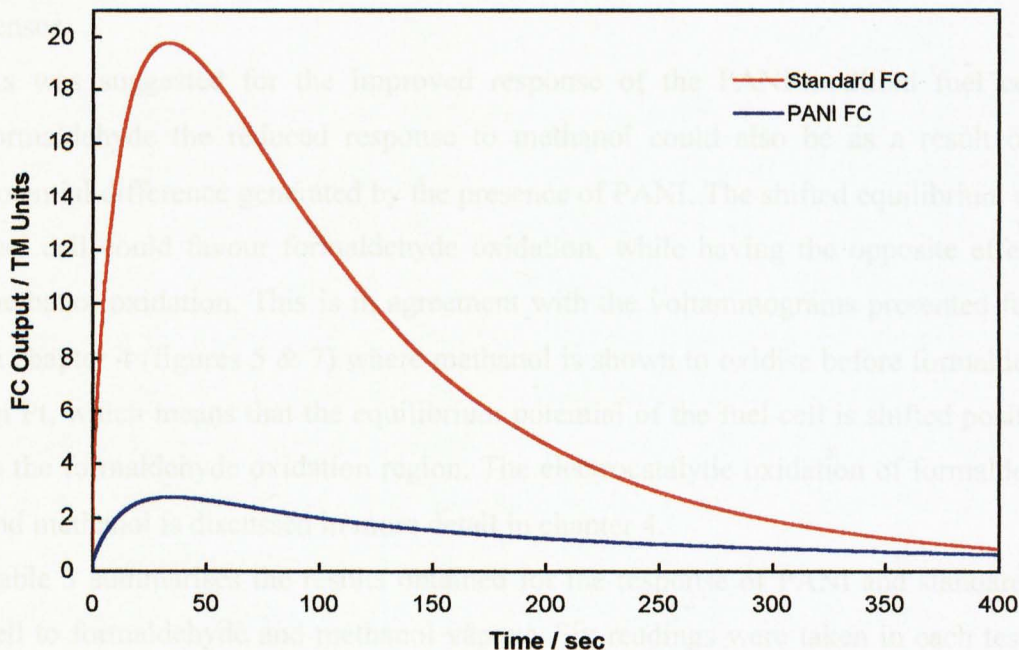
Figure 43 Comparison of fuel cell responses to 100 ppm methanol.
Vapour generator run at 18 °C & 40 % RH

113

In comparison to the response to formaldehyde the response to methanol is much broader with the maximum intensity occurring at 36 seconds, approximately 26 seconds later than formaldehyde. It is thought that this slower response is due to the complexity of the MeOH molecule in comparison to HCHO. The oxidation involving 6e⁻ for MeOH and 4e⁻ for HCHO. The performance of fuel cell electrodes towards the electro-oxidation of methanol has proved to be relatively poor due to the slow kinetics of the process [129-131]. The reaction is poorly catalysed on conventional platinum electrodes since the surface of the electrode is covered at low potentials by strongly poison and adsorbed intermediates such as –CO and ≡C-OH [132-134].

As low concentrations of methanol were difficult to detect using the PANI-modified fuel cell, which was exactly the requirement for a specific fuel cell for formaldehyde, a more concentrated methanol vapour had to be generated in order to facilitate comparison between the fuel cells. It is immediately visible that the response of the PANI-modified fuel cell is much smaller than the standard fuel cell by approximately 8 times which is a significant improvement on the standard fuel cell. It is therefore clear that the presence of PANI on the cathode improves the behaviour of the fuel cell sensor.

As was suggested for the improved response of the PANI-modified fuel cell to formaldehyde the reduced response to methanol could also be as a result of the potential difference generated by the presence of PANI. The shifted equilibrium of the fuel cell could favour formaldehyde oxidation, while having the opposite effect on methanol oxidation. This is in agreement with the voltammograms presented further in chapter 4 (figures 5 & 7) where methanol is shown to oxidise before formaldehyde on Pt, which means that the equilibrium potential of the fuel cell is shifted positively to the formaldehyde oxidation region. The electrocatalytic oxidation of formaldehyde and methanol is discussed in more detail in chapter 4.

Table 3 summarises the results obtained for the response of PANI and standard fuel cell to formaldehyde and methanol vapour. Six readings were taken in each test; the average is shown in the table.

Fuel Cell	HCHO (2 ppm)			MeOH (100 ppm)			MeOH / HCHO
	Direct Output	Response / PPM	Response Time	Direct Output	Response/ PPM	Response Time	
PANI FC	2.9	1.45	10	2.7	0.027	36	0.018
Standard FC	1.45	0.725	13	20	0.20	36	0.275

Table 3 Response of PANI-modified and standard fuel cell to 2 ppm formaldehyde and 100 ppm methanol. Also shown are methanol/formaldehyde ratios. All tests performed at 18°C and 40 % RH

The MeOH/HCHO ratio gives a direct comparison of the fuel cell specificity, the smaller the ratio the more favourable the specificity of that fuel cell. It is observed that the ratio of the standard fuel cell is much higher than that of the PANI-modified fuel cell which makes it undesirable for a specific sensor for formaldehyde. The ratio of the PANI fuel cell is particularly good and is better than the 0.035 quoted in the literature [135] under the same conditions for the Formaldemeter™ fuel cell, which contains 50/50 % ratio of platinum and palladium.

3.3.4.4 Response of PANI fuel cell to mixtures of vapours

In an environment containing detectable traces of methanol and formaldehyde it is important to have a sensor that can selectively determine the concentration of formaldehyde. This environment was mimicked by mixing 1 ppm formaldehyde with 100 ppm methanol. The output of the fuel cell in comparison to individual vapours is shown in figure 44. It can be seen that the response is an additive effect peaking at 27 seconds, between those of formaldehyde (10 seconds) and methanol (36 seconds). As expected methanol is the most dominant in the mixture output. This behaviour presents a difficulty in determining the vapour concentration of formaldehyde. A modification in the software could facilitate differentiation between the two.
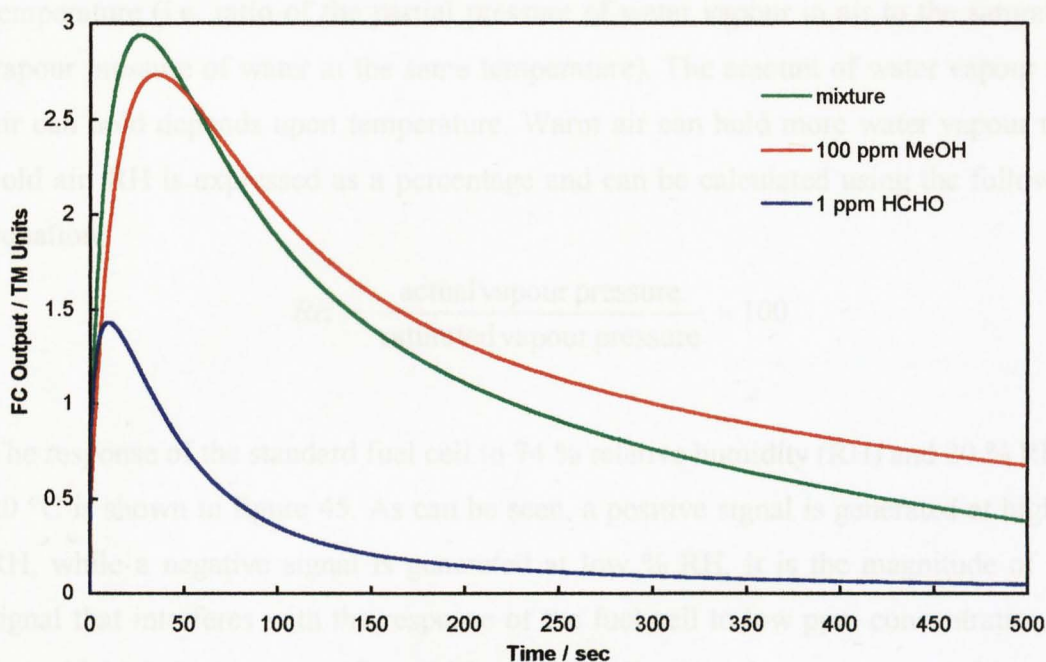
Figure 44 Response of PANI fuel cell to mixtures of vapours

Vapour generator run at 18 °C & 40 % RH

For example the peaks could be mathematically integrated and correlated to the concentration of each vapour. However, since the output depends on other variables such as temperature, pressure and presence of other interfering vapours a qualitative determination would be difficult, only estimation would be achievable. The effect of neural networks has already been investigated on the standard fuel cell [136], but up to now it has been unfruitful.

In comparison to the standard fuel cell the PANI fuel cell is better at detecting mixtures since the methanol output is much lower which has the effect of making peak shifts detectable. For the standard fuel cell the methanol output is too large for any determination of formaldehyde to be made.

3.3.4.5 Response to humidity – The humidity problem

One of the main problems with the current Formaldemeter™ is the response of the fuel cell to humidity. In general humidity is the amount of water vapour in ambient air. Relative humidity (RH) is the most commonly used measure of atmospheric humidity and it can be defined as the ratio of the actual amount of water vapour in the

air to the amount of water vapour that the air could hold if saturated at that temperature (i.e. ratio of the partial pressure of water vapour in air to the saturation vapour pressure of water at the same temperature). The amount of water vapour that air can hold depends upon temperature. Warm air can hold more water vapour than cold air. RH is expressed as a percentage and can be calculated using the following equation;

$$RH = \frac{\text{actual vapour pressure}}{\text{saturated vapour pressure}} \times 100$$

The response of the standard fuel cell to 74 % relative humidity (RH) and 20 % RH at 20 °C is shown in figure 45. As can be seen, a positive signal is generated at high % RH, while a negative signal is generated at low % RH. It is the magnitude of this signal that interferes with the response of the fuel cell to low ppm concentrations of formaldehyde in the current formaldehyde fuel cell sensor that presents a problem.

In comparison, the response of the PANI-modified fuel cell is shown in figure 46 and although the behaviour is similar, positive signal at high % RH and negative signal at low % RH, the magnitude of the signal is much lower, approximately ten fold, which is a substantial improvement on the standard fuel cell. The response is so small in fact that the signal is in the noise region, as demonstrated by the jagged transients.
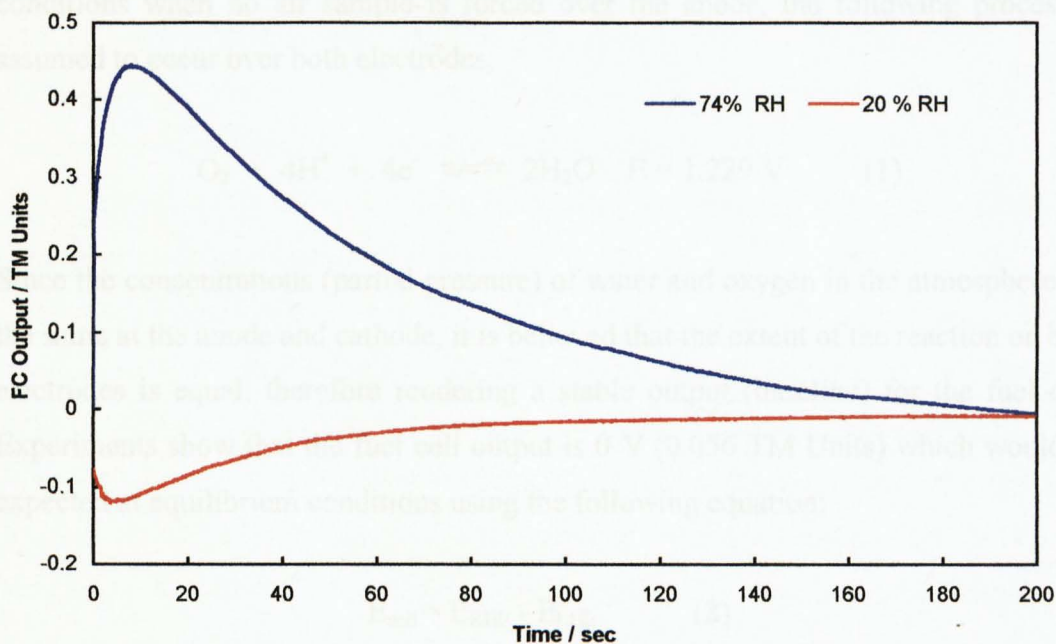
Figure 45 Response of standard fuel cell to 20 % RH and 74 % RH at 20 °C

117
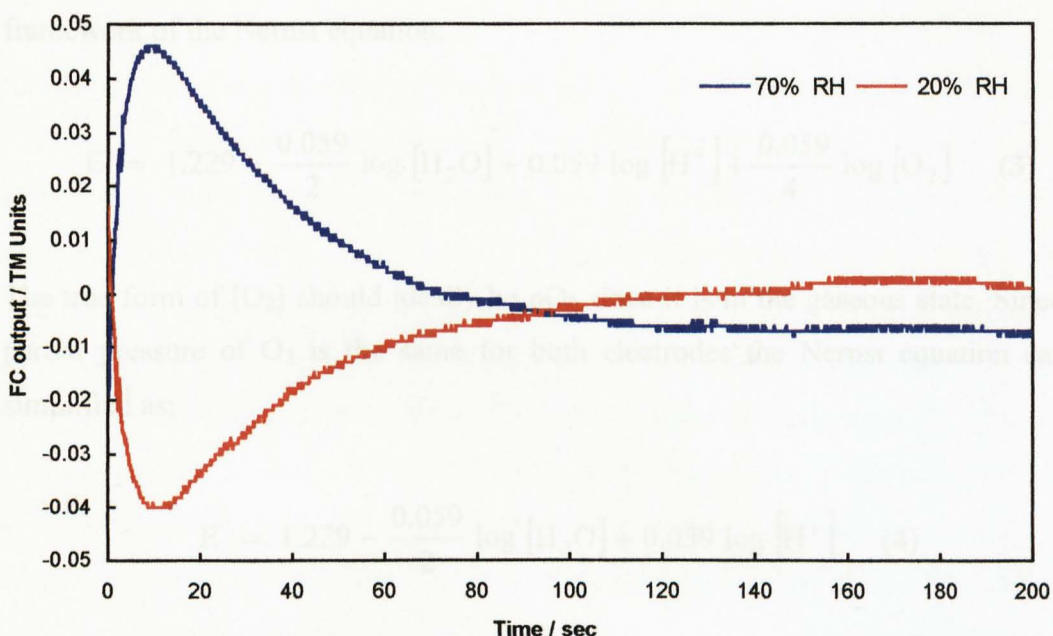
Figure 46 Response of standard fuel cell to 20 % RH and 70 % RH at 20 °C

To explain this improvement it is necessary to investigate the origin of the humidity signal. The first general assumption that can be made is that high % RH contains wet air, and that low % RH contains dry air in comparison to the ambient air of the laboratory (40 % RH) where the measurements were performed. At equilibrium conditions when no air sample is forced over the anode, the following process is assumed to occur over both electrodes,

$$O_2 + 4H^+ + 4e^- \rightleftharpoons 2H_2O \quad E = 1.229 \text{ V} \quad \textbf{(1)}$$
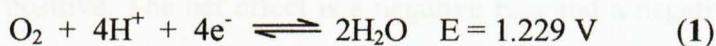
Since the concentrations (partial pressure) of water and oxygen in the atmosphere are the same at the anode and cathode, it is believed that the extent of the reaction on both electrodes is equal, therefore rendering a stable output (baseline) for the fuel cell. Experiments show that the fuel cell output is 0 V (0.056 TM Units) which would be expected at equilibrium conditions using the following equation;

$$E_{cell} = E_{RHE} - E_{LHE} \quad \textbf{(2)}$$

118

Introduction of wet air or dry air at the anode will greatly influence this equilibrium and based on this concentration dependence, reaction (1) can be considered within the framework of the Nernst equation;

$$E = 1.229 - \frac{0.059}{2} \log [H_2O] + 0.059 \log [H^+] + \frac{0.059}{4} \log [O_2] \quad (3)$$

The true form of $[O_2]$ should ideally be pO_2 since it is in the gaseous state. Since the partial pressure of O_2 is the same for both electrodes the Nernst equation can be simplified as:

$$E = 1.229 - \frac{0.059}{2} \log [H_2O] + 0.059 \log [H^+] \quad (4)$$

The two concentration terms which can influence the value of E after the introduction of an air sample. Of the two terms it is thought that the concentration of water is the controlling factor. Considering the reaction at high % RH, the concentration of H_2O will inevitably increase; as a result the value of E will become less. The net effect according to the governing equation (2) is a positive E_{cell} and a positive signal for the fuel cell response is given. The influence of the second process (H^+) is thought to be minimal, although over a long period of time it will result in dilution of the electrolyte leading to poor conductivity. Conversely when a dry air sample (low % RH) is introduced to the anode, H_2O concentration will decrease and the value of E will become more positive. The net effect is a negative E_{cell} and a negative signal for the fuel cell response is given. The long term effect would be the drying of the electrolyte due to the continuous removal of water.

From the response of the PANI fuel cell to humidity, figure 46, it is thought that the same processes occur but only to a slight extent due to the presence of PANI. The behaviour of the cell will be dominated by the redox chemistry of the polymer.

It is shown that a fuel cell constructed with a PANI cathode reduces the response of the fuel cell to humidity, however the signal could completely diminish if a humidity sensor was incorporated in the detecting instrument. Through electronic adjustments the response to humidity could be compensated. The significantly lower response of the fuel cell to water vapour means qualitative formaldehyde measurements can be

performed in variable humid conditions; up to now this has been very difficult to achieve with the current Formaldemeter™ sensor.

3.3.4.6 Long-term behaviour of the fuel cell

Due to the significant improvement in sensitivity, selectivity and reduced humidity response in the PANI fuel cell, the sensor was investigated for its long term stability 2 years after initial set up. The fuel cell showed no observable degradation in response and showed excellent consistency which suggests that the modified fuel cell has excellent shelf life, a property that is essential if the fuel cell is marketed. As only one PANI fuel cell was initially tested and to prove that the fuel cell was not a "one off" a replica was constructed. Similar responses as the initial fuel cell were obtained, the fuel cell also showed no signs of degradation and excellent performance and consistency over a period of 1 year. Going by the stability results obtained, it is anticipated that the shelf life of the fuel cells could be much longer. Only future experiments can determine the true shelf life of the fuel cell.

The excellent performance and stability of the fuel cell is especially intriguing when considering the results obtained on the stability of PANI in H_2SO_4 in section 3.2. It was shown that the degradation of the polymer was particularly rapid in this medium. Although cyclic voltammetry and open circuit measurements indicated that the degradation of the polymer was rapid in H_2SO_4, regardless of the concentration, the stability and improved performance of the PANI fuel cell suggests that the polymer is still active. This might be due to the thickness and high surface area of the polymer, whereas maybe a thinner film would show signs of fuel cell deterioration.

3.3.5 Conclusions

The activity of a PANI-modified fuel cell is dependent on the acid electrolyte and the substrate onto which it is coated. Whilst the activity of PANI fuel cells in HCl and H_3PO_4 were poor, the activity of a fuel cell containing a PANI-coated Pt-black cathode in H_2SO_4 was excellent. Interestingly this fuel cell also exhibited a positive direct fuel cell output, in contrast to all the other fuel cells which exhibited a negative output. Future experiments will have to be performed to elucidate the relationship between direct fuel cell output and fuel cell activity.

Compared to a standard fuel cell containing identical Pt-black electrodes, the PANI-modified fuel cell showed improved sensitivity (twice as sensitive to formaldehyde), improved selectivity (8 times less sensitive to methanol) and a substantial reduction in the response to humidity (10 times less sensitive to water vapour). It is thought that the enhanced sensitivity and selectivity is due to the shifted equilibrium potential of the PANI fuel cell; the presence of PANI on the cathode is thought to minimise the humidity reaction. A faster response time and exceptional reproducibility was also demonstrated by the PANI-modified fuel cell, which may be related to the fast switching time of PANI.

Over the long term (2 years) the fuel cell showed excellent performance and stability. Future experiments will have to be performed to determine the true shelf life of the fuel cell.

3.4 General Conclusions to Chapter 3

1. SEM investigations of the polymers indicate that the growth condition greatly influences the morphology. The nature of the anion in the growth medium is of particular importance with PANI films deposited from SO_4^{2-} electrolyte displaying a highly fibrilar and porous morphology. PANI films from Cl⁻ electrolyte show a much more dense and compact nature, which is consistent with work carried out by other authors [24,65].

2. Open circuit investigations of PANI suggest that the polymer attains a stable equilibrium potential in the emeraldine salt oxidation state, regardless of the initial applied potential. In the presence of oxygen the reduced polymer switches rapidly to the emeraldine salt oxidation state, especially in H_2SO_4. This is of great importance for the fuel cell application where oxidation of the polymer to the emeraldine salt state is required to make multiple sampling possible. It was also shown that the same process occurs under completely degassed conditions but at a much slower rate. A reaction of the polymer with a species in solution or on the chain itself (disproportionation or comproportionation) is proposed, however, more experiments utilising *in situ* ESR technique is required to confirm this.

3. A negative shift in the equilibrium potential of the polymer was observed when Na_2SO_3 was added into solution. In addition three definable equilibrium potentials for PANI were clearly demonstrated. It is thought that these corresponds to different conformations of the polymer; α, β and a metastable state as proposed by Albery *et*

al. [102]. *In situ* ESR and *in situ* IR experiments should be used in future experiments to confirm the exact conformation of the polymer at these equilibrium potentials.

4. The stability of PANI strongly depends on the nature of the anion in which the polymer is stored. Degradation increased in the order HCl < H_3PO_4 < H_2SO_4. In H_2SO_4 the degradation was particularly rapid which is in agreement with other authors who have suggested the catalytic effect of SO_4^{2-} and HSO_4^- on PANI degradation [114]. The fast degradation may be related to the size of the anion in a shielding model theory whereby the sulfate and bisulfate anions are too small to effectively preclude the approach of nucleophilic constituents such as H_2O and OH^- compared to the large Cl^- anion which has a protecting effect. The greater stability in HCl was also attributed to the stability of the ion pairs. On Pt-black the same degradation pattern was observed but to a more rapid extent. The large surface area and porous nature of the Pt-black/PANI/SO_4^{2-} polymer was thought to promote the degradation.

5. The stability of the polymer was also shown to be dependent on the growth condition. PANI deposited from HCl solutions were much more stable than polymers deposited from H_2SO_4. The compact morphology of the PANI/Cl^- films was thought to minimise the degradation compared to the porous morphology of the PANI/SO_4^{2-} film which is more prone to nucleophilic attack.

6. Greater stability was observed in H_2SO_4 + Na_2SO_3 than in the base electrolyte. It is thought that Na_2SO_3 has a reducing effect on the polymer, thus keeping it in the polaronic form which is less liable to nucleophilic attack by solution constituents.

7. Although PANI degradation was shown to be particularly rapid in H_2SO_4 the activity and performance of the corresponding fuel cell was for more superior. Thus, it is anticipated that degradation does not lead to a completely inactive film. The blocking of the catalytic surface by Cl^- and PO_4^{3-} anions due to their greater adsorption strengths was thought to be the cause of the poor activity in HCl and H_3PO_4 respectively.

8. Compared to a standard fuel cell, the PANI modified fuel cell (in H_2SO_4 electrolyte) has improved sensitivity, selectivity, and a reduced response to humidity. In addition the fuel cell has a faster response time, good reproducibility and a long shelf life. The shifted equilibrium potential of the fuel cell was thought to favour formaldehyde oxidation, while having the opposite effect on methanol oxidation. The

physical presence of PANI on the cathode was thought to minimise the humidity reaction. The fast switching of PANI was thought to speed up the response time.

Based on these conclusions it is proposed that a fuel cell containing a PANI based cathode, which relies on the fast switching of PANI, is an attractive and reliable alternative to a standard fuel cell that relies on the diffusion of oxygen at the cathode.

3.5 References

1   M. Kalaji, L. M. Peter, L. Abrantes, J. C. Mesquita, *J. Electroanal. Chem.* 274 (1989) 289

2   J. Kankare, I. A. Vinokurov, *Anal. Chem.*, 69 (1997) 2337

3   H. Okamoto, T. Kotaka, *Polymer*, 40 (1999) 407

4   C. Q. Cui, L. H. Ong, T. C. Tan, J. Y. Lee, *Synth. Met*, 147 (1993) 58

5   G. de T. Andrande, M. J. Aguirre, S. R. Biaggio, *Electrochim. Acta.*, 44 (1998) 633

6   E. M. Geniès, A. Boyle, M. Lapkowski, C. Tsintavis, Synth. Met., 36 (1990) 139

7   W. S. Huang, B. D. Humphrey, and A. G. MacDiarmid, *J. Chem. Soc., Faraday Trans.* 82 (1986) 2385

8   B. Wang, J. Tang, and F. Wang, *Synth. Met.*, 18 (1987) 323

9   G. Horányi and G. Inzelt, *J. Electroanal. Chem.*, 264 (1989) 259

10 G. Sandí and P. Vanýsek, *Synth. Met.*, 64 (1994) 1

11 B. Pfeiffer, A. Thyssen, and J. W. Schultze, *J. Electroanal. Chem.*, 260 (1989) 393

12 T. Boschi, G. Montesperelli, P. Nunziante, G. Pistoia, and P. Fiordiponti, *Solid State Ionics,* 31 (1989) 281

13 A. D. Jannakoudakis, P. D. Jannakoudakis, N. Pagalos, and E. Theodoridou, *Electrochim. Acta,* 38 (1993) 1559

14 A. Calderone, R. Lazzaroni, and J. L. Brédas, *Synth. Met.*, 55-57 (1993) 4620

15 S. K. Dhawan, M. K. Ram, B. D. Malhotra, and S. Chandra, *Synth. Met.*, 75 (1995) 119

16 G. Mengoli, M. T. Munari, and C. Folonari, *J. Electroanal. Chem.*, 124 (1981) 237

17 B. Wessling, *Adv. Mater.*, 6 (1994) 226

18 C. M. A. Brett, A. M. C. F. O. Brett, J. L. C. Pereira, and C. Rebelo, *J. Appl. Electrochem.*, 23 (1993) 332

19 R. M. G. Rajapakse, A. D. L. Chandani, L. P. P. Lankeshwara, and N. L. W. L Kumarasiri, *Synth. Met.,* 83 (1996) 73

20 S. M. Lin and T. C. Wen, *Electrochim. Acta,* 39 (1994) 393

21 H. N. Dinh, V. I. Birss. *J. Electroanal. Chem.,* 147 (2000) 3775

22 P. Nunziante, G. Pistoia, *Electrochim. Acta* 34 (1989) 223

23 G. Zotti, S. Cattarin, N. Comisso, *J. Electroanal. Chem.* 235 (1987) 259

24 G. Zotti, S. Cattarin, N. Comisso, *J. Electroanal. Chem.* 239 (1988) 387

25 T. Osaka, S. Ogano, K. Naoi, N. Oyama, *J Electrochem. Soc.* 136 (1989) 306

26 P. M. Williams, *Ph.D Thesis,* University of Wales, Cardiff, (1978)

27 I. D. Harrison, *Ph.D Thesis,* University of Wales, Cardiff, (1982)

28 C. A. Marrese, *Anal. Chem.,* 59 (1987) 217

29 F. Gloaguen, J. M. Leger, C. Lamy, A. Marmann, U. Stimming, R. Vogel, *Electrochim. Acta,* 44 (1999) 1805

30 C. H. Hamann, A. Hamnett, W. Vielstich, *"Electrochemistry,"* Wiley VCH Weinheim, (1998)

31 W. Vielstich, *"Fuel Cells",* Wiley-Interscience, London, (1968)

32 D. E. Stilwell, S. M. Park, *J. Electrochem. Soc.* 135 (1988) 2491

33 S. Y. Cui, S. M. Park, *Synth. Met.,* 105 (1999) 91

34 H. N. Dinh, P. Vanýsek, V. I. Birss, *J. Electrochem. Soc,* 146 (1999) 3324

35 F. Fusalba, P. Gouerec, D. Villers, D. Belanger, *J. Electrochem. Soc,* 148 (2001) A1

36 M. P. Sumino, S. Shibata, *Electrochim. Acta.,* 37 (1992) 2629

37 Y. B. Shin, M. S. Won, S. M. Park, *J. Electrochem. Soc,* 137 (1990) 538

38 H. N. Dinh, J. Ding, S. J. Xia, V. I. Birss, *J. Electroanal. Chem,* 459 (1998) 45

39 D. C. Trivedi, in H. S. Nalwa (Ed.), *"Handbook of Conducting Molecules and Polymers",* Vol. 2, Wiley, Chichester, England, (1997)

40 S. M. Park, in in H. S. Nalwa (Ed.), *"Handbook of Conducting Molecules and Polymers",* Vol. 3, Wiley, Chichester, England, (1997)

41 D. M. Mohilner, R. N. Adams, W. J. Argersinger, *J. Am. Chem. Soc.,* 84 (1962) 3618

42 Southampton Electrochemistry Group, *"Instrumental Methods in Electrochemistry,"* Ellis Horwood (1990)

43 J. C. LaCroix, K. K. Kanazawa, A. Diaz, *J. Electrochem. Soc.* 136 (1989) 1308

44 V. W. Jones, M. Kalaji, G. Walker, C. Barbero, R. Kotz, *J. Chem. Soc. Faraday Trans.*, 90 (1994) 2061

45 V. W. Jones, *PhD Thesis*, University of Wales, Bangor (1995)

46 A. F. Diaz, J. A. Logan, *J. Electroanal. Chem.*, 111 (1980) 111

47 T. Kobayashi, H. Yonemana, H. Tamura, *J. Electroanal. Chem.*, 161 (1984) 419; 177 (1984) 281, 293

48 P. M. McManus, S. C. Yang, R. J. Cushman, *J. Chem. Soc., Chem. Commun.*, (1985) 1556

49 A. Watanabe, K. Mori, Y. Iwasaki, Y. Nakamura, S. Niizuma, *Macromolecules*, 20 (1987) 1793

50 E. M. Geniès, M. Lapkowski, *J. Electroanal. Chem,* 220 (1987) 67

51 W. E. Rudzinski, L. Lozano, M. Walker, *J. Electrochem. Soc.*, 137 (1990) 3132

52 M. Kalaji, L. Nyholm, L. M. Peter, *J. Electroanal Chem.*, 313 (1991) 271

53 D. Orata, D. A. Buttry, *J. Am. Chem. Soc.*, 109 (1987) 3574

54 C. Barbero, M. C. Miras, O. Haas, R. Kotz, *J. Electroanal. Chem.*, 310 (1991) 437

55 G. Horányi, G. Inzelt, *Electrochim. Acta.*, 33 (1988) 947

56 C. Barbero, M. C. Miras, O. Haas, R. Kotz, *J. Electrochem. Soc.*, 138 (1991) 669

57 T. Matencio, E. Vieil, *Synth. Met,* 44 (1991) 349

58 M. Lapkowski, E. M. Geniès, *J. Electroanal. Chem.*, 284 (1990) 127

59 H. Q. Tang, A. Kitani, M. Shiotani, *Electrochim. Acta.*, 41 (1996) 1561

60 L. Duic, Z. Mandic, F. Kovacicek, *J. Polymer Sci. Part A: Polymer Chemistry*, 32 (1994) 105

61 F. Rourke, J. A. Crayston, *J. Chem. Soc. Faraday Trans*, 89 (1993) 295

62 Y. Lu, J. Li, W. Wu, *Synth. Met.*, 30 (1989) 87

63 L. Doubova, G. Mengoli, M. M. Musiani, S. Valcher, *Electrochim. Acta.*, 34 (1989) 337

64 R. Córdova, M. A. Del Valle, A. Arratia, H. Gómez, R. Schrebler, *J. Electroanal. Chem.*, 377 (1994) 75

65 A. Q. Zhang, C. Q. Cui, J. Y. Lee, *Synth. Met.*, 72 (1995) 217

66 C. Mailhe-Randolph, A. J. McEvoy, *Ber. Bunsenges. Phys. Chem.*, 93 (1989) 905

67 J. C. LaCroix, A. F. Diaz, *J. Electrochem Soc.* 135 (1988) 1457

68 J. R. Ellis in T. A. Skotheim (ed.) *"Handbook of Conducting Polymers"*, Vol. 1, Marcel Dekker, New York, (1986)

69 S. Pitchumani, V. Krishnan, *Bull. Electrochem.*, 3 (1987) 117

70 A. P. Monkman, P. N. Adams, P. J. Laughlin, E. R. Holland, *Synth. Met.*, 69 (1995) 183

71 P. Novak, B. Rasch, W. Vielstich, *J. Electrochem. Soc.*, 138 (1991) 3300

72 P. J. Nigrey, A. G. MacDiarmid, A. J. Heeger, *J. Chem. Soc., Chem, Commun.*, (1979) 598

73 D. MacInnes Jr, M. A. Druy, P. J. Nigrey, D. P. Nairns, A. G. MacDiarmid, A. J. Heeger, *J. Chem. Soc., Chem, Commun.*, (1981) 317

74 N. L. D. Somasiri, A. G. MacDiarmid, *J. Appl. Electrochem.* 18 (1988) 92

75 E. W. Paul, A. J. Ricco, M. S. Wrighton, *J. Phys. Chem.*, 89 (1985) 1441

76 C. Barbero, M. C. Miras, B. Schryder, O. Haas, R. Kotz, *J. Mater. Chem.*, 4 (1994) 1775

77 R. Ansari. W.E. Price, C.G. Wallace, *Polymer*, 37 (1996) 917

78 A. A. Shaikh, S. M. J. Zaidi, *React. Kinet. Catal. Lett.*, 64 (1998) 343

79 P. M. Wilkinson, B. Doldersum, P. H. M. R. Cramers, L. L. Vandierendonck, *Chem. Eng. Sci.,* 48 (1993) 933

80 H. J. Popel, M. Wagner, *Water Sci. Technol.,* 23 (1991) 1941

81 K. P. Bulmaga, S. I. Zhdanov, *J. Appl. Chem-Engl Tr.,* 64 (1991) 976

82 E. Alper, B. Abusharkh *AICHE J.* 34 (1988) 1384

83 F. H. B. Decastro, M. E. M. Sancho, M. G. Garzon, A. C. Chena, *Afindad,* 41 (1984) 419

84 W. S. Huang, A. G. MacDiarmid, A. J. Epstein, *J. Chem. Soc., Chem. Commun.,* 23 (1987) 1784

85 D. E. Stilwell, S. M. Park, *J. Electrochem. Soc.* 135 (1988) 2497

86 S. J. Choi, S. M. Park, *J. Electrochem. Soc.,* 149 (2002) E26

87 G. Mengoli, M. M. Musiani, G. Zotti, *J. Electroanal. Chem.,* 202 (1986) 217

88 L. M. Doubova, G. Mengoli, S. Valcher, G. Zotti, *Mater Chem. Phys.* 22 (1989) 401

89 C. Q. Cui, J. Y. Lee, *J. Electroanal. Chem.,* 367 (1994) 205

90 J. Kankare, I. A. Vinokurov, *Anal. Chem.,* 69 (1997) 2337

91 Y. B. Shim, D. E. Stilwell, S. M. Park, *Electroanalysis,* 3 (1991) 31

92 D. W. DeBerry, *J. Electrochem. Soc.,* 132 (1985) 1022

93 J. R. Santos, L. H. C. Mattosom A. J. Motheo, *Electrochim. Acta.,* 43 (1998) 309

94 M. A. Malik, M. T. Galkowski, H. Bala, B. Grzybowska, P. J. Kulesza, *Electrochim. Acta.,* 44 (1999) 2157

95 R. Gasparac, C. R. Martin, *J. Electrochem. Soc.* 148 (2001) B138

96 M. C. Bernard, S. Joiret, A. H. L. Goff, P. V. Phong, *J. Electrochem. Soc.,* 148 (2001) B12

97 A. Kitani, M. Kaya, K. Sasaki, *Denki Kagaku,* 52 (1984) 847; 53 (1985) 592; *Chem. Lett.,* (1986) 147

98 S. H. Glarum, J. H. Marshall, *J. Electrochem. Soc.* 134 (1987) 2160

99 S.H. Glarum, J. H. Marshall, *J. Phys. Chem.* 92 (1988) 4210

100 R. Mažeikienè, A. Malinauskas, *Synth. Met.,* 123 (2001) 349

101 W. S. Huang, A. G. MacDiarmid, *Polymer,* 34 (1994) 1833

102 W. J. Albery, Z. Chen, B. R. Horrocks, A. R. Mount, P. J. Wilson, D. Bloor, A. T. Monkman, C. M. Elliott, *Faraday Discuss. Chem. Soc.,* 88 (1989) 247

103 S. W. Feldberg, *J. Am. Chem. Soc.* 106 (1984) 4671

104 A. R. Hillman, S. Bruckenstein, *J. Chem. Soc. Faraday Trans.,* 89 (1993) 339

105 A. R. Hillman, S. Bruckenstein, *J. Chem. Soc. Faraday Trans.,* 89 (1993) 3779

106 M. Pasquali, G. Pistoia, R. Rosati, *Synth. Met.,* 58 (1993) 1

107 A. Redondo, E. A. Ticanelli, S. Gottesfield, *Mol. Cryst. Liq. Cryst.,* 160 (1988) 185

108 R. L. Hand, R. F. Nelson, *J. Am. Chem. Soc.,* 96 (1974) 850

109 R. L. Hand, R. F. Nelson, *J. Am. Chem. Soc.,* 125 (1978) 1059

110 R. U. Bruners, G. Ya. Lisitis, A. V. Vosekalns, *Izv. Akad. Nauk. Lat. SSR, Ser. Khim.,* 4(1986) 450

111 C. D. Batich, H. A. Laitinen, H. C. Zhou, *J. Electrochem. Soc.,* 137 (1990) 883

112 H. Okamoto, T. Kotaka, *Polymer,* 39 (1998) 4349

113 J. Lippe, R. Holze, *J. Electroanal. Chem.,* 339 (1992) 411

114 D. E. Stilwell, S. M. Park, *J. Electrochem. Soc.,* 136 (1989) 688

115 A. G. MacDiarmid, D. Hill, N. L. D. Somasiri, *US Patent* 5,023,149 (1991)

116 L. W. Niedrach, *J. Electrochem. Soc.,* 111 (1964) 1309

117 E. J. Cairns, *Adv. Electrochem. Eng.,* 8 (1991) 337

118 J. J. Llopis, *Catal. Revs. Sci. Eng.,* 2 (1969) 161

119 P. N. Ross, *J. Electrochem. Soc.,* 126 (1979) 79

120 C. Lamy, J. M. Leger, *J. Chim. Phys.,* 88 (1991) 1649

121 N. M. Markovic, H. A. Gasteiger, B. N. Grgur, P. N. Ross, *J. Electroanal.Chem.*, 467 (1999) 157

122 V. Stamenkovic, N. M. Markovic, P. N. Ross Jr, *J. Electroanal.Chem.*, 200 (2001) 44

123 J. Sobowski, A. Wieckowski, *J. Electroanal.Chem.*, 41 (1973) 373

124 J. Sobowski, K. Franaszczuk, K. Dobrowolska, *J. Electroanal.Chem.*, 330 91992) 529

125 S. Chen, T. Noles, M. Schell, *J. Phys. Chem. A.*, 104 (2000) 6791

126 T. J. Schmidt, U. A. Paulus, H. A. Gasteiger, R. J. Behm, *J. Electroanal.Chem.*, 508 (2001) 41

127 V. S. Bagotsky, Y. B. Vassilyev, J. Weber, J. N. Pirtskhlava, *J. Electroanal.Chem.*, 16 (1971) 1511

128 Formaldemeter™ 3 Technical Specifications, PPM Technology Ltd, Parc Menai, Bangor, Gwynedd, Wales, UK

129 K. Scott, W. Tamma, J. Cruikshank, *J. Appl. Electrochem.*, 28 (1998) 289

130 M. Webster, J-T. Wang, S. Wasmus, R. F. Savinell, *J. Electrochem. Soc.*, 143 (1997) L158

131 W.-F. Lin, J.-T. Wang, R. F. Savinell, *J. Electrochem. Soc.*, 144 (1997) 1917

132 R. J. Nichols, *Ph.D Thesis,* University of Southampton (1989)

133 R. Parsons, T. VanderNoot, *J. Electroanal. Chem.*,257 (1988) 9

134 S. Wasmus, A Kuver, *J. Electroanal. Chem.*, 461 (1999) 14

135 R. L. Nurton, *MSc. Thesis*, University of Wales, Cardiff, (1985)

136 A. B. Ben-Rashed, *PhD Thesis*, University of Wales, Cardiff, (1995)

Chapter IV - The Catalytic Activity of Fuel Cell Electrodes – Electrocatalysis

4.0 Introduction

As previously mentioned in section 1.5.5 two methods of improving the response of the fuel cell sensor to formaldehyde were investigated in this work. In this chapter the effect of the nature of the metal on the electrocatalytic oxidation of formaldehyde and other small organic molecules is reported. The work is divided into two sections. Firstly, before the preparation of the fuel cells, the electrocatalytic behaviour of various noble metal and alloys was investigated to determine the best-suited electrocatalysts for formaldehyde oxidation; this was achieved by cyclic voltammetry. In the second part of the work, fuel cells were constructed and their performance evaluated. This was carried out with the aid of a calibrated vapour generator. The choice of the electrodes used in the fuel cells was based on the electrochemical results obtained in the first part of the work. As electrocatalysis of small organic molecules is a rapidly developing field in electrochemistry a review of the subject is presented here.

4.0.1 Electrocatalysis

In the late 1950s concern about the impending energy crisis and already acute environmental problems led to a search for alternative sources of energy. One of the areas that held great promise at that time was electrochemical energy conversion and its subsequent development gave rise to the branch of heterogeneous catalysis known as Electrocatalysis. The term electrocatalysis was first used by Kobosev and Monblanova [1] in 1934, but it was not until 1963 that Grubb used it to describe the processes occurring at electrode surfaces [2]. Today, electrocatalysis has become one of the most active research fields in electrochemistry in response to its many applications and in particular due to the rapid advance in fuel cell development.

Many electrochemical reactions, such as those involved in the energy conversion process, in fuel cells, or those leading to a selective transformation of organic materials, are catalysed by the electrode surface. This constitutes the important field of electrocatalysis, which can be defined, in a first approach as the heterogeneous catalysis of electrochemical reactions by the electrode material. The determining rôle

played by the electrode material was very soon recognised, and particularly the effect of adsorbed species on electrode surfaces, for driving the kinetics and thermodynamics of electrochemical reactions [3]. Therefore most electrocatalytic reactions are mainly controlled by an adsorption process, the rate of which depends strongly on the nature and the structure of the catalytic electrode [4].

Many chemical reactions, although, thermodynamically very favourable, do not by themselves occur at a significant rate. For such reactions to be useful, it is necessary to find a catalyst that will increase the rate of reaction, maybe by several orders of magnitude. In the absence of a catalyst, many electrode reactions occur, if at all, only at very high overpotentials because of poor kinetics (i.e. electrode has low exchange current density). The objective of electrocatalysis is to provide alternative, lower energy of activation pathways and hence to permit such reactions to occur at high current density close to the equilibrium potential [5].

The most extensively studied reactions are those of the hydrogen and oxygen electrode reactions and to a lesser extent the electrode reactions of simple hydrocarbons. Typical values of the exchange current density for electrode reactions of interest in electrochemical energy conversion are shown in table 1, from which it follows that the rate of electrode reaction is dependent on the material from which the electrode is constructed [6]. High values of exchange current density correspond to the fastest rates of reaction and hence indicate the most catalytically active materials.

Metal	$I_0 / A\ cm^{-2}$		
	Hydrogen Evolution[*]	Ethylene Oxidation[*]	Oxygen Reduction[+]
Pt	1×10^{-3}	1×10^{-10}	1×10^{-10}
Pd	1×10^{-3}	1×10^{-10}	1×10^{-10}
Rh	6×10^{-4}	5×10^{-11}	3×10^{-13}
Ru	-	5×10^{-11}	1×10^{-8}
Au	4×10^{-6}	2×10^{-11}	4×10^{-15}
Ni	6×10^{-6}	-	5×10^{-15}

Table 1. Typical values of the Exchange Current Density (I_0) for different metals [6]

* acid electrolyte, +alkali electrolyte,

Most of the electrocatalytic materials are based on noble metals or transition metal elements, in the pure form or as alloys. A good electronic conductivity is needed in most applications. Moreover, the electrode material must have the required mechanical, chemical and electrochemical stability, particularly in contact with aggressive electrolytic media (strong acids or bases). These conditions restrict the choice of an electrocatalytic material to a few metals; in the case of the fuel cell sensors used in this work noble metals are the obvious choice in an acid electrolyte.

It is not sufficient for an electrode material to exhibit good catalytic properties under laboratory conditions. In practise it is often essential for the electrode to catalyse specifically only one reaction. The selection of electrocatalysts for a particular reaction remains largely an empirical process, and catalyst design is still very much a goal for the future. However due to rapid progress in fuel cell research in recent years many suitable catalysts for the oxidation of small organic molecules are slowly being revealed.

4.0.2 Electrooxidation of small organic molecules

Several reviews have appeared over the years on the theoretical and mechanistic aspects of electrocatalysis [7-12], however it was not until 1988, that Parsons published a benchmark review on the electrochemistry of small organic molecules in relation to fuel cell research [13]. The paper has become a standard reference for the collection of work in this area prior to 1988. Today, research in the electrochemistry of small organic molecules remains vigorous, particularly in support of fuel cell applications. New approaches are emerging in the study of electrode kinetics, reaction pathways, electrode materials and electrode surface characterisation techniques [14-21].

Studies on the electrooxidation of such small organic molecules in the 1960s and 1970s were essentially limited by the classical current/voltage/time techniques then available; although providing a wealth of kinetic data [10,13], they lacked the ability to provide essential molecular information. Major breakthroughs in the understanding of the mechanism at the electrode/electrolyte interface were triggered in particular by the development at the beginning of 1980s of *in situ* electrochemical infrared (IR) techniques [14,15] and of the evolution of experimental protocols for the production of ordered and well-defined single crystal electrodes of the Pt-group metals [22,23]. Research into single crystal electrodes has laid the foundations for some basic

understanding of methanol electrocatalysis. Some authors claim that results obtained using single crystals allow conclusions for fuel cell type electrodes [24,25]

The oxidation of small organic molecules, such as formaldehyde, methanol and formic acid, on Pt and other noble metal electrodes have been the subject of a number of investigations in the past few decades [13,17,23]. The studies gained particular interest due to the promising features of the organic fuels as potential energy sources due to their high energy density; this is especially true for methanol which is used in the Direct Methanol Fuel Cell [17]. The electrooxidation of formaldehyde has also attracted considerable interest because of its possible use in fuel cells and its electrochemical detection and measurement in the environment with a sensor [26-29]. Formaldehyde and formic acid also play a key rôle as a representative C1 species in the understanding of related oxidation processes [29].

Because of their simple structure small organic compounds should have the simplest and most straightforward reaction mechanism of all the possible organic fuels. However the oxidation reactions are still generally complex and involve the formation of poisons and reactive intermediates adsorbed on the electrode surface. The reaction mechanism, commonly known in the literature as the dual path reaction mechanism, can be presented in a general form as [10,12,13,30]:
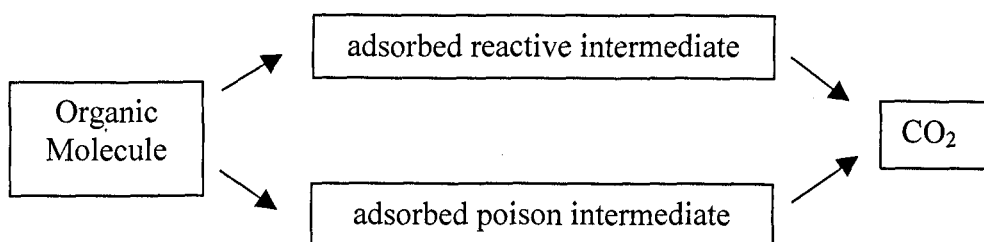
Figure 1 General mechanism of the oxidation of small organic molecules.

A serious problem in electrocatalytic oxidation of organic fuels on noble metal electrodes is the self-poisoning effect of electrodes. Generally, adsorbed reaction intermediates strongly influence the catalytic activity of noble metal electrodes. The major poison on Pt, according to a number of reports based on spectroscopic and electrochemical measurements, is adsorbed CO [13,30]. The formation of chemisorbed CO on the Pt surface acts as a 'poison' by blocking surface sites and

inhibiting further oxidation of the organic molecule. The catalytic activity of the platinum electrode also depends on the nature of the electrode surface, for example the involvement of adsorbed reactive oxygen-containing species (OH_{ads}). This is believed to be involved in the oxidation of both poison and reactive intermediates [17,32]. Accumulation of strongly adsorbed intermediates leads to poor electrode performance [13].

4.0.3 Electrooxidation of formaldehyde

While studies on the electrocatalytic oxidation of methanol are plentiful due to its use in fuel cells only a few reports exist on the electrocatalytic oxidation of formaldehyde. The preference for methanol is probably due to the fact that its complete oxidation to CO_2 generates 6 electrons compared to 4 and 2 for formaldehyde and formic acid respectively; as well as the instability and toxicity of formaldehyde. In the case of formaldehyde, the overall reaction in acid solution is

$$H_2CO + H_2O \longrightarrow CO_2 + 4H^+ + 4e^-$$
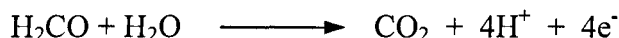
Of the literature published most authors agree that in aqueous media formaldehyde is almost completely hydrated to methylene glycol,

$$HCHO + H_2O \rightleftharpoons CH_2(OH)_2 \qquad K_{eqm} \approx 10^3$$
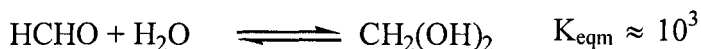
Olivi *et al.* have studied the reaction in perchloric acid and it has been shown that this hydration-dehydration equilibrium plays an important rôle [30,33]. The non-hydrated formaldehyde forms strongly adsorbed CO species, which is responsible for electrode poisoning in the less positive potential region.

$$HCHO \longrightarrow CO_{ads} + 2H_{ads}$$
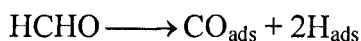
At lower CO coverage there is adsorption of a bridge-bonded species. As coverage increases a linearly bonded form is favoured. Parsons and VanderNoot propose the following mechanism for poison formation [13].
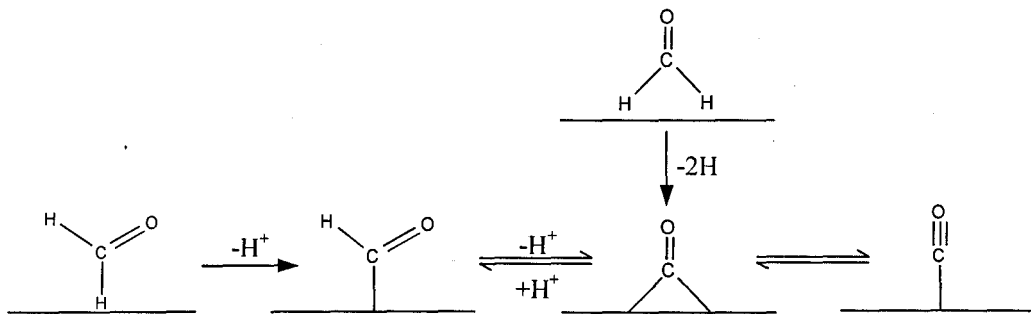
Figure 2 Proposed mechanism for poison formation of formaldehyde on Pt [13]

IR data has also given evidence of an adsorbed methylene glycol and carboxylic acid in the reaction pathway.

$$CH_2(OH)_{2,ads} \longrightarrow HCOOH_{ads} + 2H^+ + 2e^-$$

It has been suggested that formic acid may be further oxidised by a path suggested by Capon and Parsons whereby formic acid is oxidised directly to CO_2 or oxidised *via* a strongly bound intermediate such as adsorbed CO [12,34].

A process involved in the oxidation of formaldehyde on Pt in common with methanol and formic acid is the reaction by which reactive oxygen-containing species adsorbed on the electrode surface are formed, which can be presented as;

$$H_2O \rightleftharpoons OH_{ads} + H^+ + e^-$$
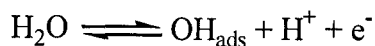
The oxidative removal of adsorbed reactive and poison intermediates from the electrode surface occurs through the reactions of the same with OH_{ads} species, the reaction with adsorbed CO is

$$CO_{ads} + OH_{ads} \longrightarrow CO_2 + H^+ + e^-$$
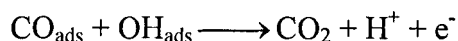
Clearly, from the little investigations conducted on the electrooxidation of formaldehyde there is still a lot of research to be done to understand the process fully.

The information is necessary to avoid a purely empirical approach for the search for better catalysts.

4.0.4 Modification of electrocatalysts

In electrocatalytic processes where the rate determining step is a surface reaction, the measured current density (in terms of geometric area of the electrode) depends on both the genuine catalytic activity of the surface and also the real surface area *i.e.* the roughness of the surface. Hence, in catalytic electrode design the surface should be as rough as possible to give the highest apparent current density.

The challenge in electrocatalysis is to enhance the kinetics of the electrocatalytic oxidation of small organic molecules such as methanol and formaldehyde at low overpotentials by avoiding or limiting the poisoning phenomena observed with pure platinum. Such enhancement can only be obtained by modification of the structure and the nature of the electrode. It is only by modifying the superficial structure of the platinum catalyst by addition of a second or a third metal that it becomes possible to greatly improve the activity of the electrodes [13,32]. The presence of an alloying metal either:

1. Modifies the electronic nature of the surface
2. Modifies the physical structure
3. Blocks the poison formation reactions
4. Adsorbs oxygen/hydroxyl ions which can then take part in the main oxidation reaction.

In this sense, one metal atom adsorbs the reactant molecule and the other absorbs the oxygen which will be required; the two sites together give the complete reaction unit. In other words, the second metal component may act as a catalyst speeding up the removal or otherwise chemical reaction of the inhibitor. The search for possible catalyst materials for the electrooxidation of a wide range of organic substrates has been focused for some time upon binary or ternary alloys [13].

The rôle of Pt remains central to electrocatalysis in fuel cell applications. A variety of alloys, with platinum as the common component, have been explored for enhancing the catalytic oxidation of small organic molecules [13,27,29]. These have been prepared by simultaneous electrodeposition or casting. Such alloy electrodes display a

synergistic effect, with each constituent serving a different purpose in a bifunctional mechanism [17,29]. The greatly enhanced catalytic activity has been attributed to the minimisation of poison formation, as well as the alteration of the electronic structure. Recent advances have shown that Pt-based bimetallic or multimetallic catalysts exhibit enhanced efficiency for methanol oxidation. Alloy electrodes such as Pt-Ru, Pt-Rh, Pt-Rb, Pt-Re and Pt-Sn have been studied [17,35,36], with binary Pt-Ru catalysts showing the highest activity towards the oxidation of methanol [19,36-40]. Ruthenium is critical to the activity of this binary catalyst; although itself essentially inactive towards the oxidation of methanol, it is believed to provide oxygen-containing species at a significantly lower potential than platinum which, in turn can promote CO oxidation [21]. Although the PtRu alloy has been recognised as the best anode catalyst, it is currently thought that platinum intermixed (alloyed) with ruthenium and osmium constitutes the most promising catalyst for the direct methanol fuel cell [20,41]

4.0.5 Electrocatalysts for formaldehyde oxidation

The electrocatalytic oxidation of formaldehyde has been studied on a variety of single metals [13,27,42] including Pt [30,35,43,44] Pd [45], Au [28,46-48] Cu [49, 50], single crystal electrodes [23,48] and a combination of alloys [27,29,51-54] in basic and acidic media. In basic solutions the most promising electrode has been reported to be gold, as it does not get poisoned in such an environment [13,28]. In addition platinum-gold (Pt-Au) alloys have been identified as even better catalysts for the electrooxidation of formaldehyde under the same conditions [29,51,52]. Baltruschat *et al.* reported on the development of a formaldehyde sensor based on this alloy [28]. In this work the electrocatalytic behaviour of metals for formaldehyde oxidation in acidic environments is of interest.

Due to the poisoning effect in acidic environments efficient electrocatalysts for formaldehyde oxidation have been difficult to find. Particularly challenging has been the search for a catalyst that is specific only to formaldehyde. The electrocatalytic oxidation of formaldehyde at platinum-silver (Pt-Ag) and platinum-gold (Pt-Au) alloys has been investigated in several fundamental studies in connection with the possible rôle in fuel cells [29]. Cataldi *et al.* reported on the amperometric monitoring of aldehydes at a glassy carbon electrode coated with mixed valent ruthenium oxide-ruthenium cyanide films [54]. Similarly Wang *et al.* investigated a host of different

metals and alloys for the amperometric detection of formaldehyde; their results revealed that platinum-palladium (Pt-Pd) and platinum-gold (Pt-Au) deposited on glassy carbon were the most active [27].

A comprehensive review of the literature reveals that Pt-Pd alloy is best suited for formaldehyde electrooxidation in acid. This is in agreement with the work carried out in the 1980s by Nurton in the development of the Formaldemeter™ [26]. However, very little work has been done on non-platinum alloys for most small organic molecules. It is therefore clear that a fundamental investigation into the electrooxidation of formaldehyde on various noble metals and alloys is required to develop further the fuel cell in the Formaldemeter™.

4.0.6 Electrocatalysts investigated in this work

The amount of different metals and alloys that can be investigated for the electrocatalytic oxidation of small organic molecules is endless. In addition, not only can different alloys be prepared but also the composition of each metal in the alloy can be varied. It is also well known that varying the preparation method can also influence the activity of the electrocatalyst. It is therefore accepted that there are many routes possible to investigate electrocatalysts for formaldehyde oxidation.

In this study the oxidation of formaldehyde and methanol on pure metals were initially investigated. Binary alloy mixtures of these single metals were then investigated for their modified behaviour. The effect of changing metal composition on the activity of Pt-Pd alloys was also investigated. Finally ternary alloys of Pt-Pd-X (X = Ru, Rh) were examined. Slow sweep voltammetry was utilised to study the mechanistic aspects of the oxidation of formaldehyde; this technique was only performed on Pt-Pd deposits.

4.1 Experimental

Although fuel cell electrodes used in this work were mostly deposited on gold, the depositions carried out in this fundamental investigation were performed on a glassy carbon electrode (0.7 cm^2). Glassy carbon is relatively easy to work and is the preferred substrate in the literature reports. More details on the preparation techniques can be found in the following experimental section.

4.1.1 Electroplating solutions

Standard solutions of pure metal ions solutions were prepared; the amount used was calculated according to the atomic weight of the metal rather then the salt. This was necessary to give equal loading of metals onto the electrode. The assumption was made here was that the rates of deposition were similar. All electroplating solutions were prepared by dissolving the chloride salt of the metal in 20 ml HCl (1 mol dm^{-3}). The total metal content of each solution was calculated to give 0.0475 g of the required metal or alloy. The table below summarises the electroplating solutions prepared and used for electrodeposition in this study.

Metal / Alloy	Atomic Ratio %
Pt	100
Pd	100
Rh	100
Pd-Pt	50:50
Pd-Pt	75:25
Pd-Pt	25:75
Pd-Rh	50:50
Ru-Pd	50:50
Rh-Pd-Pt	33:33:33
Ru-Pd-Pd	33:33:33

Table 2 Metal and alloys used in this work. Atomic ratio indicates the theoretical composition of the alloys investigated.

Electroplating solutions were prepared from the following salts which were supplied by Johnson Matthey Chemicals;

Platinum (II) Chloride (5 % w/v)	$PtCl_2$
Palladium (II) Chloride	$PdCl_2$
Rhodium (III) Chloride	$RhCl_3 \, 3H_2O$
Ruthenium (III) Chloride	$RuCl_3.3H_2O$

4.1.2 Electrodeposition method and procedure

The electrodeposition of the pure metals and alloys was carried out potentiodynamically. Before deposition the bare glassy carbon electrode was polished using successively finer grades of alumina (1µm, 0.3µm, 0.05µm) on a polishing cloth. The electrode was then thoroughly washed with pure deionised water, and placed in an ultrasonic bath of deionised water for five minutes, to remove any impurities remaining. The electrode was finally left to dry in air at room temperature. Electrodepositions on the clean glassy carbon electrodes were carried out in a clean 25 ml beaker using a saturated calomel electrode (SCE) as the reference electrode and a platinum gauze counter electrode.

Electrodepositions were carried in a similar manner to that described by White et al. [55] and Gunasingham and Tan [56] unless otherwise stated. All electrodepositions were performed by cycling the potential of the glassy carbon electrode between 0 and –200 mV at a sweep rate of 50 mV s^{-1}. As the number of deposition cycles was varied in some experiments to investigate the effect of growth condition, the number of cycles is given at all times. The quality and behaviour of the deposits were then investigated by cyclic voltammetry.

4.1.3 Cyclic voltammetry experiments

Figure 3 shows a diagram of the cell used for voltammetric studies. The cell was fitted with a SCE reference electrode and a polycrystalline Pt counter electrode (1 cm^2). The behaviour of the electrodeposits was investigated in sulfuric acid (1 mol dm^{-3}) electrolyte and then in solutions of formaldehyde (0.1 mol dm^{-3}) and methanol (0.1 mol dm^{-3}) in the same acid electrolyte. Prior to all experiments, the solutions were degassed with nitrogen for 20 minutes to remove traces of oxygen in solution.

Gas inlet

Gas outlet

Reference electrode

GC Working electrode (disc)

Pt counter electrode
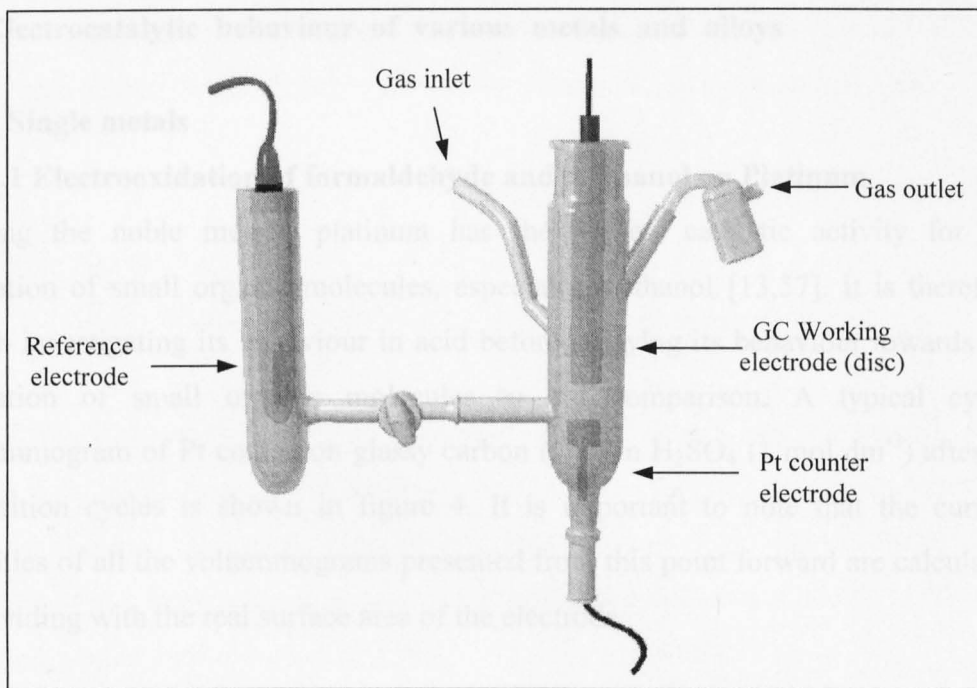
Figure 3 Diagram of the three electrode cell used for electrocatalytic investigation of metallic deposits

The behaviour of the electrodeposits was investigated by cycling the potential between the hydrogen and oxygen evolution regions of the metal. For most deposits the electrode was cycled between limits of -200 mV and $+1000$ mV.

In all experiments the real surface area was used to calculate current density. The real surface area was estimated from the amount of charge for the anodic desorption of the adsorbed hydrogen.

4.2 Electrocatalytic behaviour of various metals and alloys

4.2.1 Single metals

4.2.1.1 Electrooxidation of formaldehyde and methanol on Platinum

Among the noble metals, platinum has the highest catalytic activity for the oxidation of small organic molecules, especially methanol [13,57]. It is therefore worth investigating its behaviour in acid before studying its behaviour towards the oxidation of small organic molecules to aid comparison. A typical cyclic voltammogram of Pt coated on glassy carbon (GC) in H_2SO_4 (1 mol dm^{-3}) after 10 deposition cycles is shown in figure 4. It is important to note that the current densities of all the voltammograms presented from this point forward are calculated by dividing with the real surface area of the electrode.
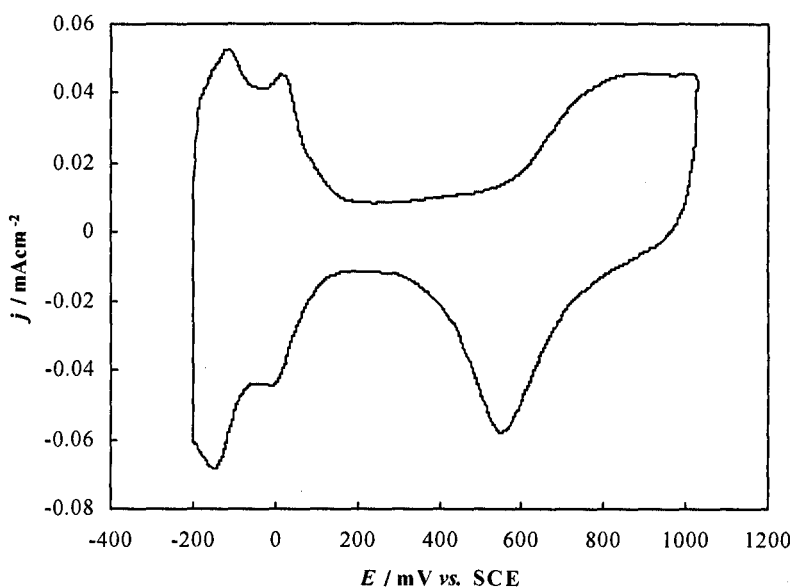
Figure 4. Voltammogram of platinum coated glassy carbon (Pt/GC) in H_2SO_4 (1 mol dm^{-3}) after 10 deposition cycles (RSA=3.7 cm^2).

Interpretation of the voltammogram is well established [58]. The curve consists of several distinct regions. Between −200 and 100 mV hydrogen is adsorbed on the negative sweep and desorbed on the positive sweep. Hydrogen adsorbs reversibly on platinum, the voltammogram being almost symmetrical in this region. Between 100 and 400 mV the double layer region occurs in which the current is low and

mainly corresponds with the charging of the double layer. At potentials above 400 mV oxygen chemisorption commences on the anodic sweep with the process;

$$Pt + OH^- \longrightarrow Pt\text{-}OH + e^-$$

And above 600 mV

$$Pt\text{-}OH + OH^- \longrightarrow Pt\text{-}O + H_2O + e^-$$
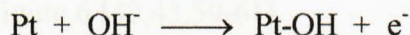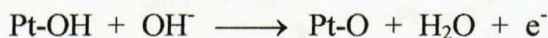
At potentials above 1 V oxygen evolution occurs. On the reverse sweep, any dissolved oxygen present in the neighbourhood of the electrode is reduced together with the chemisorbed oxide layer, though recent research has demonstrated that reduction of the oxide may give rise to a roughened platinum surface that only re-attains an equilibrium morphology [58].

A typical cyclic voltammetry curve of Pt in HCHO (0.1 mol dm^{-3}) in H$_2$SO$_4$ (1 mol dm^{-3}) is shown in figure 5. Two voltammograms are shown, the blue line corresponding to 10 electrodeposition cycles and the red corresponding to 20 electrodeposition cycles. As expected the 20 cycle electrodeposit is more active due to the larger surface area, 5.4 cm^2 compared to 4 cm^2.
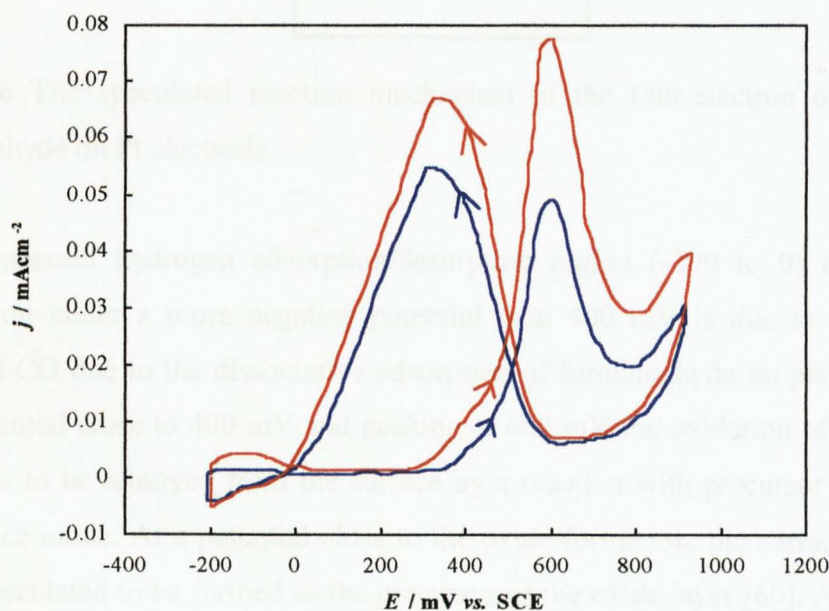
Figure 5 Cyclic voltammograms of platinum coated glassy carbon (Pt/GC) in HCHO (0.1 mol dm^{-3}) in H$_2$SO$_4$ (1 mol dm^{-3}) red – 20 cycle deposit (RSA = 5.4 cm^2), blue – 10 cycle deposit (RSA = 4 cm^2)

142

The general features of these voltammograms are consistent with literature results, which are well documented [30,33,42,43,59-61]. The reaction mechanism speculated so far for the electrooxidation of formaldehyde on a platinum electrode is schematically shown in figure 6 [42,43,59-61]
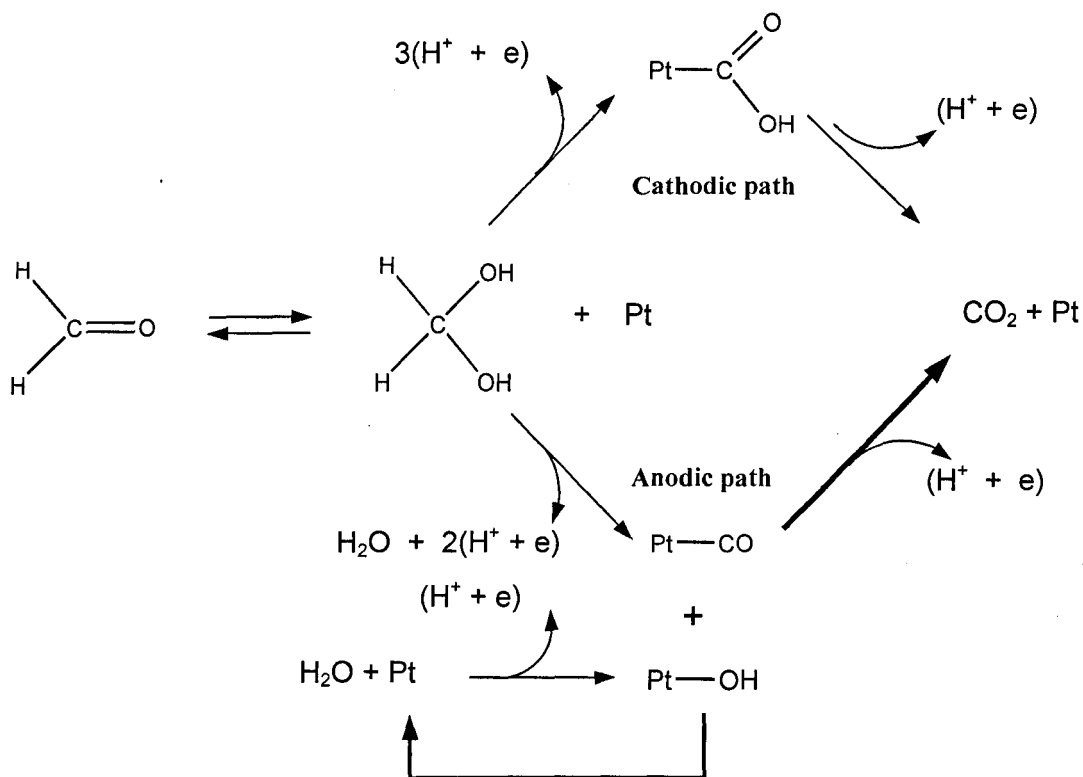
Figure 6 The speculated reaction mechanism of the four-electron oxidation of formaldehyde on Pt electrode

The suppressed hydrogen adsorption/desorption region (-200 to 0) and current passivation under a more negative potential than 400 mV is due to the surface adsorbed CO due to the dissociative adsorption of formaldehyde on platinum [42]. At a potential close to 400 mV and peaking at 600 mV the oxidation of CO begins and starts to be removed from the surface by a reaction with precursor species for the surface oxide. At a potential close to the oxide formation, the surface adsorbed OH is speculated to be formed as the precursor of the oxide layer [60]. As shown in the anodic reaction path, the adsorbed CO is removed by a bimolecular reaction with adsorbed OH species [17,43,59,62,63]. The removal of CO is speculated to occur by the following reaction [43];

$$-CO + -OH \longrightarrow CO_2 + H^+ + 2\neg + e^-$$

where ¬ and e⁻ represent a vacant site on the platinum electrode surface and an electron on the electrode, respectively. The reaction is the so-called indirect path of the oxidation of formaldehyde [60].

The peak above 800 mV is attributed to the surface oxidation and electrooxidation of formaldehyde at the oxide covered electrode. On the reverse sweep reduction of the oxide at around 600 mV leaves a surface free from adsorbed or poisoning intermediates, and formaldehyde oxidation at this surface is rapid as indicated by the large positive current. The cathodic oxidation path of formaldehyde shown in figure 6 occurs [59,60]. Because this reaction proceeds without the adsorbed CO, this is sometimes called the direct oxidation path. These two peaks overlap significantly. The observed current is the sum of the reduction current for the oxide and the oxidation current of the formaldehyde. As the oxide-free platinum surface is gradually covered by CO, the current peaks at around 350 mV.

One particular problem inherent in studying the electrooxidation of the adsorbed fragments, by potential step or potential sweep methods, is deconvoluting the current due to the oxidation of the adsorbed fragments from superimposed current arising from the bulk reaction. Looking closer at the peak at 600 mV on the forward sweep it is evident that there are actually two peaks. A shoulder that peaks at around 400 mV is observed before the main CO oxidation peak. This left shoulder has been previously observed in voltammograms of methanol electrooxidation, and attributed to two adsorbed species [64]. The species were suggested to be a kind of surface bonded water (Pt-OH$_2$) in addition to Pt-OH [65].

Identification of the poisoning intermediates in the electrooxidation of formaldehyde on Pt has proved to be particularly difficult as in aqueous solution, formaldehyde is mainly present in its hydrated form, i.e. methylene glycol, which results from an equilibrium which has a constant for the dehydration reaction of about 10^{-3} [33,66]. This shows that two active species are always in equilibrium in solution, and this increases the complexity of the analysis of the electrooxidation reaction.

Figure 7 shows the cyclic voltammetric response of the same Pt deposits in the presence of methanol. Although the profile is quite different to that of formaldehyde oxidation, the peaks follow the same trend.

144
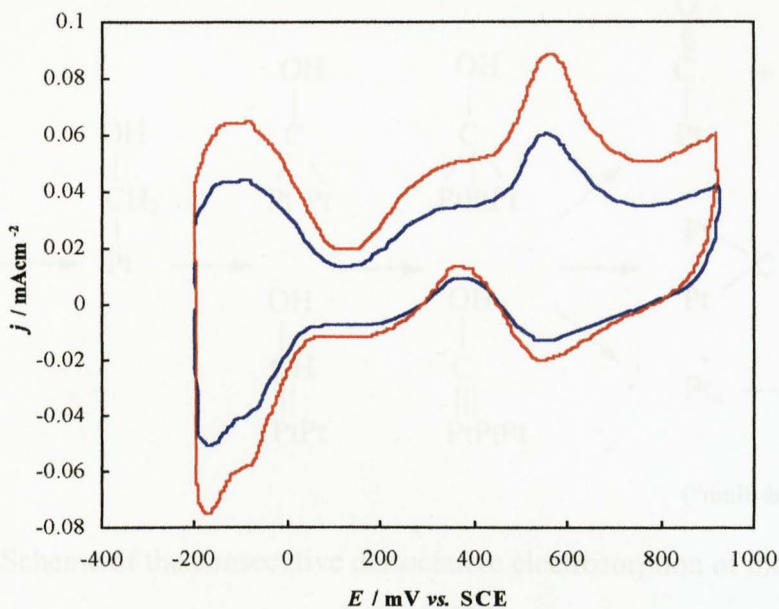
Figure 7 Cyclic voltammograms of Pt/GC in MeOH (0.1 mol dm^{-3}) H$_2$SO$_4$ (1 mol dm^{-3}), red – 20 cycle deposit, (RSA = 5.4 cm^2), blue – 10 cycle deposit, (RSA = 4 cm^2)

On the forward sweep a small oxidation shoulder at 300 mV is clearly seen before the main oxidation peak at 600 mV where oxidation of the adsorbed/poison intermediates occur. Literature reports suggest that the main poison is adsorbed CO (linear, bridge or multiple site) [13,17,23,64], however it has been suggested that COH could also be a poisoning species in the reaction. The identification of the poison has been a major objective over the years and recent investigations suggest that COH is firstly formed with the formation of CO occurring after subsequent reaction steps [27]. The following reaction scheme for poison formation on Pt was proposed.

145

$$
\begin{array}{c}
\\
\\
\text{OH} \\
| \\
\text{CH}_2 \\
| \\
\text{CH}_3\text{OH} \longrightarrow \quad \text{Pt} \longrightarrow
\end{array}
$$

Figure 8 scheme:

```
                                              O
                                              ||
            OH          OH                    C     + 2 Pt
            |           |                     |
     OH     C           C                     Pt
     |     / \         /|\
     CH2   Pt-Pt       PtPtPt      /
     |                              
CH3OH —→  Pt  —→           —→          —→    Pt
                                             \
            OH          OH                    >C=O   + Pt
            |           |                     /
            CH          C              \     Pt
            ||          |||             \
            PtPt        PtPtPt           \→  Ptx ---- C=O
                                                     + (3-x) Pt

                                             ("multi-bonded" CO)
```
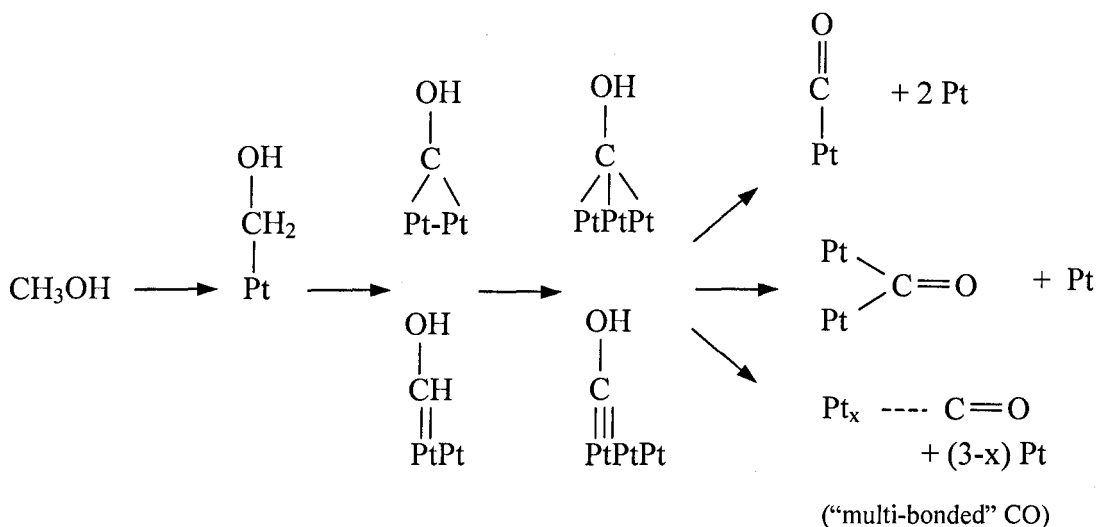
Figure 8 Scheme of the consecutive dissociative electrosorption of methanol at a Pt electrode [27]

Based on this generalised chemisorption scheme, neglecting structural influences of Pt surface heterogeneities one can conceive that three adjacent Pt sites are initially needed for the dissociative methanol adsorption to COH, with up to two of these sites liberated again during subsequent reaction steps yielding either linear bonded – CO or bridge-bonded =CO species which subsequently poison the surface.

The left shoulder observed in the voltammogram is consistent with the results obtained by Shimazu *et al.* [65] which was suggested to be the oxidation of surface bonded water ($Pt-OH_2$) in addition to Pt-OH. At more positive potentials oxidation of bulk methanol occurs. On the reverse sweep at approximately 550 mV reduction of platinum oxide occurs exposing the clean surface to methanol, which causes its oxidation. The hydrogen adsorption-desorption is still very prominent in the presence of methanol compared to the near complete suppression of the same region in formaldehyde, this suggests that the dissociative adsorption of formaldehyde is much faster, which may be due to the simpler nature of the molecule [33].

4.2.1.2 Electrooxidation of formaldehyde and methanol on Palladium

Although Pt and Pd have very similar properties (same group of the periodic table, same fcc crystal structure, similar atomic size), they have different electrochemical

behaviour. Figure 9 shows the typical cyclic voltammetry of Pd coated glassy carbon in H_2SO_4 (1 mol dm^{-3}) after electrodeposition for 10 cycles.
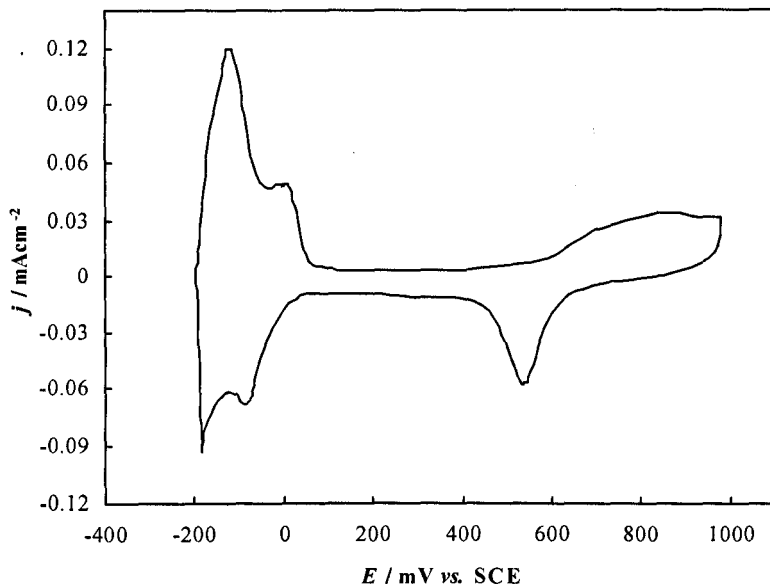
Figure 9 Cyclic voltammogram of Pd/GC electrode in H_2SO_4 (1 mol dm^{-3}),
(RSA = 4 cm^2)

The voltammogram is quite similar to that of platinum under the same conditions, however, there is a very large activity in the region of hydrogen desorption and adsorption between −200 and 0 mV. It is well known that palladium can adsorb large quantities of hydrogen (up to 250 times its own weight) [67]. Based on this property Tateishi *et al.* demonstrated that surface modification of palladium could be used to discriminate between adsorbed and absorbed hydrogen [68].

Figure 10 shows the response of the Pd/GC to HCHO (solid line) and MeOH (dotted line). Compared to the response of formaldehyde it can be seen that there is very little activity towards the electrooxidation of methanol. This may be explained by the hydrogen adsorption/desorption region, where only a little suppression in the region is observed which suggest that methanol does not dissociatively adsorb as well as on the surface as Pt. Dalbay *et al.* have observed a similar behaviour for the electrooxidation of ethylene glycol with Pd being completely inactive [69].
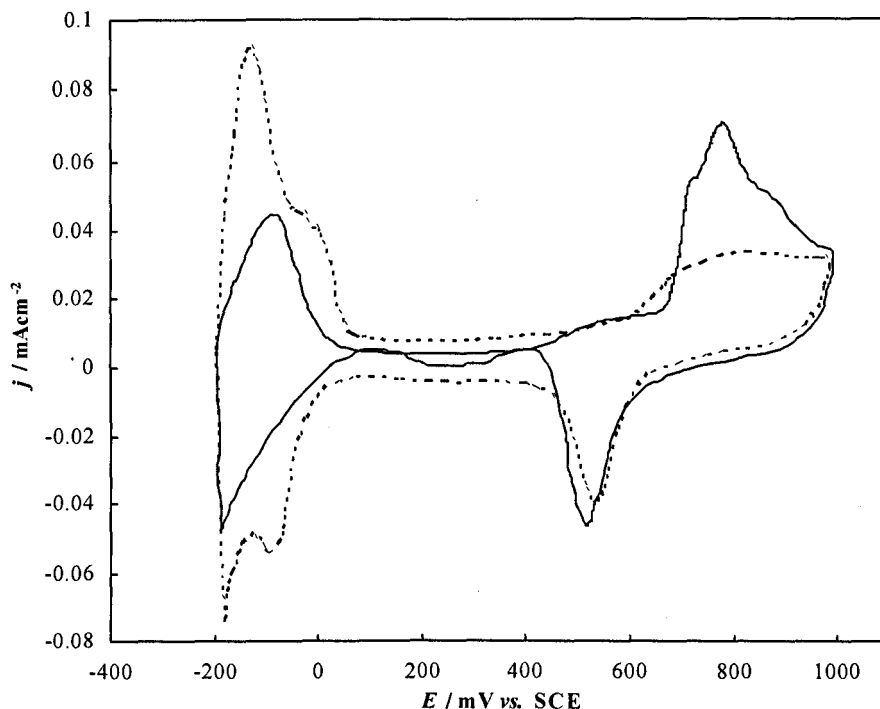
Figure 10 Cyclic voltammogram of Pd/GC in HCHO (0.1 mol dm^{-3}) in H$_2$SO$_4$ (1 mol dm^{-3}) (solid line), MeOH (0.1 mol dm^{-3}) in H$_2$SO$_4$ (1 mol dm^{-3}) (dotted line); (RSA = 5.4 cm^2)

The voltammetric response of Pd/GC to formaldehyde is particularly interesting. It can be seen that the strong hydrogen adsorption on Pd is suppressed in the presence of formaldehyde, indicating the presence of adsorbed intermediates on the surface which is thought to be CO [30,33]. However, this is not as suppressed as was seen for formaldehyde oxidation on Pt. The region 400 to 900 mV is especially interesting. Before the main oxidation at 700-900 mV a small shoulder is clearly visible between 400-700 mV. The position of the shoulder is very similar to the shoulder observed in the voltammogram of formaldehyde oxidation on Pt (figure 5), which was attributed to the oxidation of two types of adsorbed intermediates, -OH$_2$, and –OH [64], it is possible that the same species also adsorb on Pd. At potentials greater than 700 mV a sharp increase in current is observed (peaking at 800 mV) which corresponds to the oxidation of strongly adsorbed intermediates, particularly CO. Compared to the same peak on Pt, the peak occurs 200 mV more positive which suggests that the poisoning species are bound stronger to Pd than on Pt. It is also clear that the peak is in fact a combination of three peaks. In addition to the main peak a sharp peak is observed at 725 mV and a broad peak is observed at 886

mV. This type of behaviour has not been previously reported for Pd and could be as a result of different types of adsorbed intermediates being oxidised. It could also correspond to the adsorption of the same intermediate but in a different configuration on the metal, such as CO linear-, bridge- or multi-bonded.

During the reverse scan, a broad anodic peak spread over 400 mV is observed after the reduction of the PdO at 570 mV. In fact the peak has substructure, indicated by two peaks at 380 mV and 100 mV. These oxidation peaks are related to the oxidation of bulk formaldehyde as a result of PdO reduction.

Zhang *et al.* have indicated that the potential region active for the electrochemical oxidation of HCHO on Pd electrodes depends on the size of the palladium particles which affects the stability of the surface oxygen on palladium. It was also suggested that fresh metallic surfaces of Pd formed by electrochemical reduction give very high catalytic activity for HCHO oxidation [45].

4.2.1.3 Electrooxidation of formaldehyde and methanol on Rhodium

Rhodium is the hardest and the most chemically stable of the platinum-group metals, but it is also one of the most expensive. [70]. The behaviour of rhodium in acidic solution is similar to platinum, as far as the surface processes of hydrogen desorption/adsorption and processes of surface oxidation/reduction are concerned. However, hydrogen is less strongly bonded to the metal than at platinum and its adsorption occurs at less positive potentials. The surface oxidation starts at 0.6 V (*vs.* RHE) at a potential less positive than the oxidation of platinum in sulfuric acid. When the oxidation of the rhodium surface is extended to more positive potentials, the reduction of the oxide species formed proceeds in the reverse scan by a more irreversible electrode reaction [71].

Figure 11 shows the cyclic voltammograms of rhodium coated on glassy carbon (after 40 cycles electrodeposition cycles) in H_2SO_4 (1 mol dm^{-3}), HCHO (0.1 mol dm^{-3}) in H_2SO_4 (1 mol dm^{-3}) and MeOH (0.1 mol dm^{-3}) in H_2SO_4 (1 mol dm^{-3}).
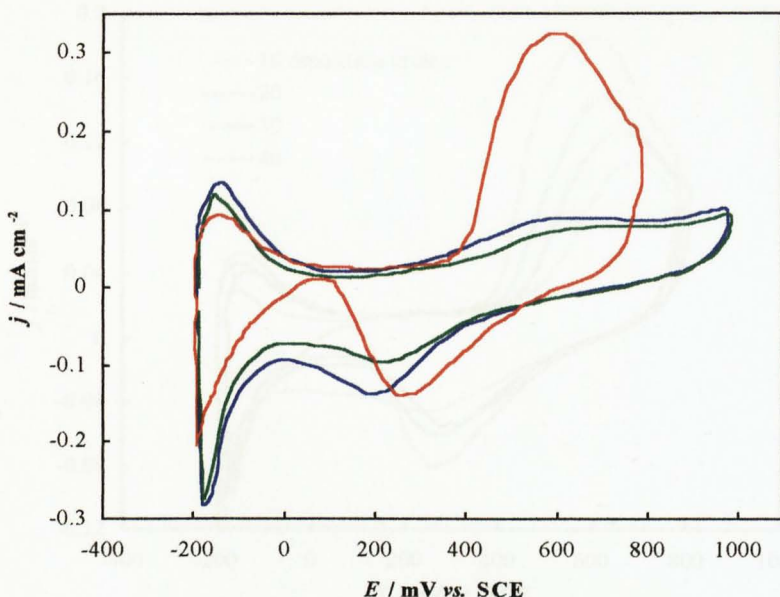
Figure 11 Cyclic voltammograms of Rh/GC (40 deposition cycles) in H_2SO_4 (1 mol dm^{-3}) (blue), HCHO (0.1 mol dm^{-3}) in H_2SO_4 (1 mol dm^{-3}) (red) and MeOH (0.1 mol dm^{-3}) in H_2SO_4 (1 mol dm^{-3}) (green). (RSA = 0.74 cm^2)

The behaviour in H_2SO_4 is similar to that of Pt and Pd in that it exhibits hydrogen adsorption and desorption peaks in addition to the formation and reduction of surface oxides. Little difference can be seen between the cyclic voltammogram of Rh/GC in H_2SO_4 (1 mol dm^{-3}) and in MeOH (0.1 mol dm^{-3}) in H_2SO_4 (1 mol dm^{-3}). However, the reduction in current indicates some degree of poisoning of the surface. This is in contrast to the electrooxidation of formaldehyde where a broad oxidation peak 600 mV can be seen on the positive sweep. The processes occurring are analogous to the electrooxidation of formaldehyde on platinum.

The effect of varying the number of deposition cycles on the electrooxidation of formaldehyde can be seen in figure 12. It is clear that increasing the number of deposition cycles produces, not only a larger surface area, but also a more active catalyst for the electrooxidation of formaldehyde.

It can be seen that the peak potential corresponding to the oxidation of HCHO shifts towards less positive values with increasing number of deposition cycles. Figure 13 shows the relationship between the number of deposition cycles and the real surface area of the electrode; it also shows how the real surface area is related to the potential of the oxidation peak.

150
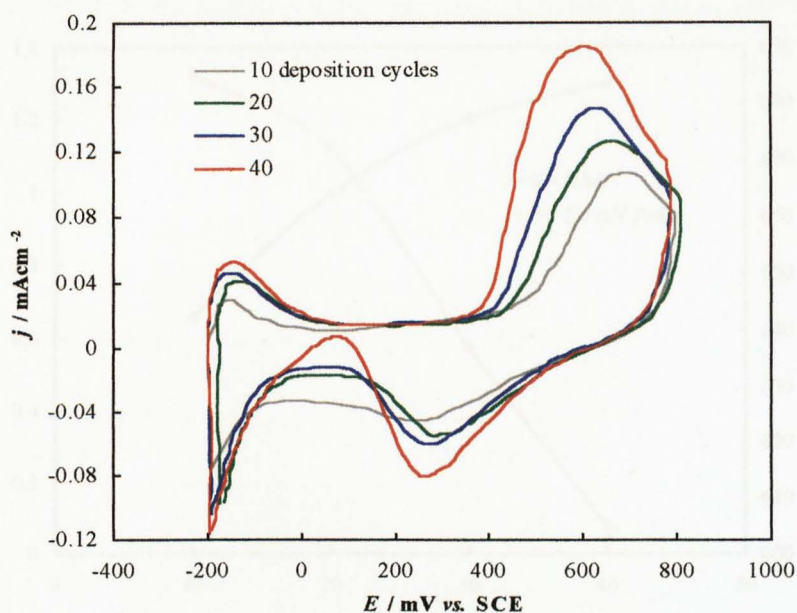
Figure 12 Cyclic voltammogram of various deposits of Rh/GC in HCHO (0.1 mol dm^{-3}) in H$_2$SO$_4$ (1 mol dm^{-3}); j calculated by dividing with real surface area (RSA shown in figure 13)

It is clear from the plot that there is a strong relationship between the number of deposition cycles and real surface area. With increasing number of cycles the real surface area of the rhodium electrode increases. It is also noticeable that the surface area starts to level off after 40 deposition cycles. It is possible that increasing the number of deposition cycles increases the particle size of the metal. The curve suggests that the particle size cannot increase any further over 40 – 50 cycles, i.e. a particle size threshold has been reached.

The 'particle size effect' or the 'crystallite size effect' is only a recent phenomenon in fuel cell research and controversy still exists over its true existence [17]. Generally, the majority of investigators agree that catalysis by small particles is different from that at smooth electrodes [72]. Lee *et al.* explained how platinum supported on high surface area materials is of great significance to obtain effective catalysts [73]. Yahikozawa *et al.* have demonstrated that increasing the particle size of platinum increases the activity towards the oxidation of small organic molecules [47]. However it has also been proposed that "no size effect exists" or "the decisive factor influencing the electrocatalytic oxidation must be an inter-crystallite distance, not a particle size" [45].
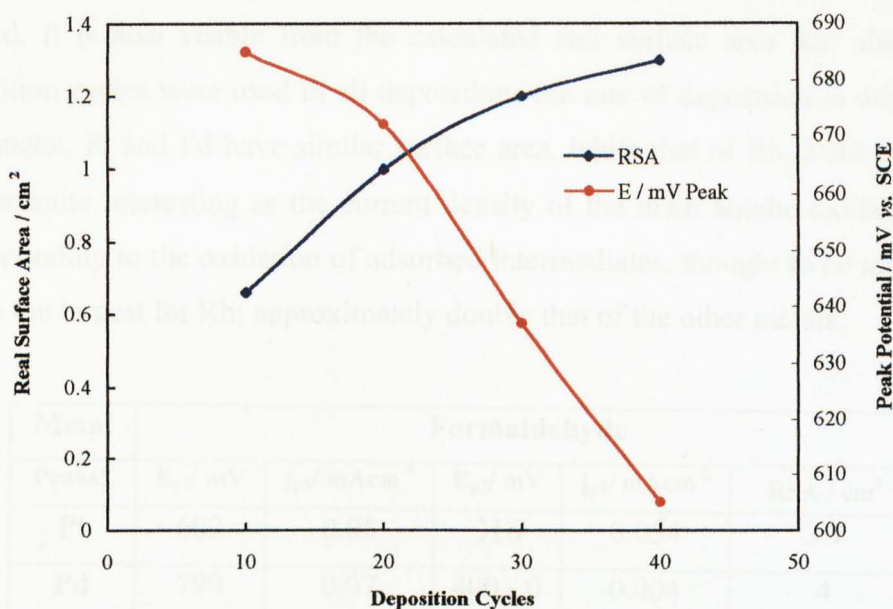
Figure 13 Relationship between the number of deposition cycles, real surface area and oxidation peak potential

The shift in the oxidation peak potential to more negative values with increasing surface area is particularly interesting. It is possible that a higher surface area electrode necessitates a lower overpotential to oxidise the strongly adsorbed intermediates. Yahikozawa *et al.* suggested that the shift of the anodic peak potential for the oxidation of small organic molecules must be related to the particle size dependency on the formation of the fresh surface of the metal particles [47]. Napporn *et al.* proposed that the negative shift in potential indicates that less poisoning species are formed on the surface [74].

4.2.1.4 Conclusions from single metal investigations

From these initial investigations on Pt, Pd and Rh it is evident that the choice of metal plays a significant rôle in the efficient electrooxidation of small organic molecules. In addition it has been demonstrated that the catalytic activity depends on the preparation procedure. Table 3 summarises the results obtained from deposits of the pure metal. P1 corresponds to the oxidation of adsorbed CO and P2 corresponds to the oxidation of bulk formaldehyde or methanol on the reverse sweep. Also shown is the calculated real surface area of the electrocatalysts.

It can be seen that methanol oxidation only occurs on Pt at the concentration levels studied. It is also visible from the calculated real surface area that although 10 deposition cycles were used in all depositions the rate of deposition is different for each metal, Pt and Pd have similar surface area, while that of Rh is six times less. This is quite interesting as the current density of the main anodic oxidation peak, corresponding to the oxidation of adsorbed intermediates, thought to be mainly CO, is also the largest for Rh; approximately double that of the other metals.

Metal	Formaldehyde				
Peaks*	E_{p1}/ mV	j_{p1}/ mAcm^{-2}	E_{p2}/ mV	j_{p2}/ mAcm^{-2}	RSA / cm^2
Pt	602	0.05	316	0.054	3.7
Pd	790	0.07	400 - 0	0.004	4
Rh	685	0.108	45	-	0.66
	Methanol				
Pt	570	0.06	360	0.013	4
Pd	-	-	-	-	4
Rh	-	-	-	-	0.66

Table 3 Values of peak potentials and peak current densities for the electrooxidation of HCHO (0.1 mol dm^{-3}) in H$_2$SO$_4$ (1 mol dm^{-3}) and MeOH (0.1 mol dm^{-3}) in H$_2$SO$_4$ (1 mol dm^{-3}) for different metals coated on glassy carbon. All metals deposited for 10 cycles. * p1 and p2 refer to the anodic peaks in the forward and reverse scan, respectively.

It would be expected that the metal deposit with the largest surface area would give the highest current density for the oxidation; as this is clearly not the case the enhanced catalytic activity must be related to the particle size of the metal deposit. This would have to be confirmed in future experiments where the utilisation of techniques such as Transmission Electron Microscopy (TEM) would be advantageous to confirm the particle sizes.

Comparing the position of the anodic oxidation peak, the oxidation of mainly adsorbed CO, the peak potential increases in the order Pt < Rh < Pd which suggests that the intermediates bind more strongly in the same order. The shift in potential is most probably related to the surface characteristic of the metal which affects the bonding of the adsorbed intermediates, however it is difficult to confirm this with

the data presented here, future experiments should include surface characterisation techniques such as '*in situ*' FTIR.

The ultimate objective of this work is to find a suitable catalyst for specific oxidation of formaldehyde. In summary platinum shows a good electrocatalytic activity to formaldehyde but its also very active to methanol. In comparison, palladium is active towards the oxidation of formaldehyde but shows negligible activity to methanol. Rhodium is also active towards formaldehyde and not methanol. It is with these results in mind that alloys of the metals are investigated.

4.2.2 Binary alloys

4.2.2.1 Electrooxidation on Platinum-Palladium alloys

Since Platinum-Palladium (Pt-Pd) alloy has been previously shown to have superior activity for the electrooxidation of formaldehyde [26], it was decided to investigate this alloy first. The current fuel cell in the Formaldemeter™ contains electrodes of 50:50% atomic ratio Pt-Pd. In this study the effect of changing the atomic ratio of Pt:Pd on the activity of the catalyst is investigated. Three alloys of Pt-Pd were investigated of atomic ratios 50:50%, 25:75% and 75:25%. Due to the differing rates of deposition of each metal it makes it very difficult to predict the atomic ratio of each metal on the surface of the electrode. Therefore atomic ratios referred to in this work apply to electroplating solutions only, not the surface composition of the electrode. The cyclic voltammograms of the alloys in H_2SO_4 (1 mol dm^{-3}) after the same number of deposition cycles is shown in figure 14.
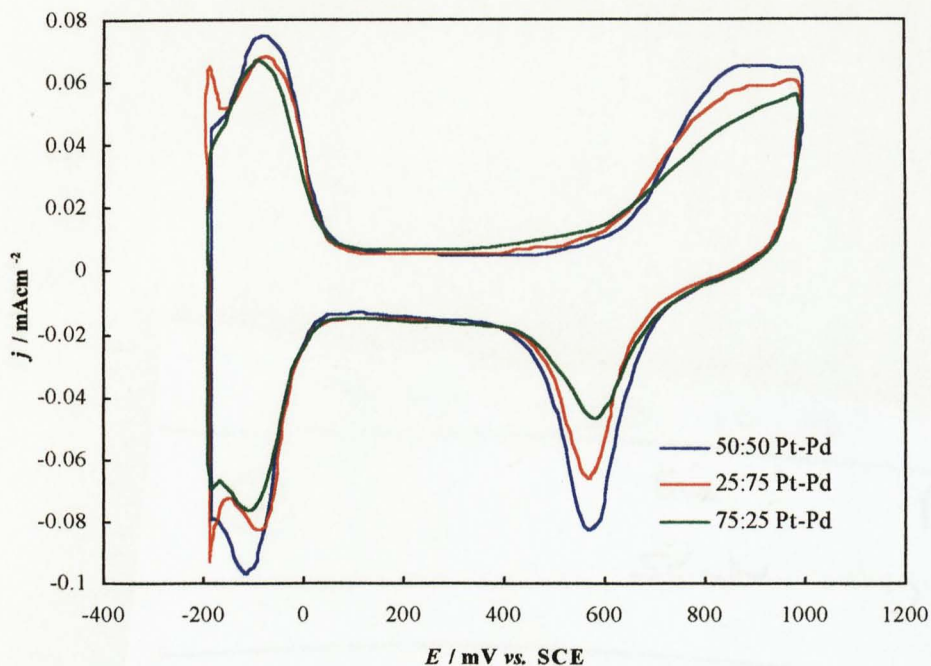
Figure 14 Cyclic voltammogram of the different Pt-Pd/GC alloys in H_2SO_4 (1 mol dm^{-3}). Deposited for 5 cycles. (RSA 50:50 Pt-Pd = 4.05 cm^2; RSA 25:75 Pt-Pd = 2.60 cm^2; RSA 75:25 Pt-Pd = 2.11 cm^2)

The current peaks on each voltammogram occur at potentials between those at which the corresponding peaks appear for the separate component metals; the actual value depends on the proportion of the pure metals. These observations support the conclusion that characteristics of the chemisorption of hydrogen and oxygen on these alloy systems are a composite of the properties of the individual metals as shown previously by Dalbay *et al.* [69] and Rand *et al.* [75] The intensity of the peaks also reflects the composition of the metals. At high Pt loading (75:25 Pt-Pd) it can be seen that the hydrogen evolution region is suppressed in comparison to the others. Also the reduction peak of the surface oxides on the reverse sweep is reduced. This is typical of a platinum electrode as shown previously in figure 4. At higher Pd loading, features that are typical of Pd metal become more apparent. For example, the strong hydrogen adsorption-desorption peaks.

The effect of surface composition is clearly demonstrated in figure 15 which shows the cyclic voltammograms of the same alloys in HCHO (0.1 mol dm^{-3}) in H_2SO_4 (1 mol dm^{-3}).

155
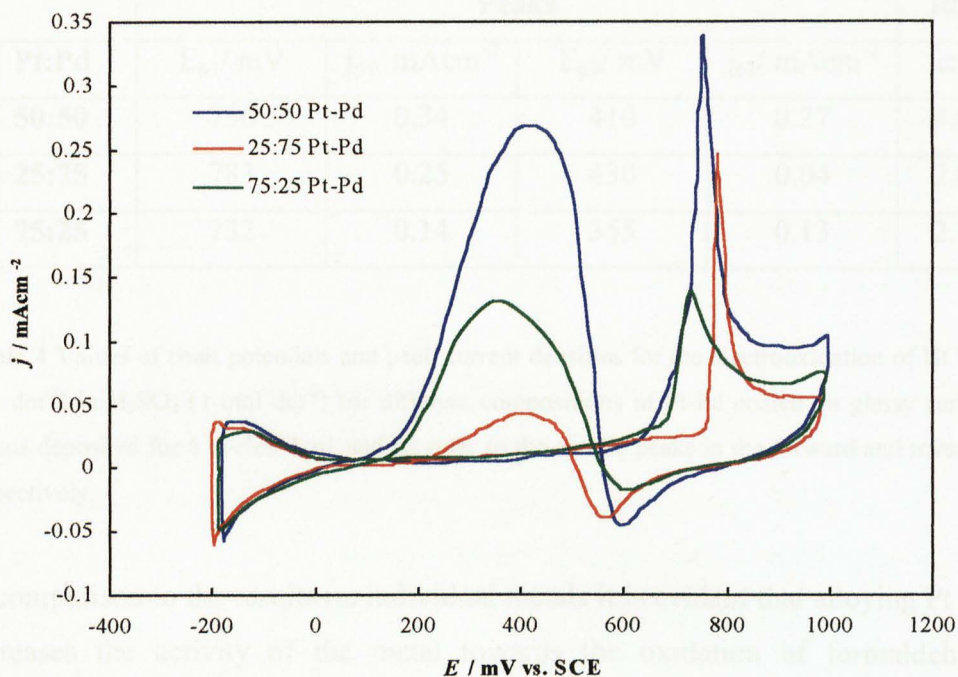
Figure 15 Cyclic voltammograms of different Pt-Pd/GC alloys in HCHO (0.1 mol dm^{-3}) in H$_2$SO$_4$ (1 mol dm^{-3}) (RSA 50:50 Pt-Pd = 3.85 cm^2; RSA 25:75 Pt-Pd = 3.07 cm^2; RSA 75:25 Pt-Pd = 2.50 cm^2)

It can be seen that the composition of the deposit has a very strong influence on the activity of the alloy towards formaldehyde electrooxidation. The peak intensities vary in addition to the peak potentials. At high Pd loading (25:75 Pt-Pd) the anodic oxidation of adsorbed CO occurs at 780 mV. With increasing Pt composition, 50:50 Pt-Pd and 75:25 Pt-Pd the peak position shifts negatively to 745 and 732 mV respectively. These peak positions are a composite of the individual properties of the metals. In the previous experiments on single metals summarised in table 3 it was shown that the anodic oxidation peak of formaldehyde on Pd occurred at 790 mV while that of Pt occurred at 600 mV. Therefore increasing the Pd content in the alloy shifts the peak positively, while increasing Pt content shifts the potential negatively. This behaviour is also shown in the oxidation on the reverse sweep. A summary of peak positions, peak current density and real surface area are presented in table 4.

156

| Pt:Pd | Peaks | | | | RSA |
	E_{p1}/ mV	j_{p1}/ mAcm^{-2}	E_{p2}/ mV	j_{p2}/ mAcm^{-2}	cm^2
50:50	756	0.34	410	0.27	4.05
25:75	783	0.25	430	0.04	2.60
75:25	732	0.14	355	0.13	2.11

Table 4 Values of peak potentials and peak current densities for the electrooxidation of HCHO (0.1 mol dm^{-3}) in H$_2$SO$_4$ (1 mol dm^{-3}) for different compositions of Pt-Pd coated on glassy carbon. All metals deposited for 5 cycles. * p1 and p2 refer to the anodic peaks in the forward and reverse scan, respectively.

In comparison to the results on individual metals it is evident that alloying Pt and Pd increases the activity of the metal towards the oxidation of formaldehyde as indicated by the large current density of the oxidation peaks on the anodic and cathodic sweeps. The greatly enhanced catalytic activity can be attributed to changes in the adsorption features of the surface, and particularly to the suppression of the formation of adsorbed intermediates (which block the oxidation on pure Pt surfaces) [27,44]. The exact values of peak potential and peak current density, however, must be treated with caution as the electrodes differ in real surface area, even though they were deposited for the same number of cycles.

An interesting feature common to the Pt-Pd alloys is the sharp nature of the CO oxidation peak on the positive scan. These are very sharp in comparison to oxidation on the individual metals. The alloy containing most Pd is the sharpest, while the alloy containing most Pt is the broadest; however, this peak is very sharp compared to Pt alone.

The oxidation potentials and peak sharpness suggest the oxidation of the CO intermediately occurs at a particular environment which is different on each alloy due to the Pt:Pd ratio, i.e. different neighbouring atoms. Motoo and Watanabe proposed that each atom plays a definite rôle in the overall oxidation process [77]. This explanation may apply to the results obtained in the work where each alloy has a different atomic structure. Thus, a different atomic structure of the catalyst may cause the bonding of CO in only one configuration (linear, bridged or multibonded), which could result in the sharpness of the peak. The oxidation of formaldehyde on

the 25:75 Pt-Pd is extremely narrow and occurs only over a range of approximately 100 mV.

In all three voltammograms the hydrogen adsorption-desorption region is suppressed compared to the same alloys in acid. This was also observed for the oxidation of formaldehyde on single metals due to the adsorption of poison/reaction intermediates as a result of formaldehyde dissociation. However, in comparison to formaldehyde oxidation on Pt there is reduced suppression for all the alloys suggesting that less poisoning occurs on the Pt-Pd alloys.

Although the alloys show superior catalytic activity for the electrooxidation of formaldehyde it is also important for the sensor application that the activity of the catalyst is reduced towards methanol. Figure 16 shows the cyclic voltammograms of the same alloys in MeOH (0.1 mol dm^{-3}) in H$_2$SO$_4$ (1 mol dm^{-3}).
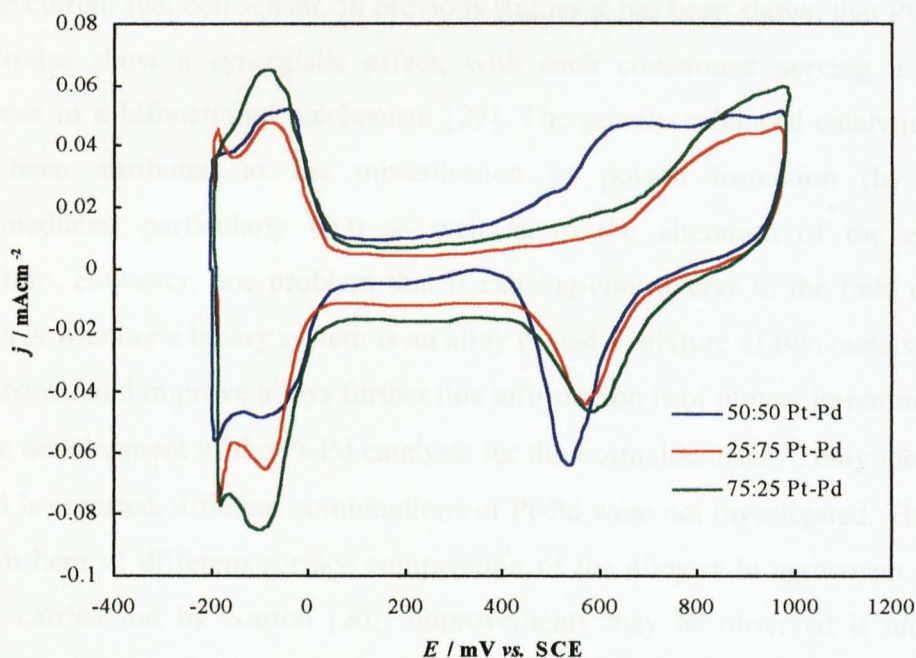
Figure 16 Cyclic voltammograms of the different alloys in MeOH (0.1 mol dm^{-3}) in H$_2$SO$_4$ (1 mol dm^{-3}) (RSA 50:50 Pt-Pd = 3.60 cm^2; RSA 25:75 Pt-Pd = 3.07 cm^2; RSA 75:25 Pt-Pd = 2.11 cm^2)

The surface composition again has a very strong influence on the activity of the alloy towards methanol electrooxidation. The activity of all the alloys towards methanol oxidation is very low, with only 50:50% Pt-Pd showing a small response. Increasing the Pd content (25:75 Pt-Pd) has the effect of reducing catalytic activity towards methanol. In a previous experiment on Pd coated on GC, figure 10, it was

shown that Pd was indeed inactive towards methanol. A similar effect has been observed by Kadirgan *et al.* [78] for methanol and by Dalbay *et al.* [69] for ethylene glycol oxidation. Increasing the Pd in the alloy reduced the catalytic activity. In both cases the effect was attributed to the inactivity of Pd towards the oxidation of methanol or ethylene glycol.

Recalling the mechanism shown in figure 8 proposed for poison formation from the oxidation of methanol, it is possible that alloying Pt with Pd dilutes the Pt sites preventing the presence of the three adjacent sites necessary for the formation of the COH intermediate. As a result the reaction mechanism would favour the adsorption of CO, and thus a decrease in activity for methanol.

Although the 50:50% Pt-Pd alloy shows a small response to methanol oxidation, its activity towards formaldehyde justifies it as the preferred composition of the alloy in the current fuel cell sensor. In previous studies it has been shown that Pt-Pd alloy electrodes show a synergistic effect, with each constituent serving a different purpose in a bifunctional mechanism [27]. The greatly enhanced catalytic activity has been attributed to the minimisation of poison formation (by reaction intermediates, particularly CO) as well as to the alteration of the electronic structure. However, one problem that is causing controversy in the field of binary alloys is whether a binary system is an alloy or just a mixture of two metals [17]. To understand and improve alloys further this information is of utmost importance.

In the development of the Pt-Pd catalysts for the Formaldemeter™, only the 50:50% Pt-Pd is reported, different combinations of Pt-Pd were not investigated. The results shown here of different surface composition of the alloy is in agreement with the work carried out by Nurton [26]. Improvements may be observed if only small adjustments of ± 5-10 % of each metal were investigated. Too much Pt in the alloy would result in more poisoning, while too much Pd would reduce the activity, hence it is very important to have the right balance of each metal in the alloy.

Since the 50:50% Pt-Pd alloy showed favourable properties as a selective catalyst for formaldehyde oxidation it was decided to investigate its electrocatalytic behaviour further utilising slow sweep voltammetry.

4.2.2.2 Slow sweep voltammetry of Pt-Pd (50:50%)

The behaviour of the Pt-Pd alloy in HCHO (0.1 mol dm^{-3}) in H$_2$SO$_4$ (1 mol dm^{-3}) and MeOH (0.1 mol dm^{-3}) in H$_2$SO$_4$ (1 mol dm^{-3}) at a sweep rate of 1 mVs^{-1} is shown in figure 17.
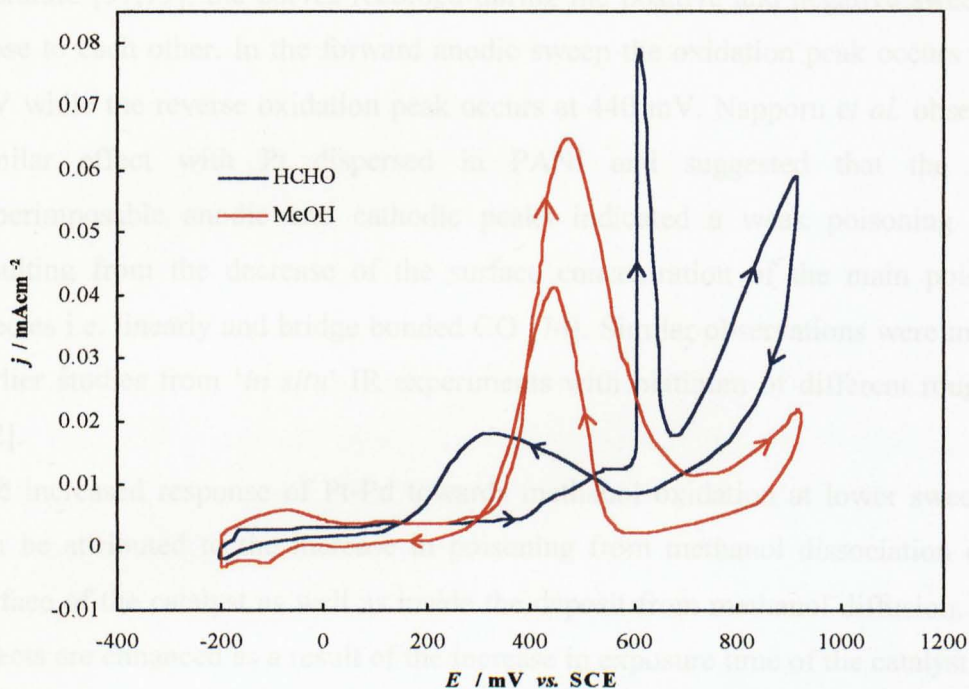
Figure 17 CVs of 50:50% Pt-Pd/GC alloy in HCHO (0.1 mol dm^{-3}) in H$_2$SO$_4$ (1 mol dm^{-3}) and MeOH (0.1 mol dm^{-3}) in H$_2$SO$_4$ (1 mol dm^{-3}), v = 1 mVs^{-1} (RSA 50:50 Pt-Pd = 2.57 cm^2)

Slowing the sweep rate has a great impact on the profiles of the voltammograms. The formaldehyde voltammogram is more detailed, especially between the ranges of 400 mV to 800 mV. The methanol voltammogram shows a substantial response to methanol, which is in complete contrast to the voltammograms at higher sweep rates (50 mVs^{-1}) where very little activity for methanol was found (figure 16).

Response to methanol

The response of the alloy to methanol is very similar to the oxidation of methanol on Pt [57,79,80]. Although the peak at 480 mV is associated with the electrooxidation of adsorbed CO, the peak has a large contribution from the readsorption of methanol and subsequent electrooxidation of the adsorbed fragments at relatively slow sweep rates. Lamy *et al.* have shown that, even at fast

sweep rates (50 Vs^{-1}) the voltammograms show contribution from the direct oxidation of methanol from solution [81].

An interesting feature of the electrooxidation of methanol on Pt-Pd is the forward and reverse anodic oxidation peak positions. In contrast to Pt reported in the literature [57,79], the curves recorded during the positive and negative sweeps are close to each other. In the forward anodic sweep the oxidation peak occurs at 484 mV while the reverse oxidation peak occurs at 440 mV. Napporn et al. observed a similar effect with Pt dispersed in PANI and suggested that the nearly superimposable anodic and cathodic peaks indicated a weak poisoning effect, resulting from the decrease of the surface concentration of the main poisoning species i.e. linearly and bridge bonded CO [74]. Similar observations were made in earlier studies from 'in situ' IR experiments with platinum of different roughness [82].

The increased response of Pt-Pd towards methanol oxidation at lower sweep rate can be attributed to the increase in poisoning from methanol dissociation on the surface of the catalyst as well as inside the deposit from methanol diffusion. These effects are enhanced as a result of the increase in exposure time of the catalyst to the dissociative adsorption of methanol at slower sweep rates. This is confirmed by the hydrogen adsorption-desorption region which is much more suppressed in comparison to the same experiment at higher sweep rate where virtually no suppression occurred.

Although it is evident that poisoning of the alloy occurs it is possible that dilution of the Pt sites with Pd forms weaker bonding with poisoning intermediates such as adsorbed COH and CO [27], in comparison to pure Pt. The fact that the oxidation potential is shifted negatively, 484 mV in comparison to 600 mV on pure Pt and that both anodic and cathodic oxidation peaks are nearly superimposable supports this assumption.

Response to formaldehyde

As briefly mentioned, voltammograms of formaldehyde on Pt-Pd obtained at slow sweep rates reveal very interesting features compared to the voltammogram at higher sweep rate (discussed in section 4.2.2.1). There is a strong suppression of the hydrogen region suggesting formation of poisonous species from the dissociative adsorption of formaldehyde. Two distinctive small pre peaks at 430 mV and 550

161

mV occur followed by an unusually large narrow peak at 610 mV. The fact that this peak is very narrow (70 mV peak width) and occurs around 600 mV strongly suggests the oxidation of linearly adsorbed CO species. Similar behaviour have been observed by Burke *et al.* who investigated the electrooxidation of CO on Pt; the narrow peak was attributed to the oxidation of a monolayer of CO [83]. This may apply to the results shown here where the very slow sweep rate could provide sufficient time for a monolayer of CO to form.

The electrooxidation of CO on Pt has been extensively studied in recent years [84]. Caram and Gutiérrez have shown that the electrooxidation of CO is greatly influenced by the admission potential [85]. Beden *et al.* detected two peaks of adsorbed CO species, dependent on both the electrode potential and the degree of coverage [86]. The existence of two peaks led them to the assumption that there were two energetically different adsorbed states differing by the nature of the bonding to Pt. By analogy with gas phase data and results of EMIRS these peaks were believed to be bridge bonded CO (0.41 V *vs.* SCE) adsorbed first at low coverage and linear CO (0.61 V *vs.* SCE) predominant at high coverage. This suggests that the pre peaks observed on Pt-Pd could be due to bridge-bonding or multi-bonded CO species. However, work by Seland [64] and Shimazu [65] suggest the pre peaks are due to adsorbed OH and OH_2. Future experiments utilising additional techniques such as *'in situ'* FTIR should be carried out to confirm the origin of the observed pre-peaks.

After the electrooxidation of CO (700 mV) the current steadily rises at a sharp rate until the potential is reversed. As the surface is clean from poisoning species the electrooxidation of bulk formaldehyde occurs at increased potential. This behaviour was also observed at higher sweep rate but to a lower extent. The same is true for the reverse sweep with surface oxides of the alloy reduced at 580 mV and the subsequent oxidation of formaldehyde occurring at 320 mV.

On the basis of the Pt single crystal work, it seems that the main oxidation reaction for HCHO involves three sites [87-89]. The number of sites required for poison formation from HCHO seems most likely to be four. It has been pointed out that the number of sites needed for a reaction to occur may not be the same as the number required for the final adsorbed product since an adjacent adsorbed species may be necessary for the reaction to occur [89]. This structural sensitivity does not seem to apply necessarily in alkaline solutions [90].

Clearly more work is needed to fully understand the processes occurring at the Pt-Pd electrode surface, as mentioned earlier '*in situ*' IR techniques should be used in future experiments to yield more details about the oxidation mechanism and the nature of the adsorbed species.

4.2.2.3 Electrooxidation on Platinum - Rhodium alloys

Although there have been many investigations on Pt alloys, there have been relatively few reports on Pt-Rh alloy. Methanol oxidation has been studied on a range of Pt-Rh alloys prepared by selective dissolution of rhodium from an alloy with an initial content of 75 % Rh [91]. It was shown that at low potentials, alloys containing small percentages of rhodium were more active than pure platinum. Also Pt-Rh alloys have been investigated for the oxidation of formic acid in aqueous H_2SO_4 [92]. Wang *et al.* have investigated the amperometric response of this catalyst for formaldehyde oxidation [27]; however, it was shown that Pt-Pd had superior catalytic activity. Figure 18 shows the activity of a 50:50 % Pt-Rh alloy in H_2SO_4 (1 mol dm^{-3}), HCHO (0.1 mol dm^{-3}) in H_2SO_4 (1 mol dm^{-3}) and MeOH (0.1 mol dm^{-3}) in H_2SO_4 (1 mol dm^{-3}).
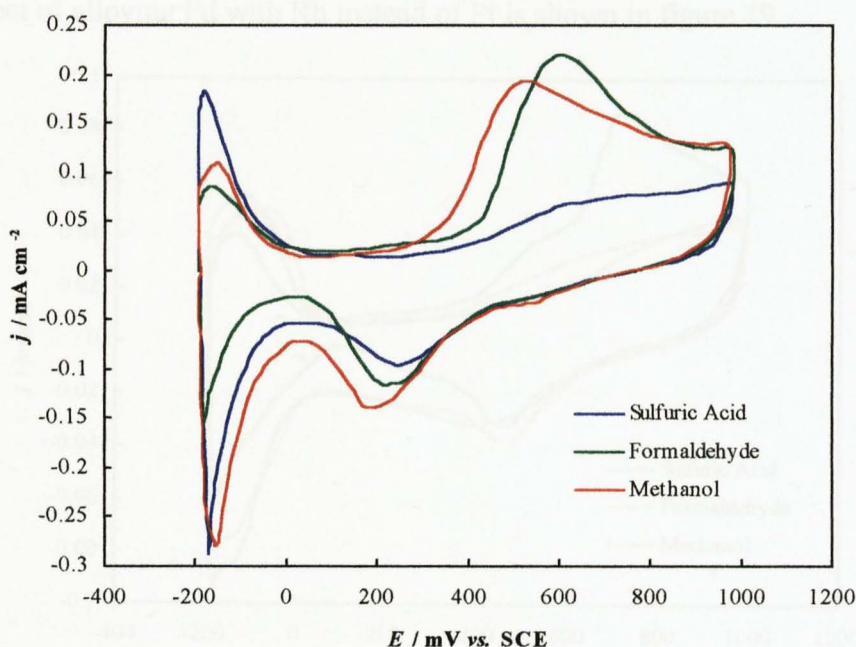
Figure 18 Cyclic voltammograms of 50:50% Pt-Rh/GC in H_2SO_4 (1 mol dm^{-3}), HCHO (0.1 mol dm^{-3}) in H_2SO_4 (1 mol dm^{-3}) and MeOH (0.1 mol dm^{-3}) in H_2SO_4 (1 mol dm^{-3}). Deposited for 5 cycles. (RSA = 0.90 cm^2)

163

It can be seen that the alloy is active towards both formaldehyde and methanol with the voltammetric response being a composite of the single metals. While Rh was inactive towards methanol at the range of concentration studied, the alloy with Pt shows a good electrocatalytic activity towards methanol oxidation. It is possible that the Pt atoms in the alloy provide a site for the adsorption and subsequent oxidation of methanol or its intermediates. A good characteristic of this alloy is the large current densities of the peaks compared to the same number of deposition cycles for the single metals. The hydrogen adsorption-desorption region (-200 to 0 mV) is much reduced in formaldehyde which is in agreement with the formaldehyde oxidation on other metals. This is due to the dissociative chemisorption of formaldehyde and it is assumed that the same poisoning species, mainly CO is formed, similar to Pt and Pt-Pd.

Although the alloy shows a strong activity for formaldehyde electrooxidation as indicated by the large peak current density, its possible use as an electrode in a fuel cell sensor is likely to be hampered by its activity towards methanol.

4.2.2.4 Electrooxidation on Palladium - Rhodium alloys

The effect of alloying Pd with Rh instead of Pt is shown in figure 19.

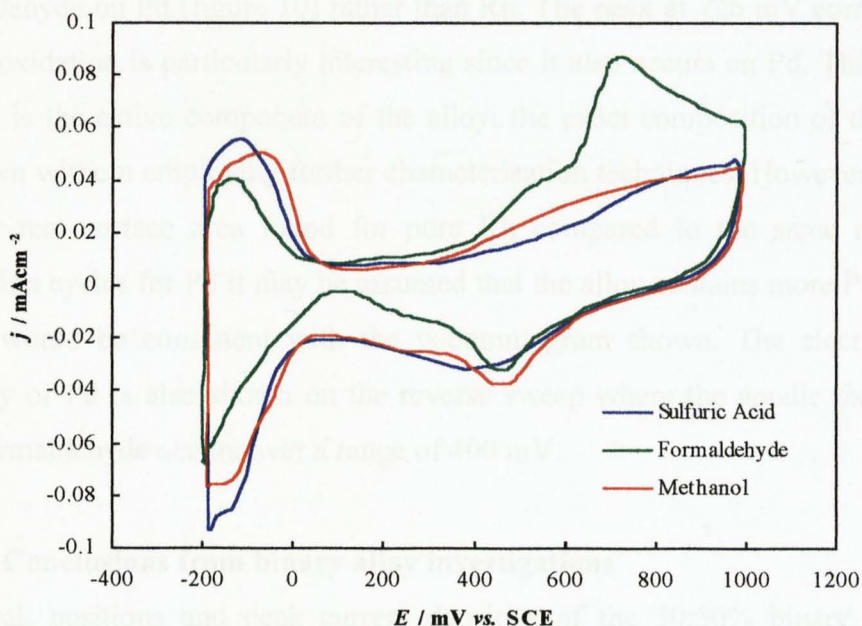
Figure 19 Cyclic voltammograms of 50:50% Pd-Rh/GC in H_2SO_4 (1 mol dm^{-3}), HCHO (0.1 mol dm^{-3}) in H_2SO_4 (1 mol dm^{-3}) and MeOH (0.1 mol dm^{-3}) in H_2SO_4 (1 mol dm^{-3}). Deposited for 5 cycles. (RSA = 1.51 cm^2)

The voltammogram shows the activity of the alloy in H_2SO_4 (1 mol dm^{-3}), HCHO (0.1 mol dm^{-3}) in H_2SO_4 (1 mol dm^{-3}) and MeOH (0.1 mol dm^{-3}) in H_2SO_4 (1 mol dm^{-3}). It can be seen that the activity of Pd-Rh is quite different to that of Pt-Rh alloy. The voltammogram is again a composite of the individual metals. It was previously shown that Pd and Rh alone exhibit enhanced activities towards the oxidation of HCHO but not MeOH; hence, an alloy containing both metals would not be expected to show activity for methanol oxidation. This is indeed the case where only the oxidation of formaldehyde is observed in the voltammogram.

The suppressed hydrogen adsorption/desorption region shows evidence of the dissociative adsorption of formaldehyde intermediates. In comparison no such suppression is seen in the voltammogram of methanol oxidation, probably due to the inactivity of the Pd constituent for methanol, as discussed earlier.

The anodic oxidation of formaldehyde intermediates (adsorbed CO) occur at potentials between that of pure Rh and Pd. In addition a shoulder can be clearly seen peaking at 530 mV before the main oxidation peak at 726 mV, the shoulder could be as a result of adsorbed species such as $-OH_2$ or $-OH$ as was described previously for formaldehyde oxidation on Pt or different types of CO bonding (bridge or multibonded). In general the voltammogram resembles the oxidation of formaldehyde on Pd (figure 10) rather than Rh. The peak at 726 mV corresponding to CO oxidation is particularly interesting since it also occurs on Pd. This suggests that Pd is the active component of the alloy; the exact composition of the alloy is unknown without employing further characterisation techniques. However, from the smaller real surface area found for pure Rh compared to the same number of deposition cycles for Pd it may be assumed that the alloy contains more Pd than Rh, which would be consistent with the voltammogram shown. The electrocatalytic property of Pd is also shown on the reverse sweep where the anodic oxidation of bulk formaldehyde occurs over a range of 400 mV.

4.2.2.5 Conclusions from binary alloy investigations

The peak positions and peak current densities of the 50:50% binary alloys for formaldehyde and methanol electrooxidation are summarised in table 5. P1 corresponds to the oxidation of adsorbed CO and P2 corresponds to the oxidation of bulk formaldehyde or methanol on the reverse sweep. Also shown is the calculated real surface area of the electrocatalysts.

It can be seen that the anodic peak potential is shifted positively in the presence of Pd which is analogous to the peak potential of pure Pd. It can also be seen that the alloys containing Pd (Pt-Pd and Pd-Rh) have a reduced catalytic activity towards methanol oxidation in comparison to Pt-Rh, which has a good catalytic activity towards both formaldehyde and methanol oxidation. The inactivity of Pd alloy is in agreement with the behaviour of pure Pd, which was shown to be very inactive towards methanol oxidation. Although the Pd-Rh alloy shows specific oxidation to formaldehyde the peak current density is not as large as Pt-Pd which shows excellent activity. This is in agreement with the work by Wang *et al.* who found a similar observation for the amperometric oxidation of formaldehyde [27].

Metal	Formaldehyde				
Peaks*	E_{p1}/ mV	j_{p1}/ mAcm^{-2}	E_{p2}/ mV	j_{p2}/ mAcm^{-2}	RSA / cm^2
Pt-Pd	756	0.34	410	0.27	4.05
Pt-Rh	600	0.22	20	0	0.904
Pd-Rh	740	0.09	400-100	0.004	1.51
	Methanol				
Pt-Pd	661	0.04	-	-	4.05
Pt-Rh	515	0.19	-	-	0.904
Pd-Rh	600	0.02	-	-	1.51

Table 5 Values of peak potentials and peak current densities for the electrooxidation of HCHO (0.1 mol dm^{-3}) in H$_2$SO$_4$ (1 mol dm^{-3}) and MeOH (0.1 mol dm^{-3}) in H$_2$SO$_4$ (1 mol dm^{-3}) for 50:50% Pt-Rh and Pd-Rh coated on glassy carbon. All metals deposited for 5 cycles. * p1 and p2 refer to the anodic peaks in the forward and reverse scan, respectively.

The results, however, must be treated with caution due to the differing deposition rates of the metals, as indicated by the real surface area. Nevertheless, as the results seem to coincide with literature reports it may be assumed that a correct representation of the catalytic activity is given [27].

In summary, alloying particular metals improves the catalytic activity towards the oxidation of formaldehyde or methanol. From all the binary alloys studied, 50:50% Pt-Pd showed the best activity towards the oxidation of formaldehyde. At the same time its response to the same concentration of methanol was negligible. Therefore it is the best-suited catalyst for the formaldehyde fuel cell sensor. Of the other alloys

studied Pt-Rh showed a good activity to the oxidation of both organic molecules. However its suitability in a fuel cell sensor specific for formaldehyde is questionable.

4.2.3 Ternary alloys

In addition to binary alloys it is also possible to utilise alloys composed of more metals. Studies for methanol catalysis have revealed attractive properties for PtRuSnW [93], PtRuOs [94] and PtWO$_{3x}$ [95] to name a few. However, reports on ternary alloys for formaldehyde oxidation are scarce. In this work the ternary alloys Pt-Pd-Rh and Pt-Pd-Ru were investigated in a 33:33:33 % composition.

4.2.3.1 Electrooxidation on Platinum-Palladium-Rhodium alloys

Figure 20 shows the cyclic voltammograms of Pt-Pd-Rh in H$_2$SO$_4$ (1 mol dm^{-3}), HCHO (0.1 mol dm^{-3}) in H$_2$SO$_4$ (1 mol dm^{-3}) and MeOH (0.1 mol dm^{-3}) in H$_2$SO$_4$ (1 mol dm^{-3}).
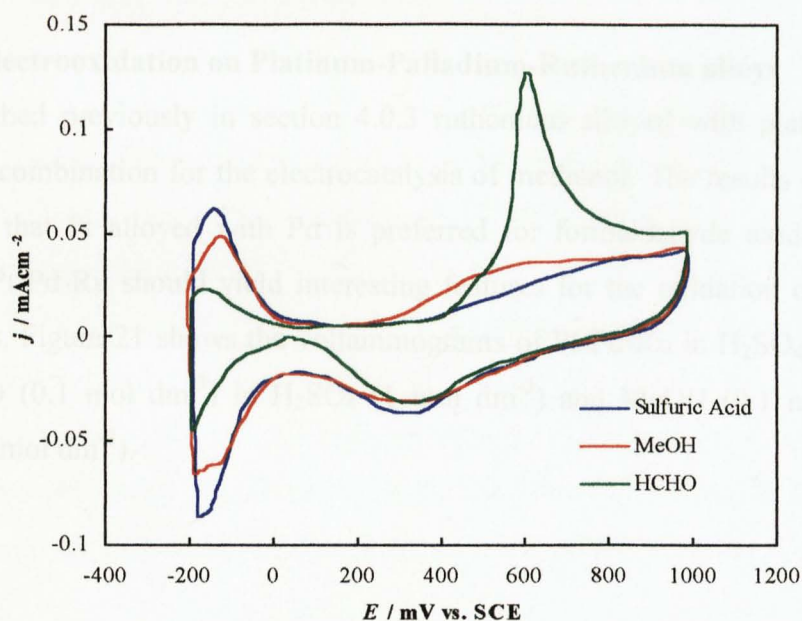
Figure 20 Cyclic voltammograms of 33:33:33% Pt-Pd-Rh/GC in H$_2$SO$_4$ (1 mol dm^{-3}), HCHO (0.1 mol dm^{-3}) in H$_2$SO$_4$ (1 mol dm^{-3}) and MeOH (0.1 mol dm^{-3}) in H$_2$SO$_4$ (1 mol dm^{-3}). Deposited for 5 cycles. (RSA = 2.95 cm^2)

Several interesting features can be seen. The voltammograms follow the same patterns as those of the binary alloys with the response being a composite of the individual metals under the same conditions. The voltammogram of Pt-Pd-Rh in H_2SO_4 is similar to that of Rh or Pt with the reduction of the oxide on the reverse sweep occurring between the positions on respective pure metals.

Although there is a small response to methanol the catalyst is much more active towards formaldehyde oxidation as indicated by the larger peak current density. The peak for the oxidation of adsorbed intermediates (mainly CO) occurs at 610 mV. This peak position is possibly due to the influence of Pt atoms, as 600 mV is the oxidation potential on Pt itself. The oxidation peak takes place over a wide potential region, 400-800 mV, which is also indicative of Pt atoms. In comparison to formaldehyde oxidation on Pt the hydrogen evolution region is not as suppressed, indicating the formation of less poisoning species on the electrode surface. However in comparison to the voltammogram of the alloy in acid the effect of poisoning is clearly visible.

4.2.3.2 Electrooxidation on Platinum-Palladium-Ruthenium alloys

As described previously in section 4.0.3 ruthenium alloyed with platinum is the favoured combination for the electrocatalysis of methanol. The results discussed so far show that Pt alloyed with Pd is preferred for formaldehyde oxidation. Thus, alloying Pt-Pd-Ru should yield interesting features for the oxidation of respective molecules. Figure 21 shows the voltammograms of Pt-Pd-Ru in H_2SO_4 (1 mol dm^{-3}), HCHO (0.1 mol dm^{-3}) in H_2SO_4 (1 mol dm^{-3}) and MeOH (0.1 mol dm^{-3}) in H_2SO_4 (1 mol dm^{-3}).
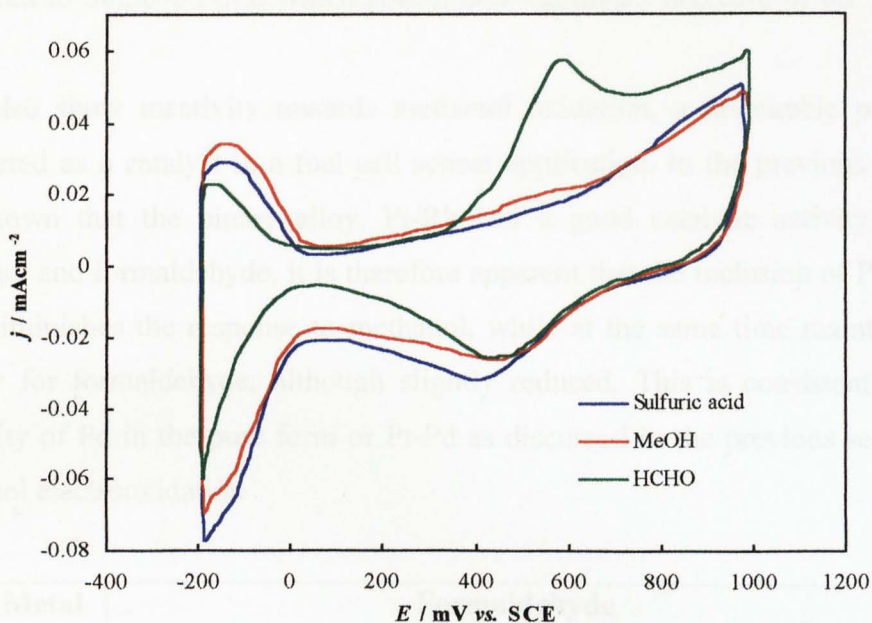
Figure 21 Cyclic voltammograms of 33:33:33% Pt-Pd-Ru/GC in H_2SO_4 (1 mol dm^{-3}), HCHO (0.1 mol dm^{-3}) in H_2SO_4 (1 mol dm^{-3}) and MeOH (0.1 mol dm^{-3}) in H_2SO_4 (1 mol dm^{-3}). Deposited for 5 cycles. (RSA = 2.95 cm^2)

The voltammograms are quite different to those of Pt-Pd-Rh; the effect of replacing Rh with Ru is clearly seen. The alloy is active towards formaldehyde oxidation but is inactive towards the same concentration of methanol. This is quite surprising considering that Pt-Ru binary alloys are very active towards its oxidation. The inclusion of Pd, which has been previously shown to be inactive towards methanol oxidation [69,78], has a major influence on the activity of the alloy. On the other hand, the inclusion of Ru into the alloy reduces the activity of the catalyst towards formaldehyde oxidation as indicated by the smaller peak current density on the anodic sweep of 0.06 $mAcm^{-2}$ compared to 0.34 $mAcm^{-2}$ for the 50:50% Pt-Pd binary alloy.

4.2.3.3 Conclusions from ternary alloy investigations

The peak positions and peak current densities of the 33:33:33% ternary alloys for formaldehyde and methanol electrooxidation are summarised in table 6. As can be seen the Pt-Pd-Rh has better catalytic activity for formaldehyde oxidation than Pt-Pd-Ru as evidenced by the peak current densities. However, the main anodic oxidation peak of adsorbed CO is shifted negatively by 0.1 V for both ternary alloys

169

compared to 50:50% Pt:Pd which confirms a significant decrease of the poisoning effect.

Both also show inactivity towards methanol oxidation, a favourable property if considered as a catalyst in a fuel cell sensor application. In the previous section it was shown that the binary alloy, Pt-Rh had a good catalytic activity for both methanol and formaldehyde, it is therefore apparent that the inclusion of Pd into the alloy diminishes the response to methanol, while at the same time maintaining its activity for formaldehyde, although slightly reduced. This is consistent with the inactivity of Pd in the pure form or Pt-Pd as discussed in the previous sections for methanol electrooxidation.

Metal	Formaldehyde				
Peaks*	E_{p1}/ mV	j_{p1}/ mAcm^{-2}	E_{p2}/ mV	j_{p2}/ mAcm^{-2}	RSA / cm^2
X=Rh	610	0.13	30	0	2.95
X=Ru	580	0.06	33	0	2.95
	Methanol				
X=Rh	510	0.03	-	-	2.95
X=Ru	-	-	-	-	2.95

Table 6 Values of peak potentials and peak current densities for the electrooxidation of HCHO (0.1 mol dm^{-3}) in H_2SO_4 (1 mol dm^{-3}) and MeOH (0.1 mol dm^{-3}) in H_2SO_4 (1 mol dm^{-3}) for 50:50% Pt-Pd-X/GC. All metals deposited for 5 cycles. * p1 and p2 refer to the anodic peaks in the forward and reverse scan, respectively.

From these initial investigations it has been shown that the responses of ternary alloy mixtures are further changed in comparison to the single metals and the binary alloy mixtures. There are a number of metallic interactions possible in a ternary alloy mixture, which could favour different types of adsorption on the surface and ultimately the electrooxidation mechanism, thus influencing the catalytic properties of the alloy. Possible adsorbed species include –OH in addition to CO in the linear, bridge and multibonded conformation; however, it is difficult to ascertain the identity of the adsorbed species without complimentary techniques such as 'in situ' IR spectroscopy.

The statistical distribution of atoms in the metal plays a very important rôle in the activity of the catalyst. Although some of these catalysts exhibit attractive properties, this approach seems to be somewhat arbitrary, particularly since today even binary systems are not completely understood, let alone ternary or even quaternary systems with possible metallic interactions which are a multitude of those likely in binary systems. An understanding of alloy systems is vital towards the development of new catalysts to avoid a purely empirical approach in the search for new electrocatalysts.

4.3 Fuel cell preparation and characterisation

From the fundamental investigations on the electrocatalytic behaviour of various noble metals and alloys towards the oxidation of formaldehyde and methanol, it was decided to prepare and incorporate the following electrodes in fuel cells for use as sensors;

1. Pt-Pd (50:50%)
2. Rh
3. Pt-Rh (50:50%)

Pt-Pd was an obvious candidate as it showed superior response in comparison to all other catalysts studied. It was also shown to be more specific towards the oxidation of formaldehyde compared to methanol. Rh also responded to the oxidation of formaldehyde with a high current density, its response was also shown to be specific. Although Pt-Rh showed a good response to the electrooxidation of methanol, its response to formaldehyde was also very good, therefore it was decided to investigate this alloy.

4.3.1 Experimental

All the fuel cells used in this work were prepared using the electrodeposition procedure described in section 2.3.3. In each case the supporting material onto which the metal electrodes were deposited, consisted of a thin layer of gold, coated onto a porous PVC substrate. After electrodeposition it was usual to subject the metal electrodes to a number of pre-treatment procedures described in section 2.3.3.5, the effect of which on the structure of the metal deposit was uncertain. In order to obtain a better understanding of the pre-treatment procedures on the composition and morphology of the metal deposits, a study of the fuel cell electrodes was undertaken by means of scanning electron microscopy and EDAX, experimental details of which are described in section 2.6.

The composition and operating conditions of the electroplating baths used in the preparation of the different metal electrodes are shown in table 7.

Metal to be deposited	Electroplating solutions Made up to 20 ml	Operating Conditions
Platinum-Palladium 1:1 Ratio	0.016 mol dm^{-3} PtCl$_2$ 0.03 mol dm^{-3} PdCl$_2$ in 1 mol dm^{-3} HCl	I = 40 mA t = 10 h pH = 0
Rhodium	0.5 mol dm^{-3} RhCl$_3$3H$_2$O in 1 mol dm^{-3} HCl	I = 40 mA t = 14 h pH = 0
Rhodium	0.5 mol dm^{-3} RhCl$_3$3H$_2$O in 1 mol dm^{-3} HCl	I = 40 mA t = 3 h pH = 0
Rhodium	0.5 mol dm^{-3} RhCl$_3$3H$_2$O in 1 mol dm^{-3} HCl	Potentidynamically 100 cycles pH = 0
Platinum-Rhodium 1:1 Ratio	0.016 mol dm^{-3} PtCl$_2$ 0.03 mol dm^{-3} RhCl$_3$3H$_2$O in 1 mol dm^{-3} HCl	I = 40 mA t = 14 h pH = 0

Table 7 Electroplating solutions and experimental conditions

It is important to note that alloyed catalysts of the Pt-Pd type are very difficult to characterise and as yet no electrochemical method is commonly accepted for their characterisation. In the case of fuel cell catalysts, the situation is far more complex. It is not only the electrochemically active surface area which determines the activity, but also the preparation method, the kind of supporting material and the pre-treatment which influence catalyst performance [17].

4.3.2 Gold-coated porous PVC substrate

The function of the porous PVC substrate is two fold;

1. to separate and support the catalytic electrodes,
2. to retain the cell electrolyte in contact with both electrodes, such that ionic exchange may take place between them.

In order to use the porous PVC discs in the preparation of the metal electrodes in the fuel cells it was necessary to coat the faces of the discs with a thin layer of gold. This was necessary to provide a base onto which the metal electrodes could be deposited. The deposition of gold was carried out by means of gold sputtering as described in section 2.3.3.2.

Although the electrodes were pressed after electrodeposition of the metal on the gold-coated substrate, the effect of compression on the pore structure of the gold-coated PVC was initially examined as it would be difficult to examine after deposition of the metal. The compression technique is described in section 2.3.3.5. SEM images of the as-deposited and pressed gold-coated porous PVC substrate are shown in figure 22. These reveal that the material is composed of a network of PVC nodules linked at different points and intersected by a random pore structure. The pore structure is asymmetrical with a mean pore diameter of 30 μm. The pore size must be such that sufficient electrolyte is held to minimise the internal resistance of the cell. Large pores would render the electrolyte more prone to atmospheric evaporation. Closer examination of the SEM images reveals that the pore structure of pressed gold-coated PVC substrate, is, as expected, less open than that of the unpressed PVC sample. As a result of compression the electrode have smooth shiny visual appearance.
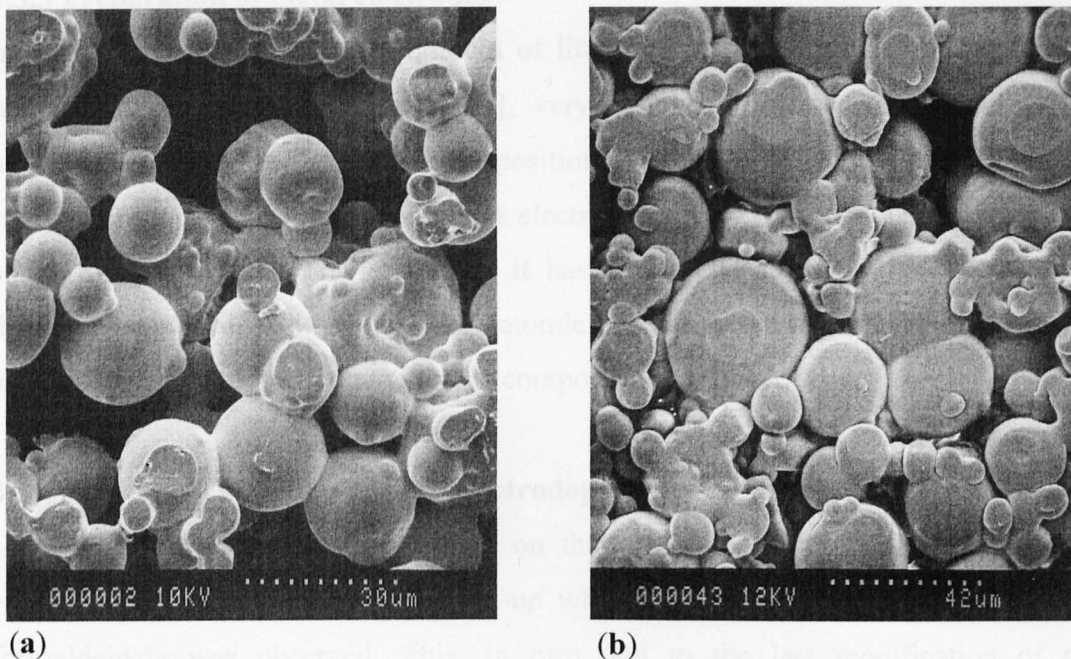
(a)　　　　　　　　　　　**(b)**

Figure 22 SEM images of **(a)** unpressed gold-coated PVC　**(b)** pressed gold-coated PVC at 5 tons for 10 minutes

A comparison of these images with pristine PVC (without gold coating) reveals little difference under the electron microscope; this is in marked contrast to their visual appearances – the uncoated PVC substrate being a fawny colour, while the colouration of gold was clearly visible on the gold-coated PVC substrate. The presence of gold is also proved in the EDAX spectra in figure 23. Strong signals are also observed for chlorine, corresponding to the chemical makeup of the PVC substrate
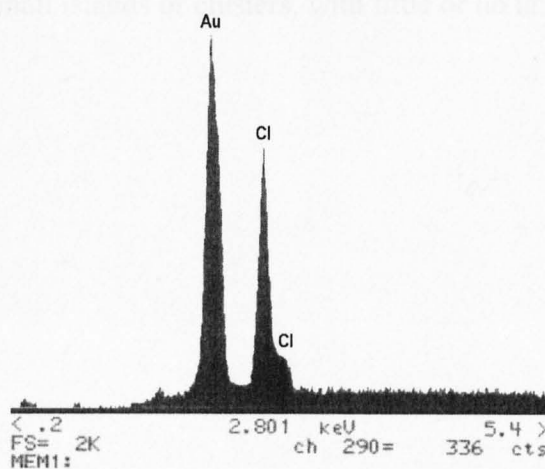

Figure 23 EDAX of the gold-coated PVC substrate, showing strong signals for gold and chlorine

4.3.3 Preparation of metal electrodes

In marked contrast to the vast amount of literature dealing with the preparation of platinum-black deposits [6,26,96-100], very little information was found to be available concerned with the electrodeposition of other metals and alloys chosen for study. Consequently, initial attempts at electrodeposition were conducted on a 'trial and error' basis. In a previous study it has been suggested that the metals have different rates of deposition, therefore atomic ratios referred to in this work apply to electroplating solutions and not surface composition of the electrode [26].

4.3.4 Platinum-Palladium (Pt-Pd) electrodeposits

Very little work has been performed on the electrodeposition of Pt-Pd and only Nurton [26] has studied a similar set-up where an increase in selectivity towards formaldehyde was observed. This, in turn, led to the last modification of the Formaldemeter™ fuel cell in 1985.

Electrodeposition was achieved from a solution of palladium (II) and platinum (II) chloride containing equal noble metal content. SEM images of the deposit are shown in figures 24a-c, these reveal an open structure, in which the crystallites are confined to the gold-coated portions of the PVC nodules. As can be seen in figure 24a the deposit is present as small islands or clusters, located on the protruding portions of the gold electrode. Closer examination of the deposit (figure 24b-c) reveals 'boulder' type growths on the surface of the deposit. This type of deposit is different to that of individual platinum and palladium; platinum alone has been reported to have a protruding dentritic growth with lateral growth while that of palladium has been shown to be fragile small islands or clusters, with little or no lateral growth [6].
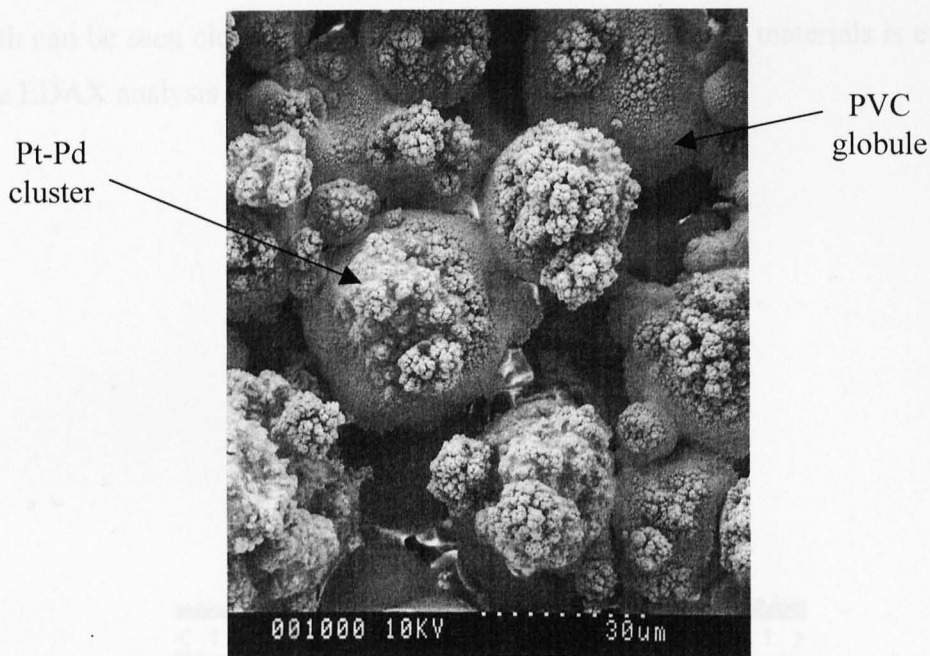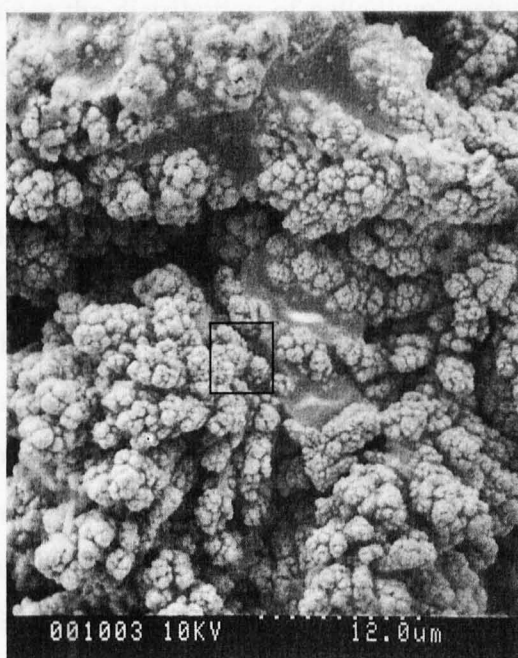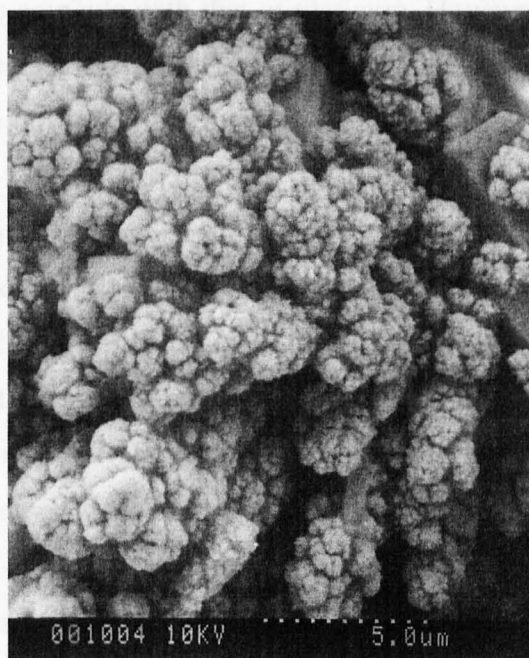
Figure 24a SEM image of Pt-Pd deposit 50/50 % atomic ratio (× 1000 magnification)

(b)   **(c)**

Figure 24b Close-up of one of the Pt-Pd clusters (× 2500) (c) Magnification of region enclosed in (b) (× 6000)

The images suggest that Pt-Pd is a combination of both types of deposit, lateral growth can be seen clearly in figure 24b. The presence of both materials is evidenced by the EDAX analysis of the deposit shown in figure 25.
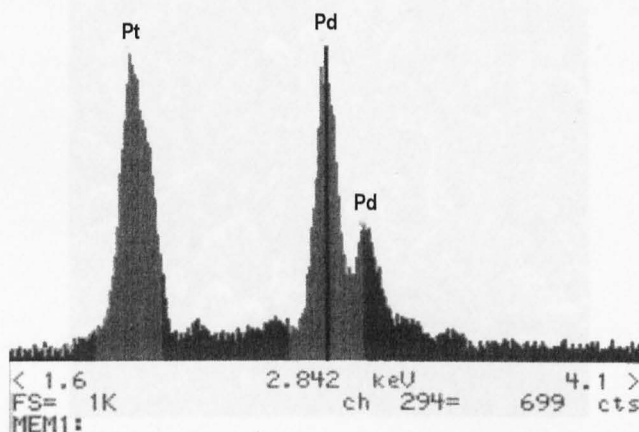

Figure 25 EDAX analysis of the Pt-Pd deposit

The x-ray distribution of metals in the alloy electrodeposit is particularly interesting since the distribution of palladium seems to coincide with that of platinum. However, in order to quantify a 50/50 % ratio of the metals in the deposit techniques such as XPS would be required, this should be done in future experiments.

4.3.5 Compression of the Pt-Pd electrodeposits

The effect of compression on the Pt-Pd deposit is shown in figure 26. Comparisons of the SEM image of the pressed deposit, with those obtained for the unpressed deposit in figure 24a reveal the dramatic effect compression has on the deposit. The protruding crystallite growths have been completely flattened and the deposit is now much more compact than that of the unpressed deposit. Several interesting features arise as a result of compression of the Pt-Pd electrodeposit; (i) several cracks and fractures appear in the deposit. This suggests that on compression the Pt-Pd layer is very brittle, Harrison [6] has also observed this effect and it has been suggested that cracks and fractures appear along the lines of stress in the deposit pointing to the uneven nature of the porous PVC substrate, this is especially true for the substrate used in this study.
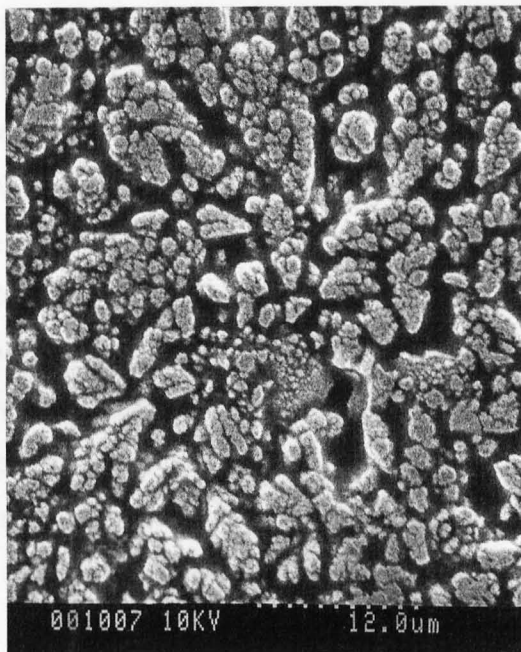
Figure 26 SEM image of compressed Pt-Pd electrodeposit (× 2500)

From this it follows that the effect of the compression procedure is to force the Pt-Pd deposit down into the porous PVC substrate and produce a smooth, tightly packed structure. Kurlbaum suggested that the shiny appearance is due to compression forcing the Pt-Pd crystallites together into a smaller number of larger particles with less internal reflection [101]. It would be expected, by comparison with the pressed gold-coated PVC substrate, figure 22b, that the compression procedure also has the effect of bringing the Pt-Pd deposit and the conductive gold layer into a more intimate contact.

4.3.6 Effect of pre-treatment procedure on the Pt-Pd electrodeposit

The activation procedure has been shown to increase the catalytic activity of fuel cell electrodes; the procedure, as described in section 2.3.3.6 consisted of cycling the potential between the hydrogen and oxygen evolution regions for 1 hour / 75 cycles. Various theories have been proposed for this increase in catalytic activity and have been reviewed by Shibata [102] who discounted the theory that the effect was due to the removal of impurities from the electrode surface and showed, instead that a

change in actual surface structure was responsible. This structure slowly reverted to its original preactivation state, thus causing the activity of the catalyst to decay slowly with time. Later, Shibata and Sumino [103] ascribed the activity change to the adsorbed oxygen in the anodic cycle which caused the rearrangement of the platinum atoms. Results by Williams supports this theory and it was proposed that anodic/cathodic polarisation has the effect of leaving the surface of the platinum atoms in a loosely packed, high energy and thus highly catalytic state [96]. It was also proposed that activation results in the platinum to be in the reduced form, i.e. platinum hydroxide, which is thought to be the active species for the oxidation of small organic molecules, such as ethanol [96].

The effect of the activation procedure on the Pt-Pd deposit is shown in figure 27.
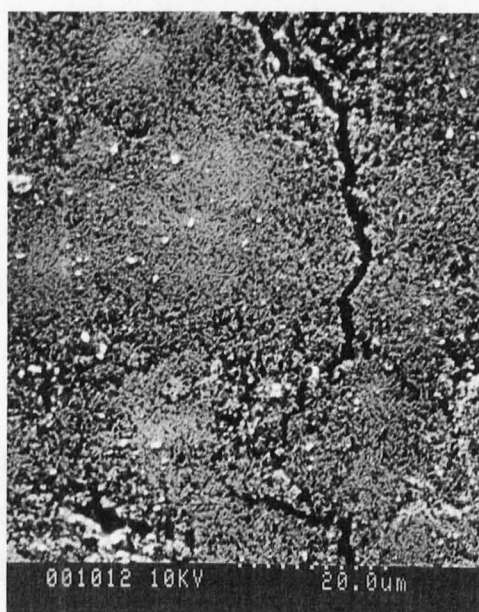
Figure 27 SEM image of activated Pt-Pd electrodeposit (× 1500)

The SEM image reveals a marked increase in the roughness of the deposit compared with the unactivated deposit shown in figure 26. It has been reported that the repetitive oxidation and reduction of the oxide layers increases the roughness factor of platinum-black by a factor of 100 or more [104]. This has been attributed to;

1. repeated penetration and removal of hydrogen on the cathodic cycle [105], with the resultant expansion and contraction of the platinum-lattice breaking up the metal surface,

179

2. the repeated formation and breaking of strong Pt-O bonds [106], resulting in a weakening of the Pt-Pt interactions.

However it seems most likely that the net result, in either case, is an increase in the surface area of the electrode. More investigations utilising cyclic voltammetry are needed to confirm the exact effect of pre-treatment on the catalytic activity of the electrode. Other experimental techniques such as TEM to determine the particle size and X-ray radiation methods such as XRD and XPS to determine qualitative and quantitatively the surface composition would also be extremely useful.

Cracks and fractures are still visible in the activated electrode but to a much lesser extent than the unactivated electrode. It is thought that the apparent closure of the cracks and fractures in the activated, pressed deposit arises as a result of platinum, dissolved on the anodic cycle, being redeposited on the cathodic cycle [107]. It has also been reported that activation of an unpressed deposit results in the complete stripping of the deposit [6]. The compression procedure, therefore, has a stabilising effect on the deposit. It has also been concluded that the effect of activation on the electrodeposit is two fold, (i) to increase the surface roughness (area) of the platinum deposit (ii) to effect the redistribution of the existing Pt-Pd crystallites [6].

4.3.7 Rhodium electrodeposits

The rhodium electrodes used in this work were prepared by electrodeposition from solutions of rhodium (III) chloride. Three sets of fuel cell electrodes were prepared, one was performed potentiodynamically whilst the other two were deposited galvanostatically but with different deposition times, 3 h and 14 h. SEM images of the rhodium deposits, are shown in figures 28a,b and c.

Cracking exposing Au layer
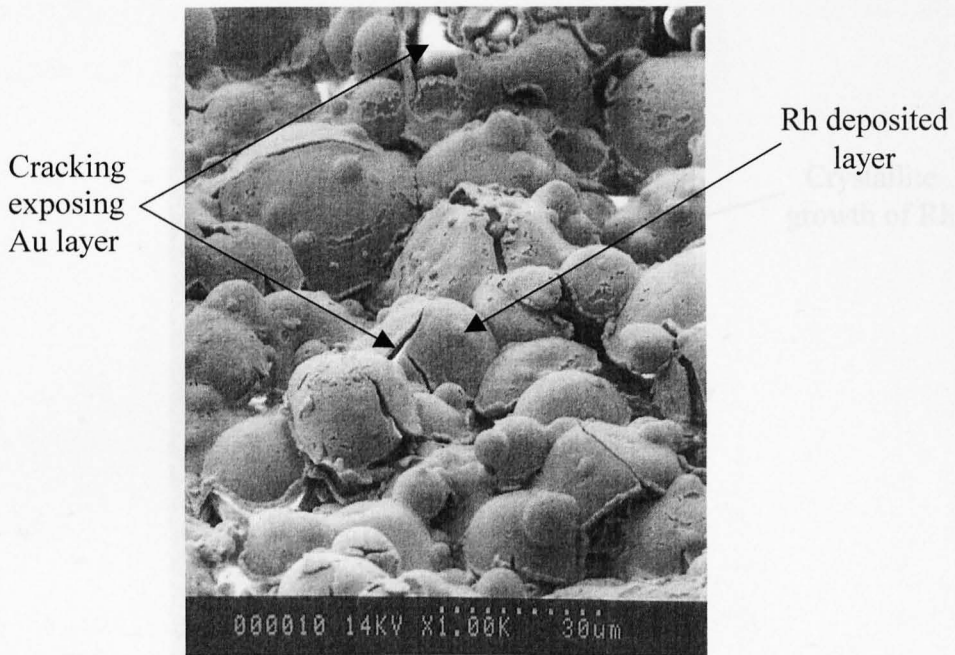
Rh deposited layer

Figure 28a SEM image of rhodium deposited by potential cycling for 100 cycles (× 1000)

Rh deposited layer

Rh crystallitic growth
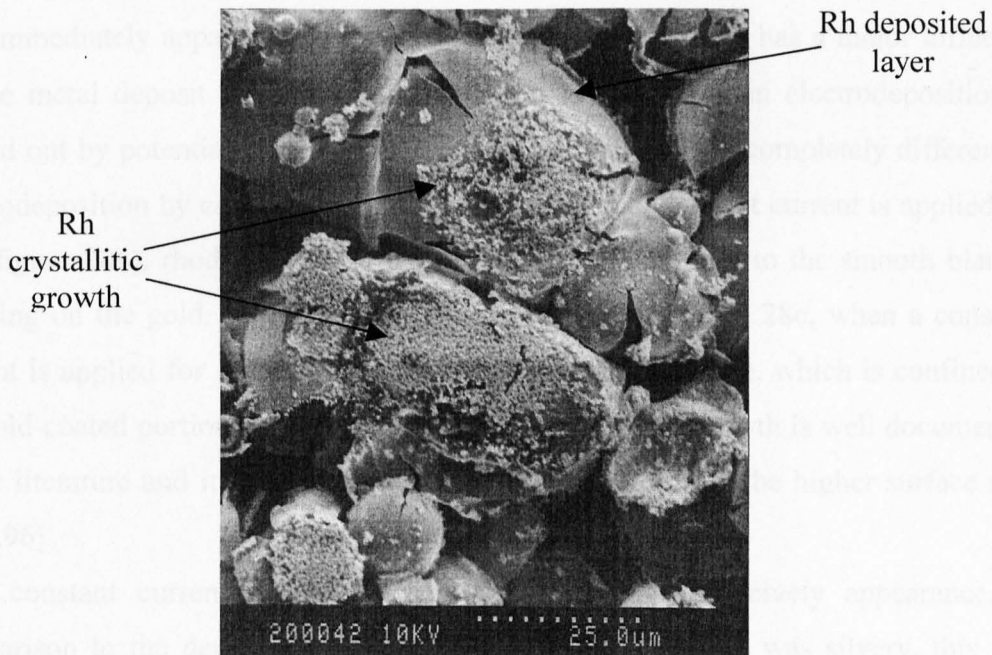
Figure 28b SEM image of rhodium deposited galvanostatically for 3 hours (× 1200)

Crystallite growth of Rh

200026 10KV 20.0um

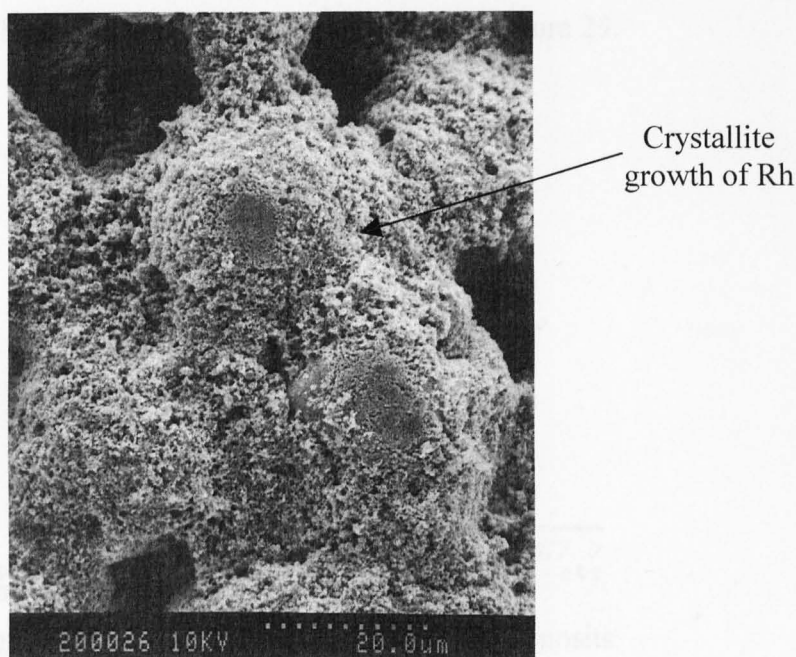**Figure 28c** SEM image of rhodium deposited by galvanostatically for 14 h (× 1500)

It is immediately apparent that the electrodeposition technique has a major influence on the metal deposit. A 'blanket' of rhodium is formed when electrodeposition is carried out by potential cycling as seen in figure 28a which is completely different to electrodeposition by constant current methods. When a constant current is applied for 3 h (figure 28b), rhodium crystallites can be seen in addition to the smooth blanket covering on the gold. In comparison, as can be seen in figure 28c, when a constant current is applied for 14 h only the crystallite growth is visible, which is confined to the gold-coated portions of the PVC nodules. This type of growth is well documented in the literature and it is the preferred type of deposit due to the higher surface area [6,26,96].

Both constant current deposited electrodes had a black velvety appearance, in comparison to the deposit formed by potential cycling which was silvery, this was also visibly brittle. This behaviour can be attributed to the preparation condition where potential cycling causes the repeated penetration and removal of hydrogen on the cathodic cycle, with the resultant expansion and contraction of the rhodium-lattice. This could have the effect of causing a weaker adherence to the gold-coated PVC substrate.

EDAX analysis of all the deposits confirmed the presence of rhodium without contamination from the preparation procedure, as shown in figure 29.
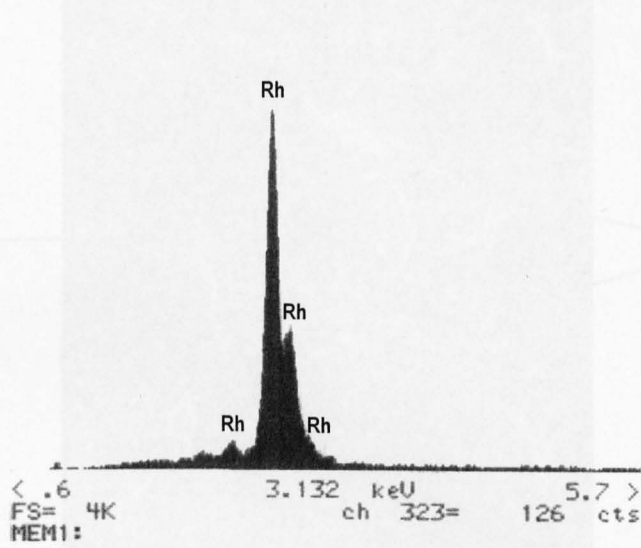
Figure 29 EDAX analysis of the rhodium deposits

The effect of compression on the three different deposits are shown in figure 30a,b and c; like the Pt-Pd deposits this procedure has a marked effect on the surface characteristics.
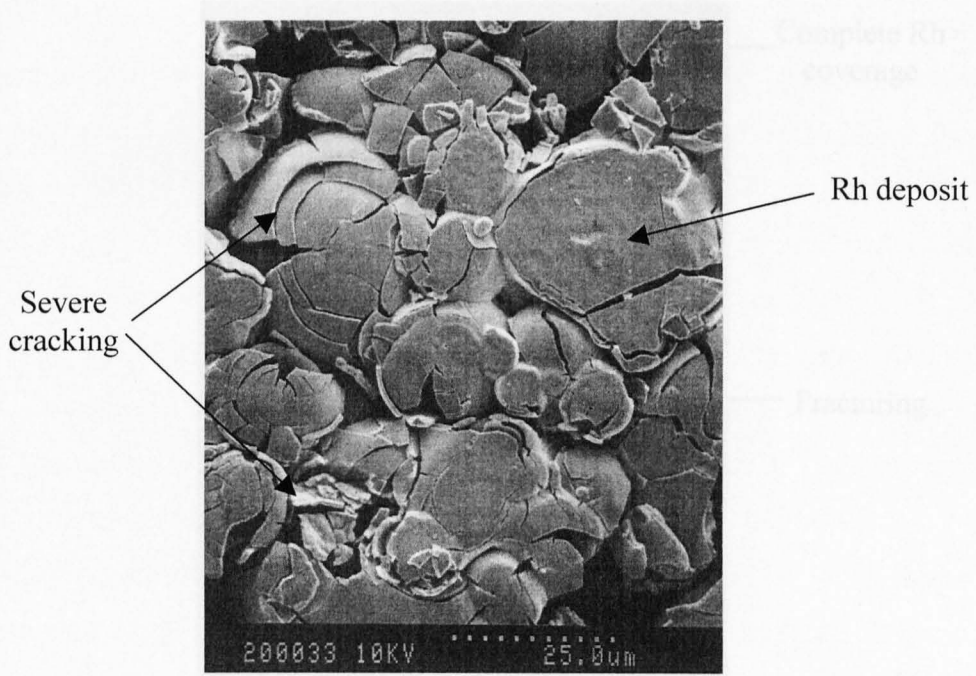
Figure 30a SEM image of compressed rhodium after potentiodynamic deposition of 100 cycles ($\times$ 1200)

Compressed
Rh deposit

Incomplete
coverage
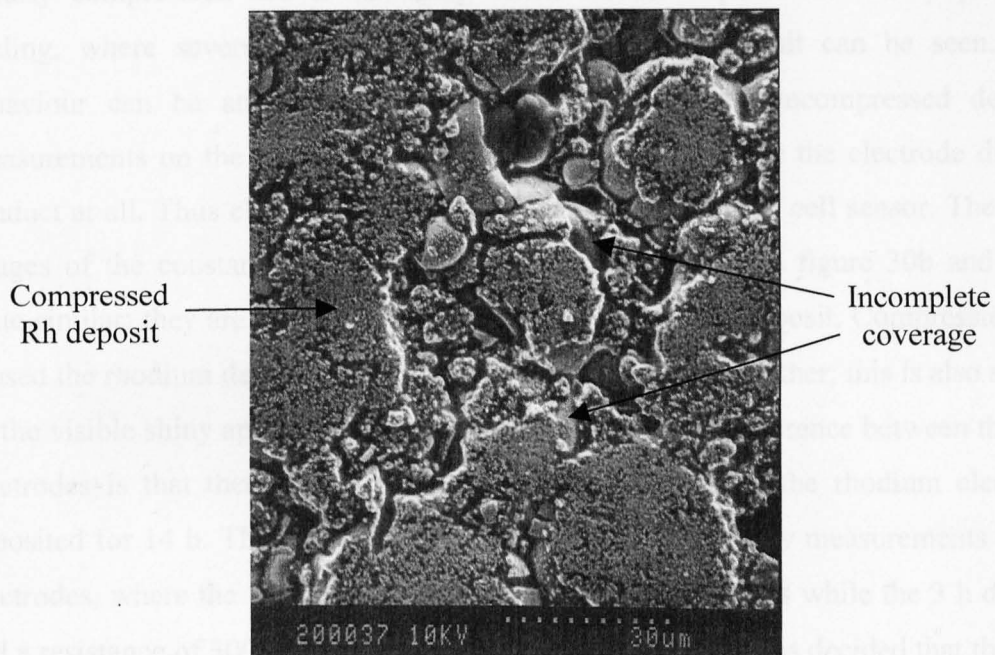
Figure 30b SEM image of compressed rhodium after galvanostatic deposition
for 3 hours (× 1000)

Complete Rh
coverage

Fracturing
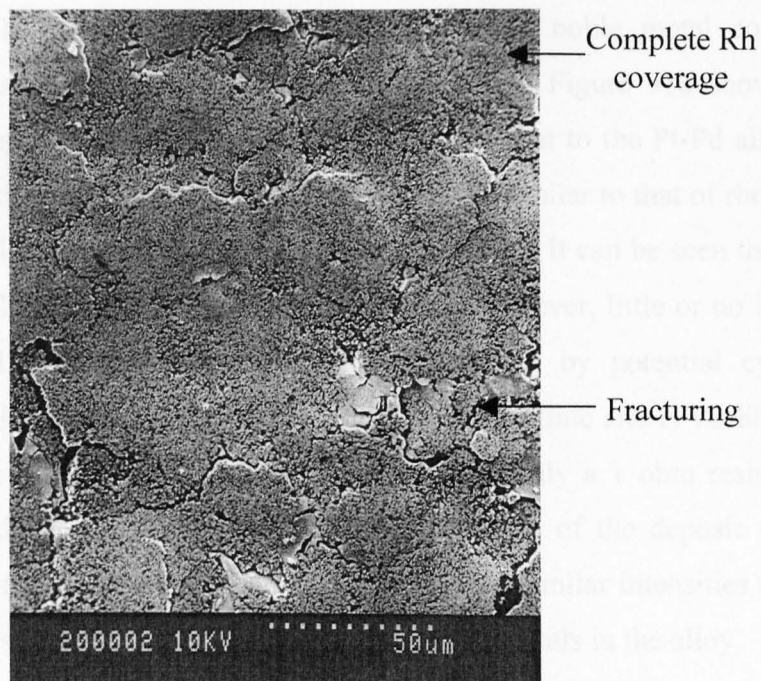
Figure 30c SEM image of compressed rhodium after galvanostatic deposition
for 14 hours (× 600)

Clearly compression has a damaging effect on the deposit formed by potential cycling, where severe cracking and shattering of the deposit can be seen. This behaviour can be attributed to the brittle nature of the uncompressed deposit. Measurements on the resistance of the electrode revealed that the electrode did not conduct at all. Thus eliminating its use as a catalyst in the fuel cell sensor. The SEM images of the constant current deposited electrodes shown in figure 30b and c are quite similar; they are also similar to the compressed Pt-Pd deposit. Compression has caused the rhodium deposit to be more compact and closer together; this is also shown by the visible shiny appearance of the electrode. The main difference between the two electrodes is that there is much better surface coverage on the rhodium electrode deposited for 14 h. This was also demonstrated by conductivity measurements of the electrodes, where the 14 h deposit had a resistance of 0.3 ohms while the 3 h deposit had a resistance of 300 ohms. Based on these observations it was decided that the 14 h deposit was the preferred catalyst for the fuel cell sensor.

4.3.8 Platinum – Rhodium (Pt-Rh) electrodeposits

The platinum – rhodium (Pt-Rh) electrodes were prepared from a solution of rhodium (III) and platinum (II) chloride solutions containing equal noble metal content. Electrodeposition was performed galvanostatically for 14 h. Figure 31a shows an SEM image of the deposit. The Pt-Rh deposit is quite different to the Pt-Pd alloy in that it has no cluster crystallite growth, in fact the deposit is similar to that of rhodium deposited by potential cycling techniques shown in figure 28a. It can be seen that the deposit covers the gold-coated PVC nodules completely. However, little or no lateral growth has occurred. Compared to the rhodium deposited by potential cycling methods this deposit is bound strongly to the gold-coated substrate and is visibly less fragile. The electrode also showed good conductivity with only a 1 ohm resistance between opposite ends of the electrode. The EDAX analysis of the deposit which shows the presence of Pt and Rh is shown in figure 31. The similar intensities of the Pt and Rh peak suggest that there is good distribution of the metals in the alloy.
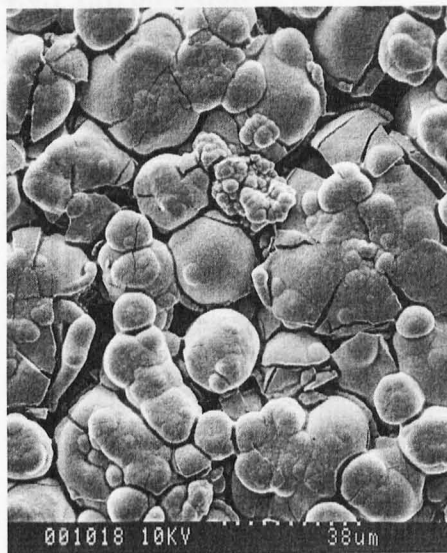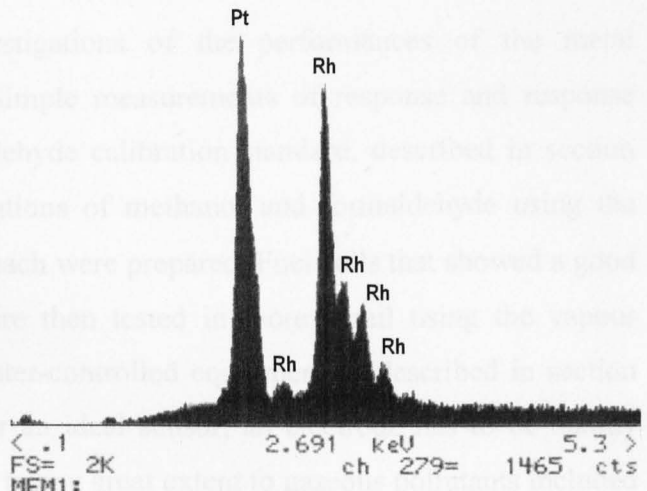
(a)   **(b)**

Figure 31 (a) SEM image of Pt-Rh electrodeposit (50/50 % atomic ratio) (× 800) **(b)** EDAX analysis of the same deposit.

4.3.9 Conclusions

Although SEM and EDAX techniques show a lot of detail about the deposit, other methods would have to be utilised in future experiments to fully characterise the deposit. Methods employing X-ray radiation have proved to be invaluable for the characterization of technical catalysts – either supported or unsupported – and complete fuel cell electrodes. X-ray diffraction (XRD) and X-ray photo electron spectroscopy (XPS) are the most frequently used of these methods. Alone or in combination with other methods, important information about some characteristics of the catalyst can be derived. These include crystallinity, crystallite size, composition, oxidation state of species and possible interactions of the catalyst with the substrate.

186

4.4 Performance of fuel cells

4.4.1 Introduction

After preparation of the electrodes, the fuel cells were assembled and placed in the Formaldemeter™. Preliminary investigations of the performances of the metal electrodes were then carried out. Simple measurements of response and response times were taken using the formaldehyde calibration standard, described in section 2.4.4, and known vapour concentrations of methanol and formaldehyde using the vapour generator. Two fuel cells of each were prepared. Fuel cells that showed a good response to a particular vapour were then tested in more detail using the vapour generator combined with the computer-controlled equipment as described in section 2.5.3. It is worth reminding that for an ideal sensor, an electrode has to be mainly specific for that gas and not respond to any great extent to gaseous pollutants included in the sample volume. In this study it is desirable that the methanol/formaldehyde ratio is low. Other desirable characteristics include maximum response to a standard gas concentration, fast response and clearing times to enable a greater number of measurements in a given time and a reduced humidity signal.

4.4.2 Preliminary testing of the fuel cells

The preliminary results for all the fuel cells are summarised in table 8. Six readings were taken in each test; the average is shown in the table. Also shown are the methanol/formaldehyde ratios.

Fuel Cell	HCHO (2 ppm)			MeOH (25 ppm)			MeOH / HCHO
	Direct Output	Response / PPM	Response Time	Direct Output	Response/ PPM	Response Time	
Pt-Pd 1	1.56	0.78	18.9	0.32	0.0128	22.9	0.016
Pt-Pd 2	1.6	0.8	18.9	0.34	0.0136	21.9	0.017
Rh x 2	Response negligible			Response negligible			-
Pt-Rh x 2	Response negligible			Response negligible			-

Table 8 Response of various fuel cells to 2 ppm formaldehyde and 25 ppm methanol. Also shown are formaldehyde/methanol ratios. All tests performed at 18 °C and 50 % RH

187

As can be seen consistent readings were given for the Pt-Pd fuel cells, which also showed a good selectivity to formaldehyde; however, the Rh and Pt-Rh fuel cells gave disappointing results with little or no response to the vapour concerned. Both Pt-Pd fuel cells showed similar behaviour with the response to formaldehyde and methanol nearly identical, peaking around 19 seconds for formaldehyde and 22 seconds for methanol. An attractive feature of the Pt-Pd fuel cell is the very low methanol/formaldehyde ratio per ppm of the sample, and justifies its use as the preferred catalyst for the current Formaldemeter™ fuel cell. As the Pt-Pd catalyst exhibited the best performance in these initial investigations, its behaviour was analysed further. Firstly however, the origin of the poor performances of the Rh and Pt-Rh fuel cells are discussed.

4.4.3 Rhodium fuel cell

The poor response of the Rh fuel cell was quite surprising as the SEM images of the Rh deposit (figure 30c) were very similar to those of the Pt-Pd deposit, which showed excellent homogeneous surface coverage after compression. The low activity of Rh for formaldehyde and methanol oxidation is most probably due to the nature of the oxide layer. The electrochemical behaviour of the Rh/oxygen system has been investigated by a number of workers [75,108,109] and it is believed that an equilibrium of the type;

$$RhO \ + \ 2H^+ \ + \ 2e^- \ \rightleftharpoons \ Rh \ + \ H_2O$$
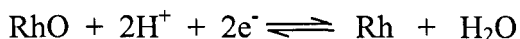
is formed on rhodium in aqueous solutions. Rand and Woods have shown that the oxide layer so formed is strongly bound to the electrode surface [75].

Luo *et al.* recently reported that the presence of water vapour along with gaseous oxygen catalyses oxide formation on rhodium [108]. This would suggest that the source of the poor activity of the rhodium fuel cell is·the almost total coverage of the surface by a layer of strongly bound oxygen which hinders the rate of adsorption and oxidation of the molecules.

In comparison to rhodium, palladium and platinum form oxides having a lower thermodynamic stability (*i.e.*, less negative free energies of formation). This difference is reflected in the ca. 0.3 V higher electrode potentials at which the surface

oxides are formed and removed on the latter two metals in aqueous electrochemical environments [109].

The poor performance of the fuel cell also relates well to the voltammogram shown previously in figure 11. It can be seen that the main oxidation peak, corresponding to the oxidation of poisoning CO at 600 mV occurs at exactly the same point as oxide formation; this is further evidenced by the nature of the broad peak. Another feature in the voltammogram that could explain the poor activity of Rh fuel cell is the hydrogen evolution region. Only a little suppression in the region is observed in the presence of formaldehyde, suggesting that formaldehyde does not dissociatively adsorb as efficient as it does on Pt or Pt-Pd where near passivation in the region is observed due to the adsorption of CO.

4.4.4 Platinum-Rhodium fuel cell

Along with Rh the response of the Pt-Rh fuel cell was also very disappointing. It was thought from initial voltammetry investigations of formaldehyde oxidation on Pt-Rh/GC, described in section 4.2.2.3, that the catalyst could be used in fuel cell sensors due to the large current density of the oxidation of the adsorbed poisoning species CO. Although the voltammogram obtained in this work did not show particular specificity for formaldehyde, Nurton studied the response of a Pt-Rh fuel cell previously and a low methanol/formaldehyde ratio was demonstrated [26], which is a desirable property for a specific fuel cell sensor for formaldehyde. However, the poor millivolt response of the fuel cell ruled out its further development.

There are many factors which could affect the performance of the Pt-Rh fuel cell prepared in this work. The surface of the electrode could be coated with a strongly bound oxide layer due to the presence of Rh which has a tendency to form a strong oxide layer as discussed in the previous section. Similar to the voltammogram of formaldehyde oxidation on Rh the CO oxidation peak on Pt-Rh shows a significant contribution from the formation of the oxide layer as can be seen in figure 18.

The poor response could also be as a result of the nature of the Pt-Rh deposit. Although the electrode showed a good conductivity the morphology of the electrode was completely different to the Pt-Pd electrode. The deposit was confined to the PVC nodules with little or no lateral growth as previously shown in figure 31. Thus it would be fair to assume that the surface area of the electrode is reduced in comparison to the Pt-Pd electrode. The confined morphology could also lead to poor

electrochemistry at the electrode-electrolyte interface which is essential for an efficient fuel cell [6,58]. Future experiments should include depositing Pt-Rh for a longer time period, to ensure a surface similar to Pt-Pd. However, another disadvantage of the Pt-Rh alloy has been reported by de Tacconi *et al.* who showed that rhodium is leached from platinum alloy in sulfuric acid solutions [92]. With this observation and the results presented in this work in mind the use of Pt-Rh as a fuel cell catalyst would be unwise.

4.4.5 Platinum-Palladium fuel cell

The response of the Pt-Pd fuel cell to 1 ppm, 2 ppm formaldehyde and 25 ppm methanol is shown in figure 32. As can be seen, the fuel cell demonstrates excellent linearity with the response to 2 ppm approximately double that of 1 ppm formaldehyde. In addition the fuel cell recovers relatively quickly with the output returning to the baseline after approximately 200 seconds. The general fuel cell response and processes have been discussed previously in section 3.3.5.
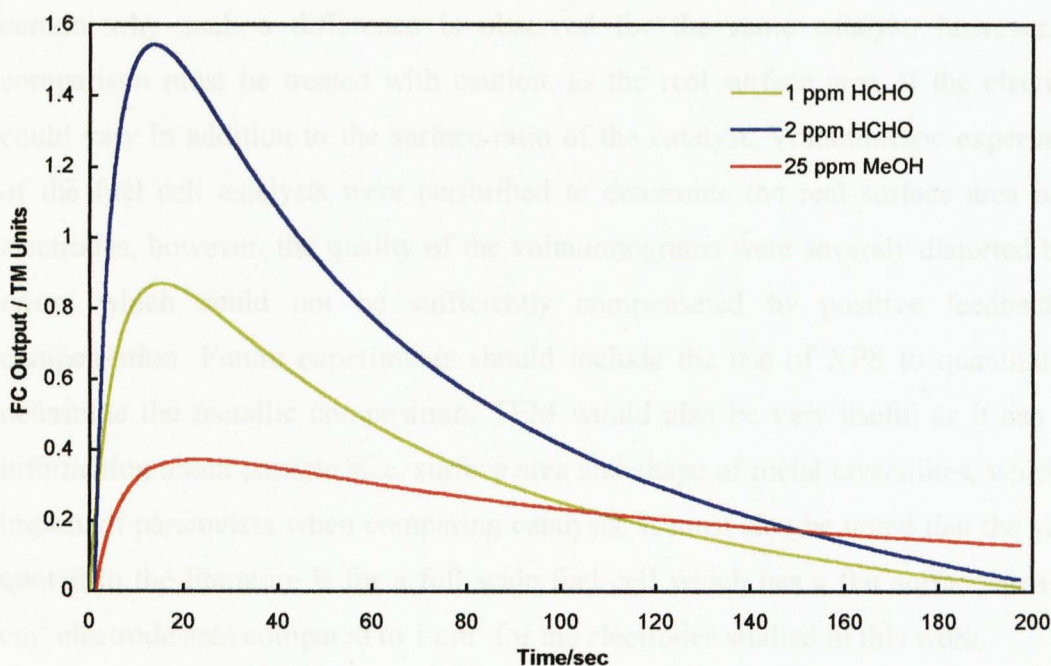

Figure 32 Pt-Pd fuel cell output to 1 ppm, 2 ppm formaldehyde and 25 ppm methanol. Vapour generator run at 18°C and 50 % RH

190

Also shown on the same figure is the response of the fuel cell to 25 ppm methanol. In comparison to the response to formaldehyde the response to methanol is broader with the maximum peak intensity occurring at 23 seconds. The broad nature was observed previously for the Pt-black fuel cell and the PANI fuel cell and was attributed to the slow kinetics of the oxidation process due to formation of strongly bound poison and adsorbed intermediates such as CO and COH [110-112]. Evidence of strong poisoning is also shown at the end of the time scale, where the fuel cell still maintains an output of 0.2 TM Units after 3 minutes, compared to both curves for formaldehyde, which recover to the baseline. However, as mentioned in the previous section a good property of this electrode is the low response to methanol and the respective low methanol/formaldehyde ratio. This follows the behaviour observed previously in the voltammograms of 50:50 % Pt-Pd in figures 14 and 15, where a better catalytic activity was observed for formaldehyde oxidation and reduced activity for methanol oxidation was shown. The average ratio for both fuel cell tested is 0.0165, which is particularly good and is better than the 0.035 quoted in the literature [26] for the Formaldemeter™ fuel cell which is also composed of 50:50% ratio Pt-Pd. It is not certain why such a difference is observed for the same catalyst, however, the comparison must be treated with caution, as the real surface area of the electrodes could vary in addition to the surface ratio of the catalyst. Voltammetric experiments of the fuel cell catalysts were performed to determine the real surface area of the electrodes, however, the quality of the voltammograms were severely distorted by iR errors which could not be sufficiently compensated by positive feedback iR compensation. Future experiments should include the use of XPS to quantitatively determine the metallic composition. TEM would also be very useful as it can give information about particle size, surface area and shape of metal crystallites, which are important parameters when comparing catalysts. It must also be noted that the values quoted in the literature is for a full scale fuel cell which has a flat surface area of 8 cm^2 electrode area compared to 1 cm^2 for the electrodes studied in this work.

4.4.6 Response of Pt-Pd fuel cell to humidity

Although the fuel cell shows good specificity towards formaldehyde, a low response to humidity is also required. The response of the Pt-Pd fuel cell to various levels of humidity at 20°C is shown in figure 33.
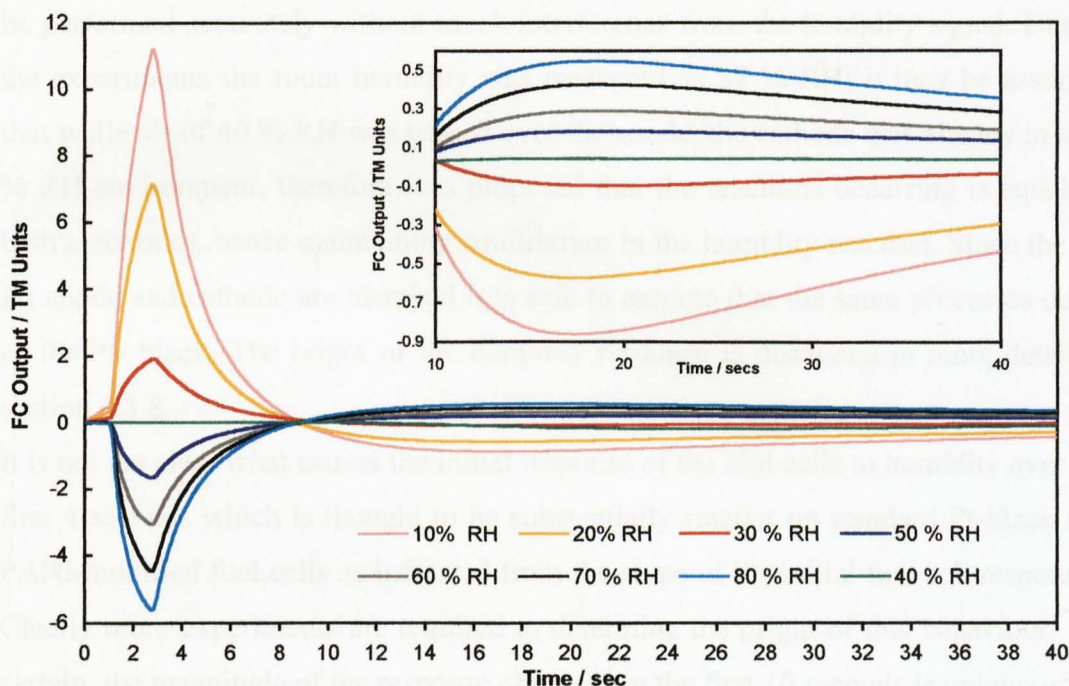
Figure 33 Response of Pt-Pd fuel cell to various levels of humidity at 20°C.

Inset, close-up between 10 and 40 seconds

As can be seen, the response is quite different to the standard Pt-black and PANI fuel cell discussed in section 3.3.8. However, in this study the effect of humidity was measured during the sampling procedure, whereas in the previous study the measurements were taken immediately after sampling. Samples were taken after 1 second, and the pump run time was 1.7 seconds, which is represented on the profile: An increase or decrease in the signal occurs just after 1 second when sampling starts, and a peak maximum occurs at 2.7 seconds when sampling or the pump stops. The signal then approaches the baseline within 4 seconds.

In general the more positive RH values (50-80% RH) give an initial negative peak during the sampling procedure and then increase in value where a positive peak maximum at 19 seconds is given. Values of 10-30 % RH follow the opposite trend, with a sharp positive peak during sampling, then a negative peak at around 19

192

seconds. The response from 10-40 seconds is shown in more detail inset in figure 33. In the previous investigations the humidity peak was shown to occur at around 13 seconds, therefore it may be assumed that the humidity peak for the Pt-Pd fuel cell is the second peak which occur at 19-20 seconds.

It can be seen that 40 % RH is the only humidity level that sample measurement can be performed accurately without much interference from the humidity signal. During the experiments the room humidity was measured as 37 % RH; it may be assumed that while air of 40 % RH was passed over the anode, the cathode was already in a 37 % RH environment, therefore it is proposed that the reactions occurring is equal on both electrodes, hence maintaining equilibrium in the humidity reaction. Since the Pt-Pd anode and cathode are identical it is safe to assume that the same processes occur as for Pt- black. The origin of the humidity response is discussed in more detail in section 3.3.8.

It is not yet clear what causes the initial response of the fuel cells to humidity over the first 4 seconds which is thought to be substantially smaller on standard Pt-black and PANI-modified fuel cells as indicated from the slope of the initial fuel cell responses. Clearly more experiments are required to determine the origin of this behaviour. For certain, the magnitude of the response observed in the first 10 seconds is unfavourable when low ppm measurements of formaldehyde are required.

4.4.7 Conclusions

Of the fuel cells studied containing Rh, Pt-Rh and Pt-Pd catalysts, only the Pt-Pd fuel cell showed good activity. It is thought that the poor activity of Rh and Pt-Rh is related to the greater strength of the oxide layer, especially for Rh. Pt-Pd on the other hand is active as the individual metals have surface oxides of lower thermodynamic stability.The response of the Pt-Pd fuel cell to formaldehyde and methanol, in comparison to the PANI-modified fuel cell and standard fuel cell composed of two separate Pt-black electrodes, discussed previously in section 3.3, is shown in table 9.

Fuel Cell	Formaldehyde		Methanol		MeOH / HCHO
	Response / PPM	Response Time	Response/ PPM	Response Time	
PANI	1.45	10	0.027	36	0.018
Pt-black	0.725	13	0.2	36	0.275
Pt-Pd	0.79	19	0.013	23	0.016

Table 9 Comparison of the fuel cell responses given by i) PANI-modified, ii) Standard Pt-black, iii) Pt-Pd

Compared with the Pt-black fuel cell it can be seen that an alloy containing both Pd and Pt has a marked effect on the response to methanol. While maintaining a good catalytic activity for formaldehyde its response to methanol is reduced by a factor of 15. Clearly the presence of Pd introduces specificity to the alloy, and is in agreement with the solution based voltammetry experiments, where little change was seen in the voltammogram of Pt-Pd in the presence of methanol compared to Pt. The decrease in catalytic activity was attributed to the inactivity of the Pd sites for methanol, while the increase in activity for formaldehyde was attributed the changes in adsorption features of the surface, in particular to the suppression of the poisoning (CO) intermediates.

An interesting feature of the Pt-Pd fuel cell in comparison to the other fuel cells is the slower response time to formaldehyde and the faster response time to methanol. In a previous study the response time of identical fuel cells have been shown to vary depending on the depositing solution used, which result in a different surface area of the electrodes [6]. The method of preparation is also thought to effect the fuel cell response; type I fuel cell electrodes are produced from deposition and compression of a slurry of Pt-black, while type II fuel cell electrodes are produced by electrodeposition of Pt-Pd onto gold-coated PVC. The different deposition methods are certain to affect the surface area and surface adsorption sites of the electrodes. Future experiments should include techniques to quantitatively determine the real surface area of the electrodes including the quantity of the individual metals in an alloy, such as TEM and XPS experiments.

Although voltammetric experiments were employed in order to determine the surface area of the electrodes, the magnitude of the iR errors greatly influenced the

quantitative information; in future the electrodes could be cut into smaller sizes of exact dimensions which would not produce as much iR drop, and thus a voltammogram of better quality.

From the table it can be seen that the PANI-modified fuel cell has the fastest response time to formaldehyde; as mentioned earlier faster response and clearing times enable a greater number of samples to be taken in a given time. The fast response time has been discussed previously in section 3.3 and attributed to the fast and effective switching of the PANI-coated cathode. An important advantage of the PANI-modified fuel cell in addition to the low methanol/formaldehyde ratio over the other two fuel cells is the significantly reduced response to humidity. It is therefore concluded that although a fuel cell containing Pt-Pd catalyst has a reduced methanol/formaldehyde ratio the PANI-modified fuel cell is favoured due to its low methanol/formaldehyde ratio in addition to reduced humidity response.

4.5 General Conclusions to Chapter 4

1. The anodic oxidation of formaldehyde is thought to occur by the indirect oxidation method where the reaction proceeds with the adsorption of the poisoning species CO formed from the dissociative adsorption of formaldehyde. The main anodic oxidation peaks in the voltammograms of formaldehyde electrooxidation is thought to be the oxidation of adsorbed CO. Slow sweep voltammetry indicate the presence of two pre peaks before the main CO oxidation peaks. At present, the origin of these pre peaks are unknown, however, it is speculated that they might be due to the oxidation of adsorbed OH and OH_2. The pre peaks could also be due to the oxidation of adsorbed CO in a different configuration, *i.e.* linear, bridge or multi-bonded. A similar oxidation process is thought to occur for methanol electrooxidation; however, investigations suggest that the strongly bound intermediate COH is firstly formed with the formation of CO occurring after subsequent reaction steps [27]. The identities of all the intermediates should be studied in future experiments utilising surface characterisation techniques such as *'in situ'* IR techniques. This should yield important information about the oxidation mechanisms.

2. The choice of metal has a significant effect on the electrooxidation of formaldehyde and methanol. Electrooxidation of formaldehyde occurred on all the metals studied, however, Pd and Rh showed a poor electrocatalytic activity towards the oxidation of methanol. Pd has been previously reported to be inactive for

methanol electrooxidation [69,78]. The inactivity of Rh for methanol could be due to the nature of the strong oxide layer [109].

3. Even though the deposition solutions contained equivalent atomic % of the metals, the rate of deposition was different for each of the pure metals. For the same number of deposition cycles, Pt and Pd had similar surface area, while that of Rh was six times less. However, a greater peak current density was observed for CO oxidation on Rh, which could be related to a particle size effect.

4. Alloying particular metals improves the catalytic activity towards the oxidation of formaldehyde; this is due to the change in adsorption features of the surface. Voltammograms indicate that alloys are a composite of the individual metals, which is in agreement with previous work [69,75]. From all the alloys studied, 50:50 % Pt-Pd had the best activity towards formaldehyde oxidation, while at the same time its activity towards methanol was much reduced compared to Pt alone. The greatly enhanced catalytic activity was attributed to the minimisation of poison formation (particularly adsorbed CO) and the reduced response to methanol was attributed to the presence of Pd, which is inactive for methanol electrooxidation. Future experiments should include the use of XPS to quantitatively determine the composition of all the alloys studied.

5. SEM characterisation of the electrodes indicates that the surface morphology is strongly dependent on the deposition time and technique. Potentiodynamic methods of deposition forms a weak coating of the metal, while galvanostatic deposition leads to a strongly bound crystalline morphology; the deposition time governing the surface coverage. EDAX analysis of the surfaces reveal a good distribution of the metal in the alloys, however, methods based on X-ray radiation should be used in future experiments to fully characterise the surface structure and composition. XPS would be essential to quantitatively determine the surface composition.

6. Of the fuel cells studied (Rh, Pt-Rh, Pt-Pd catalysts), only the Pt-Pd fuel cell showed good activity. The responses of the other fuel cells were particularly poor. It is proposed that the inherent activity of different metal electrodes is dependent on the nature of the adsorbed oxygen layer. The strength of the oxide layer is especially strong for Rh, which is thought to be the origin of the poor activity of the Rh and Pt-Rh fuel cells.

7. Compared to standard Pt-black fuel cells, the fuel cell containing Pt-Pd electrodes showed enhanced activity for formaldehyde and a substantially reduced response to

methanol (15 times smaller) giving a low methanol/formaldehyde ratio. This is analogous to the activity of the catalyst in voltammetric experiments. However, similar to the standard Pt-black fuel cell a substantial interference from humidity was shown. Future experiments should concentrate on an improved humidity response for the Pt-Pd fuel cell. As was shown in Chapter 3 for fuel cells consisting of Pt-black, a favourable option would be to coat the Pt-Pd cathode with PANI which was greatly shown to minimise the humidity reaction.

4.6 References

1   N. Kobosev, W. Monblanova, *Acta. Physiochem. URSS*, 1 (1934) 611

2   W. T. Grubb, *Nature*, 198 (1963) 883

3   F. C. Anson, *Acc. Res.*, 8 (1975) 400

4   A. J. Appleby, Electrocatalysts, in *Modern Aspects of Electrochemistry* (Ed B. E. Conway and J. O. M. Bockris), Vol 9, p369, Plenium Press, New York (1974)

5   Southampton Electrochemistry Group, "*Instrumental Methods in Electrochemistry,*" Ellis Horwood (1990)

6   I. D. Harrison, *Ph.D Thesis*, University of Wales, Cardiff, (1982)

7   B. D. McNicol, *J. Electroanal. Chem.*, 118 (1981) 71

8   S. Srinivasan, *J. Electroanal. Chem.*, 118 (1981) 51

9   A. J. Appleby, *J. Electroanal. Chem.*, 118 (1981) 31

10 A. Capon, R. Parsons, *J. Electroanal. Chem.*, 45 (1973) 205

11 N. A. Hampson, M. J. Willars, B. D. McNicol, *J. Power Sources*, 4 (1979) 191

12 A. Capon, R. Parsons, *J. Electroanal. Chem.*, 44 (1973) 239

13 R. Parsons, T. VanderNoot, *J. Electroanal. Chem.*, 257 (1988) 9

14 A. Bewick, K. Kunimatsu, S. Pons, *Electrochim. Acta.*, 25 (1980) 465

15 S. Pons, *J. Electroanal. Chem.*, 150 (1983) 495

16 T. D. Jarvi, E. M. Stuve, J. Lipkowski, P. N. Ross (Eds) "*Electrocatalysis*", Wiley-VCH, New York, (1998) Chapter 3, p 75

17 S. Wasmus, A Kuver, *J. Electroanal. Chem.*, 461 (1999) 14

18 C. Cattaneo, M. I. S. Pinto, H. Mishima, B. A. Mishima, D. Lescano, L. Cornaglia, *J. Electroanal. Chem.*, 461 (1999) 32

19 D. Kardash, C. Korzeniewski, N. Markovic, *J. Electroanal. Chem.*, 500 (2001) 518

20 A. Crown, I. R. Moraes, A. Wieckowski, *J. Electroanal. Chem.*, 500 (2001) 333

21 W. F. Lin, P. A. Christensen, A. Hamnett, *Phys. Chem. Chem. Phys.*, 3 (2001) 3312

22 J. Clavilier, *J. Electroanal. Chem.*, 107 (1980) 211

23 C. Lamy, J. M. Léger, *J. Chim. Phys.*, 88 (1988) 1649

24 A. Wieckowski, W. Chrzanowski, E. Herrero, "*Proceedings of the first international symposium on new materials for fuel cell systems*", Montreal, July 9-13 (1995) 326

25 N. Markovic, H. Gasteiger, P. N. Ross, *J. Electochem. Soc.,* 144 (1997) 1591

26 R. L. Nurton, *MSc. Thesis*, University of Wales, Cardiff, (1985)

27 J. Wang, P. V. A. Pamidi and G. Cepria, *Anal. Chim. Acta,* 330 (1996) 151

28 H. Baltruschat, N. A. Nastasijevic, M. Beltowska-Brzezinska, G. Hambitzer, J. Heitbaum, *Ber. Bunesenges. Phys. Chem.* 94 (1990) 996

29 J. Stelmach, R. Holze, M. Beltowska-Brzezinska, *J. Electroanal. Chem.*, 377 (1994) 241

30 P. Olivi, L. O. S. Bulhoes, J. M. Léger, F. Hahn, B. Beden, C. Lamy, *J. Electroanal. Chem.*, 370 (1994) 241

31 J. Sobkowski, K. Franazczuk, K. Dobrowolska, *J. Electroanal. Chem.*, 330 (1992) 529

32 B. Beden, C. Lamy, J. M. Léger, J. O. M. Bockris, B. E. Conway, R. E. White (Eds.), "*Modern Aspects of Electrochemistry*" Vol 22, Plenium, New York, 1992, 97

33 P. Olivi, L. O. S. Bulhoes, B. Beden, F. Hahn, J.-M. Léger and C. Lamy, *J Electroanal. Chem.,* 330 (1992) 583

34 M. T. M. Koper, M. Hachkar and B. Beden, *J. Chem. Soc., Faraday Trans.,* 92 (1996) 3975

35 B. Beden, F. Kadirgan, C. Lamy, J. M. Léger. *J. Electroanal. Chem.*, 127 (1981) 75

36 T. C. Hable, M. S. Wrighton, *Langmuir*, 7 (1991) 1305

37 A. Hamnett, B. J. Kennedy, *Electrochim. Acta.*, 33 (1988) 1613

38 T. Iwasita, H. Hoster, A. John-Anacker, W. F. Lin, W. Vielstich, *Langmuir*, 16 (2000) 522

39 J. W. Long, R. M. Stroud, K. E. Swider, D. R. Rolison, *J. Phys. Chem. B*, 104 (2000) 9772

40 W. Chrzanowski, A. Wieckowski, *Langmuir,* 14 (1988) 1967

41 E. Reddington, A. Sapienza, B. Gurau, R.Viswanathan, S. Sarangapani, E. S. Smotkin, T. E. Mallouk, *Science*, 280 (1998) 1735

42 P. Bindra, J. Roldan, *J. Electrochem. Soc.* 132 (1985) 2581

43 S. Nakabayashi, I. Yagi, N. Sugiama, K. Tamura, K. Uosaka, *Surface Science*, 386 (1997) 82

44 T. Zerihun, P. Grundler, *J. Electroanal. Chem.*, 441 (1998) 57

45 X. G. Zhang, Y. Murakami, K. Yahikozawa, Y. Takasu, *Electrochim. Acta.*, 42 (1997) 223

46 H. Yang, T. H. Lu, K. H. Xue, S. G. Sun, S. P. Chen, *J. Appl. Electrochem.*, 27 (1997) 428

47 K. Yahikozawa, K. Nishimura, M. Kumazawa, N. Tateishi, Y. Takasu, K. Yasuda, Y. Matsuda, *Electrochim. Acta.*, 37 (1992) 453

48 R. R. Adzic, M. L. Amramov-Ivic, A. V. Tripkovic, *Electrochim. Acta.*, 29 (1984) 1353

49 L. D. Burke, K. J. O'Dwyer, *Electrochim. Acta.*, 36 (1991) 1937

50 R. Ramanauskas, I. Jurgaitiene, A. Vaskelis, *Electrochim. Acta.*, 42 (1997) 191

51 M. Beltowska-Brzeziska, J. Heitbaum, *J. Electroanal. Chem.* 183 (1985) 167

52 M. Beltowska-Brzeziska, *Electrochim. Acta.*, 30 (1985) 1193

53 M. Watanabe, Y. Fuuruchi, S. Motoo, *J. Electroanal. Chem.* 191 (1985) 367

54 T. R. Cataldi, C. Campa, D. Centonze, *Anal. Chem.*, 67 (1995) 3740

55 S. F. White, A. P. F. Turner, R. D. Schmid, U. Bilitewski, J. Bradley, *Electroanalysis*, 6 (1994) 625

56 H. Gunasingham, C. B. Tan, *Electroanalysis*, 1 (1989) 223

57 R. J. Nichols, *Ph.D Thesis*, University of Southampton (1989)

58 C. H. Hamann, A. Hamnett, W. Vielstich, *"Electrochemistry,"* Wiley VCH Weinheim, (1998)

59 S. Nakabayashi, A. Kira, *J. Phys. Chem.* 96 (1992) 1021

60 S. G. Sun, J. Clavilier, A. Bewick. *J. Electroanal. Chem.* 240 (1988) 147

61 S. G. Sun, Y. Lin, N. H. Li, J. Q. Mu, *J. Electroanal. Chem.* 370 (1994) 273

62 F. Raspel, M. Eiswirth, *J. Phys. Chem.*, 98 (1994) 7613

63 S. C. Chang, M. J. Weaver, *J. Phys. Chem.*, 94 (1990) 5095

64 F. Seland, D. A. Harrington, R. Tunold, *"2001 Joint International Meeting, September 2 – 7, 2001, the 200th Meeting of The Electrochemical Society, the 52nd Meeting of the International Society of Electrochemistry"* Abstract No. 60

65 K. Shimazu, H. Kita, *J. Electroanal. Chem*, 341 (1992) 361

66 L. C. Gruen, P. T. McTigue, *J. Chem. Soc.*, (1963) 5217

67 M. Pourbaix, "*Atlas of Electrochemical Equilibria*", Pergamon Press, Oxford (1966)

68 N. Tateishi, K. Yahikozawa, K. Nashimura, M. Suzuki, *Electrochim Acta*, 36 (1990) 1235

69 N. Dalbay, F. Kadirgan, *Electrochim Acta.*, 353 (1991) 36

70 D. Pletcher, R. I. Urbina, *J. Electroanal. Chem.* 421 (1997) 137

71 M. Vuković, *J. Electroanal. Chem.* 242 (1988) 97

72 P. A. Christensen, A. Hamnett, G. L. Troughton, *J. Electroanal. Chem.* 362 (1993) 207

73 S. –B. Lee, S. –I. Pyun, *J. Appl. Electrochem.*, 30 (2000) 795

74 W. T. Napporn, H. Laborde, J. –M. Léger, C. Lamy, *J. Electroanal. Chem*, 404 (1996) 153

75 D. A. J. Rand, R. Woods, *J. Electroanal. Chem*, 36 (1972) 57

76 P. Olivi, L. O. S. Bulhoes, J. M. Léger, F. Hahn, B. Beden, C. Lamy, *Electrochim Acta.*, 41 (1996) 927

77 M. Watanabe, S. Motoo, *J. Electroanal. Chem.*, 60 (1975) 267

78 F. Kadirgan, *These de Doctorat de 3eme Cycle*, Univ. de Poitiers (1980)

79 K. Yahikozawa, Y. Fujii, Y. Matsuda, K. Nishimura, Y. Takasu, *Electrochim. Acta.*, 36 (1991) 973

80 M. A. Abdel Rahim, M. W. Khalil, H. B. Hassan, *J. Appl. Electrochem.*, 30 (2000) 1151

81 A. Papoutis, J. -M. Léger, C. Lamy, *J. Electroanal. Chem.*, 234 (1987) 315

82 B. Beden, F. Hahn, J. -M. Léger, L. Lamy, C. Perdriel, N. de. Tacconi, R. O. Lezna, A. J. Arvia, *J. Electroanal. Chem.*, 301 (1991) 129

83 L. D. Burke, M. A. Horgan, L. M. Hurley, L. C. Nagle, A. P. O'Mullane, *J. Appl. Electrochem*, 31 (2001) 729

84 J. M. Murday, *MSc. Thesis*, University of Wales, Bangor, (1993)

85 J. A. Caram, C. Gutiérrez, *J. Electroanal. Chem.*, 346 (1993) 451

86 N. Collas, B. Beden, J. -M. Léger, C. Lamy, *J. Electroanal. Chem.*, 186 (1985) 287

87 S. Motoo, N. Furuya, *J. Electroanal. Chem.*, 184 (1985) 303

88 S. Motoo, N. Furuya, *J. Electroanal. Chem.*, 197 (1986) 209

89 S. Motoo, M. Shibata, *J. Electroanal. Chem.,* 139 (1982) 119

90 C. Lamy, J. –M. Léger, J. Clavilier, *J. Electroanal. Chem.,* 135 (1982) 321

91 D. F. A. Koch, D. A. J. Rand, R. Wood, *"Binary Electrocatalysts for Organic Oxidation"*

92 N. R. de Tacconi, J. –M. Léger, B. Beden, C. Lamy, *J. Electroanal. Chem,* 134 (1982) 117

93 A. S. Arico, Z. Poltarewski, H. Kim, A. Morana, N. Giordano, V. Antonucci, *J. Power Sources,* 55 (1995) 159

94 K. L. Ley, R. X. Liu, C. Pu, Q. B. Fan, N. Leyarovska, C. Segre, E. S. Smotkin, *J. Electrochem. Soc.,* 144 (1997) 1543

95 P. K. Shen, A. C. C. Tseung, *J. Electrochem. Soc.* 141 (1994) 3082

96 P. M. Williams, *PhD Thesis,* University of Wales, Cardiff (1978)

97 M. Feltham, M. Spiro, *Chem. Rev.,* 71 (1971) 177

98 C. A. Marrese, *Anal. Chem.,* 59 (1987) 217

99 W. Levason, D. Pletcher, A. M. Smith, A. R. Berzins, *J. Appl. Electrochem.,* 28 (1998) 18

100 W. Jeffrey Basirun, D. Pletcher, *J. Appl. Electrochem.,* 28 (1998) 167

101 F. Kurlbaum, *Ann. Phys. Chem.,* 67 (1899) 846

102 S. Shibata, *Bull. Chem. Soc. Japan,* 36 (1963) 525

103 S. Shibata, M. P. Sumino, *Electrochim. Acta.,* 16 (1971) 1511

104 S. D. James, *J. Electrochem. Soc.,* 116 (1969) 1681

105 J. P. Hoare, *"The Electrochemistry of Oxygen",* Wiley Interscience, New York, (1968)

106 T. Biegler, *J. Electrochem. Soc.,* 116 (1969) 1131

107 J. Weber, B. Posiril, *J. Electroanal. Chem.,* 38 (1972) 417

108 H. Luo, S. Park, Y. H. Chan, M. J. Weaver, *J. Phys Chem. B,* 104 (2000) 8250

109 H. Y. H. Chan, S. Zou, M. J. Weaver, *J. Phys Chem. B,* 103 (1999) 11141

110 K. Scott, W. Tamma, J. Cruikshank, *J. Appl. Electrochem.,* 28 (1998) 289

111 M. Webster, J-T. Wang, S. Wasmus, R. F. Savinell, *J. Electrochem. Soc.,* 143 (1997) L158

112 W.-F. Lin, J.-T. Wang, R. F. Savinell, *J. Electrochem. Soc.,* 144 (1997) 1917

Chapter V – General Conclusions and Recommendations

The work has shown that it is possible to improve the performance and reliability of fuel cells by either utilising PANI as a cathode or by changing the electrocatalyst itself.

In the first part of the work the possibility of replacing the oxygen reduction reaction on the cathode with that of a conducting polymer (PANI) was investigated. The suitability and redox behaviour of various PANI-coated electrodes were initially examined by cyclic voltammetry and open circuit potential measurements. The results indicate that the stability of PANI depends on the nature of the anion in which the polymer is stored. Degradation increased in the order $HCl < H_3PO_4 < H_2SO_4$. Degradation is promoted in H_2SO_4 and can be related to the catalytic action and the small size of the anion where SO_4^{2-} and HSO_4^{-} are too small to effectively preclude the approach of nucleophilic constituents such as OH^{-} and H_2O. SEM studies indicate that the stability is also related to the polymer morphology. PANI/Cl^{-} coated Pt-black has a compact morphology which minimises degradation while Pt-black coated with PANI/SO_4^{2-} has a porous morphology, which promotes degradation by exposing the polymer interior.

Open circuit investigations of PANI films deposited on polycrystalline Pt indicate that the polymer attains a stable equilibrium potential in the emeraldine salt oxidation state, regardless of the initial applied potential. In the presence of oxygen the reduced polymer switches rapidly to the emeraldine salt oxidation state. The results also indicate that the same process occurs under completely degassed conditions but at a much slower rate. A reaction of the polymer with species in solution other than oxygen or on the PANI chain itself (comproportionation or disproportionation) is proposed. Mathematical treatment of the potential transients supports this assumption, however, future experiments should include the use of *in situ* ESR to determine the exact nature of the reacting species. In the presence of the reducing agent Na_2SO_3 the equilibrium potential of the polymer shifts negatively; three definable equilibrium potentials are demonstrated which could be due to different α, β and metastable forms of the polymer. However future *in situ* ESR and *in situ* IR experiments should be preformed to verify this. The presence of Na_2SO_3 in H_2SO_4 electrolyte also improves the stability of the polymer by maintaining the polymer in the more stable polaronic form of the polymer which is less liable to nucleophilic attack.

By incorporating the PANI-modified fuel cells into the Formaldemeter™ instrument and evaluating the performance on a calibrated vapour generator it has been shown that the activity of the fuel cells depends on the electrolyte and the substrate onto which PANI is coated. Fuel cells containing HCl and H_3PO_4 electrolyte display poor fuel cell performance due to the greater strength of adsorption of the corresponding anions which block the catalytic surface. Although open circuit measurements indicate a fast degradation of the polymer in H_2SO_4 the fuel cell shows excellent performance. Thus, degradation of the polymer does not lead to a completely inactive film. Compared to a standard fuel cell composed of two Pt-black electrodes which depends on the diffusion of oxygen at the cathode, the PANI-modified fuel cell has improved sensitivity (twice as sensitive to formaldehyde), improved selectivity (8 times less sensitive to methanol) and a significantly reduced response to humidity (10 times less sensitive). In addition the fuel cell has a faster response time, good reproducibility and a long shelf life. The shifted equilibrium potential of the fuel cell is thought to favour formaldehyde oxidation, while having the opposite effect on methanol oxidation. The presence of PANI on the cathode minimises the humidity reaction. The fast switching of PANI from the oxidised state to the reduced state and the rapid oxidation of the polymer by oxygen back to its original state is thought to speed up the response time and improve the reproducibility of the fuel cell.

In the second part of the work various noble metals and alloys deposited on glassy carbon were evaluated for their electrocatalytic activity. Cyclic voltammetry has shown that the choice of metal has a significant effect on the electrooxidation of formaldehyde and methanol. The results indicate that while Pt is active towards methanol and formaldehyde Pd and Rh are inactive towards the oxidation of methanol. Calculation of the real surface area of the electrodes indicates that the metals have different deposition rates even though the solutions were of identical metal content. Alloying particular metals improves the catalytic activity towards the electrooxidation of formaldehyde; this is due to the change in adsorption features of the surface. Cyclic voltammograms indicate that alloys are a composite of the individual metals. From all the alloys studied, 50:50 % Pt-Pd has the best activity towards formaldehyde oxidation, while at the same time its activity towards methanol is significantly reduced. The greatly enhanced catalytic activity is attributed to the minimisation of poison formation (particularly adsorbed CO) and the reduced response to methanol is attributed to the presence of Pd, which is inactive for

methanol electrooxidation. It is suggested that future work be directed towards the characterisation of the electrode surfaces, including the use of XPS to quantitatively determine the composition of all the alloys studied.

The inherent activity of different metal electrodes is dependent on the nature of the adsorbed oxygen layer. Of the fuel cells studied (Rh, Pt-Rh, Pt-Pd catalysts), only the Pt-Pd fuel cell shows good activity. The responses of the other fuel cells were particularly poor due to strength of the oxide layer, which is especially strong for Rh. Fuel cell containing Pt-Pd electrodes show enhanced activity for formaldehyde and a substantially reduced response to methanol (15 times smaller). This is analogous to the activity of the catalyst in voltammetric experiments. However in comparison to the PANI-modified fuel cell a significant interference from humidity is shown. An improved humidity response for the Pt-Pd fuel cell could be achieved by coating the Pt-Pd cathode with PANI and therefore should be subjected to further development in the future.

Future attempts at sensor development should examine the durability, reproducibility and accuracy of the sensors over long periods of time and under conditions appropriate to their use, as these may be far removed from those observed in the laboratory environment.